The Mechanism of BAM-assisted OMP Folding

Anna Juman Higgins

Submitted in accordance with the requirements for the degree of

Doctor of Philosophy

The University of Leeds

Astbury Centre for Structural Molecular Biology

School of Molecular and Cellular Biology

September 2018

Intellectual Property and Publications

The candidate confirms that the submitted work is her own, except where work which has formed part of jointly authored publications has been included. The contribution of the candidate and the other authors to this work has been explicity indicated below. The candidate confirms that appropriate credit has been given within the thesis where reference has been made to the work of others. This copy has been supplied on the understanding that it is copyright material and that no quotation from this thesis may be published without proper acknowledgement.

Throughout this thesis the work directly attributable to the candidate is as follows:

(i) Literature research and compilation of the manuscript stated above.

(ii) The candidate performed all the experimental work and data analysis unless otherwise stated.

Chapter 4 includes discussion of protein purification and cryo-EM and Chapter 5 includes functional assays from the following publication: Higgins, A.J.*, Iadanza, M.G.*, Schiffrin, B., Calabrese, A.N., Brockwell, D.J., Ashcroft, A.E., Radford, S.E., Ranson, N.A. 2016. Lateral opening in the intact B-barrel assembly machinery captured by cryo EM. Nature Communications 7, 12865. The author contribution reads: S.E.R., D.J.B., A.J.H. and B.S. designed functional assays. A.J.H. expressed and purified proteins, and performed functional assays (Figures1,7, SupFig1,4 & 10). M.G.I. and N.A.R. designed electron microscopy experiments. M.G.I. performed electron microscopy sample preparation, data collection, image processing and model building. A.C. performed MS experiments. All authors contributed to data analysis and interpretation. M.G.I., A.J.H., N.A.R., S.E.R., B.S., D.J.B. and A.N.C. prepared the manuscript. M.G.I., A.J.H., A.N.C. and N.A.R. contributed figures to the manuscript.

Chapter 3 includes functional assays on tOmpA folding by BamA variants from the following publication: Schiffrin, B., Calabrese A.N.*, Higgins A.,J.*, Humes, J.R., Ashcroft, A.E., Kalli, A.C., Brockwell, D.J., Radford, S.E. 2017. Effects of Periplasmic Chaperones and Membrane Thickness on BamA-Catalyzed Outer-Membrane Protein Folding. Journal of Molecular Biology 429, 3776. I expressed

and purified BamA proteins and performed functional assays and folding gels for BamA variant proteins (Figure 5 &SupFig9). B.S. performed all other functional assays and MD simulations. A.N.C. performed MS experiments. J.R.H. carried out MST experiments. A.E.K. assisted with MD simulations and data analysis. I contributed the noted figures noted and to the editing of the manuscript. The manuscript was written by B.S. with contribution and editing by all authors.

Acknowledgements

Abstract

Outer membrane proteins (OMPs) mediate the survival and pathogenicity of Gram negative bacteria. The biogenesis of these proteins, however, presents problems as they must be transported to, inserted and folded correctly in the outer membrane in the absence of ATP. This problem is resolved by the β-barrel assembly machinery (BAM) complex: a ~203 kDa complex of five proteins (BamA-E) that enables the membrane insertion and folding of substrate OMPs on a physiological timescale. Despite available crystal structures, the mechanism of this vital protein complex remains poorly understood.

In this thesis I use a variety of structural and biochemical tools to probe the nature of BAM-assisted OMP folding, particularly the role of BamA dynamics. Successful purification of the intact BAM complex in the detergent DDM allowed the first cryo-electron microscopy structure of the complex to be obtained, at a resolution of 4.9 Å. This reveals the intact BAM complex with BamA in a laterally-open conformation in which the first (β1) and last (β16) strands of the barrel are no longer hydrogen bonded.

In addition, biochemical assays provide the first *in vitro* evidence of the functional importance of BamA lateral gating in OMP folding. These assays demonstrate that in a reconstituted system utilising the BAM complex, inhibiting the lateral gating of BamA by incorporating new disulphide bonds diminishes the ability of BAM to assist substrate folding. This is shown with two different OMP substrates, tOmpA (the β-barrel domain of OmpA) and OmpT. In synthetic lipids, however, the presence of prefolded BamA is sufficient to aid substrate folding and inhibition of lateral gating by disulphide bonding in this case does not diminish the catalytic effect. The results indicate that BamA likely adopts different roles depending on substrate and lipid.

Furthermore, this thesis discusses preliminary experiments towards determining the significance of the β-signal: a conserved sequence found towards the C-terminus of OMPs hypothesised to be important for recognition by BamA. The results show that while some mutations may slow the protein's intrinsic folding into the membrane they do not affect the apparent BamA-catalysed folding rate. However, other single amino-acid substitutions appear to incur a large energetic penalty, rendering the protein incapable of adopting its stable β-barrel structure. Combined, the data allow us to begin dissecting the mechanism of BAM-assisted

folding of OMPs, particularly the role of BamA in passive membrane destabilization or active lateral opening.

Table of Contents

List of Figures

xvii

List of Tables

List of Abbreviations

A

ABC	ATP-binding cassette
AFM	Atomic force microscopy
APS	Ammonium persulphate
ATP	Adenosine triphosphate
Au	Absorbance units
AUC	Analytical ultracentrifugation

B

BAM	β-barrel assembly machinery
BCA	Bicinchoninic acid
BN-PAGE	Blue native polyacrylamide gel electrophoresis
BSA	Bovine serum albumin

C

CD	Circular dichroism
CL	Cardiolipin
CPP	Cell-penetrating peptide
CryoEM	Cryo-electron microscopy

D

dH2O	Deionised water (greater than 15 MΩ resistance)
DDPC	Didecanoyl phosphatidylcholine
DDPE	Didecanoyl phosphatidylethanolamine
DDM	Dodecyl maltoside
DTT	Dithiothreitol
DLPC	Dilauroyl phosphatidycholine
DLS	Dynamic light scattering
DMPC	Dimyristoyl phosphatidylcholine
DMSO	Dimethyl sulphoxide
DNA	Deoxyribonucleic acid
DTPC	Ditridecanoyl phosphatidylcholine
DUPC	Diundecanoyl phosphatidylcholine

E

EDTA	Ethylenediaminetetraacetic acid
EM	Electron microscopy
ER	Endoplasmic reticulum
ESI	Electrospray ionisation
EtBr	Ethidium bromide
EtOH	Ethanol

F

FES	Fluorescence Emission Spectrscopy/Spectra
FRET	Förster resonance energy transfer

G

GuHCl	Guanidine hydrochloride

H

HT	His-tagged

xx

HDX	Hydrogen-deuterium exchange
HSQC	Heteronuclear single quantum coherence
I	
IM	Inner membrane
IMS	Ion mobility spectrometry
IPTG	Isopropyl-β-d-thiogalactoside
K	
Kd	Equilibrium dissociation constant
L	
LB	Lysogeny broth
LDAO	Lauryldimethylamine-N-oxide
Lol	Localisation of lipoproteins
LPR	Lipid to protein ratio
LPS	Lipopolysaccharide
Lpt	Lipopolysaccharide transport
LUV	Large unilamellar vesicle
M	
MD	Molecular dynamics
MDR	Multidrug resistance
Mla	Maintanence of OM lipid asymmetry
MRE	Mean residue ellipticity
MS	Mass spectrometry
MWCO	Molecular weight cut-off
N	
NMR	Nuclear magnetic resonance
NOE	Nuclear Overhauser effect
O	
OD	Optical density
OM	Outer membrane
OMP	Outer membrane protein
ORF	Open reading frame
P	
PAGE	Polyacrylamide gel electrophoresis
PagP	PhoP/Q activated gene P
PC	Phosphatidylcholine
PCR	Polymerase chain reaction
PDB	Protein data bank
PE	Phosphatidylethanolamine
PG	Phosphatidylglycerol
PMSF	Phenylmethanesulfonylfluoride
POTRA	Polypeptide transport-associated
PPIase	Peptidyl-prolyl isomerise
PPIs	Protein-protein interactions
R	
Rg	Radius of gyration

rpm	Rotations per minute
RMSD	Root mean square deviation
S	
SDS	Sodium dodecyl sulphate
SDS-PAGE	Sodium dodecyl sulphate polyacrylamide gel electrophoresis
SEC	Size exclusion chromatography
SEM	Standard error of mean
Skp	Seventeen kilodalton protein
SMFS	Single molecule force spectroscopy
SurA	Survival protein A
SUV	Small Unilamellar Vesicle
T	
TCEP	Tris(2-carboxyethyl)phosphine (TCEP)
TEMED	Tetramethylethylenediamine
TEV	Tobacco etch virus
TF	Trigger factor
TM	Transmembrane
TMD	Transmembrane domain
Tris	Tris (hydroxymethyl)-aminomethane
TBS	Tris-buffered saline
U	
UV	Ultraviolet
W	
WT	Wild-type

1   Introduction

Gram-negative bacteria are important pathogens in the modern world[1-3], the increasing incidence of antibiotic resistance means there is a strong pressure to develop novel antibiotic candidates[2-5]. The outer membrane (OM) of Gram-negative bacteria represents their principal line of defence[5-9], but may also present an antibacterial target[6,7,10]. Outer membrane proteins (OMPs) are vital in Gram-negative bacteria, forming a core component of the OM and performing a wide variety of roles[7,11-19].

Over the last 15 years our understanding of OMPs and OMP biogenesis has dramatically increased. Moving from the most simplistic notion of the two membranes of Gram-negative bacteria[15,20,21] we now have detailed knowledge of the protein players in every aspect. However, many aspects of OMP biogenesis, their journey to the OM, assembly and folding remain unclear. While the proteins vital in this pathway are generally known, their mechanisms are yet to be elucidated.

The β-barrel assembly machine (BAM) is vital and highly conserved across Gram-negative bacteria[21-23]. Its absence is lethal and its depletion causes severe defects in OMP folding and assembly[21,24,25]. The central component BamA was identified as a member of the Omp85 superfamily, of which a homologue is present in all Gram-negative bacteria, mitochondria and chloroplasts[26-29]. Despite knowing that BAM is crucial for the correct assembly of OMPs, the mechanism by which it does this, and by which OMPs arrive to the OM is not clear[14,19,21,30-35].

Moving from the bacteria, to OMP sequences, I will summarise what is known in these fields, and how it has been studied, before moving to the fundamental question: how does BAM, particularly BamA, catalyse the folding of OMPs?

1.1   Gram-negative bacteria

Bacteria can be classified on the basis of their Gram staining[20,36]. The simple staining method identifies Gram-positive bacteria, which possess a thick peptidoglycan cell wall, as stained with crystal violet dye, and remain purple following washing. In Gram-negative bacteria the thin peptidoglycan layer allows

extensive washing to remove the crystal violet and cells can subsequently be stained with a red dye, typically safranin or fuchsin[20,36].

Gram-negative bacteria are characterised by possessing both an inner and an outer membrane (IM and OM), with a thick periplasmic space (100- 210Å)[37,38] containing a layer of peptidoglycan (Figure 1-1), with this structure revealed by electron microscopy (EM) in 1969[39]. The combination of these elements makes the bacteria difficult to target, resistant to the influx of both hydrophilic and hydrophobic molecules. The OM is connected to the peptidoglycan by Braun's lipoprotein or Lpp[40], the most abundant lipoprotein in enteric bacteria. Lpp is capable of lengthening and controls the dimensions of the periplasm[41].

Gram-positive bacteria are protected by thicker layers of peptidoglycan, 30-100 nanometres thick, as opposed to the few nanometres characteristic of Gram-negative bacteria (Figure 1-1)[13]. Peptidoglycan is made up of repeating units of the disaccharide N-acetyl glucoamine-N-acetyl muramic acid[42]. The peptidoglycan is rigid in Gram-positive bacteria and determinant of cell shape[42]. In addition, in Gram-positive bacteria, anionic polymers, known as teichoic acids thread through the peptidoglycan, accounting for ~60% of the mass of the cell wall[13,43]. In the absence of an OM, surface-expressed proteins in Gram-positive bacteria are tethered into the cell wall.

Partly due to their protective outer layers and intractability as a target, Gram-negative bacteria represent the causative agents of many human bacterial diseases. They are key contributors to nosocomial infections and show widespread development of antibiotic resistance[1-7,44]. The WHO 2017 priority list on bacteria for which antibiotics are urgently needed highlighted many Gram-negative bacteria, with all of the "critical" priority, including *Enterobacteriaceae,* being Gram-negative[45] (Table 1-1).

Priority 1: Critical	
Acinetobacter baumannii	Carbapenem-resistant
Pseudomonas aeruginosa	Carbapenem-resistant
Enterobacteriaceae	Carbapenem-resistant, 3rd generation cephalosporin-resistant
Priority 2: High	
Enterococcus faecium	Vancomycin-resistant
Staphylococcus aureus	Methicillin-resistant Vancomycin-intermediate
Helicobacter pylori	Clarithromycin-resistant
Campylobacter	Fluoroquinolone-resistant
Salmonella spp.	Fluoroquinolone-resistant
Neisseria gonorrhoeae	3rd generation cephalosporin-resistant fluoroquinolone-resistant
Priority 3: Medium	
Streptococcus pneumoniae	Penicillin-non-susceptible
Haemophilus influenza	Ampicillin-resistant
Shigella spp.	Fluoroquinolone-resistant

Table 1-1: WHO Priority Pathogens List for development of new antibiotics.
The list shows pathogenic bacteria for which research and development of antibiotics is required, their priority, as well as their current antibiotic resistance. Gram-negative bacteria are highlighted in grey. *Enterobacteriaceae* include: *Klebsiella pneumonia, Escherichia coli, Enterobacter* spp*., Serratia* spp*., Proteus* spp*., Providencia* spp*,* and *Morganella* spp*.* Figure reproduced from WHO 2017[45].

Many current antibiotics target elements of the cell envelope of Gram-negative bacteria. β-lactam antibiotics, including pencillin and cephalosporin, target production of peptidoglycan[6,44]. These have been the primary antibiotic of choice for many years[4], but many Gram-negative bacteria now possess extended-spectrum β-lactamases, enzymatic against multiple β-lactam antibiotics[44]. Other elements that constitute the bacteria's first layer of defence, the proteins and lipids of the outer membrane, also represent excellent targets as they are essential, conserved and surface exposed[10,46-49]. Therefore, improving our understanding of the mechanisms behind the biogenesis of the cell envelope may

improve the ability to specifically target cell envelope formation, and thus create new antibiotics. The work carried out in this thesis was conducted on *E.coli* OM biogenesis. The focus in this introduction, therefore, will principally be on the proteins and mechanisms of this species, but in general these apply to other Gram-negative bacteria.
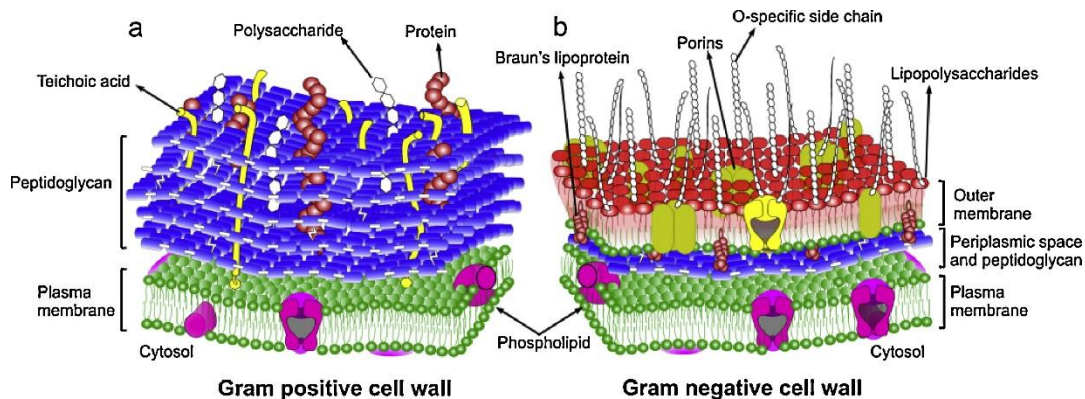
Figure 1-1: Gram- negative and -positive cell walls. Schematic comparing the cell walls of (a) Gram-positive bacteria, which possess a thick layer of peptidoglycan, and (b) Gram-negative bacteria which have a thin layer of peptidoglycan and an Outer Membrane. Figure reproduced from Tripathi *et al.*, (2012)[50].

1.2 The outer membrane

The outer membrane (OM) of Gram-negative bacteria represents their first, and critical layer of defence[5-9,51-53]. A crowded asymmetric bilayer, the OM possesses an outer leaflet of lipopolysaccharide (LPS) and an inner one of phospholipids[54], numerous lipoproteins and transmembrane proteins[13,19,55-57]. All of these components must be transported to, and assembled in, the OM following synthesis in the cytoplasm. Despite initial evidence showing areas of fusion between the IM and OM, known as Bayer bridges[58] which would facilitate the flux of protein and lipid between the membranes, it now appears this is unlikely and all of these components have evolved their own protein-based pathways for transport across the periplasm[15,21,31,35,51,59-64]. The transport mechanisms and ultimate assembly of these components are fascinating as while ATP can assist initial transport across the IM, the periplasm is devoid of nucleotide[65]. Therefore, an intricate energetically-favourable pathway, powered only by protein conformations and affinities, has evolved to facilitate OM assembly in every case. As they constitute vital elements of the OM, the nature and transport of OM lipids,

LPS and lipoproteins will be briefly discussed, before further emphasis on the pathway of interest for the work presented in this thesis: OMP biogenesis. In most cases the pathway and proteins responsible have gradually been elucidated[31,34,52,61], but the OMP pathway has perhaps proved the most intractable, with the mechanisms still largely unclear. OMPs constitute vital, conserved, defensive elements for Gram-negative bacteria and therefore their biogenesis is an important area to study, especially given the urgent need to develop new antibiotics in today's world[2,3,5,7,8,45].

1.3 Outer membrane lipids and lipid transport

Whereas most bacteria exhibit high diversity in the makeup of their lipid bilayer, *E.coli* is unusual in possessing only three phospholipids with an abundance higher than 1%(ref. 56). Both inner and outer membranes of *E.coli* are composed primarily of phosphatidylethanolamine (PE), phosphatidylglycerol (PG) and cardiolipin (CL) (Figure 1-2)[54]. These three lipids are all synthesised from simple building blocks, via the Kennedy pathway and transported across the periplasm[66]. The outer membrane is enriched in phosphatidylethanolamine, comprising ~90% by weight, as opposed to 70% in the inner membrane[67].

While either CL[68] and PE[69] are dispensible for *E.coli* cell viability, mutants lacking both are not viable[70]. The lack of requirement is perhaps most surprising for PE which makes up a large proportion (70-80%) of total glycerophospholipid in *E.coli* cells[70]. Depletion of PE in the OM can be compensated by increased proportion of the other, anionic lipids (such as CL) and divalent cations, such as Mg^{2+} and Ca^{2+} (ref. 56,69,70). This implies that the role of the membrane lipids is primarily structural, with reduced dependence on the specific type of lipid. In addition, the outer membrane is enriched in saturated fatty acids, of which palmitic acid (16:0) is the major contributor, making up approximately 30% (ref. 54). As will be discussed further (Section 1.8) a large number of studies on the folding of OMPs have been carried out in synthetic bilayers, usually composed principally of phosphatidylcholine (PC), despite the native OM makeup of PE and PG (Figure 1-2).
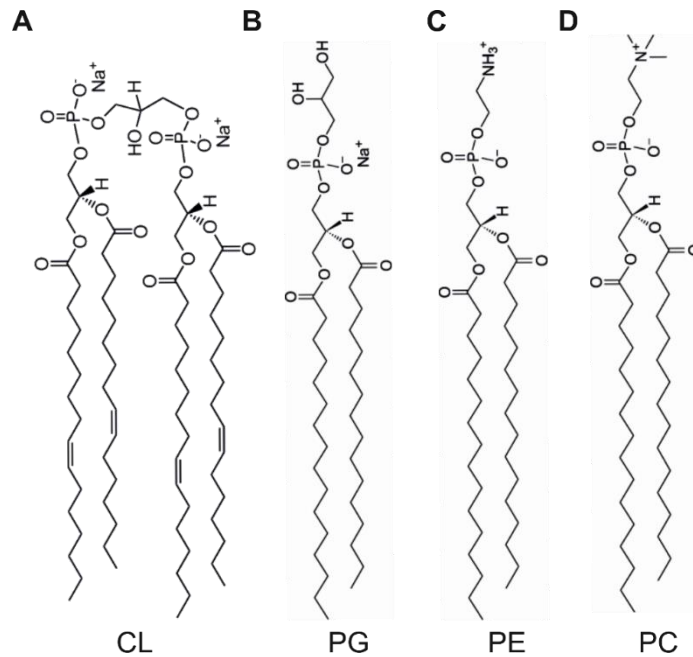
Figure 1-2: Schematic of lipids. A) Cardiolipin; B) phosphatidylglycerol; C) phosphatidylethanolamine and D) phosphatidylcholine. A, B, and C are the lipids commonly found in the OM while D (phosphatidylcholine) is commonly used in folding assays[71,72]. Shown is the dihexadecanoyl (16:0) form of PG, PE and PC, eg. DPPC, and the 16:1 form of cardiolipin. Chain lengths used in folding assays commonly vary from 10-16 carbons[71,72].

Intriguingly the exact mechanism for lipid transport to the OM is not yet clear[48,61]. Vital components have been identified, such as MsbA which flips lipid A (for LPS) and phospholipids across the inner membrane and Mla (maintenance of lipid asymmetry) proteins[53,73]. The Mla proteins were identified as functioning to move phospholipids away from the outer membrane, via retrograde transport to the inner membrane[53]. MlaA is an OM lipoprotein[53] which maintains the asymmetry between the inner and outer leaflets by cooperation with the porin OmpC, removing phospholipids that migrate into the outer leaflet (Figure 1-3)[74]. The asymmetry of the OM is critical to strong barrier function in Gram-negative cells[9,53,75]. In growth or stress conditions, phospholipids appear in the outer leaflet, and disrupt the LPS, leading to leaky patches. Proteins MlaF, E, D, B and C also function to return phospholipids from the OM to the IM. Recent evidence suggests these form a complex[76] and interaction with related MCE proteins allows transport of phospholipids across the periplasm (Figure 1-3)[61]. Whether the same pathway is used for initial transport from IM to OM is unclear.

6
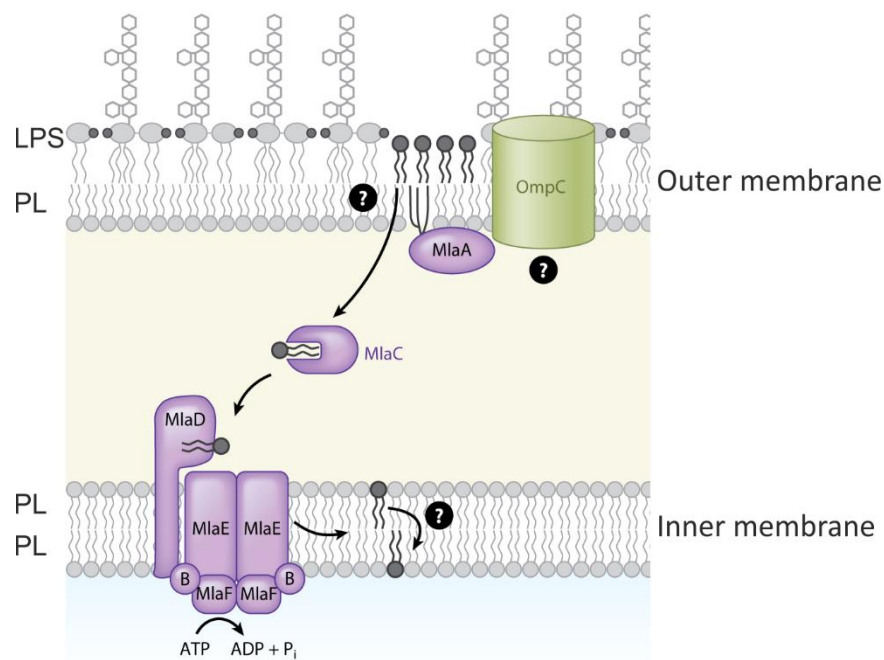
Figure 1-3: Model for the Mla lipid transport system. Schematic of the pathway by which lipids may be transported between the outer membrane (OM) and inner membrane (IM) with phospholipids (PL) and lipopolysaccharide (LPS) shown. Shown are the Mla proteins MlaF, E, D and B forming a complex in the IM, while MlaC is a soluble shuttle protein to the OmpC-MlaA complex in the OM. Figure reproduced from Henderson *et al.,* (2016)[48].

1.4 Lipopolysaccharide

Lipopolysaccharide (LPS) is a key constituent of the outer membrane in most species of Gram-negative bacteria. The LPS layer, stabilized by divalent cations, contributes to making the OM impermeable, particularly to hydrophobic molecules, which often include antibiotics[9,77]. Defects in the biosynthesis of LPS, for species that require it, leads to increased permeability of the OM and increased susceptibility to hydrophobic molecules[77,78]. The LPS of the outer membrane in *E.coli* has six fatty acyl chains, attached to a glucosamine dissacharide[79]; these are mostly 14:0 acyl chains (Figure 1-4). LPS presents another challenge for *E.coli*: how is this molecule assembled and presented on the outer surface of cells?

LptD was the first element identified of the LPS transport (Lpt) system (Figure 1-4)[25,55]. The gene was named *imp* for increased membrane permeability, a

common phenotype in its deletion[25,55,80]. The Imp protein was identified as an essential OM β-barrel and, despite evidence for Omp85 being important for lipid insertion[81], quickly became the candidate for an LPS transporter[82]. The *imp4213* allele was identified as increasing membrane permeability[83]. However these defects were partially corrected with mutations in only *bamB*[83]. As yet, the exact reason why BamB mutations may correct an LptD deficiency is unclear. Depletion of LptD and deletion strains in *N.meningitidis* where LPS is not required, helped to elucidate its role[82]. Deletion of *imp* in *N.meningitidis* causes production of less than 10% of wild-type levels of LPS, which never seem to reach the OM[62,82].

LptD is a 26 stranded β-barrel; the LptD/E complex displays unusual plug-and-barrel architecture[84] with LptE almost entirely inserted inside the β-barrel of LptD, and its protruding N-terminal forming the typical Lpt fold[85,86]. The Lpt complex requires coordination of the cell, as LptD is assembled by BAM while LptE is assembled by the Lol pathway[62,75,87,88]. There appears, however an internal checkpoint as without both components correctly folded, LptD will not adopt the correct structure to bind LptA and accept the LPS molecule[75,89]. LptD forms a crenelated β-barrel, with incomplete closure of its β1 and β26 strands and it is hypothesised that a putative lateral opening allows the translocation of LPS[90]. This would maintain the saccharide portion within the hydrophilic lumen, and lipid A at the hydrophobic interface[90,91].
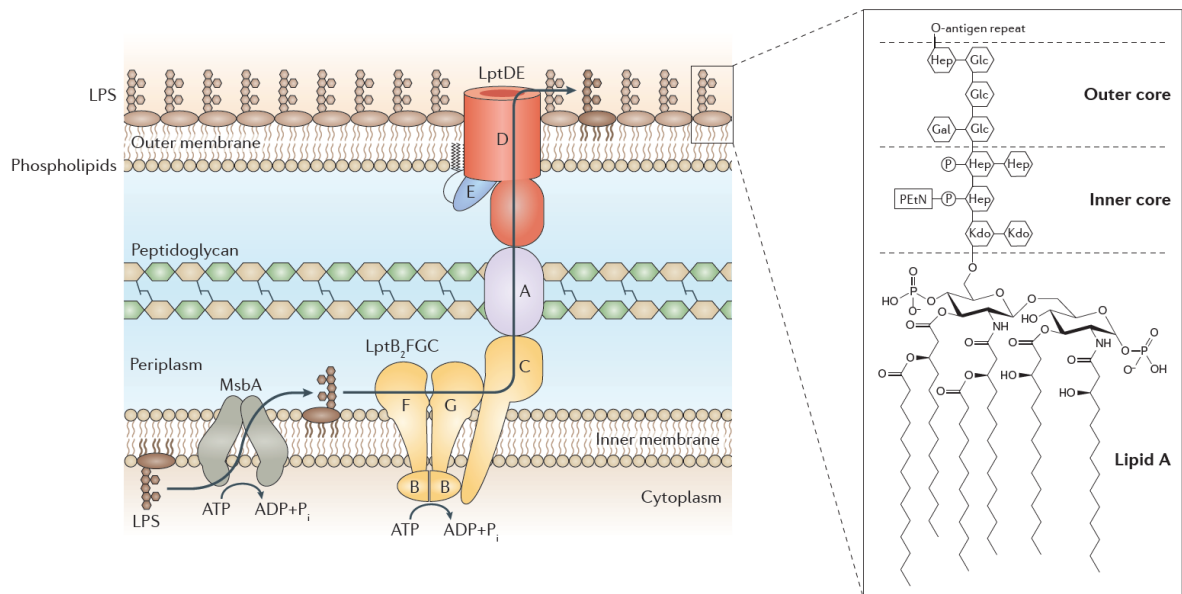
Figure 1-4: Lipopolysaccharide (LPS) transport pathway. Schematic of the transport of LPS from the inner leaflet of the cytoplasmic membrane to the outer leaflet of the OM, with all the relevant proteins. LPS is made up of lipid A, an O-antigen and a core oligosaccharide (inset). Lipid A is also known as endotoxin and is a key initiator of immune response[92]. The O-antigen repeats are synthesised in the cytoplasm and flipped across the inner membrane by an ABC (ATP-binding cassette) transporter[93]. On the periplasmic side these are polymerized and ligated to the lipid A core[93]. The lipid A core, synthesised on the inner leaflet of the IM, is flipped across the inner membrane by MsbA, an inner membrane protein of the ABC superfamily[94]. The Lpt (lipopolysaccharide transport) system is composed of seven essential proteins, in two subassemblies[51,95-97]. LPS is extracted from the IM by LptB$_2$FG, an IM ABC transporter[98], transferred to LptC[99], in one round of ATP hydrolysis before it is delivered on to LptA in a second round of ATP hydrolysis. LptA forms a periplasmic bridge, oligomerising in the presence of LPS and connecting the IM and OM[51,60,100,101]. Once reaching the OM, LptA delivers LPS to LptD and LptE, which form an insertase in the OM[84]. Figure reproduced from Okuda *et al.,* (2016)[52].

1.5 Protein transport to the OM

The initial transport pathway for lipoproteins and OMPs, as with the biogenesis of all proteins, begins the same (Figure 1-5). Proteins are synthesised on the ribosome, with an N-terminal signal sequence marking those to be secreted outside the cytoplasm[34]. For proteins destined for the inner membrane, the hydrophobic signal sequence is bound by the Signal Recognition protein (SRP) and these are co-translationally targeted to the Sec machinery to enable immediate integration into the IM following folding[102]. Periplasmic and OM proteins must be post-translationally transported to the SecYEG machinery, to be moved across the IM (Figure 1-5)[103]. However, the substrate recognition for this step has been rendered less clear by recent research[104,105]. The original

9

hypothesis was of substrate recognition by Trigger Factor, handover to SecB, then to SecA[106,107]. It now appears substrates are not exclusively intercepted by the periplasmic chaperones trigger factor (TF)[108] or SecB[109], but may be recognised by either the chaperones (TF and SecB), by SecA[104] or directly by SecY[105,110]. While it is unlikely that direct recognition by the SecYEG machinery is the preferred process for the pathway, mutants lacking SecB are viable[111,112]. SecA is the motor protein, an ATPase providing the energy source to thread the protein through the SecYEG translocon (Figure 1-6)[113]. SecYE and the motor protein SecA constitute the minimal translocase[114]. SecY forms the channel, with 10 transmembrane α-helices forming a hinge on one side and a lateral gate on the other[115]. This lateral opening allows IM proteins to be released into the membrane.
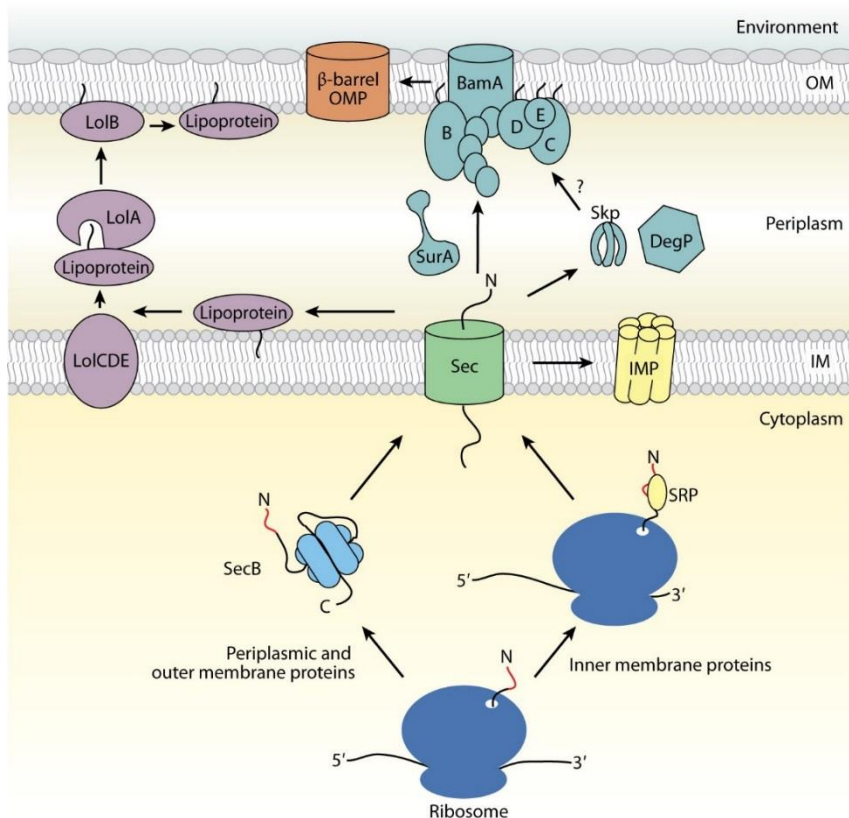
Figure 1-5: Schematic of protein biogenesis. Depicted are the pathways for Inner Membrane Proteins (IMPs), Outer Membrane Proteins (OMPs) and lipoproteins. All begin by synthesis in the cytoplasm and targeting to the Sec translocon. Figure reproduced from Hagan *et al.* (2011)[34].

There are several competing hypotheses as to the motion by which SecA drives protein through the SecYEG channel[116]. Currently favoured is the model of biased

Brownian motion[117] as depicted (Figure 1-6). This is a probabilistic model as it relies on free diffusion of polypeptide, whereas other models are processive or mixed[116]. Processive models typically require a significant conformational change in SecA on binding ATP, with a 'power stroke' that pushes substrate through SecYEG[118]. It is assumed SecA dimerization or oligomerisation is necessary to achieve this[119]. Mixed processive and probabilistic models allow for the diffusion as in the Brownian ratchet model shown, but suggest that the two helix finger of SecA pushes substrate through the channel[120,121]. This assumes a significant conformational change of the SecA two helix finger that has not yet been proven[116,122].
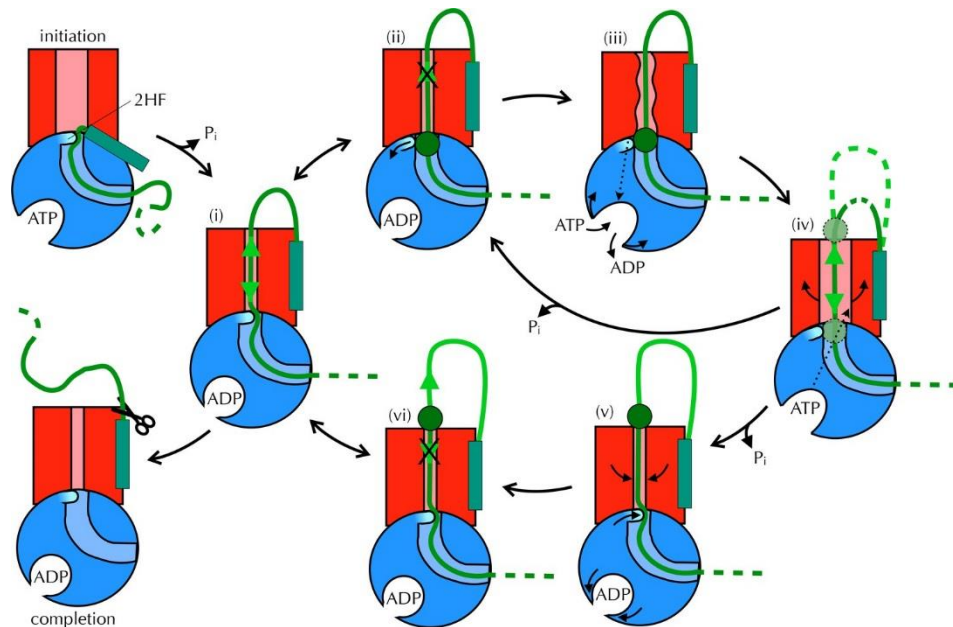
Figure 1-6: Model of SecYEG translocation by probabilistic Brownian ratchet mechanism. SecYEG (red, lateral gate in light red), is bound to SecA (blue, channel in light blue and 2-helix-finger in cyan) with substrate (green, signal sequence as turquoise rectangle) intercalated. In this model, the N-terminal signal sequence is a trigger to partially displace the plug and open the SecYEG channel, which is further opened by mature polypeptide and SecA[123]. There is free diffusion of the polypeptide through the channel until bulky amino acids (green circle), which cannot move freely through the channel, contact the two helix finger of SecA, located on the cytosolic side of the channel[117] (ii). ATP then binds SecA (iii), causing a conformational change of SecA propagated to SecYEG and fully opening the channel [117] (iv). Substrate diffuses through(iv), and ATP will hydrolyse to ADP, returning the channel to a partially open state[117] (v). Backsliding is prevented as bulky amino acids, once moved to the periplasm cannot diffuse back or trigger nucleotide exchange to open the channel (vi)[117]. Image reproduced from Allen *et al.*, (2016)[117].

11

1.5.1 Lipoprotein transport

Lipoproteins are synthesised as precursors with a signal peptide in the cytoplasm and translocated across the IM[87]. The signal peptides of lipoproteins possess a consensus lipobox sequence at the C-terminal region Leu- Leu-(Ala/Ser)-(Gly/Ala)-Cys[124]. This cysteine is modified by formation of a linkage between Cys and diacylglycerol in the IM by the enzyme Lgt[125]. The signal peptide can then be cleaved by LspA[126], and the free α-amino group acylated by enzyme Lnt[127], following which the Cys becomes the N-terminal residue of the mature lipoprotein. The amino acid following the N-terminal Cys determines the membrane specificity[128,129]. This is known as the "+2" rule[128,129], with typically an aspartate determining localisation in the inner membrane[130].

Lipoproteins that are destined for transport to the OM must first be recognised by the LolCDE complex in the IM (Figure 1-5)[131]. It is likely that an aspartate at position +2 interferes with this recognition, creating a Lol-avoidance system[132-134]. The LolCDE complex belongs to the ABC superfamily; LolC/E bind the lipoprotein in an ATP independent manner, and binding of ATP to LolD initiates a conformational change, decreasing affinity for the lipoprotein. ATP hydrolysis is required for handover to the periplasmic chaperone LolA[135], which is then able to form a water-soluble complex encapsulating the lipoprotein[136]. LolA traverses the periplasm and delivers the lipoprotein to LolB located in the OM[137], LolB possesses greater affinity for lipoproteins thus no energy is required in this step[138]. LolA and LolB both possess interior hydrophobic cavities important for transfer of lipoproteins[63] with likely similar cavities occurring in LolC and LolE.

Until recently it was assumed that lipoprotein biogenesis ended with LolB, with all known lipoproteins in *E.coli* facing the periplasm[19]. However more recently it appears this is not likely, and in addition to protein-buried (LptE[75]) or membrane-buried (CsgA[139], Wza[140]), some lipoproteins continue their biogenesis to become surface located[141,142]. This has been shown for BamC[143], as will be discussed in detail later (Section 1.7.2.2), and also Lpp[141], Pal[144] and YaiW[145]. While the majority of the pathway for lipoprotein transport is well characterised[87,142], this last step as yet remains unclear.

1.6 OMPs and their biogenesis pathways

1.6.1 Outer Membrane Proteins

Integral membrane proteins can adopt one of two characteristic structures: α-helical assemblies or β-barrels[146,147]. While α-helical membrane proteins are ubiquitous throughout eukaryotic and prokaryotic life, β-barrels are only found in the outer membranes of Gram-negative bacteria, mitochondria and chloroplasts[146,147], supporting the hypothesis of endosymbiotic origin of the latter two[26-29]. With the exception of Wza and MlaA, in the outer membrane of Gram-negative bacteria all proteins adopt a β-barrel structure[29,148]. As early as 2000 it was possible to define some of the construction rules essential to the OMP barrels[149]. These proteins possess an even number of β-strands[150] between 8-26, forming an antiparallel β-barrel[149] with N- and C-termini both in the periplasm. The β-strand tilt is around 45º, and the shear number, characterising residues of offset at closure of the β-barrel, is always positive and around n+2 for n strands[149]. The proteins display periplasmic turns and long external loops[149] and exhibit greater variability in the loops, and more conservation at transmembrane strands, with inward-pointing residues the most highly conserved[18]. Most importantly, most β-barrels have an internal hydrophilic surface, but a lipid-exposed exterior and consequently have a hydrophobic surrounding ribbon, approximately 27 Å thick[151] and two girdles of aromatic sidechains[149] (Figure 1-7).
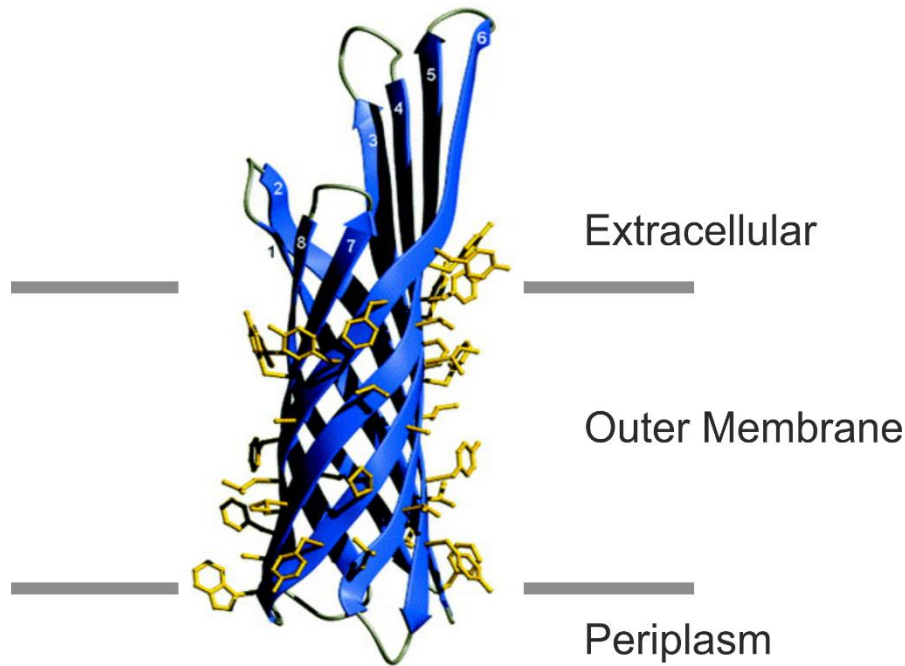
Figure 1-7: Hydrophobic girdle of OMPs. The structure of OmpX [PDB 1QJ8](152) is shown with yellow sticks depicting the residues of the aliphatic ribbon and aromatic girdle, with sidechains pointing into the membrane. The approximate position of the membrane is marked. Figure adapted from Shulz et al., (2000)(149).

OMPs are abundant in Gram-negative bacteria, constituting 2-3% of the genome[151] and making up ~50% of the mass of the OM[18]. Only two OMPs are known to be essential in *E.coli*, LptD and BamA[14]. Structurally important OMPs such as OmpA occur at ~100,000 copies/cell[18]. OMPs are hugely diverse, being 8-26 β-strands in size, taking monomeric, dimeric or trimeric forms[18] and fulfilling a huge variety of functions as enzymes[151], defensive layers[18], making up secretion apparatus[15], flagella and pili[16,17]. They can be loosely grouped by their function into six families, and one example of each in *E.coli* is shown (Figure 1-8): 1) structural proteins, such as OmpA, 2) defensins, such as OmpX, 3) porins, such as OmpF, 4) active transporters such as FhuA, 5) passive transporters such as FadL, and 6) enzymes, such as OmpT and OmpLA[18,19].
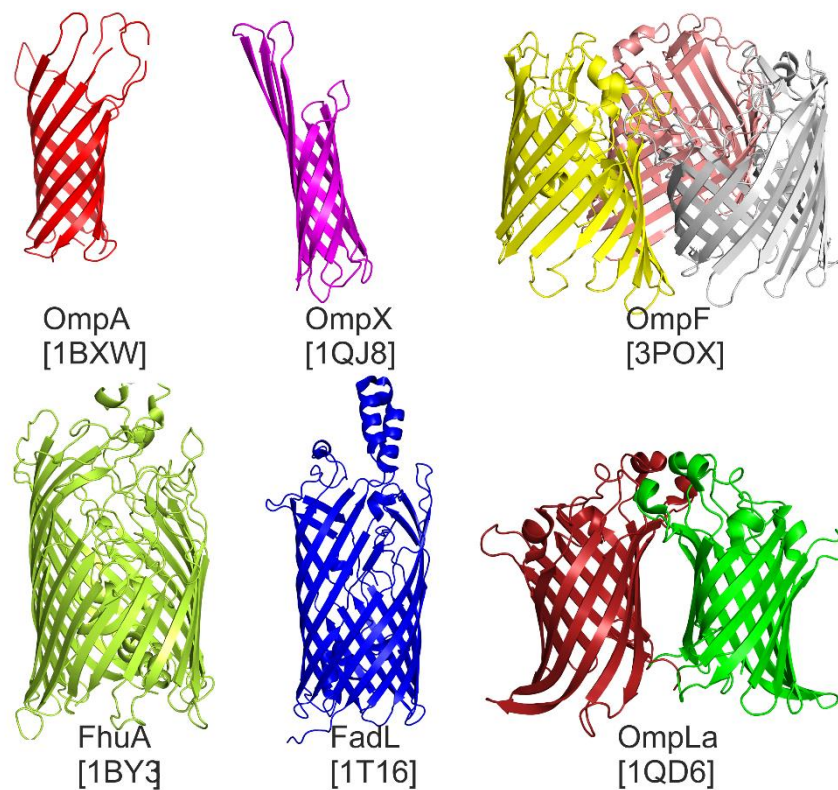
Figure 1-8: Gallery of OMPs. Shown is a representative example OMP from *E.coli* for each family of protein, showing the diversity of structures. 1) The transmembrane domain of OmpA [PDB 1BXW][153], a structural protein 2) OmpX [1QJ8][152], a defensin. 3) OmpF [3POX][154], a homotrimer and porin. 4) FhuA [1BY3][155], a siderophore transporter. 5) FadL [1T16][156], a transporter, and 6) OmpLA [1QD6][157], a phospholipase and dimer. Structures were analysed in Pymol[158] and are not shown to scale.

The long journey of OMPs from the ribosome to the OM in Gram-negative bacteria is only accomplished by the concerted action of many different proteins (Figure 1-5)[14,19,159,160]. Following translocation through the Sec machinery, the N-terminal signal is cleaved by Signal Peptidase I[159]. Periplasmic chaperones allow unfolded OMPs to navigate the periplasm and reach the outer membrane, and the BAM complex without misfolding, aggregation or unfolded protein stress response. The BAM complex fulfils the final step of OMP assembly into the OM. There are numerous questions surrounding this pathway, of which the essential players are known, but their mechanism remains unclear.

1.6.2 Chaperones involved in OMP folding

There are multiple periplasmic chaperones[160]: Spy, Skp, DegP, SurA, FkpA, PpiA, and PpiD of which the latter four have peptidyl-prolyl isomerase (PPIase) activity[19]. Three are important in the correct transport of OMPs: SurA, Skp and DegP (Figure 1-5 and Figure 1-9). Despite initial hypotheses that Skp and SurA may act sequentially[19,161] they appear to operate in partially redundant, overlapping pathways[162]. There is strong evidence against these acting sequentially as, unlike BamA, SurA is not able to release a Skp-bound OMP[163], making it likely that both chaperones deliver OMPs to the BAM complex. Skp and DegP are hypothesised to function in the same pathway, as deletion of either of these is tolerated in *E.coli* but lethal when combined with mutation of SurA[164]. In addition SurA is thought to be the principal pathway for folding OMPs in the periplasm[162]. Fascinatingly, data from single-molecule force spectroscopy experiments on FhuA demonstrated the different roles of Skp and SurA[165]. In these experiments, while Skp was able to prevent misfolding of FhuA, it increased the proportion of unfolded protein, while SurA was able to facilitate folding and increase the fraction of correctly folded protein, outlining the different roles these chaperones may play in OMP biogenesis.
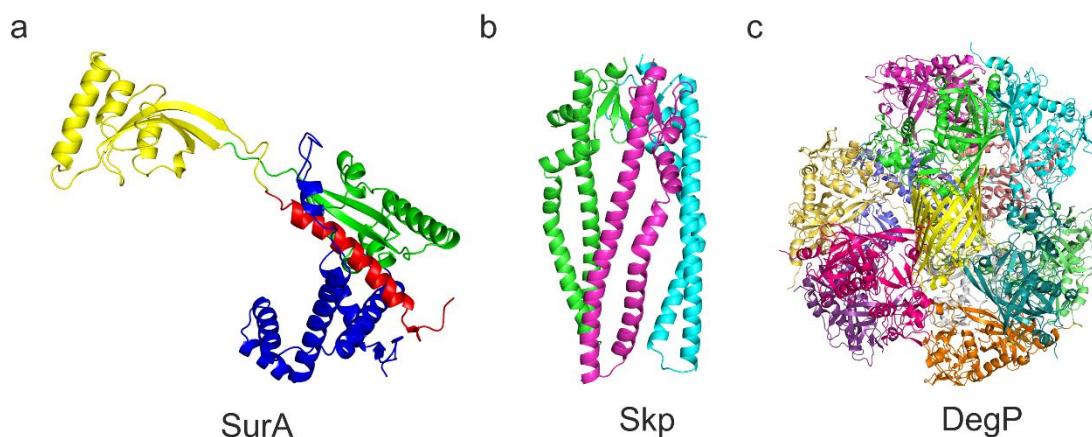
Figure 1-9: Structures of three major periplasmic chaperones. Crystal structure of SurA [PDB 1MY][166] with missing residues modelled in. The domains are coloured individually: N-terminal domain (blue), P1 (green), P2 (yellow), C-terminal domain (red). b) Crystal structure of Skp [PDB 1U2M][167] shown as a trimer, with each monomer chain coloured separately. Missing residues in chain B and C were modelled in from chain A. c) DegP [PDB 2ZLE][168] 12-mer from a cryo-EM reconstruction with a folded 16-strand porin (yellow) in the centre. Structures are not shown to scale relative to one another.

1.6.2.1 SurA

SurA is a conserved periplasmic chaperone, vital to the assembly of OMPs[169,170]. SurA possesses four domains: two parvulin-like peptide prolyl isomerase domains (P1 and P2) and N- and C-termini domains (Figure 1-9a)[166]. The PPIase activity is only found in P1, however, PPIase activity appears unnecessary for OMP chaperoning[171,172].

SurA is likely to be the principal chaperone responsible for delivery of OMPs across the periplasm, as its depletion causes severe reduction in density of the OM and slower kinetics of folding of LamB while a *skp/degP* double deletion has a less severe effect[162]. Additionally, chemical cross-linking between SurA and BamA was shown *in vivo*, with the lipoprotein BamB also able to pull-down SurA and BamA whereas other chaperones were not observed[162]. In addition, SurA has been shown to preferentially bind a distinct aromatic repeating sequence of peptide (Ar-X-Ar)[173]. This is highly similar to the "β-signal" of OMPs, with a typical $Gxx\Phi x\Phi$ motif at the C-terminus, where ϕ represents hydrophobic residues[174,175]. Therefore, while Skp/DegP are clearly important in OMP folding, and their deletion causes defects[164,176] SurA likely operates a principal pathway in OMP folding and assembly.

1.6.2.2 Skp

The seventeen-kilodalton protein (Skp) was first identified by its ability to bind unfolded OmpF by affinity chromatography[177]. Skp has broad substrate specificity, binding over 30 different proteins[178] and binds OMP substrates with low-nanomolar affinity[179]. The *skp* gene is immediately downstream of BamA[24] and regulated by the σ^E regulon.

Skp has a jellyfish-like architecture with three extended, flexible arms, held together by coordination of a 9 stranded β-barrel domain (Figure 1-9b)[167]. The tips of the protein are rich in positively charged residues, while the interior contains hydrophobic patches[167]. OMPs form interactions with Skp with nanomolar affinity, as measured by tryptophan fluorescence[179] and FRET experiments[180]. The interaction with OMPs is principally by charged residues, as above pH 11, or below pH 5, Skp and OMPs are unable to bind[179]. Consistent with this, increasing NaCl concentration from 0 to 1 molar caused a decrease in

affinity of Skp for OmpA of approximately four-fold[179]. Nuclear magnetic resonance (NMR) data demonstrate that Skp-OMPs form multiple weak, transient interactions, consistent with these mainly being electrostatic effects and with Skp providing a holding cage for unfolded OMP substrates[181]. Interestingly, Skp binds BamA with higher affinity than other OMPs (0.3 nM Kd for BamA as opposed to 12- 50 nM for other OMPs measured)[179], this may reflect necessary tighter binding in the handover of substrate OMPs.

It has been demonstrated that Skp may bind unfolded OMPs and forms a 3:1 complex, aiding identification of functional Skp as a trimer[182]. Studies have been carried out with OmpA and for this it has been demonstrated that the presence of Skp or LPS slows OMP folding into preformed lipid bilayers, but both together accelerates folding[179]. LPS binding sites were identified on the Skp monomer[167] and it was assumed that the three together form a complex[183], particularly as the presence of LPS renders a Skp-OMP complex more accessible to tryptophan quenching. However, NMR studies demonstrated LPS likely carries out a non-specific denaturing effect on Skp[184], thus explaining the apparent accelerated folding. While tryptophan fluorescence data indicate a 1:1 stoichiometry of Skp trimer to OMP substrate for OMPs of all sizes[183], later kinetic and native ESI-MS data demonstrated that a higher ratio of Skp: OMP may be necessary to sequester larger substrates[163]. The cavity within Skp could likely only accommodate a 25 kDa folded protein[167], while many OMP substrates will exceed this apparent size limit. Additionally molecular dynamics simulations demonstrate how Skp may coordinate to bind and enclose larger unfolded OMPs, creating a strong resemblance to eukaryotic chaperone prefoldin[163]. Dynamics of the helical tentacles of Skp oligomers increase the cavity size for binding larger OMPs[163].

1.6.2.3 DegP

The DegP monomer has three domains: a protease domain and two C-terminal PDZ domains for substrate binding[160]. DegP possesses protease and chaperone activities[185], and while originally thought to switch in a temperature-dependent manner, it now appears that its natural, hexamer state blocks exposure of protease sites[186] (Figure 1-9c). Deletion of *degP* alone shows a temperature-sensitive phenotype, while *E.coli* containing mutations of both *degP* and *surA* are only able to grow below 23ºC (164). Double mutants of *degP* and *surA* show a

synthetic phenotype, with reduction of envelope protein levels, but no considerable cell morphological changes, unlike that seen for *skp*/*surA* mutants[164]. DegP fulfils a crucial role as a protease[164,176]. In the presence of DegP with full protease function, the *skp*/*surA* double mutant is bacteriostatic, but when DegP is mutated to have no protease function this is bactericidal[164]. This is likely due to the toxic, high accumulation of unfolded OMPs in the absence of DegP protease function, as seen in *degP* deletion strains[164].

1.7 The BAM complex

The BAM complex in *E.coli* is a five protein complex, composed of BamA and four associated lipoproteins (BamB-E). While BamA and BamD are the only essential components of the complex[21,25,187,188], the depletion of the associated lipoproteins decreases the BAM complex catalytic activity[189] and may lead to impairment of OMP folding or membrane impermeability[21,25,176,187,190]. BamB, BamC and BamD are all expressed on the same σ^E regulon, a regulon also important for response to cell stress[187].

1.7.1 BamA

1.7.1.1 Discovery and Evolution of BamA

BamA is part of the Omp85 protein family[22]. The protein family was first identified as a D15 surface antigen, as a target of antibodies for patients infected with *H.influenza*[191]. However, the first thorough identification of the protein family came from cyanobacteria, as these bacteria contain a structural homolog of the chloroplastic protein, Toc75, in the outer membrane[22]. Identified in the cyanobacteria family *Synechocystis* and referred to as SynToc75, the sequence of this protein was used to search databases, and revealed that a member of this protein family was present in all Gram-negative bacteria genomes known at the time[22]. An Omp85 homologue has since been identified in all bacteria with an OM for which genomes are available[26]. A clear relationship is evident between Omp85 proteins, even those with low sequence homology, as all possess similar size, a proven or predicted outer membrane localization, a cleavable N-terminal signal sequence and a predicted β-strand secondary structure[22]. In addition, the

compared proteins showed areas of high sequence identity, and a highly conserved C-terminal motif[22].

The difficulty in deleting the Omp85 gene, in *Synechocystis, Haeomophilus ducreyi* and *E.coli* demonstrated that the protein is essential[22,25,192]. The conserved Omp85 family at this point had unknown function, but was a strong candidate as part of the OMP insertion machinery, for which no components were yet identified[21]. Studies using a depletion strain for Omp85 in *N.meningitidis* provided further evidence that Omp85 protein expression is essential for growth and viability[21]. It was anticipated that if Omp85 is involved in OMP insertion, then its depletion would decrease levels of OMPs detected. Intriguingly, while OMP expression levels in *N.meningitidis* did not appear to be significantly affected in the Omp85-depletion strain, PorA and B accumulated as monomers, rather than the correctly folded trimers[21,193]. The proteins also showed increased sensitivity to trypsin and extractability from the membrane[21]. Therefore, the proteins were not correctly folded into the OM. Later studies, using an Omp85-depletion strain in *E.coli* showed impaired growth, and similarly caused a decrease in the amount of folded OmpA and LamB and an increase in the unfolded OmpA and LamB detected over time[25]. In addition, immunofluorescence using antibodies directed at different OMPs demonstrated weaker labelling in the absence of Omp85, while protein expression remained constant, implying less OM localisation[21]. As opposed to the wild-type homogenous coverage of labelling, Omp85-deficient cells were irregularly labelled, with labelling absent at the cell division septa[21]. These studies, combined with the high homology to Toc75 in chloroplasts, provided strong evidence that the Omp85 protein family is involved in correct assembly and folding of OMPs.

1.7.1.2 Structure of BamA

E.coli BamA is comprised of a C-terminal β-barrel in the OM and five N-terminal polypeptide transport associated (POTRA) domains. Due to its intractability as a membrane protein, the structure of BamA was not solved until 2013[194], two years after the associated lipoproteins[195]. However, models of its structure were possible from general understanding of β-barrels and the rules that define them[149] and the structure of the loosely related FhaC[196].

Structures of the BamA β-barrel from *Haemophilus ducreyi* (*Hd*) and *Neisseria gonorrhoeae* (*Ng*) were solved in 2013, with two and five of their five POTRAs respectively[194]. Shortly after the *Escherichia coli* (*Ec*) BamA structure was solved containing the β-barrel and POTRA5 (Figure 1-10c)[11]. These structural studies confirmed the suspected architecture of the Omp85 family, in addition to fulfilling expected properties for an OMP β-barrel, with a 16 stranded β-barrel. Several interesting differences between the structures were noted: firstly there was considerable dynamics of the POTRA domains, with the POTRA domains of *Ng*BamA occluding access to the barrel[194], while the *Hd*BamA POTRAs did not, and the *Ec*BamA POTRA5 structure appears to adopt a conformation intermediate between the two[11]. Further, while the *Hd*BamA structure (Figure 1-10a) adopted the anticipated closed β-barrel, with eight H-bonds between the first and last β-strands, the *Ng*BamA structure formed only two H-bonds, with the C-terminal strand tucked inside the barrel (Figure 1-10b)[194]. The *Ec*BamA structure also showed weakly associating β1 and β16 β-strands (Figure 1-10c).
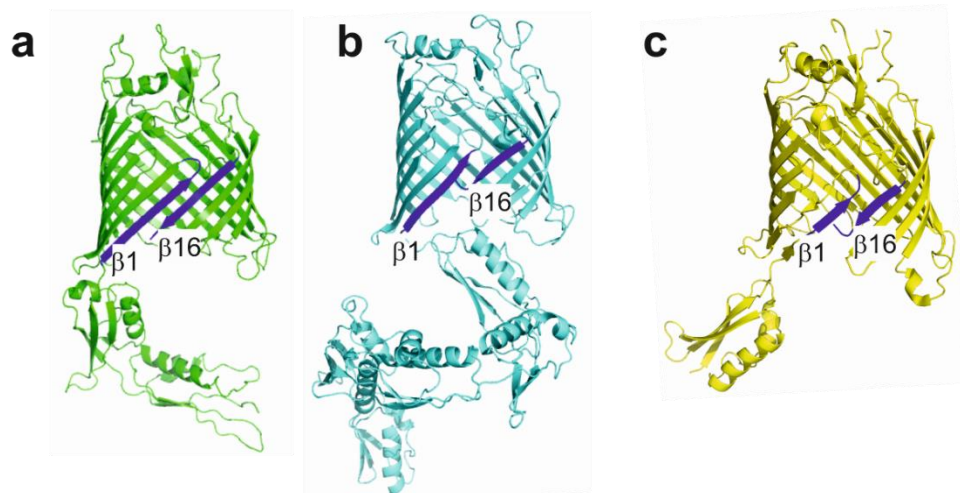
Figure 1-10: Crystal structures of BamA from three Gram-negative species. The first (β1) and last (β16) strand of each structure is highlighted in dark blue. a) The crystal structure of *H. ducreyi* BamA (construct contains POTRA4 and POTRA5) [4K3C][194] shows a close association between β-strands 1 and 16, forming eight hydrogen bonds. b) Conversely *N. gonorhoeae* BamA [4K3B][194] displays a weak interaction between β-strands 1 and 16, forming only 2 hydrogen bonds, and with a disordered C-terminus of β16 tucked inside the barrel[194]. c) *E.coli* BamA (construct contains only POTRA5) [4C4V][11] also shows a weak interaction between β-strands 1 and 16, also with only 2 hydrogen bonds, and with a disordered C-terminus.

Prior to solving the BamA structures, the most closely related structure was that of the two-partner secretion protein FhaC. This is an Omp85 family protein, but functioning as a toxin translocation pore[196] (Figure 1-11b). Comparison of the BamA structures, however, reveals several similarities to the crystal structure of Omp85 protein TamA, which also has an incompletely closed β-barrel[197] (Figure 1-11a).

For FhaC, substrates are hypothesised to thread through the lumen of the barrel[196]. The extensive contact of the β1 and β16 strands[196] (Figure 1-11b) renders lateral opening between the strands unlikely. In addition no lateral opening propensity was observed by molecular dynamics simulations unlike *Ng*BamA and *Ec*BamA (discussed further in Section 1.10.4)[194,198,199].
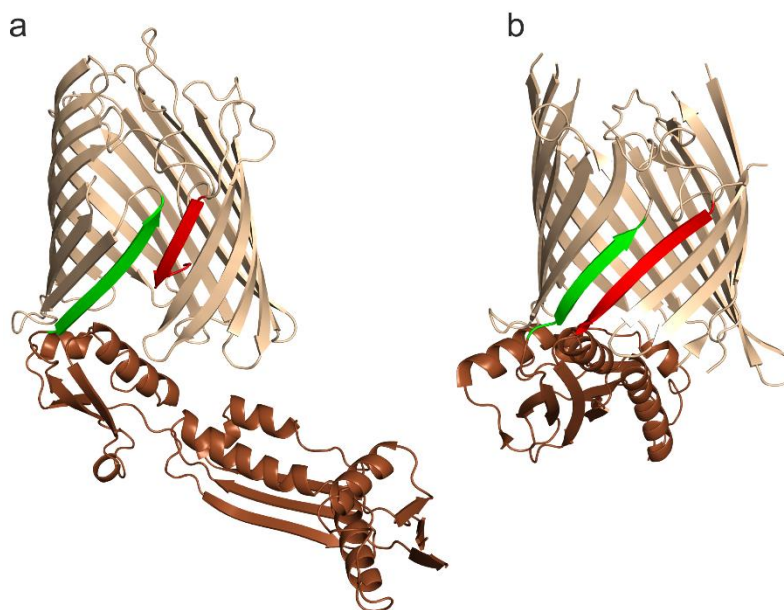
Figure 1-11: Crystal structures of a) TamA and b) FhaC highlighting differences in β-barrel closure. Structures are shown with the barrel in wheat, the periplasmic domains in brown, β1 in green and β16 in red. a) The structure of TamA [PDB 4C00][197] from *E.coli* demonstrates incomplete closure of β1 and β16 in the β-barrel, with an inward kink of β16 (red). b) The structure of FhaC [4QKY][200] from *B.pertussis* shows a more extensive interaction of β1 (green) and β16 (red) β-strands.

The structure of the majority of the periplasmic portion of BamA, the POTRA domains, was solved in *E.*coli before solution of the β-barrel structure (Figure

1-12a)[11,201]. The POTRAs structure revealed a dimer formed by a β-strand interaction between strand 2 of POTRA3 and the first residues of POTRA5[201] (Figure 1-12b). Although possibly a crystal artefact, it demonstrates a means of interaction between polypeptides and POTRA domains of β-augmentation[202]. In addition, the second structure solved for POTRA domains 1-4 showed a similar β-augmentation of POTRA3, but with the additional β-strand binding in an opposite orientation (Figure 1-12c)[203]. This supports a role for POTRA domains in assisting OMP assembly in a way that is blind to the sequence of the polypeptide chain[201].
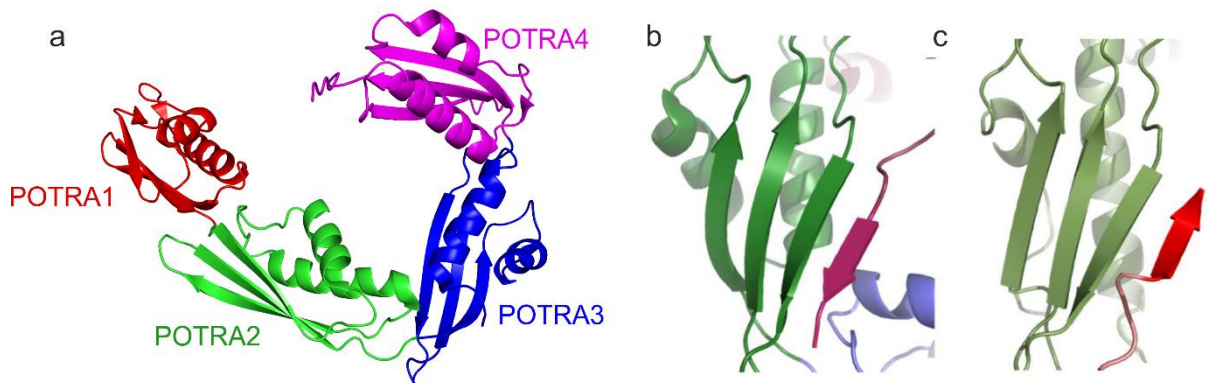
Figure 1-12: Crystal structure of *E.coli* POTRA domains and β-augmentation to POTRA3. POTRA domains 1-4 [PDB 2QDF][201], coloured red to pink. Despite possessing low sequence similarity all POTRA domains show the same structural folds. Each POTRA domain is made up of a three-stranded β-sheet and a pair of α-helices. b) β-augmentation of the β-sheet of POTRA3 with a β-strand from the N-terminus of POTRA5 in a parallel orientation(pink), from Kim *et al.*, (2007)[201]. c) β-augmentation of β-sheet of POTRA3 with a β-strand from POTRA5 (residues 345-349) in an antiparallel orientation (red). b and c) are adapted from Gatzeva-Topolova *et al.*, (2008)[203].

Studies deleting each POTRA domain individually demonstrate that these variants are all expressed, targeted correctly to the outer membrane and folded, as assessed by heat modifiability[201]. Additionally, any of the first four POTRA domains can be deleted and still maintain interactions of BamA with BamD, BamC and BamE[201]. This provided strong evidence that the periplasmic POTRA5 domain scaffolds the other four proteins.

The POTRA domains have been shown to be highly dynamic, with a potential hinge between POTRA2 and POTRA3[204,205]. This dynamic nature may be mediated by binding to BamB[204,205], binding to the membrane[206] or

conformational changes of the BamA barrel[31,207-210]. Analysis of the structures of the BAM complex[207-210] demonstrates how the dynamic nature of the POTRA domains may be mediated by lipoproteins and the BamA β-barrel and integral to the overall conformational change of BAM in substrate interaction. This is discussed in detail in Chapter 3 (Section 3.3) with analysis of the cryo-EM structure.

Studies of deletion mutants of POTRA domains *in vivo*, with and without BamA present, show that deletion of the POTRA domains further from the barrel (P1 and P2) is less damaging than deletion of those closer (P3 and P4)[201]. Deletion of P5 creates a BamA toxic to cells, likely due to mishandling β-barrel substrates[201]. Furthermore, in contrast to previous evidence of the BAM complex functioning as an oligomer[211], these studies showed it behaving as a monomer. Mobility on Blue-Native PAGE was less than 230 kDa and whereas lipoproteins were immunoprecipitated by the POTRA domain deletion mutants, BamA was not, demonstrating that oligomerisation is not occurring through BamA[201].

1.7.2 Lipoproteins of the *E.coli* BAM complex

1.7.2.1 BamB

BamB is a 42 kDa, 8- bladed β-propeller, belonging to the WD40 superfamily[195]. It is found in all α-, β- and γ- proteobacteria[195]. It possesses a ring-link structure, with closure of the propeller ring controlled by antiparallel pairing of the most N- and C-terminal β-strands[195] (Figure 1-13).

The interaction between BamA and BamB was identified as direct, occurring in a conserved region of BamB, between residues P171 to P181[190]. Specifically, mutagenesis of L173, L175 or R176 causes defects and reduces the ability of BamB to immunoprecitate BamA[190]. Disrupting the BamA-BamB interaction causes a phenotype similar to BamB deletion, suggesting that the interaction of BamB with BamA is necessary for BamB function[190]. Deletion mutants of *yfgL* (BamB) showed increased sensitivity to antibiotics and SDS, demonstrating increased OM permeability[187]. The same mutant showed a 10-fold increase in σ^E activity and reduced OMP profile[187]. A separate conserved region (V319-H328) was also shown to be needed for correct folding of BamB, but not its function[190].

The OMPs most affected by BamB deletion are larger (18-26 strands), suggesting that BamB provides additional surface area to aid folding of larger substrates[187,212-214]. In addition, BamB and SurA deletion mutants are indistinguishable[215] and the simultaneous deletion of BamB and SurA or BamB and DegP is a synthetic lethal combination[187] lending more evidence to these proteins playing overlapping, redundant roles. This also provides further evidence for BamB interacting early in the process of OMP folding. There exists a theory that SurA may deliver OMPs to BamA via BamB[215] however this is unlikely as mutants of BamB which pull down less BamA pull down equivalently less SurA[190]. Thus, it is more likely that the interaction of BamB-SurA is mediated by BamA[190]. The crystal structure of the full BAM complex confirmed the interaction between BamB and BamA POTRA2 and POTRA3 (Figure 1-17)[208] and demonstrated that the presence of BamB may link to the structural rearrangements of POTRAs in BamA dynamics[208,210], discussed in Chapter 3 (Section 3.3). Furthermore, recent studies displaying OMPs in assembly "precincts", or concentrated clusters on the cell surface have proven that BamB is required for the oligomerisation of BAM complexes[216]. It was determined that the interacting residues of BamB could be crosslinked *in situ* and also that deletion of the BamB gene, while not impacting cell growth, caused loss of assembly precincts containing the BAM complex[216]. This supports a crucial role for BamB that has not yet been determined.
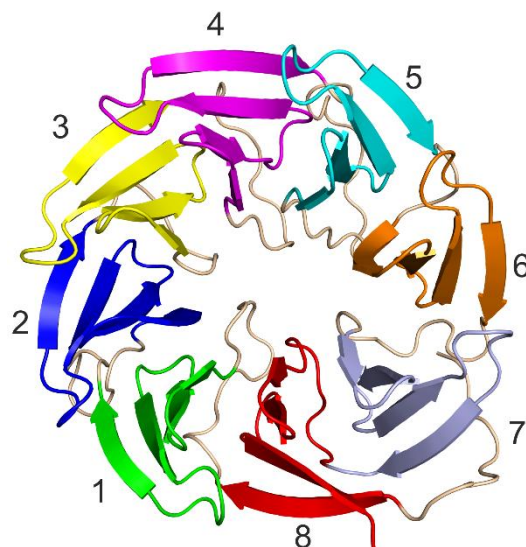
Figure 1-13: Crystal structure of BamB from *E.coli*. BamB forms an eight-bladed β-propeller with four β-strands in each blade, coloured individually and numbered 1-8. Image created with Pymol (PDB: 2YH3)[195].

1.7.2.2 BamC

BamC possesses an N-terminal segment with no regular secondary structure, ~70 amino acids in length and two independently folded helix-grip domains (Figure 1-14)[195]. Despite low sequence identity, the helix-grip domains form structurally similar folds with five antiparallel β-sheets and two α-helices[195]. The unstructured N-terminal domain is the most highly conserved region[212], and is important for interaction with BamD and BamE (Figure 1-14)[217]. Immunofluorescence demonstrated that segments of BamC are surface exposed and while the unstructured N-terminal region is in the periplasm and interacts with BamD, the helix-grip domains are likely located on the *E.coli* surface[143]. Analysis of γ-proteobacteria sequences demonstrate that there are three regions in the unstructured N-terminus of BamC which are highly conserved. The first is essential for binding BamD (residues 26-42), the second (residues 48-68) extends this interaction, while the third (residues 74-102) appears between the BamD binding segment and the two structural domains (Figure 1-14)[143]. As this third motif appears highly hydrophobic it is likely that this segment traverses the membrane, and has evolved with a sequence capable of doing so[143].

Crystal structures of the BAM complex confirmed the high flexibility of segments of BamC, with reduced electron density observed for the C-terminal domain in some cases[207] and seen interacting with BamD and POTRA 2 in others[208]. This is evidently in contrast to the suggestion of BamC being surface exposed[143], and may be due to the conditions imposed by crystallization and the detergent micelle.

The exact physiological role of BamC is unknown but it may be involved in the response to antibiotics[215]. Deletion mutants of nlpB (BamC) show increased sensitivity to the amphipathic antibiotic rifampicin, and are synthetic lethal with deletion of SurA[187]. In addition, other lipoproteins displayed an increased protease sensitivity in a BamC deletion strain[143]. Also, as previously discussed, the N-terminal 70 amino acids of BamC bind BamD[217], but the pocket of BamD observed to bind, between TPR domains 1 and 2 (Figure 1-14, green and pale blue), is also that proposed to bind the OMP targeting signal[217]. This suggests a role for BamC in regulating OMP access to BamD[190,217,218], but the functional role of these domains in OMP biogenesis remains unclear.
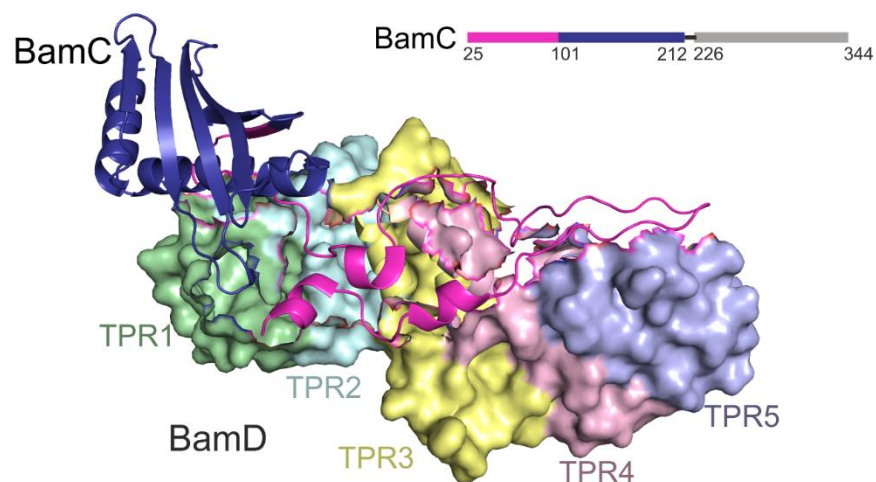
Figure 1-14: Crystal structure of BamCD subcomplex and (inset) schematic of BamC domain organisation. The crystal structure is shown with BamC in cartoon, with N-terminal domain in magenta, and the first structured domain in purple. The schematic follows the same colouring, with the C-terminal structured domain in grey, and residue numbers indicated. BamD is in a surface representation with its TPR domains individually coloured. The unstructured N-terminal domain of BamC forms a lasso structure interacting with BamD. Image created in Pymol [PDB: 3TGO][217].

1.7.2.3 BamD

BamD is entirely α-helical, composed of five tetra-tricopeptide repeat (TPR) domains[195] (Figure 1-15), which are typical for protein-protein interactions[219]. BamD is the only essential lipoprotein of the BAM complex[187].

BamD binds BamA via POTRAs 1, 2 and 5[201,208] and provides a platform on which BamC and BamE dock, confirmed in structures of the full BAM complex[208] (Figure 1-17). In addition, molecular dynamics simulations demonstrate that removal of BamD may significantly increase the dynamics of the POTRA domains[208]. The interaction between BamA and BamD is highly significant, with mutations in this interface causing low cell growth or cell death[208].

The first three TPR domains of BamD form a structural scaffold open to protein binding (Figure 1-15)[195]. In the original crystal structure, the C-terminus of the next BamD protein was found to bind within this scaffold[195], while the BamCD crystal structure revealed the unstructured N-terminal 70 amino acids of BamC binding in the same region[217] (Figure 1-14). However, the substrate groove was shown to be of appropriate dimensions for binding the conserved C-terminal six amino acids of OMPs[195]. Peptides containing typical residues conserved in this sequence could be docked to TPR1-3[195]. The role for BamD in substrate recognition and assembly is supported by further recent evidence[175,220]. The β14 strand of BamA, which contains the conserved OMP β-signal sequence, is necessary and sufficient for binding of BamA, as a substrate, to BamD[175]. In addition, trapping an incomplete folding intermediate of LptD showed interactions between BamD and LptE, normally located within the LptD barrel[220]. It is likely, therefore, that a transient periplasmic interaction with BamA and BamD facilitates OMP assembly.
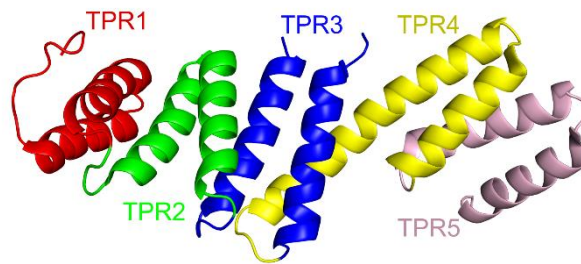
Figure 1-15: Crystal structure of BamD. TPR domains (1-5) are highlighted red-pink. TPRs1-3 are thought to form key binding sites to bind substrate proteins or BamC. Image created in Pymol (PDB: 3Q5M)[221].

1.7.2.4 BamE

BamE is the smallest, most recently discovered of the four lipoproteins of BAM[176], and non-essential, with its deletion causing no growth defects, but increased membrane permeability[176,222]. While a BamE deletion strain shows only slight deficiency in folding OMPs[176] the combination with a BamC deletion, or BamD mutant renders the cell severely defective in OMP biogenesis, while combination with BamB is synthetically lethal[176]. Additionally, the stability of the complex is shown to be compromised in its absence[176]. BamE specifically binds phosphatidylglycerol (PG), in a site near its BamD binding site[223] and was therefore hypothesised to bring the complex to sites of high concentration of PG, thus assisting OMP folding[182]. Structures of the BAM complex, however, demonstrate this binding site to remain far from the position of the membrane[207]. In BamE the N-terminal acylation site is followed by a short unstructured linker. The rest forms a structural ααββ topology fold[223] (Figure 1-16).

29
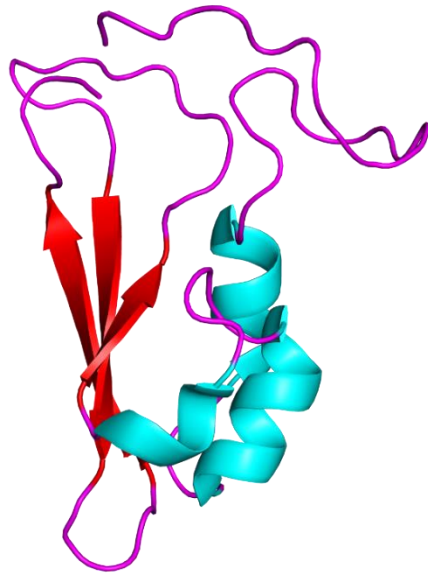
Figure 1-16: NMR structure of BamE. The BamE ααβββ topology is shown with β-strands in red and α-helices in cyan. PDB: 2KXX[224].

BamE has been shown to exist in both monomer and dimer forms[195,223,224]. The first crystal structure of BamE showed a hexameric protein complex with three intercalating dimers and a significant interface between monomers[195]. Small additional interfaces between non-conserved regions of BamE lead to hexamerization[195]. The formation of oligomeric species up to hexamer was evidenced by SEC and cross-linking, and extraction of native BamE from natural membranes with detergent demonstrated the presence of a higher molecular weight complex, suggesting that some oligomer formation occurs naturally[195]. There is evidence for the dimeric BamE being the active form due to its structural homology to β-lactamase inhibitor proteins[195] which typically operate as a tandem fold the size of dimeric BamE[225]. However, it has been demonstrated that BamE in the periplasm is principally monomeric and it may be misfolded localisation in the cytoplasm that leads to its dimerisation[223].

1.7.3   Structure of the BAM complex

Despite crystal structures of all the individual components, until 2016 there was no structure of the full BAM complex and there were unconfirmed hypotheses of how the complex may fit together[226,227]. This was well-informed, however, by several subcomplex structures, including BamCD[217], BamAB[204,228], BamAD[226] and cross-linking and pull-down studies, demonstrating which regions of each

protein are significant for interactions[25,190,201,217,223]. The first crystal structure of the BamACDE complex[207] therefore confirmed many of the suspected interfaces between proteins but also gave unique insight into the architecture of the complex. While the general conformation of the complex was oriented as anticipated, the arrangement of POTRAs and lipoproteins was more compact than hypothesised, forming a closely-associated ring at the periplasmic side of BamA (Figure 1-17). The BamD TPR motifs lie nearly parallel with the membrane and with a significant interface with the POTRA domains (buried surface area > 1100 $Å^2$), forming a large potential interaction surface for substrates[207] (Figure 1-17).

The first solved crystal structures came with a surprise, however, not in arrangement of the subunits, but in the conformation of BamA. This had previously been hypothesised as moving between the lateral closed structure observed in crystal structures of BamA alone[11] and the lateral open structure such as observed in *Neisseria gonorrhoeae* BamA[194]. The crystal structures confirmed this, showing the β-barrel of BamA to adopt one of two profoundly distinct states. The first is an "inwardly open" conformation in which the BamA β-barrel is sealed on its extracellular face and between the first (β1) and last (β16) β-strands, and open to the periplasm (Figure 1-17a). A second conformation has been observed (Figure 1-17b) in which the BamA β-barrel has undergone a large conformational rearrangement. The barrel becomes distorted by the rotation of the first six β-strands and displacement of three loops on the extracellular face. This creates the "lateral open" conformation, in which the BamA β-barrel is open to the outer leaflet of the OM and the extracellular space (Figure 1-17b).
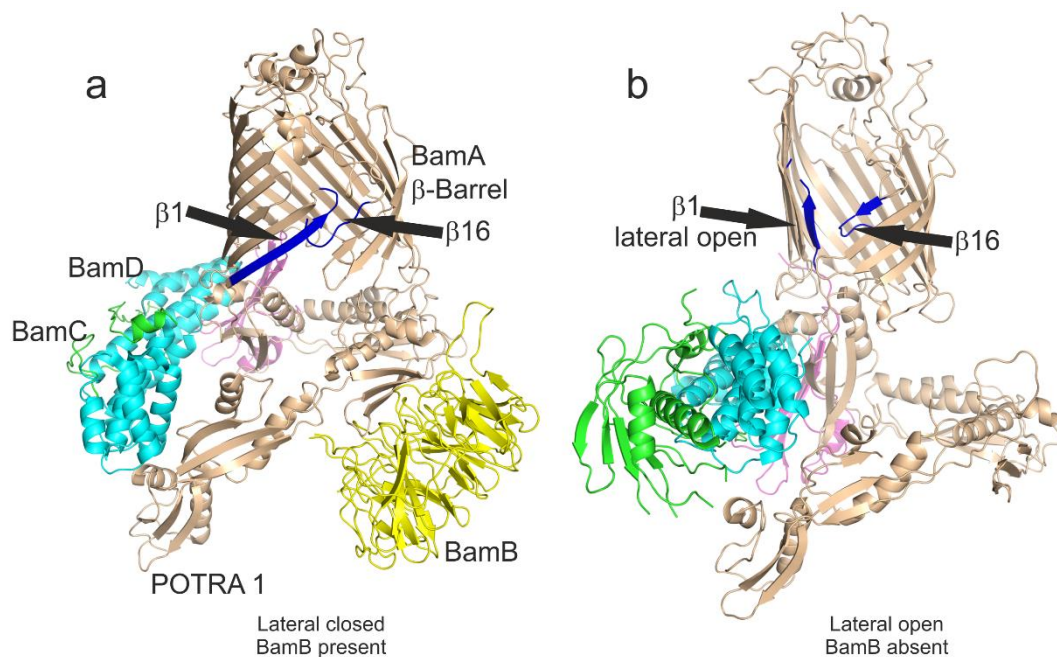
Figure 1-17: Comparison of crystal structures of the BAM complex. Crystal structure of (a) BamABCDE (PDB 5D0O)[208] and (b) BamACDE (PDB 5EKQ)[207]. BamA (brown), BamC (green), BamD (blue) and BamE(magenta) are visible in both structures in addition to BamB (yellow) in (a). The β1 and β16 strands are depicted in blue, highlighting the conformation of the BamA lateral gate in each structure. In addition, conformational changes between lateral open and closed structure are visible in the POTRA domains and in the extracellular loops at the top of the barrel.

The 'lateral open' conformations have only been observed in crystal structures of the BAM complex which lack the 42 kDa, β-propeller lipoprotein, BamB[207,208], while crystal structures of the intact complex contain a lateral-closed BamA structure similar to that published of the protein in isolation[11,208,209]. This leads to the hypothesis that changes in the BamA β-barrel conformation may represent a gating reaction driven by BamB binding. Our own structural analysis of BAM by cryo-electron microscopy has since disproved this theory[31,210], generating a structure which displays the intact BAM complex with BamA in a lateral open conformation in the presence of BamB. This will be discussed in detail in Section 3.3.

1.8 *In vitro* studies of OMP folding

OMPs must fold into the lipids of the outer membrane in the absence of an external source of energy. A huge amount of information has been gleaned from

studies of OMP folding using micelles and bilayers *in vitro*[12,33,35,71,72,79,229-246]. Typically OmpA has been used as the model folding OMP, dating from the original studies of Surrey & Jahnig demonstrating the ability to fold OmpA into micelles of the detergent β-octylglucoside[247] or lipid bilayers composed of dimyristoylphosphatidylcholine (DMPC)[243]. These studies exploited the heat modifiability of OMPs: that they will migrate as distinctive folded and unfolded populations on cold SDS-PAGE[248,249]. Since then studies have advanced apace, employing multiple techniques. Far-UV circular dichroism (CD) informs on formation of the β-sheet structure, while heat modifiability by SDS-PAGE and tryptophan fluorescence inform on the tertiary structure[79,250]. In addition, tryptophan fluorescence quenching can be utilised for single tryptophan variants monitoring insertion into a quenching environment, such as brominated lipids[237].

In addition to widespread use of SDS-PAGE, tryptophan fluorescence and CD to unravel the structures and mechanisms integral to OMP biogenesis, a plethora of further techniques have also been applied[246]. These include mass spectrometry[251,252], NMR[181,253-255], force spectroscopy[165,256,257], FRET[258-260] and molecular dynamics[246]. While considerable fundamental understanding, summarised here, has been gained through molecular biology and biochemical analyses, application of many techniques noted above to the folding of intractable outer membrane proteins remains in its infancy. With the fundamental knowledge in place however, the field may now increasingly rely on structural and biophysical techniques to resolve the finer details of OMP biogenesis.

Initial kinetic experiments suggested a multi-step model for OMP folding with a rapid initial step of hydrophobic collapse, followed by membrane adsorption, and with a slower later step of partial folding and insertion of hairpins[237,261]. This was supported by experiments with tryptophan fluorescence quenching of OmpA which demonstrated that all four β-hairpins cross the bilayer simultaneously[237]. Studies of folding of OmpA into DLPC bilayers by far-UV CD and gel electrophoresis showed similar kinetics, suggesting that secondary and tertiary structure are formed concurrently[79]. This was supported by hydrogen-deuterium exchange (HDX) studies demonstrating that when OmpX was folding into detergent micelles the rate of hydrogen bond formation between β-strands was consistent and simultaneous with tertiary structure formation[262]. The clustering of aromatic residues in the membrane interface of OMPs likely provides a critical

force in their assembly and stability[263]. It is not clear, however, how this data may fit with more recent single-molecule force spectroscopy results demonstrating that OMPs insert by sequential hairpins[256], rendering a single coordinated movement to tertiary structure unlikely.

While parallel pathways of folding have also been suggested for OmpA and other OMPs[238,264,265], more recently the mechanism of folding and insertion of OmpA has been called into question again[230]. While principally following the same pathway as previously deduced[79,237], it was shown that an intermediate was formed with more β-sheet content than the native state and populations were detected of misfolded off-pathway states[230]. Experiments used the transmembrane domain of OmpA (tOmpA) folding into bilayers of different thicknesses in studies with CD and SDS-PAGE. It is proposed this goes against the previously suggested parallel pathways and supports a "predetermined pathway with optional errors"[266]. It is concluded that the novel structure seen is likely due to transient β-strand formation by extracellular loops[230]. While plausible, the loops have also been shown to be amenable to truncation and mutagenesis[267] and therefore unlikely to be critical for folding.

Studies of OMP folding in synthetic bilayers widely employ lipids with phosphatidylcholine (PC) head groups as these support fast folding[71,72]. These conditions differ from that of the inner leaflet of the OM of *E.coli* which is comprised predominantly of PE and PG[54], and ignores the asymmetric nature of the bilayer and presence of LPS. While LPS assists the folding of some OMPs *in vivo* it is not necessary for the folding of OmpA[247] or OmpT[159,189] *in vitro*. The presence of LPS in fact retards the folding of OmpT[159], but is required for OmpT protease activity[268]. In addition, while lipid chain length varies *in vivo*, with the inner leaflet of the OM typically composed of phospholipids of 16-18 carbon acyl chains[54,67], the thickness of synthetic phosphatidylcholine bilayers typically used *in vitro* increases linearly with increasing acyl chain length[269]. In this respect, DMPC (C14) bilayers with a thickness of 23 Å[269] are closest to the hydrophobic thickness of the OM estimated from average OMP structures (23.7 Å)[270]. However, it is predominantly the 10-12 carbon acyl chain lipids that have been most extensively employed in synthetic liposomes used in OMP folding studies[71,72]. These shorter acyl chains favour OMP insertion *in vitro* compared with the inefficient folding in lipids of lengths greater than 12 carbons[71,72].

A systematic study of the folding of nine different OMPs (OmpX, OmpW, OmpA, PagP, OmpT, OmpLA, FadL, BamA and OmpF) in phosphatidylcholine LUVs showed several important general considerations previously noted for individual OMPs[72]:

1) Higher pH values increase folding efficiency, consistent with experiments on OmpF[244]. Experiments were carried out in DLPC LUVs and pH varied from 3-10, with an increased fraction folded being observed at pH 8-10. As the OMPs have a pI between pH 5 and pH 6 and will have a net negative charge at higher pH, this may promote interaction with the zwitterionic bilayer.

2) OMPs fold better in thinner bilayers. Phosphatidylcholine LUVs were used with chain length varied from 10-12 carbons: diC$_{10:0}$PC (DDPC), diC$_{11:0}$PC (DUPC) and diC$_{12:0}$PC (DLPC). All OMPs folded fastest in DDPC, in accordance with previous data on OmpA[79].

3) OMPs fold better in vesicles of smaller diameter. From comparison of folding into SUVs and LUVs of the same lipid type, the increased curvature of SUVs promotes folding, as do lipid defects[79,229,242].

4) Effects of temperature were highly variable. In variation between 30° -50°C the folding efficiency of OMPs showed no consistent trend, and properties were not correlated with OMP size. This is likely due to different aggregation propensities between OMPs at different temperatures.

While OMPs will spontaneously fold into the short acyl chain model membranes widely used (~15 Å acyl chain length for 10-carbon DDPC[269]), it is likely this would not occur at a sufficient rate in the bilayer of a cell comprised of longer lipids[71]. Additionally, the introduction of native-like lipid head groups into the bilayer, such as PE and PG, slows OMP folding[71]. A molar percentage of 20% DDPE in DDPC LUVs retarded folding of all OMPs measured (tOmpA, OmpA, OmpX and OmpLA) compared with membranes created from DDPC alone[71]. Although apparently paradoxical, this emphasises the role of BamA in relieving this kinetic barrier for OMP folding. The presence of BamA in (80:20 mol:mol) DDPC:DDPE LUVs increases the kinetics of folding of tOmpA, OmpA, OmpX and OmpLA[71]. Prefolded BamA also increases the rate of folding of OmpA and its transmembrane domain (tOmpA) in phosphatidylcholine bilayers (DUPC, DLPC, DTPC and DMPC)[241,271], and the catalytic rate enhancement of BamA increases

with increasing lipid acyl chain length[241]. Therefore it appears likely that the presence of BamA assists in overcoming energetic barriers for OMP folding, and specific localisation of BAM in the OM allows folding of OMPs in PG and PE lipid types only in that location[71], differentiating from the similar periplasmic lipids of the IM, and ensuring that OMPs are folded only into the OM.

One way in which the catalysis afforded by BAM may occur is by lipid defects[230]. OMPs fold faster at regions of lipid non-homogeneity, such as caused by lipids at their phase transition temperature[230] and BamA's principal role may be as a membrane "disruptase" or causing lipid thinning[194,241]. This model of BamA function will be discussed in full (Section 1.10.2). It has additionally been demonstrated that BamA works in a "catalytic", non-stoichiometric fashion[245], able to fold a greater concentration of substrate than total concentration of prefolded BamA. The rough turnover calculation suggests 1.7 OMPs can be folded per BamA, which is equivalent to that measured using the BAM complex (BamABCDE)[159], suggesting that the additional lipoproteins play no role in catalytic capacity or regeneration of activity. However, as will be discussed in later chapters, there are conditions in which BamA is insufficient, and it is likely that the BamBCDE subunits accelerate activity in more native lipid types[210,245].

1.8.1 *In vitro* studies with the BAM complex

Our understanding of the BAM complex mechanism is now advancing faster due to our ability to monitor substrate OMP folding by the multiprotein complex, or its sub-assemblies[159,175,189,272-274]. Originally, due to difficulties in purification of the intact BAM complex, the complex was expressed and purified as two sub-complexes: BamAB and BamCDE[189]. The choice of these two subcomplexes was due to previous knowledge that BamA binds BamB independently of BamCDE[188,201].

Studies of the *in vitro* activity of the BAM complex, dating from this original work[189], have largely used the 10- stranded β-barrel OmpT as a substrate[159,272,274]. OmpT is a protease[275] and when correctly folded it will cleave a substrate possessing sequential charged residues[268]. The subcomplexes BamAB and BamCDE were reconstituted together in *E.coli* polar lipid proteoliposomes and it was demonstrated that OmpT folding and thus activity

was significantly increased in the presence of the BAM complex[189]. Additionally, increasing concentration of SurA increased activity, while it was later demonstrated that SurA could be functionally replaced by urea[159,272]. Activity was improved when all five protein components of BAM were present, compared with either BAM subcomplex alone[159,189]. Additionally, BamABCDE yielded significantly higher activity than BamACDE[159]. These activities, measured by fluorescence, were confirmed as correlating with folding of OMP by migration of radiolabelled OmpT on SDS-PAGE[159,189].

The assembly of BamA itself into the lipid bilayer presents somewhat a "chicken and egg" problem, as BamA is the catalytic component required for OMP folding and BamA itself cannot quickly fold into empty liposomes[272]. This was solved, however, by the demonstration that the lipoproteins BamCDE aid BamA folding into *E.coli* phospholipids but are not able to exert the same effect for OmpA[272].

Subsequently the intact BAM complex was reconstituted following polycistronic expression of all five subunits and it was demonstrated that the BAM complex displays greater activity when all components are expressed together[274], as compared by the OmpT assay. This preparation of the BAM complex was demonstrated to be functional in folding the autotransporter EspP and its passenger domain correctly in proteoliposomes[274]. It additionally provided the first evidence that BAM, reconstituted in protein-supported nanodiscs is functional[274].

Most recently, a study of BAM complex catalysis in proteoliposomes composed of different lipids demonstrated that the effect of BAM is substrate-, but not lipid-, specific[273]. Using the autotransporter EspP as a substrate, the data are striking in the invariance of the observed rates and t_{50}s across different membrane thicknesses, fluidity and lipid head groups[273]. This implies that BAM is able to overcome the thermodynamic limitations conferred by the different bilayers, and catalyse folding to a consistently identical rate. For OmpA, rates are not so consistent, with BAM-catalysed OmpA folding faster in short chain lipids than in longer chain lipids. However, the range of kinetics observed are small, significantly less than for spontaneous OmpA assembly into lipids of varying lengths[79,241], and a high proportion of folding was observed in all cases[273]. BAM may accelerate folding of different substrates to different extents, but largely it is the substrate that influences the catalytic rate, not the lipid.

1.9 *In vivo* studies of BamA

Lastly, a tool that has been utilised to great effect in unravelling OMP folding mechanisms is genetic studies[21,24-27,81,83,187,201,220,276,277]. Deletion and depletion strategies have assisted identification of the roles of all BAM complex subunits and chaperones, as discussed in detail, in Sections 1.6.2, 1.7.1 and 1.7.2. For BamA studies are necessarily more complicated as the protein is essential for cell growth, and therefore BamA cannot be deleted. However, experiments have been performed by construction of a strain in which chromosomal BamA is deleted, and is replaced with the same gene under control of the araBAD promoter[25]. Using this construct the presence of BamA is regulatable by the presence of arabinose. The chromosomal copy of BamA is therefore not expressed in the absence of arabinose and cells are only viable if the compensating copy from an introduced plasmid is functional. This assay has led to great progress in the field, identifying regions or residues of BamA for which mutation is lethal[25,194,199,201,209,277] and forms the basis for the original evidence for BamA lateral gating[199], as discussed further below (Section 1.10-4).

1.10 Mechanism models of BAM function

Despite the availability of structures for the BAM complex since 2016[207-210] the mechanisms of BAM function are still unclear. Several models have been proposed[212] (Figure 1-18), outlined below, for which the concept and supporting evidence is further explained.

1) Threading (Figure 1-18a): where a substrate OMP utilizes the lumen of the BamA barrel for passage through the lipid bilayer before assembling in the adjacent membrane.

2) Membrane destabilization (Figure 1-18b), where the presence of BamA/the BAM complex in the lipid bilayer is sufficient to allow OMP insertion, possibly via interaction with one or more POTRA domains.

3) Oligomerization (Figure 1-18c): by which the BAM complex, or at least BamA multimerizes to best interact with the substrate[211], and the substrate is inserted by the cooperation of the barrels.

4) Lateral opening (Figure 1-18d) wherein BamA opens via a separation of its first (β1) and last (β16) strands and these dynamics allow substrate interaction and entry. This is linked to a second theory, that following opening of the BamA barrel, substrate OMP β-strands will attach and template on BamA, forming a hybrid super-barrel until the substrate OMP buds off into the membrane[199,212].
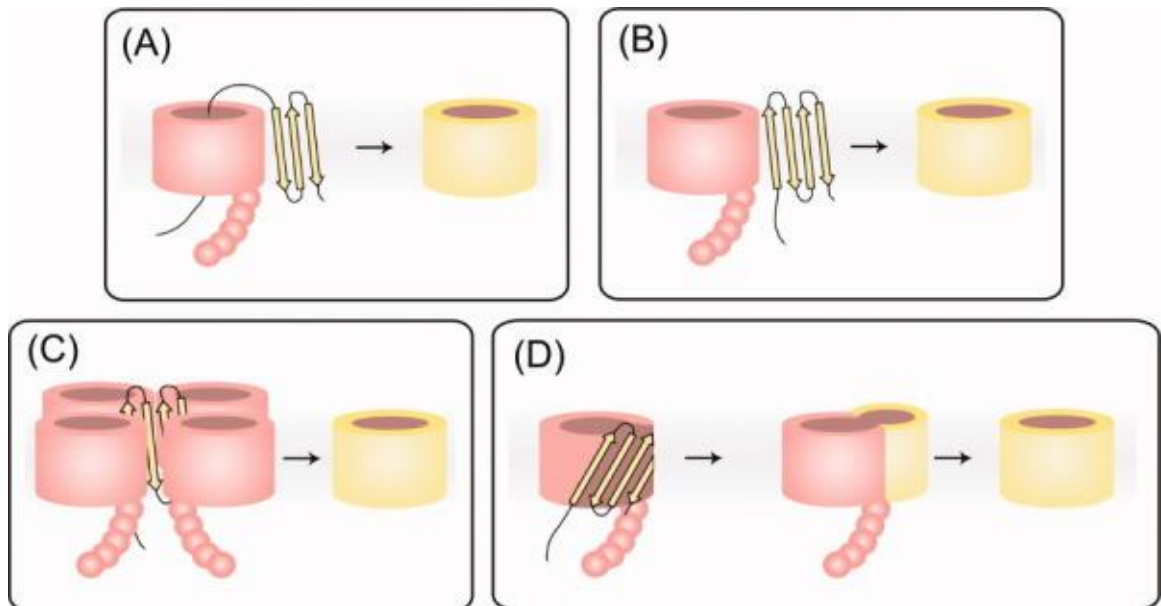
Figure 1-18: Models of BAM mechanism of action: The models show BamA (pink) as representative of the complex, assisting a substrate OMP (yellow) in insertion into the lipid bilayer. a) Threading, b) membrane destabilization, c) oligomerization, and d) lateral opening. Image reproduced from Kim (2012)[212].

1.10.1 BAM catalysis by lumen threading

The threading model of BAM-assisted OMP folding (Figure 1-18a) is possibly the least well supported by current literature. It typically hypothesises the OMP substrate moving through the lumen of the barrel and adopting hairpin folds from exterior to the cell[212]. The model appears possible, however, as it is likely that adopted by two-partner secretion protein FhaC[196,278] (Figure 1-11). In the case of FhaC the protein was originally crystallized with the first helix (H1) of the POTRAs and loop 6 (L6) of the barrel located inside the barrel pore[196]. Movement of the

39

dynamic, and essential loop 6 of the barrel allows the pore to widen to allow unfolded substrate through, where it may fold outside the membrane[196]. However, this model, when applied to OMPs, may not pay sufficient heed to the energy penalty for folding a β-barrel from the exterior of the membrane.

1.10.2 BAM catalysis by membrane destabilization

The membrane destabilisation model (Figure 1-18b) suggests that the presence of BamA/the BAM complex in the lipid bilayer destabilises the lipids in its vicinity and thus facilitates the folding of substrates. This must be a BAM-specific effect as other OMPs are not shown to catalyse folding[241,271], but there is considerable evidence supporting this model. Structural studies have shown that the exterior rim of the BamA β-barrel has a reduced hydrophobic surface on one side[194] which could produce local distortions in the OM. It has been shown that OMPs will fold faster into thinner bilayers, such as those composed of shorter chain lipids[72,79], but quicker still into bilayers possessing defects such as non-uniform phase[71,279]. Additionally, BamA alone is capable of accelerating OMP folding in synthetic lipids *in vitro*[71,245,271] and acts as a better catalyst in thicker bilayers[241]. Lastly, data presented in this thesis demonstrate that lateral opening of BamA β1 and β16 is unnecessary for it to achieve this catalytic effect (Section 4.2.5[241]), thus the presence of BamA is sufficient to facilitate OMP folding.

1.10.3 BAM catalysis by oligomerization

There remains a persistent theory that BamA or BAM complexes may oligomerize and this would assist OMP assembly[211,212,280] (Figure 1-18c). The origins of this concept for BamA derive from observation of the protein as a tetrameric species by Blue Native PAGE and size exclusion chromatography (SEC)[211]. Additionally, *Haemophilus influenza* protein HMW1B, also a member of the Omp85 superfamily, was observed in oligomeric complexes by SEC and negative stain EM[281,282]. However subsequent analysis of the individual BamA protein[201] or BAM complex[207-210] has provided no evidence towards formation of oligomers. It remains possible that optimal function of the BAM complex may be in oligomers. This is supported by identification of OMPs in concentrated "islands"[283] or "precincts"[216]. It has been observed that OMPs will exhibit unexpected clustering

behaviour, with BAM included in these clusters, which all gradually migrate towards the poles of cells[283]. Separate work appears to contradict this putative movement to the poles of cells but also demonstrates the close localisation of multiple copies of BAM, mediated by BamB in so-called BAM "precincts"[216].

However, there is evidence against BAM oligomers being the functional entity. Firstly, from early characterisation data which demonstrated that although all lipoproteins were capable of associating with BamA, BamA itself was not[201]. Secondly it is demonstrated that oligomers are likely not the functional form of Bam, from work on protein-supported nanodiscs. As nanodiscs would only hold one copy of BAM complex, demonstration that they are functional in folding the autotransporter EspP[274] and OmpT (this work, Section 3.6.3) is evidence against oligomers of BAM being the obligate functional form.

1.10.4 BAM catalysis by lateral opening

The long-abiding hypothesis[199,212] that the BamA β- barrel opens laterally to facilitate OMP folding (Figure 1-18d) was first supported by the observed weak interaction of the β1 and β16 β-strands, with only two hydrogen-bonds seen in the first crystal structure (Figure 1-10c)[11]. This is in stark contrast to *H.ducreyi* BamA with eight hydrogen bonds between β1 and β16[194] (Figure 1-10a). Molecular dynamics simulations of *Ng*BamA and a homology model of *Ec*BamA were both predicted to open laterally, with ~9Å separation of β1 and β16 in *Ec*BamA in a DMPE bilayer[199]. However, while thinning of the membrane on the side of β1/β16 side of the BamA barrel is observed relative to the other side, in all simulations in PC lipids[241] and native *E.coli* lipid[206], no lateral opening of BamA was observed for long simulation times in native lipid[206].

As discussed (Section 1.7.3), crystal and EM structures of the BAM complex subsequently published[207-210] demonstrate that the *E.coli* BamA β-barrel indeed visits both lateral open and closed conformations. While ascertaining that the lateral open state exists for *E.coli* BamA, these structures do not inform on whether opening is functionally significant or required. The first evidence that BamA β-barrel lateral opening was functionally relevant came from *in vivo* experiments[199]. Utilising a BamA knock-out strain, the two natural cysteines were

removed (C690S and C700S) and cysteines were introduced in pairs matching up the β1/16 seam (Figure 1-19)[199].
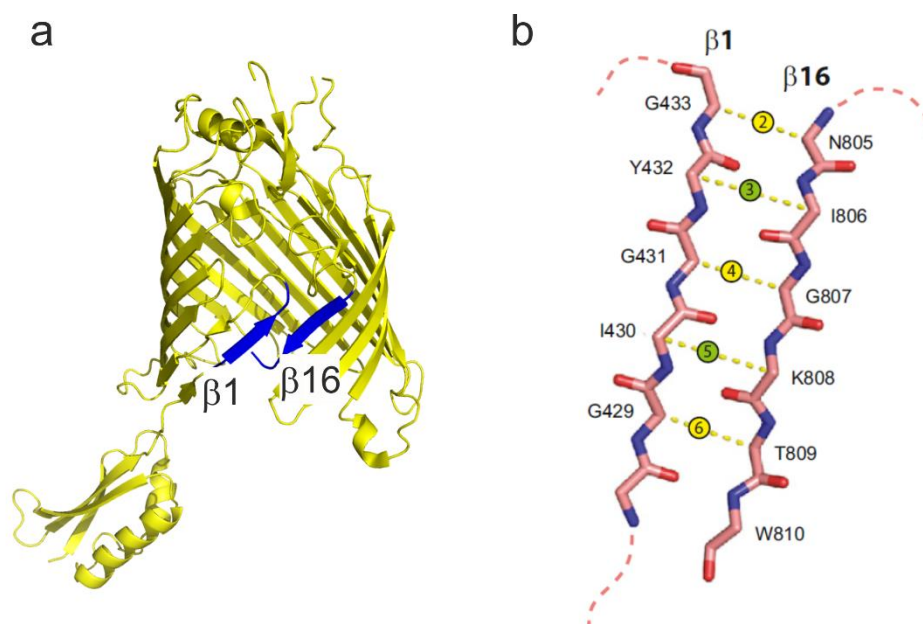
Figure 1-19: β1 and 16 double cysteine pairs lock the *E.coli* BamA β-barrel closed. a) Crystal structure of *E.coli* BamA [4C4V][11] with β1 and β16 shown in dark blue. b) Image of the pairs engineered to form disulphide cross-links, reproduced from Noinaj, 2014[199]. Yellow circles indicate disulphides that would point into the lumen of the barrel domain; green circles, disulphides that would point into the membrane.

These studies showed that BamA with disulphide linked β1 and β16 strands, such that the β-barrel was trapped closed, could not replace wild-type BamA *in vivo* causing a lethal phenotype[199]. However, these mutants were rescuable, and the bacteria viable when grown in the presence of the reducing agent TCEP[199]. Despite these *in vivo* results, the effect of lateral gating had not, until recently, been directly assessed in any *in vitro* or purified systems. Lethality in *in vivo* experiments, while a measure of functional importance, could have arisen by several means. Concurrent to work discussed in this thesis, another group tackled this question, with complementary results. The Sousa group in 2017[231] utilised disulphide pairs along the putative lateral opening of BamA and upon prefolding the protein in 80:20 mol/mol DDPC:DDPE liposomes, demonstrated disulphide-linked BamA was still capable of folding substrate OmpX at wild-type rates. This parallels results shown in Results Section 4.2.5 where the implications will be fully discussed, but demonstrates that BamA alone facilitates OMP folding, at least by a membrane disruptase effect. While lethal *in vivo,* at least for small

substrates and short-chain synthetic lipids, lateral gating appears unnecessary for OMP folding *in vitro*[231].

1.11 OMP recognition by the BAM complex

In addition to the mechanism of how OMP folding is catalysed by the BAM complex, how OMPs are recognised by BAM remains unknown, and one of the key questions within the field. As OMPs display high conservation, at both structural and residue level it has long been hypothesised there is a 'signal sequence' to direct OMPs to BAM encoded within the sequence, known as the β-signal.

This is typically the C-terminal membrane-spanning fragment, or β-strand, as it has been found this is essential for membrane localisation for many OMPs[284]. This so called β-signal is particularly conserved, and involves a pattern of alternating hydrophobic residues, and a highly conserved terminal Phe[285]. Lipid bilayer experiments show that the 12 terminal amino acids of an OMP, forming this 'β signal' are capable of mimicking a substrate OMP's abilities to induce channel-opening in BAM[211]. The experiments confirmed importance of the terminal Phe, but also displayed significant species specificity, as PorA from *N.meningitidis* was unable to cause channel opening with *E.coli* BamA[211]. While the C-terminal end of PorA appears to conform to the C-terminal OMP signature sequence, the lack of channel opening was attributed to the charged residue at the penultimate position of *Neisserial* OMPs[211]. Subsequent bioinformatics analysis suggests that the incompatibility between the two is more likely due to a histidine three residues from the C-terminus[286].

Studies on BamA are yet more complicated, as while the sequence of β-strand 16 sequence mirrors the consensus β-signal[71], it is a segment on strand 14 that is capable of stalling BAM function[175], suggesting that the β-signal of BamA resides in β14. In addition, deletion of the C-terminal Phe of two small OMPs was shown not to affect their intrinsic folding rate, but to slow BamA-catalysed folding[71].

The concept of the β-signal anticipates specific recognition of a β-strand of substrate OMPs by a β-strand of the Omp85 protein. This overlaps with the hypothesis of lateral gating[199,212], as this would be most effectively managed in

cases where lateral opening provides accessibility to the C-terminal strand of BamA, with a sequence mirroring the consensus β-signal[71]. Significantly the mitochondrial Omp85-channel, Sam50, homologous to BamA, has been more fully validated as functioning with a lateral gating and β-signal recognition mechanism[287]. A series of cross-linking experiments demonstrated that Sam50 opens between β1- β16 and that the β-signal of the substrate protein is specifically recognised by Sam50 β1[287]. The precursor protein inserts in this vicinity, and the mature protein is then released into the membrane[287]. This experimental evidence, on a closely related system, strongly suggests that lateral opening is the correct model for Omp85 proteins, but whether the mechanism is conserved for different Omp85 protein complexes across mitochondria, chloroplast and Gram-negative bacteria, or for different substrates, remains to be seen.

1.12 Aims of this thesis:

This introduction has highlighted current knowledge about the OM of Gram-negative bacteria, OMP biogenesis and the BAM complex, from studies *in vitro* and *in vivo*. There remain a large number of unanswered questions about a pathway that is critical for bacterial survival. This project has taken a biochemical approach to understanding components of the pathway *in vitro*, to elucidate the roles and importance of BAM in OMP folding.

Briefly, Chapter 3 describes the optimization of purification and reconstitution of the BAM complex, which was then used for structural studies. A key assay used to examine BAM complex activity (the OmpT enzymatic assay) was optimised and explored and BAM was reconstituted into different membrane mimetics, to examine the effect of the lipid environment on activity.

Chapter 4 begins the examination of the role of lateral gating: looking at BamA-catalysed tOmpA folding. In addition, results in this chapter explore the nature of recognition by BamA, with experiments on the role of substrate β-signal.

Chapter 5 presents results utilising the optimised purification and reconstitution described in Chapter 3, to examine multiple variants of the BAM complex. Their differential activity in folding the substrates tOmpA and OmpT can inform our

understanding of the BAM complex, the role of BamA dynamics and particularly of lateral gating.

The discussion then combines the findings presented into a new model for BAM function, points the way to future experiments needed to refine this model and reviews the importance of understanding this vital pathway.

The principal question guiding throughout the research was: How does BamA/the BAM complex recognise and catalyse OMP folding in the outer membrane?

2 Materials and Methods

2.1 Materials

2.1.1 Chemicals

A	Supplier
Acetic acid, glacial	Fisher Scientific, Loughborough, UK
Acrylamide 30 % (w/v)	Severn Biotech, Kidderminster, UK
Agar	Melford Laboratories, Suffolk, UK
Agarose	Melford Laboratories, Suffolk, UK
L-(+)-Arabinose	Sigma Life Sciences, MO, USA
Aldrithiol (4,4'-dypyridyl-disulphide, 4-DPS)	Sigma Life Sciences, MO, USA
Ammonium persulphate (APS)	Sigma Life Sciences, MO, USA
Ampicillin sodium salt	Formedium, Norfolk, UK
B	
Bactotryptone	Fisher Scientific, Loughborough, UK
Benzamidine hydrochloride	Sigma Life Sciences, MO, USA
Bromophenol blue	Sigma Life Sciences, MO, USA
C	
Carbenicillin disodium	Formedium, Norfolk, UK
Chloramphenicol	Sigma Life Sciences, MO, USA
Chloroform	Fisher Scientific, Loughborough, UK
Copper Sulfate ($CuSO_4$)	Sigma Life Sciences, MO, USA
Calcium chloride ($CaCl_2$)	Sigma Life Sciences, MO, USA
D	
Dithiothreitol (DTT)	Formedium, Norfolk, UK
Diamide	Sigma Life Sciences, MO, USA
n-dodecyl β-D-maltoside (DDM)	Anatrace, OH, USA
E	
Ethidium bromide (EtBr)	Sigma Life Sciences, MO, USA
Ethanol	Sigma Life Sciences, MO, USA
Ethylenediaminetetraacetic acid (EDTA)	Fisher Scientific, Loughborough, UK
G	
Guanidine hydrochloride	Sigma Life Sciences, MO, USA
Glycerol	Fisher Scientific, Loughborough, UK
H	
Hydrochloric acid (HCl)	Fisher Scientific, Loughborough, UK
I	

Imidizole	Sigma Life Sciences, MO, USA
Instant Blue Coomassie Blue Stain	Expedeon, CA, USA
Iodine	Sigma Life Sciences, MO, USA
Isopropanol	Fisher Scientific, Loughborough, UK
Isopropyl β-D-1-thiogalactopyranoside (IPTG)	Formedium, Norfolk, UK
M	
Methanol	Fisher Scientific, Loughborough, UK
MOPS	Sigma Life Sciences, MO, USA
N	
Nickel sepharose	GE Healthcare, Buckinghamshire, UK
Nickel nitrilotriacetic acid (Ni-NTA)	GE Healthcare, Buckinghamshire, UK
P	
Phenylmethanesufonyl fluoride (PMSF)	Sigma Life Sciences, MO, USA
Potassium chloride (KCl)	Fisher Scientific, Loughborough, UK
Potassium phosphate monobasic	Sigma Life Sciences, MO, USA
Potassium phosphate dibasic	Sigma Life Sciences, MO, USA
S	
Sodium azide (NaN$_3$)	Sigma Life Sciences, MO, USA
Sodium chloride (NaCl)	Fisher Scientific, Loughborough, UK
Sodium hydroxide (NaOH)	Fisher Scientific, Loughborough, UK
Sodium dodecyl sulphate (SDS)	Sigma Life Sciences, MO, USA
Super Optimal Catabolite (SOC)	New England Biolabs, MA, USA
T	
Triton X-100	Sigma Life Sciences, MO, USA
Tris	Fisher Scientific, Loughborough, UK
Tetramethylethylenediamine (TEMED)	Sigma Life Sciences, MO, USA
Tris(2-carboxyethyl)phosphine (TCEP)	Sigma Life Sciences, MO, USA
U	
Urea	MP biomedicals, Loughborough , UK
	Fisher Scientific, Loughborough, UK
Yeast Extract	Fisher Scientific, Loughborough, UK

2.1.2 *E.coli* Bacterial Strains

E.coli DHα (NEB)

E.coli BL21(DE3) (Agilent)

E.coli BL21(DE3)pLysS (Agilent)

E.coli JCM166 (BamA depletion strain): MC4100 *ara* $^{r/-}$ Δ(λ*att-ιom*) *: : bιa* P$_{BAD}$*yaeT araC Δyaet* provided by Thomas Silhavy, Princeton

HBD150 (for expression trial of Bam complex): MC4100 *ompT::spc ΔaraBAD leuD::kan* provided by Harris Bernstein, NIH

2.1.3 Origin of Plasmids

BamA and OmpA N-terminal β-barrel domain (1-171) lacking signal sequence (*E. coli*) in pET11a vectors were both obtained from Karen Fleming, John Hopkins Univ.

His-tag(HT)-Skp clone in pET28b plasmid was obtained from Sebastian Hiller, University of Basel.

Bam complex : Full-length genes, with signal sequences of BamA,B,C,D and E. 8xHistag at C-terminus of BamE in a pTrc99a vector was a gift from Harris Bernstein, NIH.

HT-BamA: N-terminal HT, with signal sequence in pZS21 vector was obtained from Thomas Silhavy, Princeton University.

SurA: Mature SurA sequence (SurA A21-N428) with N-terminal HT in pET28b vector was obtained from Daniel Kahne, Harvard Univ.

SecB-HT in pRSFDuet-1 vector was a gift from Ian Collinson, University of Bristol.

MSP1D1 on pET28a was a gift from Stephen Sligar (Addgene plasmid # 20061)

2.1.4 Summary of proteins used in this study

Protein	Vector	Protein size (kDa)	Extinction Coefficient ($M^{-1}cm^{-1}$)	Amino acids	pI	Origin
BamA (22-810)	pET11a	88	140165	790	4.9	Fleming
BamA (22-810) C690S/C700S	pET11a	88	140040	790		*
BamA (22-810) C690S/C700S/I430C/K808C	pET11a	88	140165	790		*
BamA (22-810) C690S/C700S/G431C/G807C	pET11a	88	140165	790		*
BamA (22-810) C690S/C700S/I430C/K808C / E435C/S665C	pET11a	88	140040	790		*
HT-OmpT	pET11a	35	79760	311	5.9	
FLAG-OmpT	pET11a	35	79760	305	5.1	*
HT-OmpT(G306P)	pET11a	35	79760	311	5.9	*
HT-OmpT(G306A)	pET11a	35	79760	311	5.9	*
tOmpA (1-171)	pET11a	18	46870	172	5.7	Fleming
tOmpA (1-171)-RHK	pET11a	18.9	45380	172	6.2	
tOmpA (1-171) (G166A)	pET11a	18.9	46870	172	5.7	*
SurA (H$_6$-SurA)	pET28b	45.5	29450	412	6.2	Kahne
HT-SurA ΔP2	pET28b	35.5	18450	320	6.8	
HT-SurA N-Ct	pET28b	23.9	12950	211	8.0	
SecB-HT	pRSFduet	18.1	12950	161	4.8	Collinson
HT-Skp	pET28b	17.	1490	162	9.7	Hiller
HT-MSP1D1	pET28a	24.8	21430	212	5.9	Sligar
MSP1D1	pET28a	22.0	18450	190	5.7	
BamABCDE-HT (pJH114)	pTrc99a	200	292025	1813	5.0	Bernstein
BamABCDE-HT C690S/C700S	pTrc99a	200	292025	1813	5.0	*
BamABCDE-HT C690S/C700S/I430C/K808C	pTrc99a	200	292025	1813	5.0	*
BamABCDE-HT C690S/C700S/E435C/S665	pTrc99a	200	292025	1813	5.0	*
BamABCDE-HT C690S/C700S/G433C/N805C	pTrc99a	200	291650	1813	5.0	*
BamABCDE-HT C690S/C700S/I430C/K808C / E435C/S665C	pTrc99a	200	291650	1813	5.0	*
HT-BamA	pZS21	89.4	140040	798	5.0	Silhavy
HT-BamA C690S/C700S	pZS21	89.4	140040	798	5.0	*

HT-BamA C690S/C700S/G433C/N805C	pZS21	89.4	140040	798	5.0	*
HT-BamA C690S/C700S/I430C/K808C	pZS21	89.3	140040	798	5.0	*
HT-BamA C690S/C700S/E435C/S665C	pZS21	89.3	140040	798	5.0	*
HT-BamA C690S/C700S/E435C/S665C/ I430C/K808C	pZS21	89.3	140040	798	5.0	*

Table 2-1: Table of proteins used in this study. Details of plasmid and source. * denotes constructs made in this study, while constructs not in bold were purified by others. For all of the HT-BamA constructs, these were used solely in an *in vivo* assay and not as expression constructs for any of the work discussed in this thesis.

2.1.5 Primers for mutagenesis

All mutants were prepared using the Q5 Site-Directed Mutagenesis (NEB) kit used according to the manufacturer's instructions. All mutants of BamA (in pET11a, pTrc99a or pZS21) were originally mutated to create the Cys-free (C690S/C700S) pseudo-wild-type, followed by single rounds of mutagenesis for introduction of each cysteine. The primers used are detailed below for BamA in pET11a (Table 2-2), BAM complex in pTrc99a (Table 2-3), HT-BamA in pZS21(Table 2-4) and other proteins (Table 2-5).

Mutation	Oligo Sequence	Length	% GC	T_m	Annealing Tempe-rature (T_a)
C690S/C700S					
Forward	cgcgaaagacctgagcAAATCGGATGATGCTGTAG	35	23	57°C	59 °C
Reverse	ccgtcctgagtcgcgctTTCGTAATCATAGTCCGG	35	23	56°C	
G429C					
Forward	CTTCAACTTTtgcATTGGTTACGGTACTGAAAGTG	35	40	63°C	66 °C
Reverse	CTACCGGTGTTGCGCTCT	18	61	66°C	
I430C					
Forward	CAACTTTGGTtgcGGTTACGGTACTGAAAGTGG	33	48	63°C	66 °C
Reverse	AAGCTACCGGTGTTGCGC	18	61	67°C	
G431C					
Forward	CTTTGGTATTtgcTACGGTACTGAAAG	27	41	58°C	61 °C
Reverse	TTGAAGCTACCGGTGTTG	18	50	60°C	
G807C					
Forward	GTTTAACATCtgcAAAACCTGGTAAGATC	29	38	55°C	58 °C
Reverse	TGGAACTGTTCTGCCTTG	18	50	59°C	
K808C					
Forward	TAACATCGGTtgcACCTGGTAAGATC	26	46	57°C	60 °C
Reverse	AACTGGAACTGTTCTGCC	18	50	59°C	
T809C					
Forward	CATCGGTAAAtgcTGGTAAGATCCG	25	48	55°C	58 °C
Reverse	TTAAACTGGAACTGTTCTGC	20	40	58°C	

Table 2-2: Primers used for Q5 site-directed mutagenesis of BamA in pET11a. The base-pairs encoding the region of amino acid substitution(s) are in lower case.

51

Mutation	Oligo Sequence	Length	% GC	T_m	Annealing Temperature (T_a)
G433C					
Forward	TATTGGTTACtgcACTGAAAGTGGC	25	44	57°C	58 °C
Reverse	CCAAAGTTGAAGCTACCG	18	50	61°C	
E435C					
Forward	TTACGGTACTtgcAGTGGCGTGAG	24	54	60°C	59 °C
Reverse	CCAATACCAAAGTTGAAGC	19	42	56°C	
E435C (where I430C)					
Forward	TTACGGTACTtgcAGTGGCGTGAG	24	54	62°C	62 °C
Reverse	CCGCAACCAAAGTTGAAG	18	50	61°C	
S665C					
Forward	TGGCTTCCAGtgcAATACCATTGG	24	50	65°C	68 °C
Reverse	CGCACGGTGCTGGAACCA	18	67	69°C	
N805C					
Forward	GTTCCAGTTTtgcATCGGTAAAACCTG	27	44	60°C	61 °C
Reverse	TGTTCTGCCTTGTCTCCA	18	50	63°C	
K808C					
Forward	TAACATCGGTtgcACCTGGTAAGTG	25	48	57°C	60 °C
Reverse	AACTGGAACTGTTCTGCC	18	50	59°C	
G807C					
Forward	GTTTAACATCtgcAAAACCTGGTAAGTG	28	39	57°C	58 °C
Reverse	TGGAACTGTTCTGCCTTG	18	50	62°C	

Table 2-3: Primers used for mutagenesis of BamA in the BAM complex using pTrc99a. The base-pairs encoding the region of amino acid substitution are in lower case. Where the new primer is not specified, the corresponding BamA in pET11a primer was used.

52

Mutation	Oligo Sequence	Length	% GC	T_m	Annealing Temperature (T_a)
N805C					
Forward	GTTCCAGTTTtgcATCGGTAAAACCTG	27	44	60°C	61 °C
Reverse	TGTTCTGCCTTGTCTCCA	18	50	63°C	
G807C					
Forward	GTTTAACATCtgcAAAACCTGGTAAGTG	28	39	57°C	58 °C
Reverse	TGGAACTGTTCTGCCTTG	18	50	62°C	
K808C					
Forward	TAACATCGGTtgcACCTGGTAAGTG	25	48	59°C	60 °C
Reverse	AACTGGAACTGTTCTGCC	18	50	62°C	
T809C					
Forward	CATCGGTAAAtgcTGGTAAGTGTTC	25	44	55°C	56 °C
Reverse	TTAAACTGGAACTGTTCTG	19	37	56°C	

Table 2-4: Primers used for mutagenesis of HT-BamA using pZS21, for *in vivo* studies. The base-pairs encoding the region of amino acid substitution are in lower case. Where the new primer is not specified, the corresponding BamA in pET11a primer was used.

Mutation	Oligo Sequence	Length	% GC	T_m	Annealing Temperature (T_a)
tOmpA-G166A					
Forward	GCTGAGCCTGgcgGTTTCCTACCGTTTTG	29	59	67°C	68°C
Reverse	ATGCCGTTGTCCGGACGA	18	61	69°C	
OmpT-G306P					
Forward	CACTACTGCTccgCTTAAGTACAC	24	50	55°C	56°C
Reverse	ATGAAGTTATAGTTTTCTATACC	23	26	56°C	
OmpT-G306A					
Forward	CACTACTGCTgcgCTTAAGTACAC	24	50	57°C	57°C
Reverse	ATGAAGTTATAGTTTTCTATACC	23	26	56°C	

Table 2-5: Primers used for mutagenesis of other proteins. The base-pairs encoding the region of amino acid substitution(s) are in lower case.

2.2 Molecular Biology

2.2.1 Preparation of competent cells

Cells of the desired strain were streaked onto an LB agar plate with no antibiotics and incubated overnight at 37 °C. A single colony was selected and used to inoculate 10 mL autoclaved LB and incubated overnight at 37 °C with shaking at 200 rpm. 5 mL was used to inoculate 100 mL autoclaved LB which was grown (37 °C, 200 rpm) until the optical density (OD) at 600 nm was 0.40 – 0.45. Cells were harvested by centrifugation (4000 rpm (4000 g), 10 min, 4 °C) in a pre-chilled Beckman JS-5.3 rotor. The pellet was gently resuspended in 10 mL of filter-sterilised, pre-chilled 100 mM $CaCl_2$. After incubation on ice for 10 minutes the cells were centrifuged as described previously and the supernatant removed. The pellet was resuspended gently in 2 mL of pre-chilled 100 mM $CaCl_2$ 30% (w/v) glycerol. Cells were aliquoted (100 µl) into 1.5 mL Eppendorf tubes pre-cooled on dry ice and stored at -80 °C.

2.2.2 Transformation

For transformation of plasmid stocks 50 µL of the appropriate commercial (for BAM complex) or laboratory-prepared competent cells were thawed on ice, then transferred to a round-bottom 14 mL transformation tube. 1-2 µL of plasmid DNA (100-200 ng/µL) was added and the cells incubated on ice for 30 minutes. Subsequently the cells were heat-shocked at 42 °C for 45 seconds and returned to ice for 5 minutes. All 50 µL was plated directly onto LB agar containing relevant antibiotics (100 µg/mL carbenicillin or 50 µg/mL kanamycin).

2.2.3 Site-directed mutagenesis

Mutagenesis was carried out to create a number of different plasmid variants. Mutagenesis primers (Table 2-2-Table 2-5) were designed utilising NEBaseChanger[TM], the online NEB primer design software and primers manufactured by Eurofins Genomics.

All mutagenesis was carried out utilising Q5 Site-Directed Mutagenesis Kit and protocol (NEB). Reagents were assembled in a thin-walled PCR tube as follows:

Reagent	25 μL RXN	FINAL CONC.
Q5 Hot Start High-Fidelity 2X Master Mix	12.5 μL	1 x
10 μM Forward Primer	1.25 μL	0.5 μM
10 μM Reverse Primer	1.25 μL	0.5 μM
Template DNA (1–25 ng per μL)	1 μL	1-25 ng
Nuclease-free water	9.0 μL	

Using a Bio-RAD PCR machine the following PCR thermocycling conditions were then carried out:

STEP	TEMP	TIME
Initial Denaturation	98 °C	30 seconds
25 Cycles	98 °C	10 seconds
	50–72 °C*	10–30 seconds
	72 °C	20–30 seconds per kb
Final Extension	72 °C	2 minutes
Hold	4–10 °C	

*T_a, primer annealing temperature (Table 2-2-Table 2-5) is utilised here.

The PCR product was then visualised by agarose gel electrophoresis (see 2.2.4) and, if successful, the sample was subjected to Kinase Ligase and DpnI (KLD) treatment to circularize the plasmid and remove template DNA. Reagents were mixed as follows:

Reagent	VOLUME	FINAL CONC.
PCR Product	1 μL	
2X KLD Reaction Buffer	5 μL	1 ×
10X KLD Enzyme Mix	1 μL	1 ×
Nuclease-free Water	3 μL	

The KLD reaction was mixed thoroughly by pipetting and incubated for a minimum of 5 minutes at room temperature before being used in a transformation protocol.

For these transformations, NEB 5α competent *E.coli* cells were thawed on ice. 5 µL of the KLD mix was added and tapped to mix. Following incubation on ice for 30 minutes, cells were heat-shocked at 42 °C for 45 seconds and returned to ice for 5 minutes. 950 µL of room temperature SOC (Super Optimal Catabolite) was added and incubated for 60 minutes (37 °C, 200 rpm). Cells were mixed by tapping the tube and 50 – 300 µL spread onto LB agar plate containing relevant antibiotics (100 µg/mL carbenicillin or 50 µg/mL kanamycin). In some cases it was necessary to either dilute cells or briefly centrifuge and resuspend in lower volume to obtain an appropriate number of single colonies.

2.2.4 Agarose gel electrophoresis

Agarose gels were prepared by adding 1.5% (*w/v*) agarose to 150 mL TAE buffer and heating in a microwave until the agarose was dissolved. TAE buffer was prepared as a 50x stock containing 121 g Tris, 28.55 mL glacial acetic acid, 50 mL 0.5 M EDTA in 500 mL (pH 8.0). The agarose solution was left to cool to ~50 °C before addition of 10 mg/mL EtBr at 10 µL per 100 mL. Gels were poured into a 12 x 15 cm gel tray containing a lane comb and allowed to set. DNA samples were mixed 5:1 with gel loading buffer. Gel loading buffer was made up as a 6x stock with 0.25% (*w/v)* bromophenol blue, 0.25% (*w/v)* xylene cyanol, 40% (w/v) sucrose in H_2O. Samples containing 1 kb and 100 bp DNA ladders were included for comparison. Gels were electrophoresed in 1x TAE buffer at 100 volts for approximately 1 hour. Gels were imaged using a UV transilluminator (Syngene).

2.2.5 Preparation of Plasmids

For small scale DNA preparation, 10 mL of LB with appropriate antibiotics was inoculated with a single colony and incubated overnight (37 °C, 200 rpm). A cell pellet was obtained by centrifugation (4000 rpm, 10 minutes) and the QIAprep Spin Miniprep Kit (QIAGEN, UK) or Wizard Plus SV Minprep Kit (Promega, UK) was used as per manufacturer's instructions. DNA concentrations were obtained using a Nanodrop 2000 (Thermo Fisher Scientific, UK).

2.2.6 Sequencing

DNA sequencing was carried out by Beckman Coulter Genomics or Genewiz. The standard T7 promotor forward and reverse primers were used for sequencing

all pET vectors. For other vectors, or where these did not provide sufficient coverage, primers were designed to sequence the regions of interest.

2.2.7 Growth media

E.coli cells were grown in lysogeny broth (LB) (Miller) medium (VWR) at a concentration of 25 g/L. Medium was autoclaved for 20 minutes at 120 ºC and supplemented with antibiotics when cooled to room temperature. Antibiotics were made up as 1000x stock as follows: carbenicillin (100 mg/mL in sterile H_2O), kanamycin (50 mg/mL in sterile H_2O), chloramphenicol (25 mg/mL in 100% ethanol). These were filter sterilised prior to addition to LB.

For solid agar plates 25 g/L of LB and 15 g/L of agar were autoclaved for 20 minutes at 120 ºC. On cooling to ~50 ºC antibiotics were added to working concentration and 20-25 mL poured into sterile Petri dishes.

For expression of the BAM complex using pZS21, 2xTY medium was used, prepared as follows:

- 16 g Bacto-tryptone (Fisher Scientific)
- 10 g Yeast extract (Fisher Scientific)
- 5 g NaCl (Fisher Scientific)

This was made up to 1 L with dH_2O and autoclaved as described above. For expression medium, antibiotics were added immediately prior to inoculation.

2.3 Protein Expression

2.3.1 Expression of BamA, tOmpA and OmpT

All OMPs were expressed as described[288]. Briefly, the relevant plasmid was transformed into *E.coli* BL21[DE3] cells using the appropriate selectable marker. Single colonies were then used to inoculate starter cultures in 5-10 mL LB, which were grown overnight (37 ºC, 200 rpm) with 100 µg/mL carbenicillin. The cultures were diluted 1 in 100 into 500 mL fresh LB medium containing 100 µg/mL carbenicillin at 37 °C with shaking (200 rpm). Expression was induced with a final concentration of 1 mM Isopropyl β-D-1-thiogalactopyranoside (IPTG in dH_2O) when the culture reached an OD_{600} of 0.5-0.6, and cells were then harvested after 4h by centrifugation (5000 *g*, 15 min, 4 °C) and stored at -20 °C. Cells were

resuspended in 20 mL 50 mM Tris-HCl, pH 8.0, 5 mM EDTA, 1 mM phenylmethylsulfonyl fluoride (*PMSF*), 2 mM benzamidine (from 100x stock of both in ethanol), and lysed by sonication (6 x 1 min bursts with 1 min cooling on ice between each sonication). The insoluble fraction was collected by centrifugation (25000 *g*, 30 min, 4 °C), resuspended in 20 mL 50 mM Tris-HCl, pH 8.0, 2% (*v/v*) Triton-X-100 and incubated for 1 h at room temperature, with gentle agitation. The insoluble fraction was again pelleted (25000 *g*, 30 min, 4 °C) and the inclusion bodies washed twice by resuspension (50 mM Tris-HCl, pH 8.0), incubated for 1 h at room temperature with gentle agitation, followed by centrifugation (25000 *g*, 30 min, 4 °C). The inclusion bodies were solubilised in 25 mM Tris-HCl, 6 M Gdn-HCl, pH 8.0 and centrifuged (20,000 *g*, 20 min, 4 ºC). The supernatant was filtered (0.2 µM PVDF syringe filter, Sartorius, UK) and purified first by nickel affinity and then gel filtration or just the latter for OMPs without a His-tag (HT). For HT-OmpT, the supernatant was applied to a pre-equilibrated 5 mL HisTrap column (GE Healthcare). The column was washed with 25 mM Tris-HCl, 6 M Gdn-HCl, pH 8.0 with 20 mM imidazole, and protein eluted with buffer containing 500 mM imidazole. Fractions containing protein were then pooled and concentrated. Pooled protein (or non-purified supernatant, for those without a HT) were applied to a Superdex 75 HiLoad 26/60 column (GE Healthcare, UK) (tOmpA and OmpT), or a Sephacryl S200 26/60 (GE Healthcare) (BamA), equilibrated with 25 mM Tris-HCl, 6 M Gdn-HCl, pH 8.0. Peak fractions were concentrated to ~500 µM using Vivaspin 20 concentrators (Sartorius, UK) (5 kDa MWCO for tOmpA, 10 kDa for OmpT and 30 kDa for BamA), snap-frozen in liquid nitrogen, and stored at -80 °C. OMPs were typically buffer exchanged into 8 M urea, 50 mM glycine pH 9.5 or 8M urea, 20 mM Tris, 150 mM NaCl using Zeba spin desalting columns (Thermo Scientific, UK) prior to use.

2.3.2   Determination of protein concentration

Protein concentration was determined spectrophotometrically for all OMPs using their absorbance at 280 nm, in urea immediately prior to use. Theoretical molar extinction coefficients at 280 nm, calculated using the ExPASy Protparam server[289], are shown in Table 2-1.

2.3.3 Expression of His-tagged (HT)-Skp and HT-SurA

HT-Skp (expressed and purified by B. Schiffrin) and HT-SurA were purified using a protocol adapted from Burmann et al[181]. The pET28b plasmid, containing the Skp/SurA gene with an N-terminal 6xHis-tag and thrombin cleavage site, was transformed into *E.coli* BL21[DE3]pLysS cells. Single colonies were used to inoculate a starter culture. Following inoculation with 10 mL of starter culture (LB, supplemented with 50 µg/mL kanamycin and 25 µg/mL chloramphenicol), cells were grown in 2x 1L LB medium containing kanamycin and chloramphenicol at 37 °C with shaking (200 rpm) until the culture reached an OD_{600} of ~0.6. The temperature was then lowered to 20 °C and expression induced with 0.4 mM IPTG. Following overnight expression (~18 h) cells were harvested by centrifugation, resuspended in 25 mM Tris-HCl, pH 7.2, 150 mM NaCl, 20 mM imidazole, containing a cocktail of EDTA-free protease inhibitors (Roche), and lysed using a cell disrupter (Constant Cell Disruption Systems, UK). Following centrifugation to remove cell debris (20 min, 4 °C, 39000 g), the lysate was applied to a 5 mL HisTrap column (GE Healthcare) and washed with 25 mM Tris-HCl, pH 7.2, 150 mM NaCl, 20 mM imidazole. The protein was denatured on-column with 25 mM Tris-HCl, 6 M GuHCl, pH 7.2, and eluted with a 0-500 mM imidazole gradient over 50 mL in 25 mM Tris-HCl, 6 M GuHCl, pH 7.2. Fractions containing pure protein were pooled and the protein refolded by dialysis against 25 mM Tris-HCl, pH 7.2, 150 mM NaCl. Refolded His-tagged Skp was concentrated to ~50 µM (trimer) using Vivaspin 20 (5 kDa MWCO) concentrators (Sartorius, UK), aliquoted, snap-frozen in liquid nitrogen and stored at -80 °C. Skp has a very low molar extinction coefficient at 280 nm (1490 M^{-1} cm^{-1}) as its sequence contains no tryptophan residues, and only one tyrosine residue. Skp concentrations were determined using a Pierce bicinchoninic acid (BCA) assay (ThermoFisher), according to the manufacturer's instructions (2.3.9). Refolded His-tagged SurA was further dialysed into 50 mM Glycine NaOH pH 9.5 and concentrated to ~200 µM using Vivaspin 20 (10 kDa MWCO) concentrators (Sartorius, UK).

SurA variants SurA-ΔP2 and SurA N-Ct were generated by Julia Humes (University of Leeds) using HT-SurA in a pET28b plasmid. These were generated by removal of the P2 domain (residues 282-389) yielding ΔP2, and subsequent additional deletion of the P1 domain (residues 172-281), generating the N-Ct

variant. These were carried out by Q5-site-directed mutagenesis. The proteins were purified as for wild-type, and their properties are given in Table 2-1.

2.3.4 Expression of HT-SecB

E.coli BL21(DE3) cells were transformed with pRFSDuet-1 containing His-tagged SecB. Single colonies were used to inoculate 100 mL starter cultures (LB with 50 µg/mL kanamycin). After overnight growth (37 °C, 200 rpm) starter cultures were diluted 1/100 into 1 L TY broth containing 50 µg/mL kanamycin. Cells were grown (37 °C, 200 rpm) to OD_{600} of 0.6 and expression induced with 1 mM IPTG for 3 hours before cells were harvested by centrifugation.

The cells were resuspended and homogenized in 10 mL/L 20 mM Tris, 50 mM KCl, pH7.5, lysed with a cell disruptor (Constant Cell Disruption Systems, UK), then centrifuged (39000 g, 20 min, 4 ºC). The supernatant was filtered and applied to a 5 mL Histrap column pre-equilibrated with 20 mM Tris, 50 mM KCl, pH 7.5. The column was washed with 20 mM Tris, 50 mM KCl, 50 mM imidazole, pH 7.5, the protein was eluted with 20 mM Tris, 50 mM KCl, 330 mM imidazole pH 7.5. Protein was dialysed overnight against 20 mM Tris, 50 mM KCl at 4 ºC to remove imidazole, concentrated and further purified on a HiTrap Q HP column with a gradient of 50- 1000 mM KCl in 10 column volumes over a 20 mL bed volume.

2.3.5 Expression and purification of BamABCDE wild-type and variants in n-dodecyl-β-D-maltoside (DDM)

The complete BamABCDE complex was expressed and purified using a protocol adapted from Roman-Hernandez et al[274]. *E.coli* BL21(DE3) cells were transformed with plasmid pJH114 (see Table 2-1) containing all five Bam genes (BamABCDE-HT) and grown overnight (37 °C, 200 rpm) in LB containing 100 µg/mL carbenicillin. Cells were diluted 1:100 into fresh TY broth with the same antibiotic selection and grown (37 °C, 200 rpm) to an OD_{600} of 0.5-0.6 before addition of 0.4 mM IPTG to induce expression. Following 1.5 h expression, cells were harvested with a Beckman JLA-8.1000 rotor (4000 rpm, 15 min, 4 ºC). The cell pellet was resuspended and homogenised in 10 mL/L 20 mM Tris-HCl pH 8,

lysed with a cell disruptor (Constant Cell Disruption Systems, UK), then centrifuged (6000g, 10 min, 4 ºC). The supernatant was ultracentrifuged with a 50.2Ti rotor (244280 g, 45000 rpm, 30 min, 4 °C) to pellet membranes. Pelleted membranes were incubated with 10 mL/L cold 50 mM Tris-HCl pH 8, 150 mM NaCl, 1% (*w/v*) DDM at 4 ºC for 2 h and the ultracentrifugation repeated to remove insoluble material. Supernatants were then incubated overnight at 4 °C with 2 mL/L Ni-NTA agarose on a tube roller. Ni-NTA beads were washed with one column volume of TBS, 0.05% (*w/v*) DDM, 50 mM imidazole and BamABCDE was eluted using two column volumes of TBS, 0.05%(*w/v*) DDM, 500 mM imidazole.

The protein was concentrated to ~10 mg/mL, using a Vivaspin concentrator and further purified by gel filtration chromatography using an Analytical Superdex200, 10/300 GL column, equilibrated with TBS + 0.05 % (*w/v*) DDM running at 0.5 mL/min. 0.5 mL fractions were collected and those containing complete BamABCDE complexes were identified by SDS-PAGE, pooled and concentrated. Protein concentration was determined using the Pierce BCA Protein Assay according to the manufacturer's instructions (Section 2.3.9). The purified BamABCDE complex was concentrated to 10-15 mg/mL, flash frozen in liquid N_2, and stored at -80 ºC.

BamABCDE complexes containing BamA variants were prepared using Q5 Site-Directed Mutagenesis (NEB) kit following the manufacturer's instructions to create the Cys-free $C_{690}S/C_{700}S$ pseudo-wild-type, followed by single rounds of mutagenesis for each subsequent mutation, see Table 2-3 for primer details.

2.3.6 Expression and purification of BamABCDE in Triton X-100

Purification of BamABCDE was also initially performed in Triton X-100, as described in Roman-Hernandez *et al*[74]. In this protocol LB rather than TY broth was used for growth. In addition, during protein purification using Ni-NTA agarose resin in batch mode, the resin was washed with TBS+ 0.03% (*w/v*) DDM and the complex eluted in TBS+ 0.5% (*w/v*) Triton X-100. Gel filtration was carried out as above, however after this step, protein was concentrated to only ~1 mg/mL as yields of less than 1 mg per litre of culture grow were obtained.

2.3.7 BAM complex expression trials

Small-scale expression trials were carried out to optimize protein expression. Briefly, plasmid pJH114 was transformed into *E.coli* BL21(DE3) cells or the specific cell line HBD150 (MC4100 *ompT::spc ΔaraBAD leuD::kan*). Single colonies were used to inoculate starter cultures of 10 mL LB with 100 μg/mL carbenicillin and overnight cultures were diluted 1:50 in 100 mL of fresh LB or TY broth, containing 100 μg/mL carbenicillin. Cells were grown (37 °C, 200 rpm) to an OD_{600} of 0.5-0.6 before addition of 0.4 mM or 1 mM IPTG to induce expression. 1 mL cell samples were taken pre-induction and at various later time points, cells were diluted to the same cell density, boiled with loading buffer and analysed by SDS-PAGE(2.6.1).

2.3.8 Expression and purification of MSP1D1

Membrane Scaffold Proteins were prepared by Dr Anton Calabrese (University of Leeds) for use in nanodiscs. Briefly, *E.coli* BL21 (DE3) cells were transformed with pET28a containing His-tagged MSP1D1. Single colonies were used to inoculate 100 mL starter cultures (LB with 50 μg/mL Kanamycin). After overnight growth (37 °C, 200 rpm) starter cultures were diluted 1/100 into 1 L LB containing 50 μg/mL Kanamycin. Cells were grown (37 °C, 200 rpm) to OD_{600} of 0.6 and expression induced with 1 mM IPTG for 3 hours before cells were harvested by centrifugation.

The cells were resuspended in 15 mL/L 20 mM phosphate buffer pH 7.4 containing 1 mM PMSF. Following resuspension, 5 mg of deoxyribonuclease I was added and Triton X-100 was added to a final concentration of 1% (v/v). The cells were homogenised and lysed by sonication (6 x 1 min bursts with 1 min cooling on ice between each sonication). The lysate was centrifuged (30000 g, 10 min, 4 ºC). The supernatant was applied to a 5 mL Histrap column pre-equilibrated with 20 mM phosphate buffer, pH 7.4. The column was washed with ~100 mL each of Buffer 1 (40 mM Tris-HCl, 0.3 M NaCl, 1 % (v/v) Triton X-100, pH 8), Buffer 2 (40 mM Tris-HCl, 0.3 M NaCl, 50 mM sodium cholate, 20 mM imidazole, pH 8), Buffer 3 (40 mM Tris-HCl, 0.3 M NaCl, 50 mM imidazole, pH 8) before elution with 25 mL 40 mM Tris-HCl, 0.3 M NaCl, 0.4 M imidazole. The sample was dialysed against 20 mM Tris-HCl, 0.1 M NaCl, 0.5 mM EDTA pH 7.4

overnight at 4⁰. Protein was concentrated, filtered and snap-frozen in liquid N_2 for storage at -80 ⁰.

In some cases the HT was cleaved from MSP1D1 (for example for use with BAM where BamE also posseses a His-tag). For this the purified protein was dialysed against 20 mM Tris-HCl, 100 mM NaCl pH 8 overnight at 4 ⁰C. His_6-TEV was added to the protein at 1:50-1:100 (w/w) concentration and incubated at 4 ⁰C overnight. This was then applied to a 5 mL HisTrap column pre-equilibrated with 40 mM Tris-HCl, 0.3 M NaCl, pH 8 and recirculated over the column several times. The cleaved His_6 tag and His_6-TEV binds the column and the flow-through contains cleaved MSP1D1, which was concentrated, filtered and snap-frozen in liquid N_2 for storage at -80 ⁰.

2.3.9 Determination of BAM protein concentration by Pierce BCA Protein Assay

The protein concentrations of purified BAM complex, proteoliposomes created by dialysis (Section 2.10.2), SMALPs and nanodiscs were measured using the Pierce BCA Protein Assay (ThermoFisher). Briefly, using the 2 mg/ml Albumin (BSA) provided, a series of 10 standards from 0 µg/mL – 2000 µg/mL BSA were prepared in the buffer of choice. This included TBS (50 mM Tris, 150 mM NaCl pH 8), TBS+ 0.05 % DDM, 50 mM glycine-NaOH pH 9.5, or TBS + 10% glycerol to match the sample to be measured. The sample was diluted in the same buffer to be within the 25 – 2000 µg/mL range. Using a clear-bottom 96-well plate, 25 µL of each standard and sample (usually in triplicate) was added to 200 µL of working reagent. The plate was covered, incubated at 37 ⁰C for 30 minutes and absorbance at 562 nm was measured on the Clariostar. The average blank-corrected measurement for the standards provides a standard curve when plotted against protein concentration. This was then used to determine BAM concentration.

2.4 Mass Spectrometry (MS)

All mass spectrometry experiments detailed in this thesis were carried out by Dr Anton Calabrese (University of Leeds).

2.4.1 Non-covalent (MS)

Non-covalent MS was carried out on the BAM complex purified in TBS + 0.05 % (*w/v*) Triton X-100 for verification of intact mass. The purified BAM complex was buffer exchanged into 200 mM ammonium acetate, 0.02% (v/v) Triton X-100 pH 6.9 using Zeba spin desalting columns (Thermo Scientific, UK) immediately before MS analysis. Nanoelectrospray ionization–MS spectra were acquired using a Synapt HDMS hybrid quadrupole–travelling wave–time-of-flight mass spectrometer (Waters Corporation, UK) using in-house prepared platinum/gold-coated borosilicate capillaries. Typical instrument parameters included the following: capillary voltage 1.2–1.6 kV, cone voltage 120 V, trap collision voltage 60 V, transfer collision voltage 10 V, trap DC bias 20V and backing pressure 7 mBar. Data were processed using MassLynx v4.1, (Waters Corporation, UK) and UniDec[290].

2.4.2 Denaturing MS for molecular mass determination

Denaturing mass spectrometry was carried out on wild-type BAM complex (Section 3.2.2) in TBS + 0.05% (w/v) DDM. Purified BAM complex was precipitated by chloroform–methanol to minimize detergent contamination. For this a sample of protein (50 µL, 10 µM) was taken, and methanol (150 µL) and chloroform (50 µL) were added. The solution was mixed by vortexing, water (100 µL) was then added and the solution was mixed again before centrifuging (10,000 g, 2 min). The upper aqueous phase was removed (leaving the white protein pellet and the lower organic phase) and methanol (150 µL) was then added. The solution was mixed by vortexing, centrifuged (10,000 g, 2 min) and the supernatant removed. The precipitated protein was air dried in a laminar flow hood. The dried protein pellet was resuspended in formic acid (4 µL) and 18 MΩ H_2O (Purite) was then added (46 µL) for subsequent MS analyses. Proteins were analysed intact using online desalting liquid chromatography–MS on a nanoAcquity LC system interfaced to a Xevo G2-S mass spectrometer (Waters

Ltd., Wilmslow, Manchester, UK). The sample (2 µL) was loaded onto a MassPREP protein desalting column (Waters Ltd, Wilmslow, Manchester, UK), which was washed with 2% (v/v) solvent B in solvent A (solvent A was 0.1% (v/v) formic acid in water, solvent B was 0.1% (v/v) formic acid in acetonitrile) for 5 minutes at 40 µL/min. After valve switching, the bound proteins were eluted using a fast gradient of 2-40% (v/v) solvent B in A over 1 minute at 0.5 µL/min. The column was subsequently washed with 95% (v/v) solvent B in A for 6 minutes and re-equilibrated with 5% (v/v) solvent B in solvent A for the next injection. The column eluent was infused into a Xevo G2-S mass spectrometer (Waters Ltd, Wilmslow, Manchester, UK). Data were processed using MassLynx v4.1, (Waters Corporation, UK) and UniDec[290].

2.5 Electron microscopy

All electron microscopy in this thesis, discussed in Section 3.3 was carried out by Dr Matthew Iadanza. Analyses of structures was carried out by Dr Matthew Iadanza with assistance from Dr Bob Schiffrin (both University of Leeds).

Purified BAM complex in TBS with 0.05% (*w/v*) n-dodecyl β-D-maltopyranoside (DDM) at a concentration of 13 mg/mL was diluted 1:2 in the same buffer. A 4 µL aliquot of solution was applied to a quantifoil r3.5/1 EM grid (Quantifoil Micro Tools), allowed to incubate at room temperature and 95% humidity for 30 s, then manually blotted with a Whatman filter paper. A second 4 µL aliquot of BAM solution was added and the grid blotted and vitrified by plunging into liquid ethane using a Leica EM GP plunge freezer (Leica Microsystems).

The grids were imaged on a Titan Krios electron microscope (FEI Corporation) operating at 300 kV. Seven thousand and five hundred micrographs with a nominal defocus range of 1.5–3.5 µM were recorded with a Gatan K2 Summit energy-filtered direct detector (Gatan, Inc.) as 20 frame movies with a total electron dose of ~40e/Å^2. The sampling rate was 1.04 Å per pixel.

2.5.1 Image processing

Individual micrograph frames were combined into stacks using IMOD[291] and drift corrected using Motioncorr[292]. Individual particles were windowed manually using EMAN2[293] and automatically using Relion[294]. The raw particle set (472,857 particles) was culled through repeated cycles of two- and three-dimensional

classification using Relion[295]. The vast majority of these discarded particles were incorrectly picked by the automatic particle picking algorithms required to deal with a data set consisting of ~7,200 individual micrographs. These 'junk particles' represented carbon, ice contamination and a small amount of aggregated protein material. A total of ~120,000 particles were identified as BAM and after further classification, a total of 95,878 particles were used for structural analysis. Following alignment and three-dimensional reconstruction, the final structure was generated after performing per-particle motion correction on individual micrograph frames[296] and post-processed using Relion. Frames 4–14 of the original micrographs were used for the final reconstruction, for a total dose of 20 e/ Å^2. The local resolution of the final map was calculated using resmap[297] and it was then filtered by local resolution using LocalFilt. The final resolution was determined by 'gold standard' Fourier shell correlation of two independent half maps.

2.5.2 Atomic model fitting

An initial model of the BAM–ABCDE complex was constructed by manually fitting BAM subunits from previously published crystal structures to the EM density using UCSF Chimera[298]. BamA was constructed from 5D0Q[208] and 5D0O[208]. BamC and BamD were taken from 5D0Q[208], BamE from 5D0O[208] and BamB constructed from 3Q7O[299] and 2YH3[195]. Selenomethionines in each model were replaced with methionine. The initial model was then refined by flexible fitting to the EM density using MDFF[300] and Monte Carlo simulations with RosettaEM[301].

2.5.3 Analysis of angles between BamA POTRA domains

To calculate angles between *E. coli* BamA POTRA domains in all available structures, an arbitrary point within the loop on either side of each POTRA domain was identified. These same points in all X-ray and EM structures were the Cα atoms of F24, T93, A175, Y266, N345 and R421. The angles between each pair of POTRA domains were then calculated by placing three of these points on a plane. For example, the angle between POTRA 2 and POTRA 3 was calculated as the in-plane angle for T93-A175-Y266, the three spheres shown in the figure (Figure 3-10). This is 120º for the EM structure.

2.6 Gel electrophoresis

2.6.1 SDS gel electrophoresis

Electrophoresis was typically carried out with Tris-Tricine buffered SDS-PAGE gels (Table 2-6) made the day before use, using a 2x loading buffer (50 mM Tris-HCl pH 6.8, 2 % (*w/v*) SDS, 0.1 % (*w/v*) bromophenol blue, 10 % (*v/v*) glycerol).

Reagent	Resolving gel volumes (ml)	Stacking gel volumes (ml)
30% (*w/v*) acrylamide:0.8% (*w/v*) *bis*-acrylamide	7.5	0.83
3 M Tris, 0.3% (*w/v*) SDS (pH 8.45)	5.0	1.55
H_2O	0.44	3.72
Glycerol	2.0	-
10% (*w/v*) ammonium persulphate	0.1	0.2
N,N,N',N'-tetramethyl-ethylenediamine (TEMED)	0.01	0.01

Table 2-6: Volumes of reagents for Tris-Tricine buffered SDS-PAGE gels. The volumes indicated are sufficient to cast two 8 cm by 10 cm mini-gels using a 1.5 mm spacer.

For these gels, TEMED was added last immediately prior to pipetting of first the resolving, then stacking gels in the casting apparatus. The stacking gel was poured carefully on top of the resolving gel. After addition of loading buffer, the samples were boiled briefly before 20 µL was loaded on the gel. Precision Plus Protein™ Dual Xtra Standards (Bio-Rad, UK) were loaded into one lane to aid size determination and identification of protein bands. Gels were electrophoresed with the inner reservoir of the gel tank containing cathode buffer (100 mM Tris, 100 mM tricine, 0.1% (*w/v*) SDS, pH 8.25) and the outer reservoir containing anode buffer (200 mM Tris-HCl, pH 8.8). Electrophoresis was typically carried out with a constant current of 30 mA, or 70 mA through the stacking and resolving gels, respectively.

Following electrophoresis gels were stained with Instant Blue stain (Expedeon, UK) and imaged using the Syngene gel documentation system (Syngene, UK).

When appropriate (folding into DMPC liposomes, tOmpA assay), bandshift assays were repeated three times and quantified. The folding yield was quantified

using ImageJ[302], by analysis of each band within a lane according to Equation 2-1).

$$Fraction\ folded = \frac{folded\ band\ intensity}{(folded+unfolded)band\ intensities}$$ **Equation 2-1**

2.6.2   Semi-native PAGE and "low SDS"

Analysis of the differential migration of heat-treated (unfolded) and non-heat-treated (folded) OMPs in order to quantify folding yield can normally be carried out on any gel electrophoresis system. For BamA semi-native PAGE is necessary. For this, "low SDS" conditions were used: the Tris resolving gel buffer contained no SDS and loading buffer (2x) was 50 mM Tris-HCl pH 6.8, 0.1 % (*w/v*) SDS, 0.1 % (*w/v*) bromophenol blue, 10 % (*v/v*) glycerol. After allowing sufficient time for protein folding boiled samples were heated to 100 °C for a minimum of 30 minutes with loading buffer, while "unboiled" samples were added to sample loading buffer and immediately loaded on the gel. For the semi-native PAGE electrophoresis the gels were run using a constant current of 10 mA overnight at 4 °C.

2.6.3   Redox gels

In order to determine the redox status of BamA variants in different conditions, a number of different gel types were surveyed to resolve BamA with and without intramolecular cross-links. These include precast 4-20%(*w/v*) polyacrylamide gradient Mini-PROTEAN gels (BioRad), used with Tris-Glycine running buffer, precast 4-20%(*w/v*) polyacrylamide gradient Midi gels (Novex) with Novex Tris-Glycine buffer or 5% Tris-Tricine gels run with MOPS buffer. The latter were found to yield the high resolution between oxidized and reduced variants. Electrophoresis of all gels was carried out at 4 °C. Analysis by Tris-Tricine gels is detailed below (Table 2-7), other gels were used according to the manufacturers instructions.

To visualize the proteins, folding reactions were performed using 2 µM BamA, 1600:1 LPR (lipid: protein ratio), 0.24 M urea in 50mM glycine-NaOH pH 9.5. Folding reactions were allowed to proceed in the correct conditions (2 hours at

69

25 °C for DUPC lipids, overnight at 30 °C for DMPC). Reducing/oxidizing agents were then added to the correct final concentrations (25 mM tris(2-carboxyethyl)phosphine (TCEP), 1 mM Copper(II) Sulphate (CuSO$_4$), 25 mM dithiothreitol (DTT) or 100 µM diamide) and allowed to incubate for a minimum of 30 minutes at the required folding temperature. Half of each sample was mixed with 6x or 2x loading buffer containing 0.1 % or 0.6% SDS and boiled for 30 minutes, while the rest was mixed with loading buffer immediately prior to gel loading.

Where it was desired to visualise the redox state of BamA in the BAM complex, in either TBS + 0.05% DDM, or proteoliposomes these were diluted to a concentration of 1-2 µM with or without redox agents. Proteins were incubated with redox agents for an hour, 15 µL sample added to 5 µL 6x loading buffer containing 0.6 % SDS and boiled for 30 minutes. A variety of redox agents were used. Typically these were DTT (at 25 mM final concentration), diamide (at 100 µM final concentration) or CuSO$_4$ (at 1 mM final concentration). Additionally diamide, CuSO$_4$, iodine and aldrithiol (4,4'-dypyridyl-disulphide or 4-DPS) were assessed at concentrations 1 (4 µM), 2 (10 µM) 3 (40 µM), 4 (100 µM), 5 (1 mM), 6 (10 mM). Any alterations to conditions are noted in the main text.

For Tris-Glycine gels the resolving gel must be poured, allowed to set and then stacking gel added. For redox states of BamA, 15 µL was loaded for each sample and the gels were electrophoresed with MOPS buffer for 3 hours at 30 mA at 4 °C.

Reagent	Resolving gel Volume to add (mL)	Stacking gel Volume to add (mL)
30% (*w/v*) Acrylamide:0.8% (*w/v*) *bis*-acrylamide	2.5	0.83
H$_2$O	8.4	3.4
1.5 M Tris.HCl pH 8.8	3.8	-
1 M Tris.HCl pH 6.8	-	0.63
10% (*w/v*) SDS	0.15	0.05
10% (*w/v*) ammonium persulphate	0.15	0.05
TEMED	0.006	0.005

Table 2-7: Volumes of reagents for 5% Tris-Glycine buffered SDS-PAGE gels. The volumes indicated are sufficient to cast two 8 cm by 10 cm mini-gels using a 1.5 mm spacer.

2.6.3.1 BAM complex reduce-then-oxidize experiment

An additional experiment was carried out to determine whether the BAM complex variants could be oxidized. Protein for each variant (Lateral-lock1, Lateral-lock2 and Lid-lock) was diluted in TBS + 0.05% (*w/v*) DDM to 4 µM, with addition of DTT to 50 mM and incubated for 1 hour at room temperature. Nickel beads were prepared by washing with ddH20, TBS+DDM, TBS+DDM + 50 mM imidazole and again with TBS + DDM. These were mixed 1:1 with sample (total volume 80 µL) and incubated at 4 °C for 30 minutes with gentle agitation. The nickel beads were centrifuged and washed 4x with TBS + DDM, resuspended in 40 µL TBS +DDM + 200 µM diamide and incubated 45 minutes at room temperature. Samples were taken pre- and post- DTT treatment, of the first wash and of the final nickel beads. This was mixed with SDS loading buffer, boiled for 15 minutes and analysed by redox gel, 5% (*w/v*) acrylamide SDS-PAGE.

2.6.4 Native PAGE

Native PAGE was carried out to assess the intact state of the BAM complex in detergent, proteoliposomes, nanodiscs and SMALPs. Precast Invitrogen NativePAGE 4-16 % Bis-Tris gels were used according to the manufacturer's instructions. Approximately 10 µg of sample was mixed with 4x sample buffer and 10 µL loaded as well as 5 µL Native Mark Standard (LifeTechnologies). Electrophoresis was carried out at 150 V for 120 minutes at room temperature. Quick Coomassie staining was carried out of Native PAGE. The gels were placed in 100 mL of fixing solution (40% methanol, 10% acetic acid), microwaved for 45 seconds and shaken for 15 minutes. The process was repeated with 100 mL of destain (8% acetic acid) and shaken until bands are visible, after which the gel was washed in dH_2O.

71

2.7 Preparation of LUV liposomes

The lipids 1,2-diundecanoyl-*sn*-glycero-3-phosphatidylcholine (DUPC hereafter), 1,2-didecanoyl-*sn*-glycero-3-phosphoethanolamine (DDPE hereafter) and 1,2-dimyristoyl-*sn*-glycero-3-phosphatidylcholine (DMPC hereafter) (all purchased from Avanti Polar Lipids, AL, USA) were used in the course of this work, (see 2.17 for table of all lipids). Lipids were dissolved in 80:20 (*v/v*) HLPC grade chloroform:methanol in glass test tubes. Solvent was then removed by drying under a gentle stream of N_2, followed by further drying in a desiccator under high vacuum for > 3 h. Where mixed DUPC:DDPE (80:20 molar ratio) liposomes were required, the appropriate volumes of 25 mg/mL DUPC and 15 mg/mL DDPE lipids were mixed in their lipid solvated phase, prior to drying.

The resulting thin lipid film was resuspended in buffer (50 mM glycine, pH 9.5) to give a 40 mM lipid suspension, vortexed briefly and left to stand at room temperature for 30 min, before vortexing again. The large multilamellar vesicles that formed were disrupted by five freeze-thaw cycles. 100 nm Large Unilamellar Vesicles (LUVs) were prepared by extruding the lipid mixtures eleven times through a 0.1 µM polycarbonate membrane (Nucleopore, Whatman, Clifton, NJ) using a mini-extruder (Avanti, Alabaster, AL, USA) as described previously[72]. Where DMPC lipids were used, extrusion was carried out at 37 °C to maintain these lipids above the phase transition temperature, and in the liquid phase. All LUVs were stored at 4 ºC immediately following extrusion and used within a week.

2.8 Protein Analysis

2.8.1 Fluorescence Emission Spectra

Fluorescence emission spectra were measured using a Photon Technology International Fluorimeter (Ford, West Sussex, UK). BamA samples contained 0.8 µM BamA protein, 1.28 mM DUPC (molar LPR 1600:1), and 0.24 M urea in 50 mM glycine buffer, pH 9.5 for folded samples, or 0.8 µM BamA protein in 8 M urea, 50 mM glycine buffer, pH 9.5 for unfolded samples. Samples were folded by incubation at 25 °C for two hours prior to measurement. Each spectrum was

recorded from 280 nm to 400 nm in 1 nm increments, using an excitation wavelength of 280 nm.

Fluorescence emission spectra were additionally measured for tOmpA and OmpT variants, in studies of β-signal mutants. Here 0.4 µM protein was used, 1.28 mM DUPC (molar LPR 3200:1), and 2 M urea in 50 mM glycine buffer, pH 9.5 for folded samples, or 0.4 µM protein in 8 M urea, 50 mM glycine buffer, pH 9.5 for unfolded samples. Samples were folded by incubation at 25 °C overnight prior to measurement.

It is possible to use tryptophan fluorescence to study the folding state of a protein in LUVs, provided that certain conditions are followed[250]. An appropriate "blank" sample, containing no protein was subtracted from measurements to remove contributions due to light scattering by liposomes from the final spectra.

2.8.2   Circular Dichroism (CD)

Far-UV CD spectra were acquired on a Chirascan plus circular dichroism spectrometer (Applied PhotoPhysics) with a bandwidth of 2.5 nm, step size of 1 nm and a pathlength of 0.1 mm. Samples contained 0.8 µM BamA, 1.28 mM DUPC, and 0.24 M urea in 50 mM glycine buffer, pH 9.5 for folded samples, or 0.8 µM BamA protein in 8 M urea 50 mM glycine buffer, pH 9.5 for unfolded samples. Samples were incubated at 25 °C for two hours prior to measurement.

CD spectra were additionally measured for tOmpA and OmpT variants, in studies of β-signal mutants. For these 5 µM tOmpA/OmpT protein was used, 4 mM DUPC (molar LPR 800:1), and 2 M urea in 50 mM glycine buffer, pH 9.5 for folded samples, or 5 µM protein in 8 M urea, 50 mM glycine buffer, pH 9.5 for unfolded samples. Samples were folded by incubation at 25 °C overnight prior to measurement. The instrumentation was identical to as specified for BamA but a bandwith of 3.5 nm was used. In addition a temperature ramp was attempted for OmpT samples folded in DUPC. This was measured from 20- 90 ºC with a 1 ºC step and 120 seconds settling time for each reading.

The appropriate blank, of liposomes, or urea in glycine buffer was subtracted for each sample. The measured ellipticity in each wavelength was then converted to Mean Residue Ellipticity (MRE) by:

$$[\theta]_{MRE} = (MRW \times \theta_\lambda) / (10 \times d \times c) \qquad \text{(Equation 2-2)}$$

Equation 2-2: Calculating Mean Residue Ellipticity. Where $[\theta]_{MRE}$ is the MRE, θ_λ is the measured ellipticity at a particular wavelength, d is the pathlength in cm, and c is the concentration in g/mL and MRW is Mean Residue Weight. MRW given by: MRW = M / (N-1) where M is the molecular mass of the protein in Daltons and N is the number of amino acids it contains.

2.9 Kinetics of OMP folding determined by intrinsic tryptophan fluorescence

The kinetics of OMP folding was monitored by tryptophan fluorescence using a Photon Technology International Fluorimeter (Ford, West Sussex, UK). These experiments used a truncated form of OmpA, possessing only the transmembrane domain (residues 1-171, 18875 Da, tOmpA), as substrate and the chaperone protein Skp. Aliquots of both tOmpA and Skp were kindly provided by Bob Schiffrin, having been previously prepared and purified as detailed[288], see Methods 2.3.1 and 2.3.3.

Samples were made to a final concentration of 0.4 µM tOmpA, 1.28 mM lipid (molar LPR 3200:1 substrate), and 0.24 M urea in 50 mM glycine buffer, pH 9.5. Samples containing Skp had a two-fold molar excess of Skp trimer over tOmpA substrate, while BamA protein variants were used at a concentration of 0.8 µM of each BamA protein.

Unless otherwise indicated, samples were made up in the absence of tOmpA, and BamA (if included) was allowed to fold, for 2 hours at 25 °C. Denatured tOmpA in 8 M urea, 50 mM glycine buffer pH 9.5 was then added immediately prior to measurement. In experiments containing Skp, Skp was pre-incubated with tOmpA for 5 minutes as a 6x stock and the subreaction was then titrated into the reaction containing pre-folded BamA immediately prior to measurement.

Where oxidizing or reducing agents were used these were diluted to 10x working concentration in 50 mM glycine pH 9.5 buffer. For experiments with DUPC or DUPC:DDPE LUVs these were added prior to BamA folding, and at the following final concentrations in the reaction mixture: reducing agents Dithiothreitol (DTT 2 mM), 2-Mercaptoethanol (BME 20 µM), oxidizing agents Copper (II) Sulphate ($CuSO_4$ 100 µM), diamide (1 mM).

A timebased acquisition was used, with excitation wavelength of 280 nm, emission wavelength of 335 nm, slit widths 0.4 nm, 1 point/second and maximum duration 7200 seconds (2 hours). Four replicates were measured simultaneously. Results were analysed using Igor graphing programme (Wavemetrics) and fitted globally to either a single (Equation 2-3) or double (Equation 2-4) exponential function such that the transients share the same rate constant(s).

$$y = (A_1 * e^{-k_1 t}) + c \qquad \textbf{Equation 2-3}$$

$$y = (A_1 * e^{-k_1 t}) + (A_2 * e^{-k_2 t}) + c \qquad \textbf{Equation 2-4}$$

For experiments using DMPC lipids a similar approach was used as described above with the exceptions that BamA pre-folding reactions and measurements were carried out at 30 °C, and reactions were monitored for a maximum duration of 90,000 seconds (25 hours). Cuvettes and samples were incubated for a minimum of 20 minutes at 30 °C before measurement. In addition, where used, redox reagents were added to final concentrations of 25 mM DTT, 10 mM TCEP or 1 mM $CuSO_4$. These were added following BamA folding, for a minimum of 30 minutes with incubation at 30 °C before addition of tOmpA and measurement of folding by tryptophan fluorescence as described above. Due to difficulties with consistent fitting of exponential curves, the results were also analysed by extracting a t_{50} or time to reach 50 % of total fluorescence change. Each transient was independently analysed with a horizontal line fit to the final 10% of data containing the maximum fluorescence. A minimum of three repeats, in different liposome batches was carried out for each experiment, creating a total of 12 transients for an average t_{50}. Errors were calculated as the standard error of the mean. Error in fold change of t_{50} values for tOmpA-RHK experiments (Section 4.3) were calculated as follows:

$$\delta R = |R| \sqrt{\left(\frac{\delta X}{X}\right)^2 + \left(\frac{\delta Y}{Y}\right)^2} \qquad \textbf{Equation 2-5}$$

In Equation 2-5 δR is the error in fold change, $|R|$ is the fold change value, X and Y are the mean t_{50} values being compared and δX is the SEM value of that population.

2.10 Reconstitution of BAM complex into proteoliposomes

Three methods were used to reconstitute purified BAM complex into proteoliposomes. All utilise *E.coli* polar lipid extract solubilised at 25 mg/mL in 80:20 chloroform: methanol. In the first method ('dilution'), proteoliposomes were made by the method of dilution and ultracentrifugation following the method described by Roman-Hernandez *et al.*[274].

2.10.1   BAM proteoliposomes by dilution

Briefly, *E.coli* polar lipid extract phospholipids (Avanti Polar Lipids) were dessicated, resuspended in water at 20 mg/mL, sonicated, and 40 µL of the lipid suspension added to 200 µL of purified BamABCDE in TBS containing 0.05 % (*w/v*) DDM at 20 µM. This sample was incubated on ice for 5 minutes, then diluted with 4 mL of 20 mM Tris-HCl pH 8 and incubated for a further 30 minutes. Proteoliposomes were pelleted using a Beckman TLA 110 (50,000 rpm, 4 ºC, 30 min) and resuspended in 200 µL 20 mM Tris-HCl pH 8.

2.10.2 BAM proteoliposomes by dialysis

Alternatively, BAM complex was reconstituted into proteoliposomes using a procedure established for the outer-membrane protein FhuA ('dialysis')[257]. DDM-solubilized BamABCDE (0.3 mg) was mixed with *E. coli* polar lipid films solubilized in 200 µL of TBS + 0.05 % (*w/v*) DDM using a 1:0.5 (*w/w*) ratio of lipid to protein. This was placed into a 200 µL 12-14 kDa MWCO dialysis tube (D-tube dialyser mini, (Merck Millipore)) and dialysed against detergent-free buffer (20 mM Tris-HCl pH 8, 150 mM KCl, 0.01 % (*w/v*) sodium azide (dialysis buffer)) at 21 °C for 7 days.

To assess whether reconstitution was successful, the samples were centrifuged at 16000 *g*, the pellet resuspended in dialysis or experimental buffer and a sample of the protein-lipid pellet was boiled in SDS-containing loading buffer (50 mM Tris-HCl pH 6.8, 2 % (*w/v*) SDS, 0.1 % (*w/v*) bromophenol blue, 10 % (*v/v*) glycerol) for 10 minutes, whilst another sample was left unboiled. Samples were then analyzed by Tris-Tricine SDS-PAGE(Section 2.6.1). This showed that all five BAM complex proteins were associated with the liposome pellet, and also that BamA was folded, displaying increased electrophoretic mobility (a "bandshift") on boiling. Proteoliposomes created using this procedure resulted in the vast

majority of protein incorporated into the liposomes in marked contrast with the yields obtained using the dilution method.

Empty liposomes were made with 220 µL *E. coli* polar lipids solubilized in TBS + 0.05 % (*w/v*) DDM. For BamA-proteoliposomes, BamA in 8 M urea, 50 mM glycine-NaOH was folded by ~30-fold dilution into TBS containing 0.05 % (*w/v*) DDM, 3 M urea, and 0.3 mg was then reconstituted by dialysis into proteoliposomes as described for the BAM complex above. The folding of BamA into *E.coli* polar lipid liposomes was analyzed by low SDS-PAGE bandshift assays (Section 2.6.2)

2.10.3 BAM proteoliposomes using Biobeads

The third method utilized involved the generation of proteoliposomes using Biobeads to remove detergent, as described previously[278,303]. Briefly, *E.coli* polar lipid films were re-hydrated with water and sonicated for 10 minutes. The resuspended lipids were then diluted to 4 mg/mL in H_2O with 0.05% (*w/v*) DDM. The BAM complex, purified in TBS containing 0.05 % (*w/v*) DDM was diluted to ~ 1 mg/mL in TBS and 0.05% (*w/v*) DDM and 200 µL each of lipids and protein were mixed together. The suspension was incubated for 30 min at 4°C with gentle agitation. Meanwhile the Biobeads were prepared by washing twice with methanol, twice with ethanol, four times with distilled H_2O and twice with buffer: (TBS + 0.05% (*w/v*) DDM). All washes were done by resuspension and pelleting for 1 min at 13000 rpm in a bench-top centrifuge. The beads were resuspended in TBS containing 0.05 % (*w/v*) DDM to a final concentration of about 80 mg/mL, and 500 µL was added to the protein– detergent–phospholipid suspension. After 2 hours of incubation at 4 °C, the Bio-Beads were sedimented by a brief centrifugation in an Eppendorf centrifuge and discarded. The overlaying solution was then mixed with 40 mg of freshly washed Bio-Beads. After incubation at 4 °C for 4 h, the Bio-Beads were sedimented and the supernatant was mixed with 60 mg of fresh Bio-Beads. The mixture was finally incubated overnight at 4 °C. After sedimentation, the supernatant was collected, the Bio-Bead fraction was washed separately with 1 mL of 20 mM Tris pH 8, and the supernatants of both steps were pooled. Proteoliposomes were collected by ultracentrifugation with TLA110, 59000 rpm, 30 min, 4 °C. The liposomes were resuspended in 20 mM Tris pH 8.

2.11 Dynamic Light Scattering of BAM complex proteoliposomes

The BAM complex which had been reconstituted into *E.coli* polar lipid proteoliposomes by either dilution and ultracentrifugation or by extensive dialysis, was analysed by dynamic light scattering to assess the size distribution of the resultant proteoliposomes. Proteoliposome samples were diluted 1/120 (dilution method), or 1/60 (dialysis method). 250 µL of the samples were then injected into a Wyatt miniDawnTreos® system (equipped with an additional DLS detector) and the data analysed using Astra 6® software supplied with the instrument. Filtered (0.22 µm) and de-gassed Tris dialysis buffer was used to obtain baselines before and after sample injection. Data were plotted using Origin Pro® 8.6. DLS measures the fluctuation of scattered light as a function of time. The correlation function (Equation 2-6) determines the changes in light intensity over time.

$$g^2(\tau) = \frac{\langle I(t)I(t+\tau)\rangle}{\langle I(t)\rangle^2}$$

Equation 2-6: Correlation Function where I is intensity of scattered light, t is initial time, and $t + \tau$ is elapsed time, and brackets indicate an average over all t values.

The correlation function is based on delay т, amount the intensity trace shifts from the original prior to averaging. For a monodisperse sample, the correlation function is given in Equation 2-7:

$$g^2(\tau) = B + Ae^{(-2\Gamma\tau)}$$

Equation 2-7: B= baseline for correlation function at infinite delay, A is the correlation function amplitude at zero delay and Γ is the decay rate.

To find Γ a non-linear least squares algorithm must be fit to correlation function data. The diffusion coefficient for the particle can be found with Equation 2-8:

$$D = \frac{\Gamma}{q^2} \text{ where } q = \frac{4\pi n_0}{\lambda_0}\sin\left(\frac{\theta}{2}\right)$$

Equation 2-8: n_0 is the refractive index of the solvent, λ_0 is the vacuum λ (not in solution) of incident photon and θ is the scattering angle.

To determine the hydrodynamic radius of the particle the Stokes-Einstein Equation (Equation 2-9) is used:

$$D = \frac{kT}{6\pi\eta R_h}$$

Equation 2-9: Stokes-Einstein Equation for determining the hydrodynamic radius (R_h) of a particle using DLS. D = translational diffusion coefficient (cm^2 s^{-1}), k = Boltzmann's constant, T= absolute temperature and η = viscosity (kg $m^{-1}s^{-1}$).

Correlation function data can be fit to a single-exponential decay with Equation 2-10:

$$y = y_0 + Ae^{\frac{-(x-x_0)}{t}}$$

Equation 2-10: Single Exponential Decay equation fit to correlation function data. A is the amplitude, y_0 is the y axis intercept, x_0 is the x-axis intercept and t is time.

The correlation function assumes that the sample is monodisperse. In addition Cumulants and Regularisation analysis can be performed in the Astra software. The cumulants analysis will yield z-average (mean) radius and width (standard deviation of a solution. The values can be used to obtain a polydispersity index (Equation 2-11).

$$PDI = \frac{\sigma^2}{z^2}$$

Equation 2-11: The Polydispersity Index (PDI) is given by the width (standard deviation, σ) of the mean particle size (z-average radius, z) divided by the z-average radius squared.

Values giving a Polydispersity Index (PDI) greater than 0.7 are considered highly polydisperse, while those with a PDI lower than 0.1 are typically monodisperse. Regularisation analysis by the software determines the average hydrodynamic radii present. Plots of hydrodynamic radii are shown for each sample, where the

79

y-axis is the differential intensity fraction (log nm^{-1}) against the size of the species (nm) where values for the most intense peak (highest differential intensity fraction) are noted.

2.12 OmpT activity assays

For OmpT assays, HT-OmpT (or variant, as described) prepared according to Section 2.3.1 was buffer exchanged into 8 M urea, 50 mM Glycine-NaOH pH 9.5 prior to use. The fluoropeptide, Abz-Ala-Arg-Arg-Ala-Tyr(NO$_2$)-NH$_2$ (ARRAY) was ordered from PeptideSynthetics and resuspended in 18 mΩ H$_2$O to a 20x stock concentration. The fluorescence emission intensity following excitation at 325 nm was monitored at 430 nm with readings every 10 seconds for up to 5 hours using a Clariostar plate reader (BMG Labtech GmbH).

Following initial optimisation, urea concentrations, buffer and temperature were kept constant, as it was noted that these may impact results, and the fluorescence gain on the Clariostar was set, leading to more consistent total fluorescence. Where normalisation was necessary this was done by subtraction of the average background signal produced at the zero time point. A degree of variability is still seen in the fluorescence counts, however quantification was carried out by fitting a line to the final section of data, containing the maximum fluorescence and determining t_{50}, for which the fluorescent counts are therefore not relevant. Variability was also observed between proteoliposome preparations of the same BAM complex protein, with a narrow average distribution of t_{50}s but some significant outliers. In cases of outlying t_{50}s, comparisons are only made between conditions within the same experiment, and not included in general averaging.

2.12.1 Activity assays of wild-type and mutant BAM complexes

Following optimisation of proteoliposomes preparation and setup of OmpT assay the conditions for the OmpT assay were kept constant. The protein concentration of proteoliposomes prepared by extensive dialysis was determined by the Pierce BCA Protein Assay (Section 2.3.9) and diluted to a constant 3.5 µM. BAM complex proteoliposomes (0.5 µM) were incubated briefly with 2 mM of the fluoropeptide Abz-Ala-Arg-Arg-Ala-Tyr(NO$_2$)-NH$_2$ (Peptide Synthetics). Purified

OmpT denatured in 8 M urea, 50 mM glycine-NaOH at 100 µM was diluted 10-fold into solutions of 70 µM His$_6$-SurA in folding buffer (50 mM glycine-NaOH pH 9.5). Where concentrations of OmpT are altered these are diluted from a corresponding 10 x buffer stock, to maintain a constant urea concentration in the final assay. These SurA-OmpT solutions were mixed and instantly diluted two-fold into the proteoliposome-containing solutions. The final concentrations of the reaction components were 5 µM OmpT, 35 µM SurA, 0.25 µM BAM complex, and 1 mM fluorogenic peptide, 0.8 M urea, 50 mM glycine-NaOH pH 9.5. Assays were then performed on the Clariostar and analysed as described above.

2.12.2 BAM activity assay for dilution versus dialysis proteoliposomes

Resuspended proteoliposomes formed by dilution, with assumed BAM concentration of 10 µM were diluted two-fold into 50 mM glycine-NaOH, pH 9.5 containing 2 mM of the fluoropeptide Abz-Ala-Arg-Arg-Ala-Tyr(NO$_2$)-NH$_2$ (Peptide Synthetics). OmpT and SurA were then mixed to form a solution with final concentrations of 20 µM OmpT, 140 µM His$_6$-SurA in 50 mM glycine-NaOH pH 9.5, 1.75 M urea. This sample (SurA-OmpT 'subreaction') was then immediately diluted two-fold into proteoliposome-containing solutions to initiate the folding reaction. All OmpT folding reactions were carried out in 30 µL final reaction volume.

For proteoliposomes formed by dialysis, proteoliposomes were pelleted by centrifugation (16000 g, as above). The pellet was then resuspended in equal volume dialysis buffer to assumed 7 µM concentration and diluted to a concentration of 5 µM in 50 mM glycine-NaOH, pH 9.5 containing 2 mM of the fluoropeptide Abz-Ala-Arg-Arg-Ala-Tyr(NO$_2$)-NH$_2$ (Peptide Synthetics). This was then mixed with the same SurA-OmpT subreactions as described above.

2.12.3 OmpT assays with altered components

OmpT assays were carried out with inhibitors (Section 3.5.3). Where possible (JB-95 and L27-11) these were dissolved in glycine buffer at 20x final assay concentration. For BamD protein was buffer-exchanged (using a ZebaSpin desalting column (Thermo Scientific) into glycine buffer and used in the assay.

The potential inhibitor Peptide 2 was dissolved in DMSO, therefore an appropriate volume of DMSO was included as a control.

OmpT assays were also carried out with various chaperones and at altered concentrations of SurA (Section 3.5.4). The preparation of SurA (2.3.3), Skp (2.3.3) and HT-SecB (2.3.4) is described, as well as the generation of SurA variants (ΔP2 and N-Ct) which were purified identically to wild-type SurA. These assays were carried out as described above, with chaperones buffer exchanged into 50 mM glycine-NaOH pH 9.5 prior to use where necessary. In experiments with increased ratio of SurA: OmpT (Section 0, Figure 3-28) for some of the samples the reaction was done "in plate" with no preincubation of OmpT-SurA, to maximise final SurA concentration. However, later experiments were repeated with a more concentrated stock of SurA and show no differences.

The t_{50}s for altered components are calculated as the half-time to maximum fluorescence reached by that trace in 10,000 seconds of experiment, as many do not demonstrate substantial fluorescence increase. In order to better quantify the results comparing chaperones in the OmpT assay the initial rate was also calculated. As some variation is seen in fluorescence counts, traces were first normalised to the maximum fluorescence value observed within each individual experiment. The slope of each curve over the first 500 seconds was then quantified and compared.

OmpT assays were also carried out with OmpT folded into DUPC LUVs in the absence of BAM, in order to test inhibitors (Section 3.5.3) and OmpT variants (Section 4.4.3). For the latter, the OmpT variant protein was buffer exchanged into 8 M urea, 50 mM glycine-NaOH pH 9.5. Samples were folded by incubation at 25 °C overnight with 5 µM protein, 4 mM DUPC (molar LPR 800:1), and 2 M urea in 50 mM glycine buffer. 24 µL of folded OmpT sample was then added in the OmpT assay plate to 3 µL 10 mg/mL LPS and 3 µL 10 mM fluoropeptide. Consistent with requirement for LPS in OmpT enzymatic activity[268], following folding in synthetic LUVs it was necessary to supplement with LPS to observe protease activity. The final concentrations were 4 µM OmpT, 2.4 mM DUPC, 1 mg/mL LPS, 1 mM fluropeptide, 1.8 M urea in 50 mM glycine buffer. For the testing of inhibitors, wild-type OmpT was folded by incubation overnight at 25 ºC at 1 µM OmpT, 3.2 mM DUPC (molar LPR 3200:1), 0.3 M urea in 50 mM glycine-NaOH pH 9.5. 24 µL of folded OmpT sample was then added in the OmpT assay

plate to 3 µL 10 mg/mL LPS and 3 µL10 mM fluoropeptide. The final concentrations were 0.8 µM OmpT, 2.56 mM DUPC, 1 mg/mL LPS, 1 mM fluropeptide, 0.24 M urea in 50 mM glycine-NaOH pH 9.5. For consistency, BAM-folding of OmpT in the same assay was carried out with 0.8 µM OmpT, 5.6 µM SurA, 0.25 µM BAM complex, and 1 mM fluorogenic peptide.

2.13 tOmpA folding assay with BAM complex

An SDS-PAGE-based assay was developed to compare the activity of all BAM complex variants in folding the small substrate tOmpA under all reduced and oxidized conditions. BAM proteoliposomes formed by dialysis were resuspended in TBS (20 mM Tris-HCl pH 8, 150 mM NaCl) and protein concentration verified by Pierce BCA Protein Assay (Section 2.3.9). Two subreaction mixtures were prepared: the first contained 2 µM BAM complex proteoliposomes, and any reducing or oxidizing agents in TBS (20 mM Tris-HCl pH 8, 150 mM NaCl). The second comprised purified, denatured tOmpA (8 M urea, TBS at 20 µM) diluted 5-fold into solutions of 20 µM His_6-SurA in TBS folding buffer. These SurA-tOmpA solutions were mixed and immediately diluted two-fold into the proteoliposome-containing solutions. The final reaction mixture therefore contained 2 µM tOmpA, 10 µM SurA, 1 µM BAM complex proteoliposomes, 0.8 M urea in 20 mM Tris-HCl pH 8, 150 mM NaCl. The folding reaction was incubated at 25 ºC. When required, reducing/oxidising agents were used at a final concentration of 100 µM diamide, or 25 mM DTT, diluted from a 20-fold stock in TBS. These were incubated with the BAM subreaction for 1 hour at 25 ºC prior to initiation of the reaction. Samples were taken at time-points of 2, 5, 10, 15, 20, 30, 45, 60, 90 and 120 minutes whereupon 15 µL of the reaction mixture was quenched by addition to 5 µL of 6x loading buffer (50 mM Tris-HCl pH 6.8, 6 % (*w/v*) SDS, 0.6 % (*w/v*) bromophenol blue, 40 % (*v/v*) glycerol). The samples were not boiled, and when the reaction was complete, 15 µL of each sample was loaded on Tris-Tricine gels and electrophoresis carried out at room temperature. The identical assay was carried out to analyse folding of tOmpA or HT-OmpT mutants by BAM. The setup was as described, with only wild-type BAM proteoliposomes used, and the OMP of

interest buffer-exchanged in 8 M urea TBS and diluted to 100 µM. Time points are described when they differ from those utilised above.

The folding yield was quantified using ImageJ[302], by analysis of each band within a lane according to Equation 2-1:

$$Fraction\ folded = \frac{folded\ band\ intensity}{(folded+unfolded)band\ intensities}$$ **Equation 2-1**

The results were analysed using Igor graphing programme (Wavemetrics) and fit to a single exponential function (Equation 2-3). A minimum of three replicates was carried out for every condition of BAM mutants folding tOmpA and values averaged.

A titration of BAM concentration was also carried out for this assay (Section 5.8) using wild-type and Lateral-lock2 BAM proteoliposomes. For this the BAM subreactions were set up at 2x the required final concentration in 20 mM Tris-HCl pH 8, 150 mM NaCl (+ 50 mM DTT in the case of Lateral-lock2) and incubated at 25 °C for 1 hour. As before, the second subreaction of SurA-tOmpA was mixed and immediately diluted two-fold into the proteoliposome-containing solutions. The final reaction mixtures therefore contained 2 µM tOmpA, 10 µM SurA, 0.8 M urea, (25 mM DTT for Lateral-lock2) and BAM concentrations at 0.1, 0.2, 0.3, 0.4, 0.5, 0.6, 0.7, 0.8, 0.9 and 1 µM in 20 mM Tris-HCl pH 8, 150 mM NaCl. The folding reaction was incubated at 25 °C for one hour before quenching by addition of the sample to 6x SDS loading buffer.

2.14 Use of Styrene Maleic Acid Lipid Particles (SMALPs) to extract the BAM complex

SMA2000 was a kind gift from Dr Tim Knowles (U. of Birmingham). The protocol followed was an adaptation of that published by Lee *et al.*, (2016)[304]. BAM complex expression was carried out as described previously (see Methods 2.3.5) until the membranes were pelleted. At this stage the membranes were resuspended at 80 mg/mL in TBS buffer, (50 mM Tris, 500 mM NaCl, 1 mM DTT, pH 8) and homogenised with a Dounce homogeniser. The SMA2000 anhydrous

powder was dissolved to 5% (*w/v*) in an equal volume of the same buffer. The two solutions were mixed together, and solubilised by rotation for three hours at room temperature. Solutions were centrifuged to pellet insoluble material (25000 rpm, 30 min), the supernatant filtered and applied to a 5 mL Ni-NTA column (pre-washed with buffer), overnight at 4 °C using a peristaltic pump. The column was then washed with 4 column volumes of buffer containing 10 mM imidazole and eluted in 1 mL fractions with buffer containing 250 mM imidazole. Fractions were analysed by SDS-PAGE and fractions containing the BAM complex were pooled. Samples were concentrated to a volume < 1mL using a Generon Vivaspin20 concentrator (100 kDa MWCO). Purification was attempted by gel filtration using the Analytical Superdex S200, however no distinct elution peak was seen and fractions were analysed across the 8-14 mL elution volume.

The protocol was later repeated using a phosphate buffer. For this resuspension of the membranes was carried out in 50 mM phosphate pH 8, 500 mM NaCl, 10% (*v/v*) glycerol. The SMA solution was made up in the same buffer. Following application of the protein to a Ni-NTA column, the column was washed with 5 column volumes of buffer containing 20 mM imidazole (Wash1), 4 column volumes of buffer containing 100 mM imidazole (Wash2) and eluted in 1 mL fractions with buffer containing 500 mM imidazole. Where SEC was not carried out, samples were diluted in buffer without imidazole prior to concentration or dialysed without it.

2.15 Use of nanodiscs

The reconstitution of the BAM complex into nanodiscs was also attempted as a method to observe a more native-like system. This utilises BAM complex protein, as purified previously, MSP1D1 scaffold protein, purified by Dr Anton Calabrese and *E.coli* polar lipid extract, prepared in TBS with sodium cholate.

2.15.1 Preparation of *E.coli* polar lipid extract

The required volume of lipid extract, solubilised at 25 mg/mL was aliquoted into a clean, dry test tube, dried under a stream of N_2 and dessicated for ~ 5 hr or overnight. The lipid was then resuspended in an equivalent volume of 100 mM sodium cholate, 20 mM Tris, 150 mM NaCl. The resuspended lipids were

vortexed and sonicated (1-2 min each) several times, and run under a stream of warm water, ensuring that the lipid film is fully dissolved. The resuspended lipids were then aliquoted and stored at - 80 °C.

2.15.2 Reconstitution of BAM into MSP1D1 nanodiscs

The components were mixed together in a 1.5 mL Eppendorf tube. The molar ratios used for empty nanodiscs were 1:35 MSP1D1:lipid and for BAM containing nanodiscs 1:3:60 BAM:MSP1D1:lipid. The final concentrations in empty nanodiscs were 36 µM MSP1D1, 1.26 mM lipid, 14 mM sodium cholate in TBS + 10 % (v/v) glycerol. The final concentrations in BAM-containing nanodiscs were 6 µM BAM, 18 µM MSP1D1, 360 µM lipid, 14 mM sodium cholate in TBS + 10 % (v/v) glycerol. Typical final volume was 500 µL, although several volumes were attempted.

A small amount (~50 µL) of dry Biobeads was then added to the mixture. Prior to use, Biobeads were prepared by washing 3 times with methanol, 3 times with ddH$_2$O and washed twice with buffer immediately prior to use. The sample was incubated with fresh Biobeads 2-3 times, including one overnight incubation. In order to remove Biobeads after use, the Eppendorf containing the sample was pierced with a needle, and briefly centrifuged within a 15 mL Falcon tube such that the sample flowed out and Biobeads remained in the Eppendorf.

Formation of the Nanodiscs was verified by SDS-PAGE, Blue Native PAGE or SEC. For gel filtration chromatography ~400 µL of sample was injected on an Analytical Superdex200, 10/300 GL column. This was as with the BAM prep, but equilibrated with TBS + 10 % (*v/v*) glycerol. In addition to gel filtration with the Superdex S200 attached to the standard Akta Prime, it was also attempted with the column on an AktaMicro, where the column was run at 0.05 mL/min but smaller (100- 1000 µL) fractions could be collected in a plate. 300 µL fractions were collected, as analysed in Section 3.6.2, Figure 3-33.

In addition, BAM-Nanodisc samples were usually mixed with nickel beads and eluted in a smaller volume to increase the concentration and purity of the BAM samples. In these cases 100 µL pre-washed nickel-sepharose beads was added to 900 µL Nanodiscs mixture (estimated protein concentration 6 µM). The beads were incubated with sample, washed twice with buffer (TBS+10% glycerol) containing 50 mM imidazole and protein eluted with buffer containing 200 mM

imidazole. The sample was dialysed against TBS + 10% (v/v) glycerol using a 200 µL 12-14 kDa MWCO dialysis tube (D-tube dialyser mini, (Merck Millipore) to remove excess imidazole and protein concentration verified by the Pierce BCA Protein Assay (Section 2.3.9).
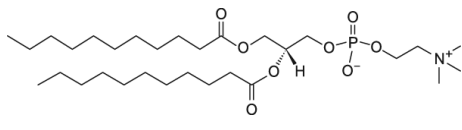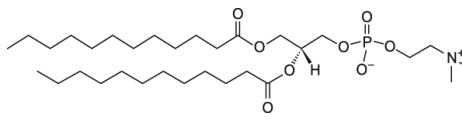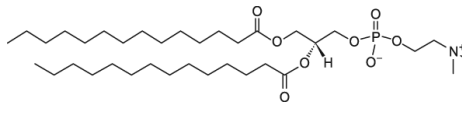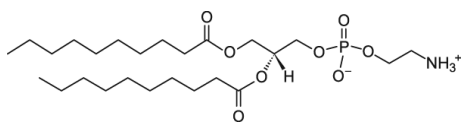
2.16 JCM166 assay

An assay was carried out to test the *in vivo* lethality of BamA mutations. This utilised JCM166 cells and a pZS21 plasmid containing HT-BamA, both kind gifts from Professor Tom Silhavy, Princeton. The pZS21 plasmid has a kanamycin resistance gene and contains HT-BamA under control of an arabinose-inducible pBAD promoter. The JCM166 cells (genotype MC4100 *ara* $^{r/-}$ Δ(λ*att-ιom*) *: : bιa* $_{PBAD}$*yaeT araC ΔyaeT*) are carbenicillin resistant, and will naturally express wild-type BamA but this is suppressed in the presence of glucose. Growth in glucose conditions is therefore only possible if the BamA on the pZS21 plasmid is functional.

All mutations of interest were introduced into the pZS21 plasmid by Q5 site-directed mutagenesis (Section 2.1.5, Table 2-4). Plasmids were transformed into JCM166 cells, with a pRSFDuet-1 plasmid used as an empty vector control. Following outgrowth with LB + 0.2 % (*w/v*) arabinose, cells were grown on LB agar + 100 µg/mL carbenicillin + 50 µg/mL kanamycin + 0.2% (*w/v*) arabinose (LB carb/kan/ara).

The following day a single colony was used to inoculate 5 mL LB carb/kan/ara which was then cultured for ~6 hours at 37 °C. 500 µl of culture was subsequently pelleted at 3000 xg for 3 minutes and the pellet washed three times to remove arabinose. The cells were then resuspended to OD_{600} of 0.1 in PBS. Cells were streaked on to LB-agar + 100 µg/mL carbenicillin + 50 µg/mL kanamycin + 0.2% (*w/v*) glucose plates and incubated overnight.

87

2.17 Table of lipids used in this work

1,2-diundecanoyl- *sn***-glycero-3-phosphatidylcholine**	DUPC	C11	$C_{28}H_{56}NO_8P$	
1,2-dilauroyl-*sn***-glycero-3-phosphocholine**	DLPC	C12	$C_{32}H_{64}NO_8P$	
1,2-dimyristoyl-*sn***-glycero-3-phosphatidylcholine**	DMPC	C14	$C_{36}H_{72}NO_8P$	
1,2-didecanoyl-*sn***-glycero-3-phosphoethanolamine**	DDPE	C10	$C_{25}H_{50}NO_8P$	

3 Results Chapter 1: The BAM complex

3.1 Introduction

Understanding of the BAM complex has advanced considerably in the time of this PhD, with multiple recently published crystal structures of the complex, enlightening the field as to its intrinsic dynamics[207-210]. At the beginning of the thesis work, there were limited studies on the activity of the BAM complex *in vitro*, with only a few examples showing active BAM in proteoliposomes[159,189,272,274]. Only one study had used intact purified BAM[274] and this demonstrated higher activity than that purified as two subcomplexes. The time was apt, therefore, for structural investigation of the BAM complex and biochemical dissection of its function. This chapter will discuss the inception of this aspect of the project and optimisation required along the way.

As will be discussed throughout this thesis, a principal aim of this project was to understand the role of lateral gating, and other dynamics in BamA function. One of the ways this is examined is by creation of variants in the BAM complex. The variants and their impact on BAM activity will be discussed in Chapter 5. However, some optimisation of the BAM preparation discussed here was carried out on both wild-type BAM (WT) and the first disulphide-lock variant created for this study (I430C/K808C).

Here I also introduce the OmpT enzymatic assay, an indirect assay which allows us to assess features of the BAM-chaperone-OMP folding system via changes in OmpT's ability to cleave a fluorogenic substrate peptide[268]. The assay is widely used for studies of BAM complex activity[34,189,274] and in this chapter I discuss some of the assay optimisation, its applications and also its limitations.

Other features of the BAM complex were also of interest, such as the membrane environment and how this may impact both structure and function. The current protocol for studies of BAM involves extraction from the native membrane, purification and subsequent structural studies using detergent and reconstitution in native-like lipids for activity assays[274]. By trialling new membrane mimetics, such as SMA-lipid particles (SMALPs)[305] and protein-supported nanodiscs[306], I could purify BAM complex in which structural and functional studies could be carried out on the same sample. In addition to the reassurance that the structure

observed was the functional form, the structure in lipid may differ from that previously seen in detergent.

Some data in this chapter were obtained with the assistance of Dr Matthew Iadanza (cryo-EM), Dr Anton Calabrese (Mass Spectrometry) and Dr Bob Schiffrin (analysis of structures). In addition, considerable parts of this chapter formed the basis for the following publication: Higgins, A.J.*, Iadanza, M.G.*, Schiffrin, B., Calabrese, A.N., Brockwell, D.J., Ashcroft, A.E., Radford, S.E., Ranson, N.A.. "Lateral opening in the intact B-barrel assembly machinery captured by cryo EM". *Nature Communications* **7**, 12865 (2016).

3.2 Purification of the intact BAM complex

The full BamABCDE complex (named herein as BAM), expressed polycistronically on a single plasmid, was expressed and purified as previously described[274], see Methods (Section 2.3.6) for details. Briefly, proteins were expressed in *E.coli* BL21 (DE3) cells, the cells were then disrupted and ultracentrifuged to pellet cell membranes. Membranes were disrupted using DDM, ultracentrifuged again and BAM purified from the soluble fraction by nickel affinity chromatography followed by size-exclusion chromatography (SEC), with the detergent Triton X-100.   BAM consistently eluted as a triple peak by SEC (Figure 3-1a). SDS-PAGE analysis showed that each peak contained all five subunits of BAM and hence different elution volumes may reflect different conformational states or differing proportions of detergent and/or lipid binding. All five protein components were verified by SDS-PAGE and seen in approximately equal stoichiometry (Figure 3-1b). A low quantity of protein (<1 mg pure protein/litre culture) was obtained from these initial purifications, and while this was taken forward and used in activity assays, work was undertaken in parallel to improve protein yield.
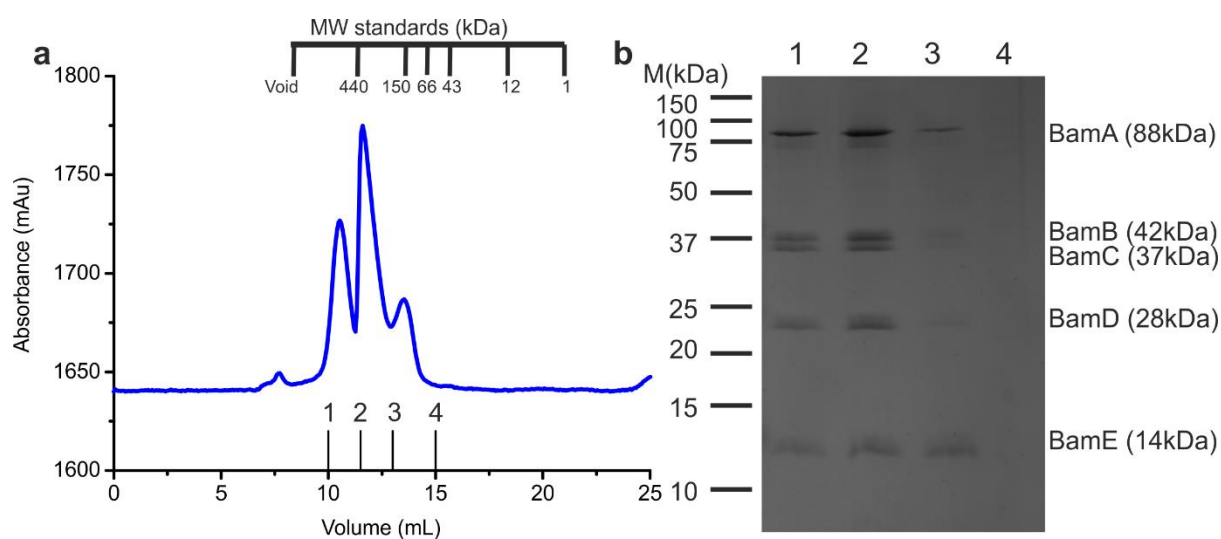
Figure 3-1: Purification of BAM complex using Triton X-100. Example trace of the elution of the BAM complex I430C/K808C variant from size-exclusion chromatography (a) using a Superdex200 10/300 column, with TBS (50 mM Tris pH 8, 150 mM NaCl) + 0.5% (*w/v*) Triton X-100. (b) Identification of protein by SDS-PAGE. Lines on the elution profile (a) indicate the beginning of the 0.5 mL fraction analysed by SDS-PAGE in (b). The protocol for purification is given in Methods, Section 2.3.6. It can be noted that the complex consistently elutes earlier on the size exclusion chromatogram than is expected considering its size relative to calibrants. However this is likely due to presence of the detergent micelle and associated lipids.

3.2.1 Optimization of BAM complex expression

Due to the low yield of the BAM complex obtained in all initial purifications using the published protocols[274], see Methods 2.3.6, persisting difficulties and loss of protein throughout, expression trials were carried out to determine whether altering the bacterial growth or protein expression conditions could improve protein yield. The triple peak seen in size-exclusion chromatography traces also gave question as to consistent protein conformation. Therefore the separate peaks were never pooled, contributing to even lower yield.

Three aspects of the expression were tested. Firstly, the protocol followed[274] is unusual in that a low IPTG concentration (0.4 mM) and short expression time (1.5 h) are used following induction of protein expression (Methods 2.3.6 for details). Changing these parameters was therefore tested. Expression was also attempted in the more nutrient-rich TY broth (Methods, Section 2.3.7), using similar induction times to determine whether an increased yield could be obtained. A small-scale expression trial was carried out for wild-type (WT) BAM

91

and a disulphide-lock variant (I430C/K808C, XL) and analysed by SDS-PAGE (Figure 3-2).
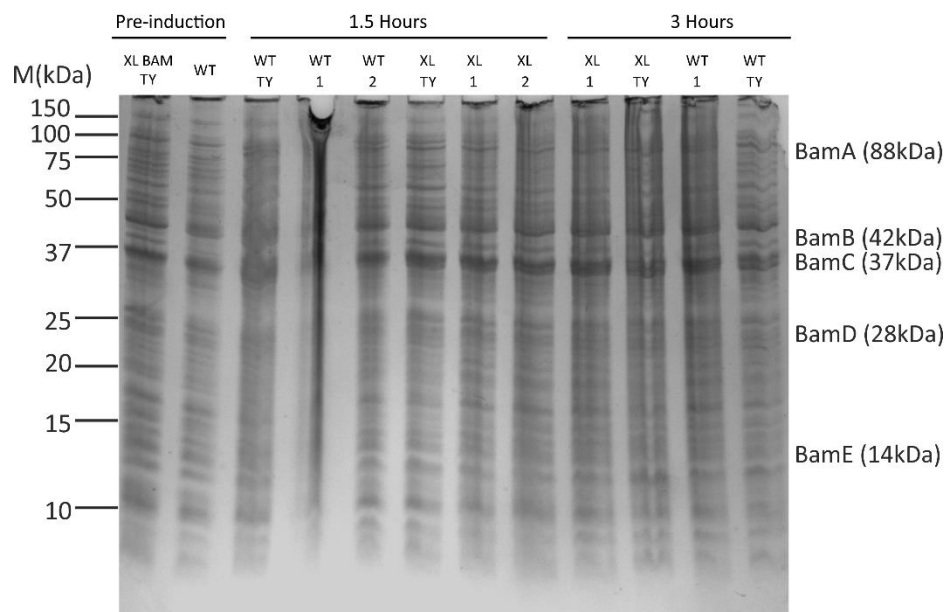
Figure 3-2: SDS-PAGE showing expression trial of BAM wild-type (WT) and cross-linked BamA$_{I430C/K808C}$BCDE variant (XL). Following transformation in *E.coli* BL21 (DE3), overnight cultures were diluted 1:50 in 100 mL of fresh LB or Terrific (TY) broth, containing 100 µg/mL carbenicillin. Cells were grown (37 °C, 200 rpm) to an OD$_{600}$ of 0.5-0.6 before addition of 0.4 mM IPTG (denoted by 1) or 1 mM IPTG (2) to induce expression. Cells in TY broth were all induced with 0.4 mM IPTG. 1 mL cell samples were taken pre-induction and at various later time points, cells were diluted to the same cell density before analysis by SDS-PAGE.

Due to the low expression level typically seen for such membrane proteins, the small scale expression trials were inconclusive (Figure 3-2). Therefore a larger scale (9 L) purification of the BAM complex was carried out, incorporating several alterations. The preparation was performed 1) utilising BL21(DE3) *E.coli* cells, and LB, 2) with BL21(DE3) cells but in TY broth or 3) utilising the *E.coli* strain HDB150 (MC4100 *ompT::spc ΔaraBAD leuD::kan*) which was used in the original BamABCDE preparation[274] with LB, with 3 L of purification by each method (the precise protocols used are detailed in Methods, Section 2.3.7). This permitted comparison of three methods (Figure 3-3), for which the size-exclusion trace of each is shown. In addition SDS-PAGE analysis of the fractions from method 2) growth with TY broth (Figure 3-3d) is shown. From visual inspection of the SDS-PAGE and final yield of protein, it was concluded that use of TY broth improved yield, while other alterations had little effect. TY broth and

transformation in BL21(DE3) cells was used, therefore, in all further preparations of the BAM complex.
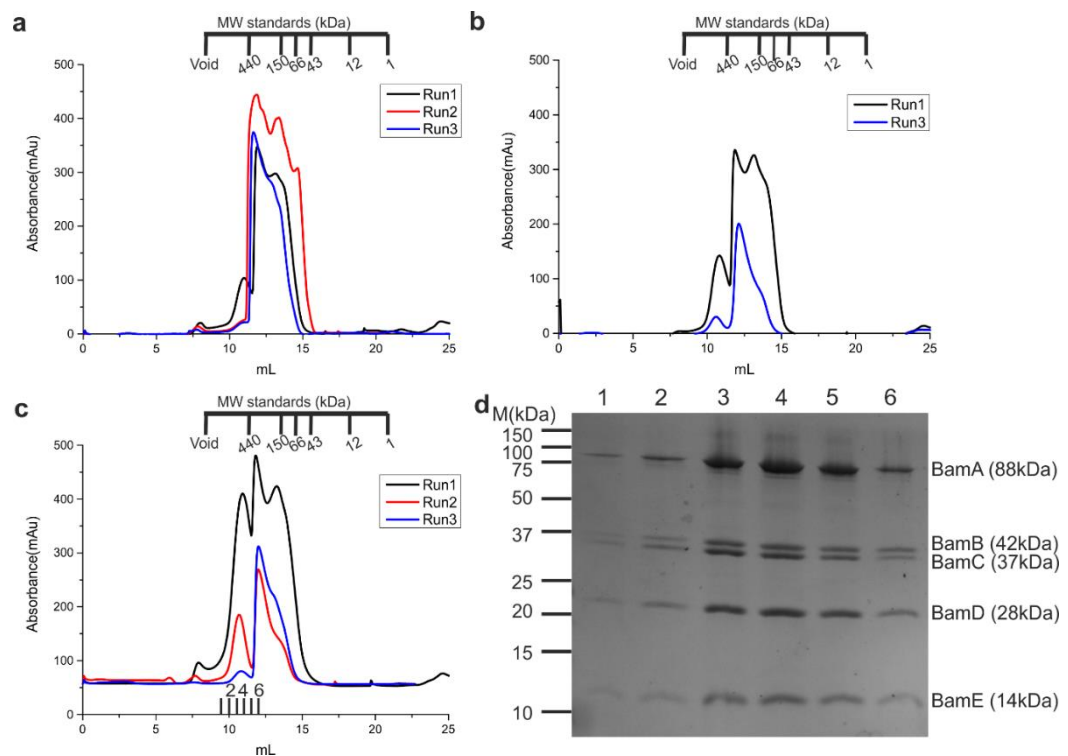
Figure 3-3: Comparison of alterations to BAM complex purification. Elution from size-exclusion chromatography with 3 runs of each, traces from a) utilising BL21(DE3) *E.coli* cells, and LB, b) utilising the *E.coli* strain HBD150 with LB, or c) with BL21(DE3) cells but in TY broth. d) Elution fractions from second elution following growth in TY (c-red line) analysed by SDS-PAGE. The 6 samples are 0.5 mL fractions from 9.5-12.0 mL shown with black marks on (c). The majority of the protein is found in the first peak (lanes2-6) which elutes at approximately 10 mL.

The protocol followed for BAM expression, as used in Roman-Hernandez et al., [274], and discussed above, uses DDM to disrupt cell membranes, but in the nickel affinity step the detergent used (necessary to keep the complex in a folded state) is switched from DDM to Triton X-100. This step appeared unnecessary, and may contribute to decreasing yield throughout the preparation. In addition, while Triton X-100 may have been chosen to render the protein more amenable to down-stream applications, the aromatic ring of Triton X-100 causes absorbance at 280 nm, commonly used for estimating protein concentration, and may therefore strongly contribute to the varied intensity in absorbance traces seen by size-exclusion in repeat runs.

It was decided to attempt a full scale purification of the BAM complex utilising DDM as the detergent throughout (see Methods Section 2.3.5). The use of detergent DDM improved the behaviour on SEC (Figure 3-4), thus allowing pooling of fractions across this peak. Also, as can be seen by the higher absorbance values of (Figure 3-4a) compared with (Figure 3-1) more protein is obtained. A single peak was routinely observed for SEC of the BAM complex, which was verified by SDS-PAGE (Figure 3-4b) to contain all five protein components. The final yield of this preparation was 1.8 mg pure BAM per litre bacterial growth.
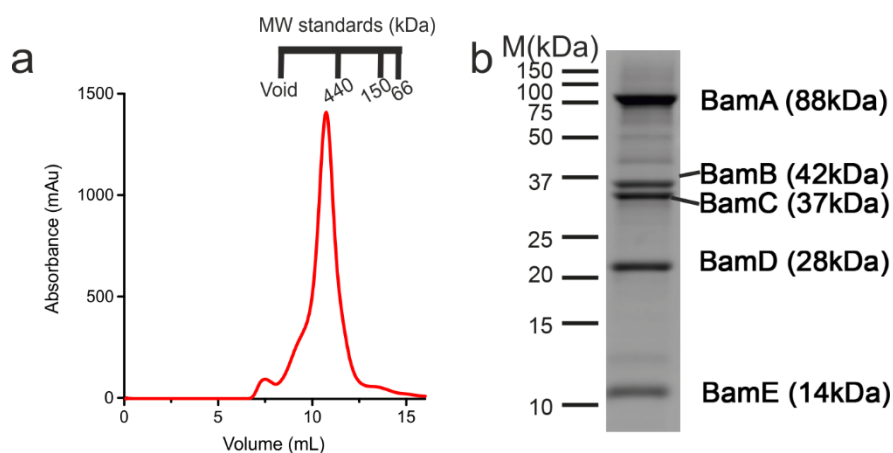
Figure 3-4: Purification of BAM complex using DDM. Shown is an example trace for elution from a Superdex S200, 10/300 GL column (a) and SDS-PAGE analysis of the central fraction(b). SEC was performed with TBS containing 0.05 % (w/v) DDM (see Methods, Section 2.3.5 for a detailed protocol).

3.2.2 Mass spectrometry of the intact BAM complex

In order to validate the complex as intact, non-covalent 'native' ESI mass spectrometry and native PAGE were carried out (Methods, Sections 2.4.1 and 2.6.4) (Figure 3-5). As noted, the complex elutes at a high molecular weight with comparison to calibrants (Figure 3-4), likely due to the presence of the detergent micelle. Native MS and PAGE (Figure 3-5) aid in confirming that this is not due to oligomers, only one copy of the complex is present. All mass spectrometry experiments were carried out by Dr Anton Calabrese on my preparation of wild-type BAM complex in Triton X-100. The spectrum showed a distinct population containing all five subunits, distributions corresponding to BamABCDE$_2$ and to the subcomplexes BamAB and BamACDE. The charge state distribution corresponding to BamABCDE is the predominant species in the spectrum, with

an observed mass of 203,456 ± 22 Da, closely matching the predicted mass of 203,218 Da. The subcomplexes observed (BamAB,BamACDE) are consistent with known architecture of the BAM complex[188,201,217] and with previous reconstitution of the complex from BamAB and BamCDE subcomplexes[159,189] and are likely due to dissociation in the gas phase. The appearance of a BamABCDE$_2$ species is also unsurprising, due to uncertainties about BamE dimerization[195,223,224] and difficulty ascertaining whether one or two copies were found in previous preparations of the complex[189]. Native PAGE of the complex in TBS+DDM confirms it is intact and that no oligomerisation is observed. The protein consistently migrates at a slightly higher molecular weight than anticipated (~200 kDa)[274], although not large enough for oligomers, and we typically see a slight doublet formation, likely corresponding to altered conformations of the proteins or detergent micelle.
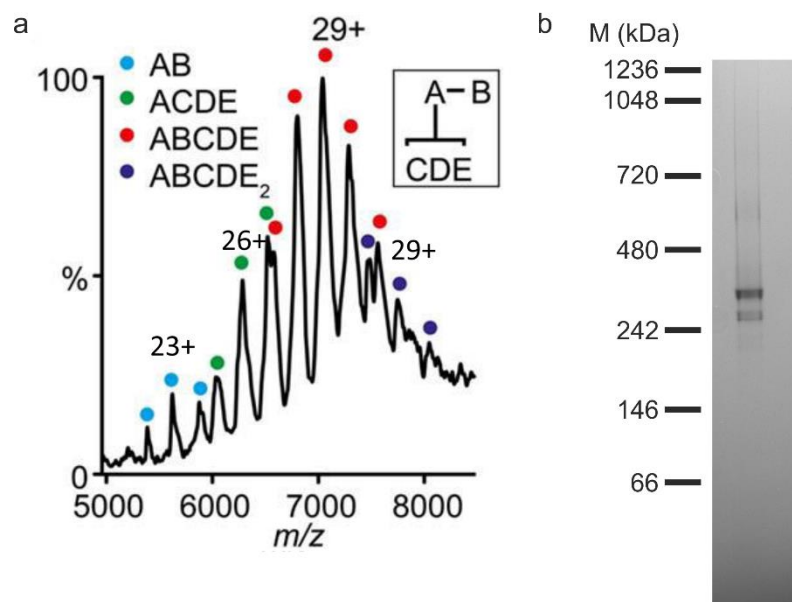
Figure 3-5: Intact BAM complex demonstrated by a) mass spectrometry and b) native PAGE. a) Charge states from the intact complex, as well as subcomplexes formed by gas phase ionization (inset) are indicated. BAM complex, purified in Triton X-100 was exchanged into 200 mM ammonium acetate, 0.02% (v/v) Triton X-100 pH 6.9. Nanoelectrospray ionization-mass spectra were acquired (see Methods Section 2.4.1). Figure reproduced from Higgins/Iadanza *et al.*(2016)[210]. b) Native PAGE of BAM complex preparation in DDM. Precast Invitrogen NativePAGE 4-16 % Bis-Tris gels were used according to the manufacturer's instructions. Approximately 10 μg of sample were loaded, as well as Native Mark Standard (LifeTechnologies). Electrophoresis is carried out at 150 V for 120 minutes at room temperature (see Methods, Section 2.6.4).

To confirm more precisely the mass of each subunit, denaturing ESI mass spectrometry was also carried out (Methods, Section 2.4.2) (Figure 3-6). Two peaks are typically seen on the chromatogram, one for the membrane-integrated and one for the soluble fraction, which following deconvolution can be determined to contain all 4 lipoproteins. This confirmed the mass of each subunit as well as determining the lipid moiety attached N-terminally to each lipoprotein subunit. Two consistent species are observed for each lipoprotein, corresponding to a mass increase of ~790 Da (3x C_{16}) or ~813 Da (2x C_{16} 1x C_{18}) however the number of double bonds in the acyl chains cannot be determined.

Protein	Theoretical mass (Da)	Measured mass (Da)	(Measured-Theoretical) (Da)	PTM
BamA	88426	88426	0	-
BamB	39853	40643	790	3x C_{16}
		40663	810	2x C_{16} 1x C_{18}
BamC	34371	35163	792	3x C_{16}
		35183	812	2x C_{16} 1x C_{18}
BamD	25790	26583	793	3x C_{16}
		26603	813	2x C_{16} 1x C_{18}
BamE	11596	12383	787	3x C_{16}
		12413	817	2x C_{16} 1x C_{18}
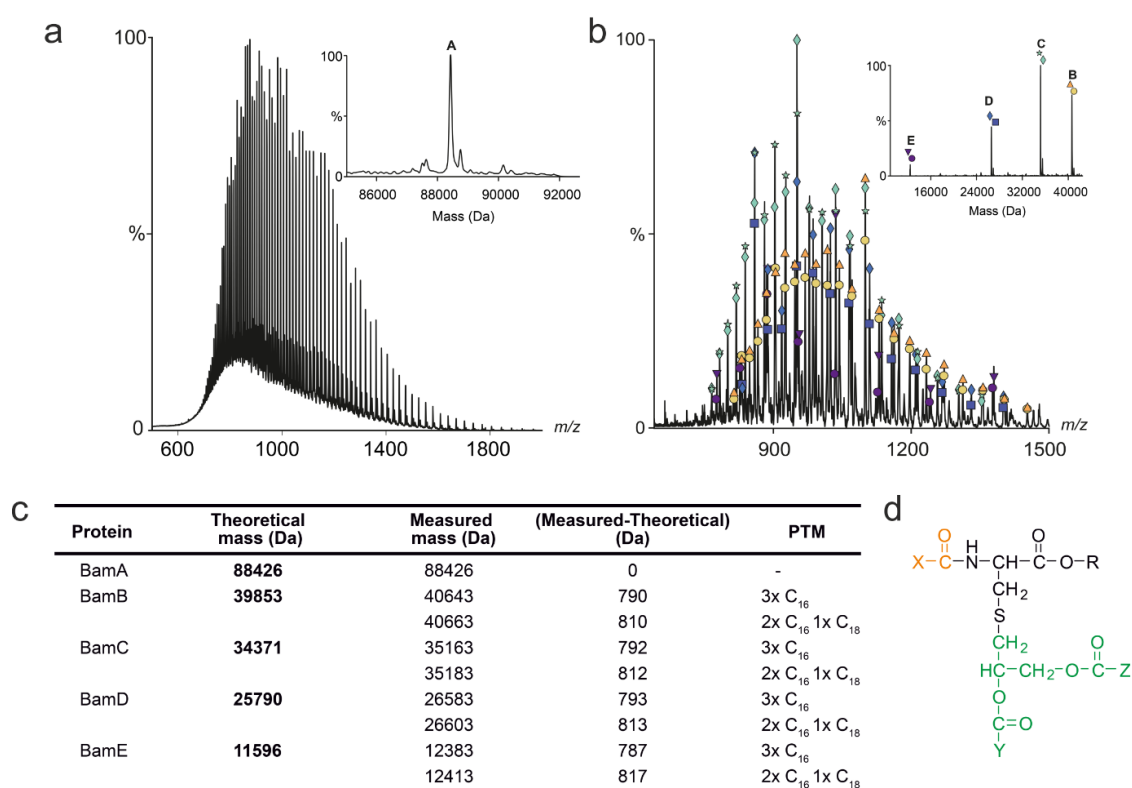
Figure 3-6: Denaturing ESI mass spectrometry of the BAM complex. (a) ESI mass spectrum of BamA. (b) ESI mass spectrum of BamB, C, D and E. Deconvoluted spectra are displayed in insets in (a) and (b). (c) Theoretical and measured masses. The mass discrepancy between the predicted and experimentally measured values is shown, along with the post-translational modification (PTM) associated with the observed mass difference. The number of double bonds in the acyl chains of the lipids cannot be determined at this resolution. (d) Chemical structure of the N-terminal modified Cys residue. X,Y, and Z denote the position of the PTMs indicated in part (c). Figure reproduced from Iadanza *et al.*(2016)[210].

3.3 Cryo-electron microscopy of the BAM complex

Having obtained high yield of a pure preparation of the BAM complex, validated as intact, and with no structures of the intact BAM complex published at the time, we turned to structural techniques, particularly cryo-EM. Optimization of the preparation of wild-type BAM complex protein in DDM allowed my colleague Dr Matthew Iadanza to begin studies using cryoEM. Samples were first assessed by negative stain EM. Following this, the sample was diluted in TBS buffer (50 mM Tris pH 8, 150 mM NaCl), at constant 0.05% (*w/v*) DDM buffer and applied to a quantifoil EM grid. Grids were imaged on a 300 kV Titan Krios electron microscope (see Methods 2.5 for details). 7803 micrographs were collected, and 95787 particles extracted for the final classification. Shown is one example micrograph and class averages determined for this dataset (Figure 3-7).

a   b
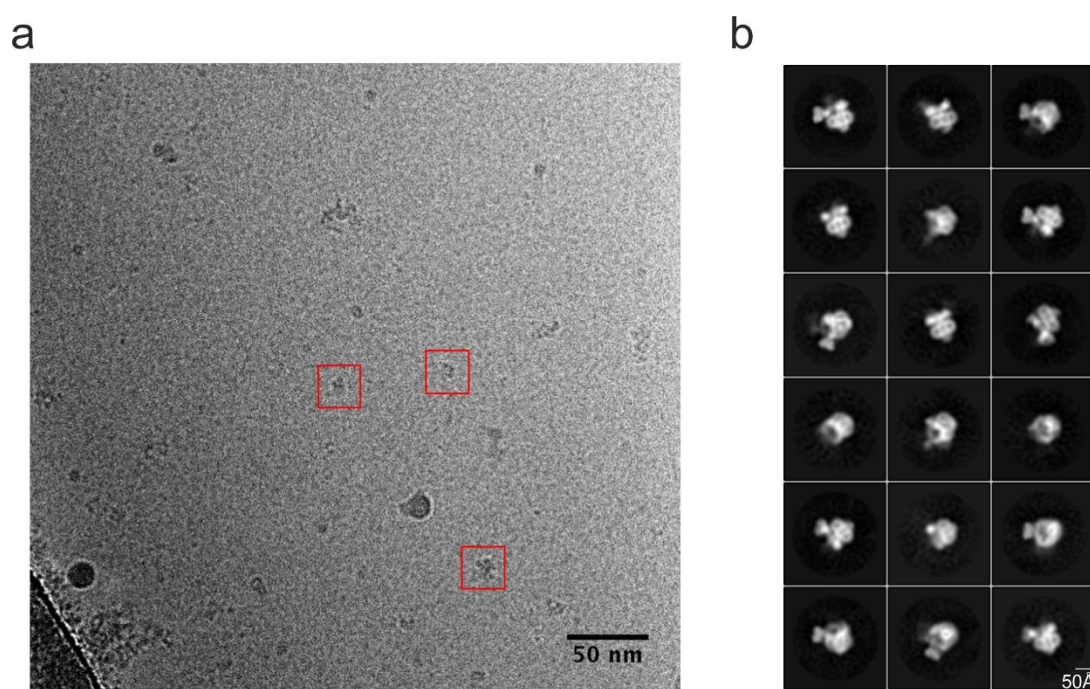
Figure 3-7: Example micrograph (a) and class averages (b) for cryo-EM on the BAM complex. Data were collected on a Titan Krios microscope using a Gatan K2 Summit energy-filtered direct detector (Gatan, Inc.) at the Electron Bioimaging Centre (eBIC, Harwell) by Dr Matthew Iadanza (University of Leeds).

Analysis of the cryo-EM map permitted reconstruction of the structure of the complex to 4.9 Å resolution. An initial model assembled from the crystal structures of each subunit was fit to the EM map: BamA from 5D0Q[208] and 5D0O[208], BamC and BamD from 5D0Q[208], BamE from 5D0O[208] and BamB from

97

3Q7O[299] and 2YH3[195]. This was refined by flexible fitting using Molecular Dynamics Flexible Fitting (MDFF)[300] and Monte Carlo Simulations with RosettaEM[301].

Shown front and back, with detergent micelle visible (Figure 3-8a) and without (b), there is clear density visible for a single copy each of BamA, B, D and E as well as the N-terminal segment of BamC (residues 26- 98). The fitting of the model to the cryo-EM density was striking in that it revealed a novel structure (Figure 3-8).

As previously discussed (Introduction 1.7.3) during the course of the previous year, a number of crystal structures were published showing the BAM complex, in varying degrees of completion and various conformations[207-209,226]. Those structural analyses show that the β-barrel of BamA can exist in two distinct conformations. In the first, the barrel is open to the periplasm (and hence is presumably an acceptor state for OMPs), known as 'inward open', but with the membrane-facing gate of the BamA β-barrel laterally closed. In the second conformation the β1 and β16 strands of the BamA barrel are open, causing it to be laterally open to the membrane, and extracellular face. Thus far, 'lateral open' conformations had only been observed in BAM crystal structures which lack the 42 kDa, β-propeller accessory protein, BamB[207,208], raising the possibility that changes in the BamA β-barrel may represent a gating reaction driven by BamB binding and dissociation.

In the cryo-EM structure, shown in Figure 3-8, BamA is in a distinctly 'lateral open' conformation, with a separation between β1 and β16. This is the first solution state structure of the BAM complex and has also allowed us to observe a novel conformation, of the 'lateral-open' form of the BamA β-barrel in the presence of BamB (Figure 3-8).
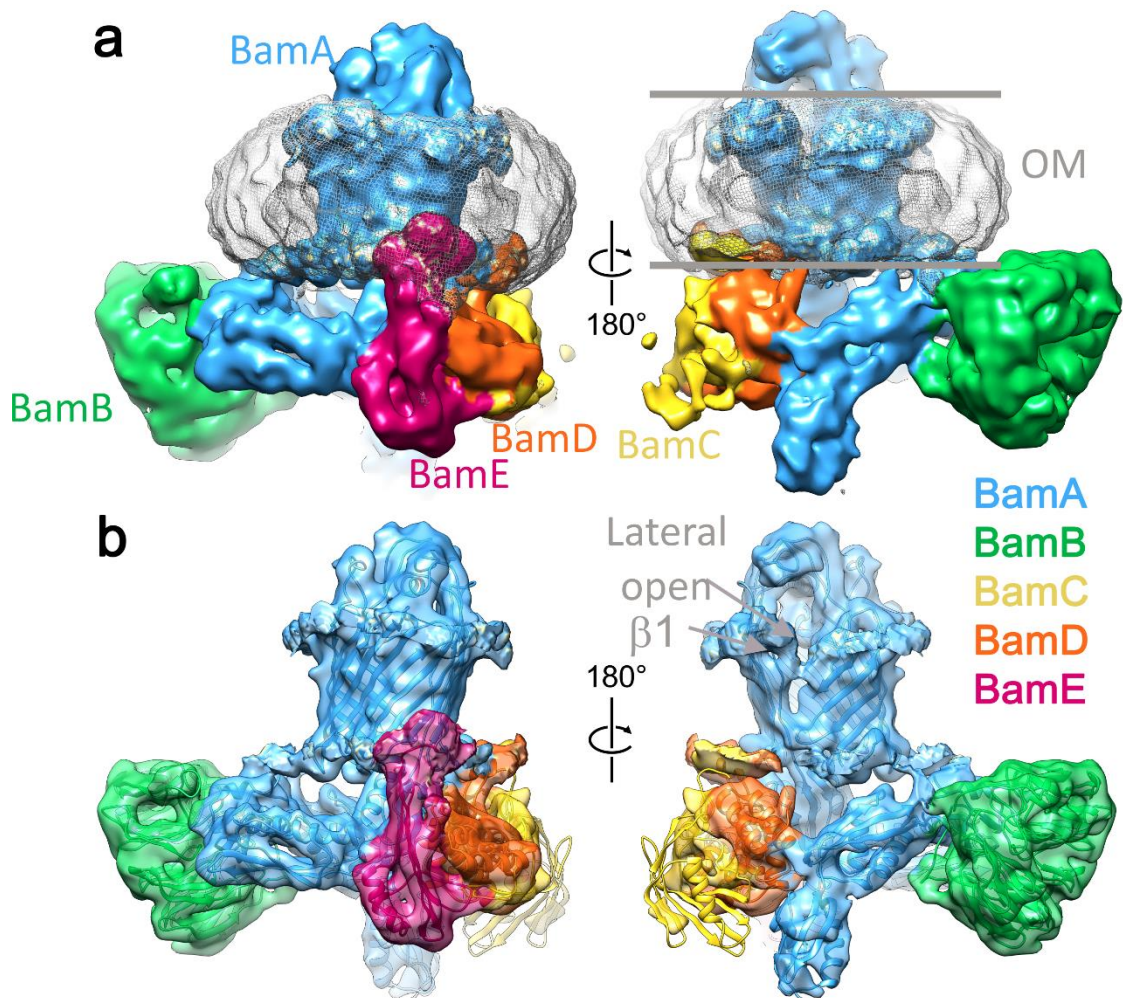
Figure 3-8: Cryo-EM structure of the BAM complex. Views of the front and back face of the cryo-EM structure of the intact BAM complex at 4.9 Å resolution. BamA is coloured blue, BamB in green, BamC in yellow, BamD in orange and BamE in magenta and the approximate position of the outer membrane (OM) is marked. Density corresponding to the micelle of n-dodecyl-β-D-maltoside (DDM) in the structure is shown as a pale grey mesh. (b) Flexible fitting of a hybrid X-ray structure into the EM density. The views and coloring are identical, but density for the micelle has been masked, and the EM density made transparent, showing the fitted pseudo-atomic model within. The location of lateral opening and position of β-strand β1 are marked. Figure adapted from Iadanza *et al.*(2016)[210].

The cryo-EM structure generated at 4.9 Å resolution allows determination of a lateral open BamA structure in the full complex. In addition, the region of lateral gating, around β1 and β16 shows high mobility evidenced by low local resolution (Figure 3-9).
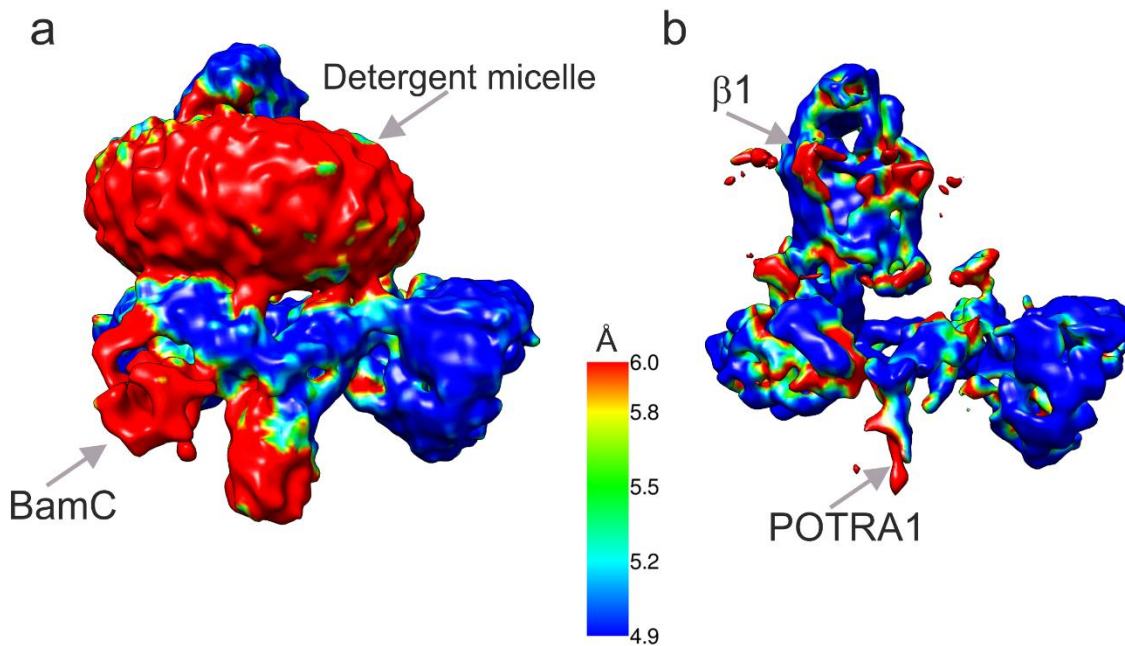
Figure 3-9: CryoEM structure coloured by estimated local resolution. Shown is a single front (β1/β16 seam)-facing view at high (a) and low (b) threshold values, so the detergent micelle is, or is not visible respectively. Resolution values are coloured according to the key. Poor local resolution is seen in more dynamic regions (eg. POTRA1, BamC N-terminal domain), the top of the β-barrel and in the detergent micelle. Figure adapted from Iadanza *et al.*(2016)[210].

A notable alteration between the cryo-EM structure and those already published[207,208] was in the conformation of the POTRA domains. The N-terminal POTRA 1 domain appears the most mobile, but in fact this results from the conformational change propagated through the POTRA domains. Comparison of the different crystal and cryo-EM structures demonstrates the angle between POTRA domains 2 and 3 is most variable, consistent with previous suggestions that this region is capable of hinge-like motions[203]. This analysis showed that the angle between POTRA2 and POTRA3 is wide (~120 º) in the lateral closed crystal structures with BamB present and more acute (~104° to ~110°) in lateral open crystal structures (Figure 3-10). The cryo-EM structure displays a wide angle between the POTRA domains, indicating this may be correlated with presence of BamB, rather than the open/closed position of the lateral gate[208,210]. However, comparison of the structures demonstrates that extension of the POTRAs vertically away from the barrel appears to more closely link to the barrel conformation than presence of BamB[210].
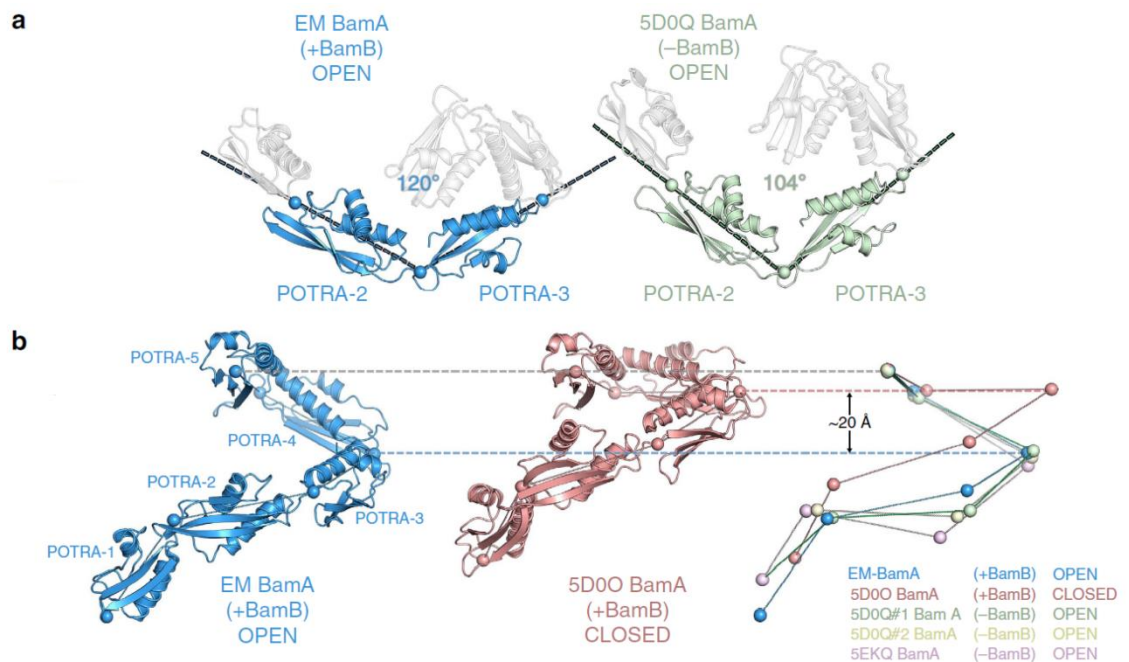
Figure 3-10: Comparison of POTRA domains across BAM complex structures. a) Comparison of the cryo-EM and 5D0Q[208] lateral open crystal structure demonstrates the obtuse angle between POTRA domains 2 and 3 appears to correlate with presence of BamB rather than lateral gate opening or closing. b) The extension of the POTRA domains away from BamA and the membrane is more closely related to lateral gate opening, noted by comparison of the cryo-EM structure to 5D0O[208]. Image reproduced from Iadanza *et al.*,(2016)[210].

The cryo-EM structure also permits us to look at the interactions with the detergent micelle, which is a mimic of the lipid membrane. The detergent micelle surrounds the BamA barrel and encapsulates the hydrophobic residues. Additional interactions are observed with the periplasmic regions of the BAM complex. Contacts with the micelle are observed for BamA from a loop in POTRA 3 (residues 196-214) which contains a hydrophobic sequence (RDE-**VPWWNVVG**-DRK) (Figure 3-11a). Additionally, the N-terminus of BamB and BamE and a conserved hydrophobic helix of BamD are observed buried in the detergent micelle.
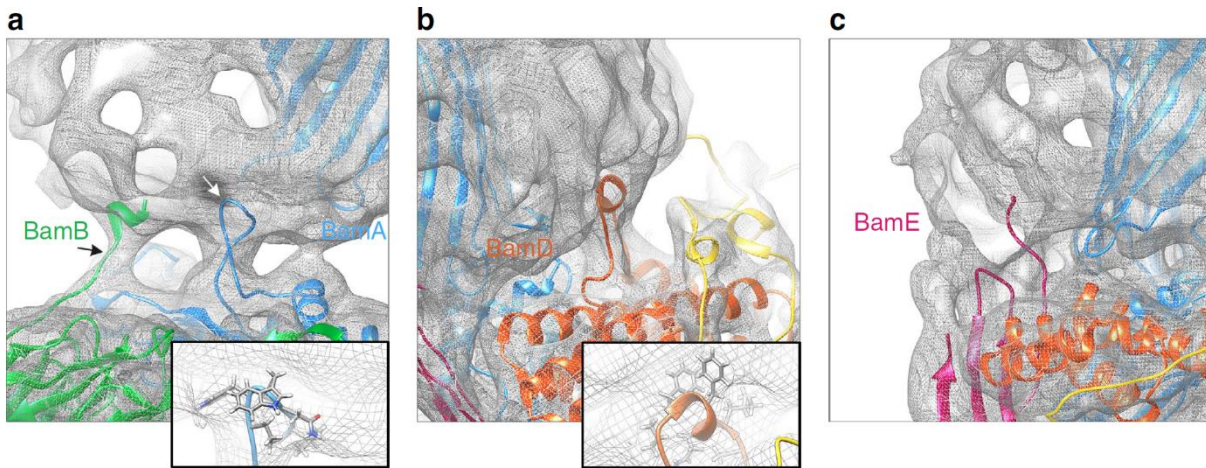
Figure 3-11: Interactions between BAM and the detergent micelle. The detergent micelle is shown as grey mesh. a) The N-terminus of BamB (green) dips into the detergent micelle. This segment is unmodelled in X-ray structures of BAM[207-209]. BamA (blue) POTRA3 also possesses a hydrophobic loop buried in the micelle, with details of the hydrophobic residues inset. (b) A hydrophobic 3_{10} helix in BamD (orange) inserts into the micelle, with hydrophobic residues buried in the hydrocarbon tail groups of the detergent (see inset) and polar residues flanking the helix placed to interact with the polar head groups of the detergent. (c) The N terminus of BamE (magenta), which is the site of the lipid anchor, also inserts into the micelle, well away from the body of the BamA β-barrel. Figure reproduced from Iadanza/Higgins *et al.*, (2016)[210].

Comparisons of structures of the BAM complex, between this 'lateral open' cryo-EM structure and 'lateral open' crystal structure 5D0Q[208] demonstrates the dynamics possible in BamD. BamD here appears to be flexible in two halves, with the C-terminal halves aligning, and the N-terminal halves not (Figure 3-12). The structures appear to differ around a hinge point, at the location where BamD is noted to contact the detergent micelle (Figure 3-11). Therefore communication with the lipid membrane may be responsible for the conformational change in this essential lipoprotein.
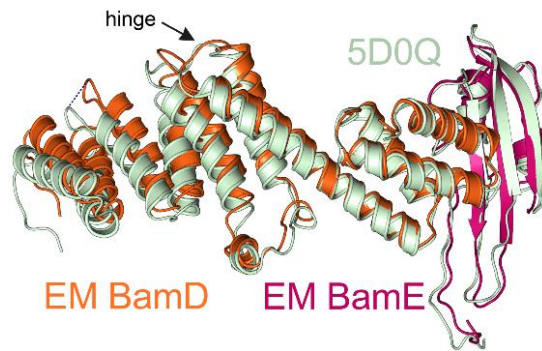
Figure 3-12: BamD conformational change between cryo-EM and crystal structures. Comparison of BamDE from cryo-EM (5LJO)[210] and crystal (5DOQ)[208] structures. Crystal structure (5DOQ) is light green throughout, cryo-EM BamD is orange with BamE magenta. Structures were aligned on BamE, and the C-terminal portion of BamD (right-hand side) aligns correctly, while the N-terminal portion(left-hand) deviates significantly between structures (orange to green). Image adapted from Iadanza *et al.*[210].

In conclusion, following considerable optimisation, the BAM complex can now be obtained at high yield and purity. This preparation of the intact BAM complex, particularly the purity and stability of the complex in DDM, facilitated analysis by native mass spectrometry and cryo-EM. The cryo-EM structure of the complex is unique in showing the intact BAM complex possessing BamA in a lateral open conformation in the presence of BamB. It remains not only the sole cryo-EM structure of the complex, but also the only structure with this particular conformation. Comparison of the cryo-EM structure to existing crystal structures has allowed some of the dynamics of the complex to be revealed. The large conformational changes observed in the swinging of the POTRA domains can be distilled to two aspects: the angle between POTRA2 and 3, which is correlated to the presence of BamB and the movement of POTRAs away from the membrane which is linked to lateral gate position. In addition BamD is noticed to conformationally change at a hinge point in the protein. The relevance of all these intricate dynamics is not yet known.

103

3.4 BAM reconstitution in proteoliposomes

On obtaining pure BAM, the next step was reconstitution in lipids for activity
assays. Prior studies, using both the intact complex, and that purified as two
subcomplexes utilise the same published protocol reported to function effectively
for reconstitution of BAM in *E.coli* polar lipid extract proteoliposomes[189,274].
Briefly, the method involves the addition of purified BAM complex to solubilized
E.coli polar lipids, a ~20 fold dilution in Tris buffer, incubation on ice, and
ultracentrifugation to pellet the proteoliposomes (see Methods Section 2.10.1 for
details). This method, ('dilution') did not appear to work effectively in my
preparation. To determine yield, the amount of protein in the supernatant and
resuspended pellet after ultracentrifugation were analysed by SDS-PAGE (Figure
3-13). The results showed that despite having been reported to reconstitute the
BAM complex into liposomes at high efficiency[159,189,274], this was not the case in
my preparation, and the majority of protein was found in the supernatant. This
preparation was originally carried out with protein prepared in Triton X-100, for
which the triple peaks typically seen (Figure 3-1) were pooled separately.
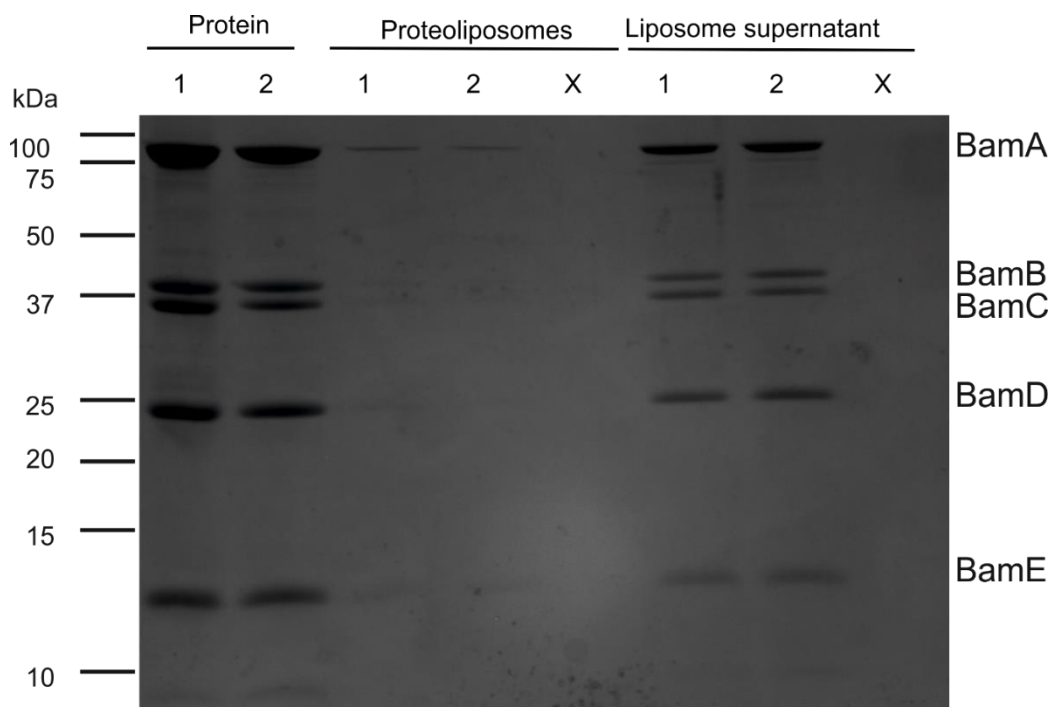
Figure 3-13: SDS-PAGE examining the efficiency of BAM complex reconstitution into proteoliposomes. Following creation of proteoliposomes by the dilution method, a sample of the protein (in detergent), the 200 μl liposome sample (both at 1:10 dilution), and the 4 mL supernatant (undiluted), were analysed by SDS PAGE. 1 and 2 designate protein from separate peaks of same prep; X designates empty liposomes. If the reconstitution has been effective, band intensity for BAM in the proteoliposome sample should nearly match that of protein, while very little protein is expected in the liposome supernatant sample.

Following the generation of larger quantities of the BAM complex using DDM, it was decided to optimize reconstitution in proteoliposomes using alternative methods. The methods tested included use of Biobeads and a new method of extensive dialysis (referred to hereafter as 'dialysis'), compared to the previous dilution method (Figure 3-14). The Biobeads method relies on the hydrophobic nature of Biobeads to bind and remove detergent, and was executed as described previously[278,303] (Methods, Section 2.10.3). This was unsuccessful as all protein was lost in this preparation (Figure 3-14). The dialysis method was carried out as reported for the outer membrane protein FhuA[257] and involved the incorporation of purified BAM complex with DDM-solubilized *E.coli* polar lipids and dialysis into detergent-free buffer over 7-days to permit the spontaneous formation of proteoliposomes (see Methods 2.10.2 for a detailed protocol). Following extensive dialysis, samples are briefly centrifuged, causing liposomes to pellet along with associated protein. This pellet is resuspended and analysed as the "Dialysis pellet" (Figure 3-14, lanes 5 & 6). These experiments showed

that the five proteins of the BAM complex are all associated with the liposomes and exhibit folded BamA. OMPs possess the property of heat modifiability, whereby they will remain folded in SDS-PAGE unless boiled[307] and the folded and unfolded forms migrate differently. While isolated BamA requires low SDS conditions to exhibit this property, BamA within the BAM complex displays a clear bandshift on boiling in standard SDS-PAGE conditions. In Figure 3-14 (lanes 5 & 6) the clear bandshift of BamA demonstrates that BamA is folded in the liposomes. Following this result, dialysis proteoliposomes were exclusively used for all the experiments described.
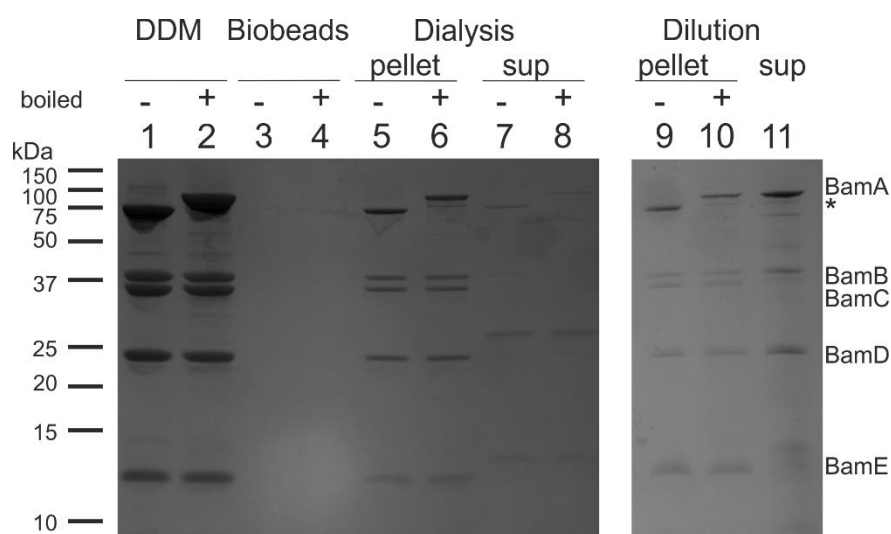
Figure 3-14: SDS-PAGE comparison of different methods to generate proteoliposomes containing the BAM complex. SDS PAGE analysis shows the purified BAM complex in DDM (lanes 1&2) and Biobeads (3&4), Dialysis (5-8) and Dilution (9-11) methods to generate proteoliposomes containing the BAM complex, with boiled (+) samples displaying the expected bandshift on unfolded BamA. A* denotes folded BamA. The original BAM protein sample, in DDM was diluted 1:10, while the resuspended dialysis pellet and all samples from ultracentrifugation were diluted 1:2, for approximate protein concentration of 3-5 µM in the final sample analysed.

3.4.1 Analysis of proteoliposomes using dynamic light scattering

Dynamic light scattering (DLS) is a powerful tool to obtain information on particle sizing[308]. This method was used to examine wild-type BAM complex proteoliposomes, generated by either the dilution or dialysis methods. It was of interest to analyse the relative sizes of liposomes generated by different methods to compare to the 100 nm LUVs previously used for BamA work (see Chapter 4), especially given that lipid curvature is known to affect the folding of membrane

106

proteins[72,309-311]. In addition, the size of the liposome may have considerable effect on efficiency of protein folding, with proteins folding more rapidly into smaller vesicles[72,79]. The particle size calculated by DLS is the hydrodynamic radius, related to the translational diffusion coefficient by the Stokes-Einstein equation[308]:

$$D = \frac{kT}{6\pi\eta R_h}$$
Equation 3-1

Equation 3-1: Stokes-Einstein Equation for determining the hydrodynamic radius (R_h) of a particle using DLS. D = translational diffusion coefficient (cm^2 s^{-1}), k = Boltzmann's constant, T= absolute temperature and η = viscosity (kg m^{-1} s^{-1}).

The hydrodynamic radius calculated is the radius of a sphere with the same translational diffusion coefficient. In addition one must recall that aspects of the surface will contribute to particle sizing, and the fact that *E.coli* polar lipids are composed of multiple lipid types, with inherent heterogeneity. Shown is the correlation function, which is calculated by Equation 3-2, for the sample and the regularised hydrodynamic radius, for which the major peak is labelled.

$$g^2(\tau) = \frac{\langle I(t)I(t+\tau)\rangle}{\langle I(t)\rangle^2}$$
Equation 3-2

Equation 3-2: Correlation Function where I is intensity of light, t is initial time, and $t + \tau$ is elapsed time, and brackets indicate an average over all t values.

The results of the DLS analysis of BAM proteoliposomes generated by dilution (Figure 3-15) indicate that there is predominantly a single population with a mean hydrodynamic radius of 91.53 ± 47 nm. The Polydispersity index is 0.278 for this sample. As samples are considered monodisperse with a PDI close to 0.1, and polydisperse with PDI > 0.6 therefore the sample is considered monodisperse[312]. The small peaks seen either side are probably contaminants and hence judged to be insignificant.
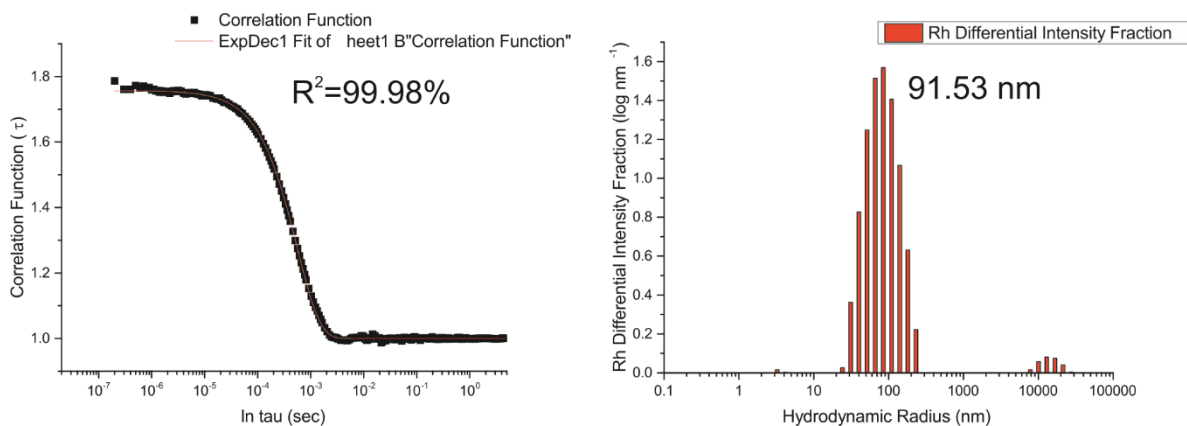
Figure 3-15: Correlation function and regularisation plot for BAM proteoliposomes generated by dilution and ultracentrifugation. Proteoliposome samples were diluted 1/120 to obtain a lipid concentration of ~50 µg/mL and 250 µL of the samples were then injected. See Methods Section 2.11 for details.

The proteoliposomes generated by dialysis appear larger with a mean hydrodynamic radius of 200 ± 167 nm (Figure 3-16). In addition to the larger error on this peak, the samples appear more polydisperse with the polydispersity index of 0.74.
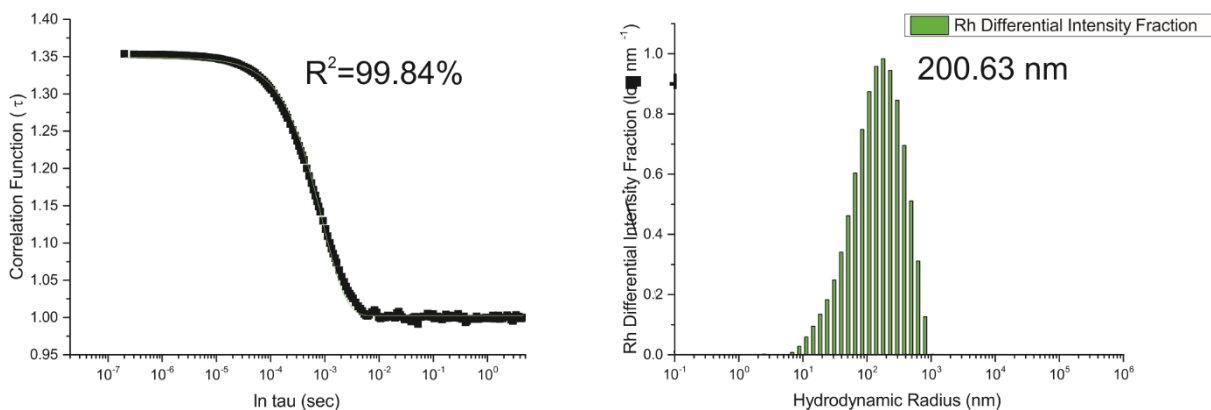
Figure 3-16: Correlation function and regularisation plot for BAM proteoliposomes generated by extensive dialysis. Proteoliposome samples were diluted 1/60 to obtain a lipid concentration of ~50 µg/mL and 250 µL of the samples were then injected. See Methods Section 2.11 for details.

The proteoliposomes generated by dialysis appear larger than those generated by dilution and ultracentrifugation and are more heterogeneous. In addition, the experiment was carried out only once for each sample, therefore replicate error is unclear. The mean hydrodynamic radius in both populations is in accordance with that reported in the literature for studies of *E.coli* polar lipid liposomes using

DLS (~200 nm diameter)[313]. The experiment was unfortunately not carried out with proteoliposomes containing other BAM variants or repeated with other preparations of wild-type proteoliposomes. However, it has now been repeated by my colleague Dr Bob Schiffrin, with his batch of dialysis proteoliposomes. The results showed more monodisperse peaks with mean hydrodynamic radii of 50-60 nm for BAM proteoliposomes and ~58 nm for empty proteoliposomes (Dr Bob Schiffrin, private communication).

3.5 OmpT assay

Reconstitution of BAM in proteoliposomes is necessary to assay its activity as an OMP folding catalyst. The enzymatic OmpT assay[189,268] has been used widely as a measure of BAM complex activity. It was employed to great effect in this project. The fluorimetric assay, first published in 2000[268], utilises OmpT's protease properties, and a substrate Abz-Ala-Arg-Arg-Ala-Tyr(NO_2)-NH_2. When excited at 325 nm the *o*-aminobenzoyl (Abz) moiety will emit fluorescence with a maximum at 430 nm. However, this is quenched by the nitrotyrosine, Tyr(NO_2), of the intact substrate. OmpT will cleave between the arginines[268,275], separating the fluorophore and quencher and producing a fluorescence readout. While possessing some limitations, particularly in that OMP folding is only indirectly measured using this assay, this section will discuss some of the optimisation and applications of this assay. BAM proteoliposomes were regularly prepared for use in this assay, and were used immediately or snap-frozen for storage at -80 °C. The fluoropeptide was ordered from PeptideSynthetics and resuspended in 18 mΩ H_2O to a 10x stock concentration. OmpT was purified from inclusion bodies (see Methods 2.3.1) and preparations of SurA were carried out by myself, Julia Humes and Dr Bob Schiffrin and used interchangeably (Methods, Section 2.3.3).

3.5.1 Optimization of the OmpT assay

The OmpT enzymatic assay works when OmpT is delivered by SurA, folded by functional BAM in proteoliposomes and is then able to cleave the fluoropeptide to produce a fluorescence signal (Figure 3-17).
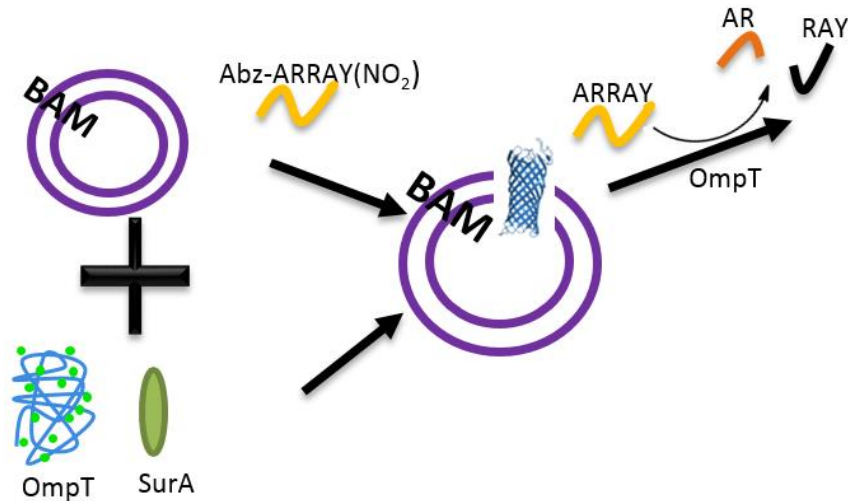
Figure 3-17: Schematic of OmpT enzymatic assay with BAM proteoliposomes. The 10-stranded β-barrel OmpT, denatured in urea, is mixed with chaperone SurA. The fluoropeptide (ARRAY) is mixed with BAM complex in *E.coli* polar lipid proteoliposomes. When the two subreactions are mixed together and OmpT is folded it is capable of cleaving the fluoropeptide, producing a fluorescence output.

While SurA can to a certain extent be replaced by urea at concentrations of 0.5-2 M[159] it appears principally to function to maintain OMP folding competence by preventing aggregation. In the absence of any of the active components, however, there is no fluorescence, and changing any of these parameters can alter the output of fluorescence intensity versus time. Controls, demonstrating the efficacy of this assay were carried out multiple times, with one representative example in optimised conditions shown below (Figure 3-18). The assay was controlled to only remove one active component in each sample and shows that BAM, OmpT, substrate and SurA are all required for a fluorescence output indicative of productive folding of OmpT.
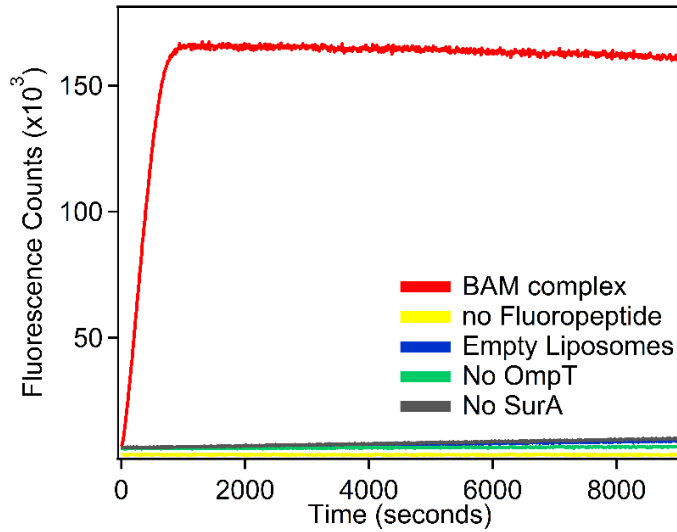
Figure 3-18: OmpT assay controls. The OmpT assay was set up with 0.25 μM BAM proteoliposomes created by the dialysis method, 5 μM OmpT, 35 μM SurA, 1 mM fluorogenic peptide, 0.8 M urea in 50 mM glycine-NaOH pH 9.5.

Initially, following creation of proteoliposomes by multiple methods, the activity of both "old" (dilution) and "new" (dialysis) proteoliposomes was assayed for the same apparent concentration of BAM (Figure 3-19). The results demonstrate the much higher activity of the dialysis method for production of BAM proteoliposomes with a fast kinetic trace and considerably shorter t_{50}.
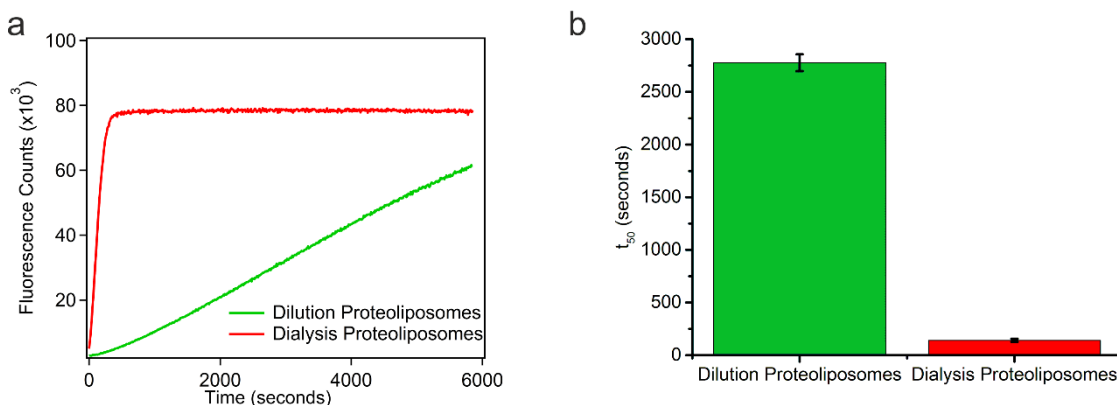
Figure 3-19: Analysis of dilution and dialysis methods for the creation of BAM proteoliposomes. (a) activity in OmpT assay and (b) t_{50} extracted from assay. Samples contained 2.5 μM BAM proteoliposomes, 10 μM OmpT, 70 μM SurA, 1mM fluoropeptide, 0.88 M urea in glycine-NaOH pH 9.5. The t_{50} utilises the average and standard error of the mean (SEM) of two repeats, one of which is shown in (a).

112

It was following this striking result (Figure 3-19) that dialysis proteoliposomes were exclusively used moving forward. Next, the conditions for the activity assay were optimised. Although experiments had been started using 2.5 μM BAM (Figure 3-19), this concentration led to a rapid apparent folding rate using the dialysis method of creation of BAM proteoliposomes. A slower initial rate was desirable to better quantify small differences in the apparent folding rate. Therefore the concentrations of different components were altered to optimise the assay. It was found that decreasing the OmpT and SurA concentration did not significantly slow the apparent folding rate. However, decreasing the BAM concentration had a marked effect, as expected (Figure 3-20).
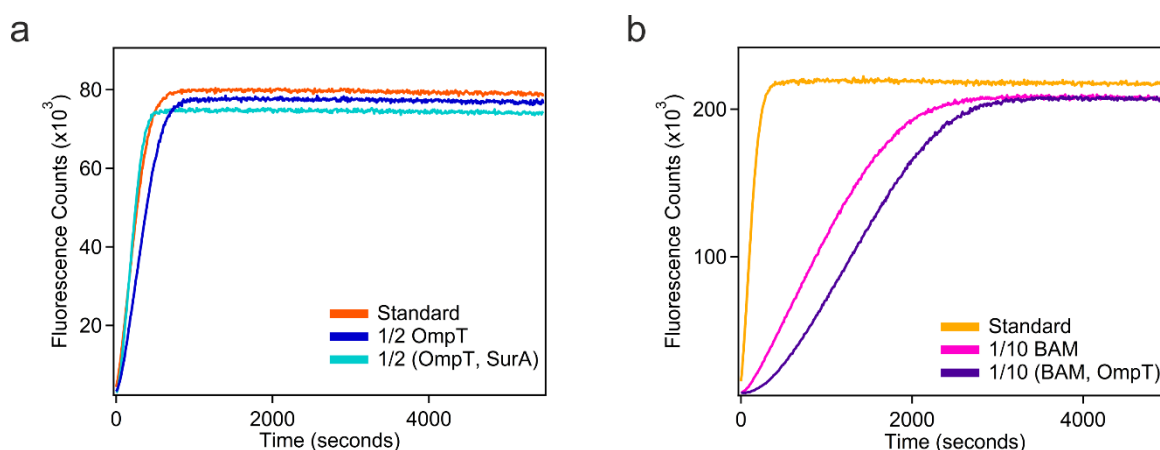
Figure 3-20: Optimisation of conditions for the OmpT activity assay with (a) changes in OmpT and SurA concentration and (b) changes in BAM and OmpT concentration. a) Initial assay conditions (Standard, orange) were 1.25 μM BAM, 10 μM OmpT, 70 μM SurA, 1 mM fluoropeptide, 0.8 M urea in 50 mM glycine-NaOH pH 9.5. This was modified by dilution to 5 μM final OmpT (blue line) or 5 μM OmpT, 35 μM SurA (cyan line) with other conditions as standard. b) Initial conditions (standard, yellow) utilised 2.5 μM BAM, 10 μM OmpT, 70 μM SurA, 1 mM fluoropeptide, 0.8 M urea in 50 mM glycine-NaOH pH 9.5. This was modified by dilution to 0.25 μM BAM (pink line) or 0.25 μM BAM, 1 μM OmpT (purple line) with other conditions as standard. Each experiment was carried out only once.

Using the results of optimisation dilutions (Figure 3-20) the conditions used for further assays were 0.25 μM BAM, 5 μM OmpT, 35 μM SurA, 1 mM fluoropeptide, 0.8 M urea, 50 mM glycine-NaOH pH 9.5 with experiments measured at 25 °C, for further details see Methods Section 2.12.1.

3.5.2 Understanding the OmpT assay

The OmpT activity assay has a number of applications, as discussed later (Sections 3.5.3, 3.5.4 and 5.5), but it was also desirable to understand how this indirect assay reports on OmpT folding, and perhaps to devise a kinetic model. To this effect, considerable work was performed varying the concentrations of all components to understand their contribution. Now working from the standard conditions (0.25 μM BAM proteoliposomes, 5 μM OmpT, 35 μM SurA, 1 mM peptide, 0.8 M urea in 50 mM glycine-NaOH pH 9.5), dilutions of BAM and OmpT were carried out. It is immediately clear that altering the concentration of the BAM complex has an effect on the measured activity in the assay as expected (Figure 3-21a). However, increasing BAM concentration does not appear to lead to a linear increase in initial rate of folding, and measurement is complicated by the appearance of a lag phase. More subtle, however, is the effect of OmpT concentration, which surprisingly has only a small effect on the apparent folding rate, with perhaps even an increase in rate at decreased concentration (Figure 3-21b). This is evidently paradoxical as correctly folded OmpT is necessary to cleave the fluoropeptide to produce a fluorescence signal. But as BAM is necessary to first fold OmpT (Figure 3-18) and it is present at a significantly lower (20-fold) concentration than its substrate OmpT, perhaps it is the effect of dropping OmpT to nearer the concentration of its catalytic enzyme. Additionally, the concentration of SurA was unchanged in this experiment, therefore at a lower concentration of OmpT there is a more significant excess of chaperone, perhaps aiding faster folding.
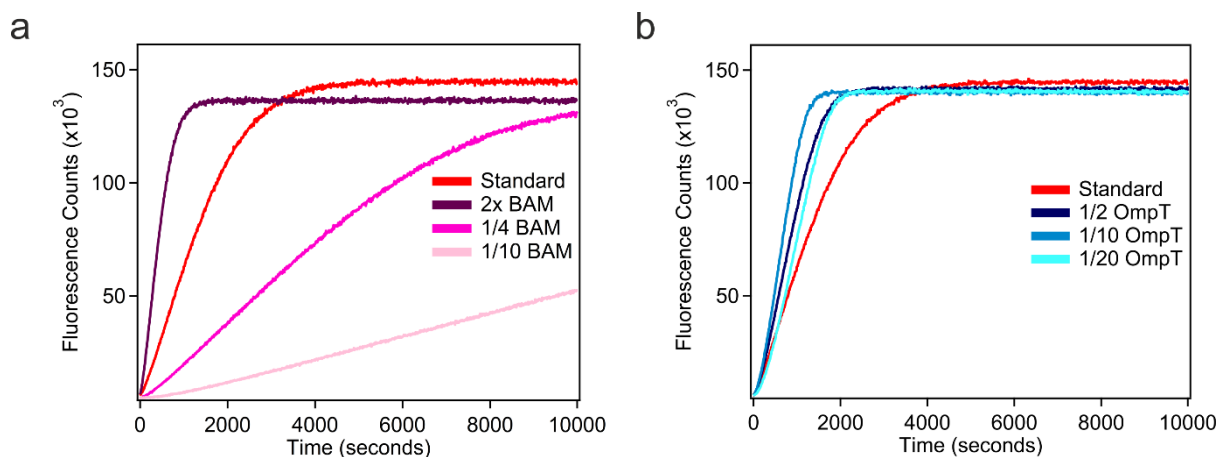
Figure 3-21: Effect of variation of (a) BAM and (b) OmpT concentration on OmpT activity assay. The standard conditions, depicted as a red line in both cases utilised 0.25 μM BAM proteoliposomes, 5 μM OmpT, 35 μM SurA, 1 mM peptide, 0.8 M urea in 50 mM glycine-NaOH pH 9.5. The results of a & b were from the same assay, which are represented separately for clarity. In (a) BAM concentration was varied: 0.25 μM, 0.5 μM, 0.06125 μM and 0.025 μM final BAM concentrations accordingly and all other concentrations remaining as standard. In (b) OmpT concentration was varied by dilution of the original stock in 8 M urea. A constant final urea concentration of 0.8 M was maintained. The final concentrations of OmpT were 5 μM, 2.5 μM, 0.5 μM and 0.25 μM with constant BAM concentration of 0.25 μM. This experiment was carried out twice for which one representative example is shown.

In addition to the direct effect of the concentration of the BAM complex, altering the concentration of BAM proteoliposomes has a confounding secondary effect, of altering the lipid: protein ratio (LPR). As dilutions of BAM are carried out by diluting the reconstituted proteoliposomes this is unavoidable when using the same set of proteoliposomes. However, to test not only the effect of the BAM complex, but also the effect of the LPR, proteoliposomes were generated with lower original concentrations of BAM. The dialysis protocol generates proteoliposomes with a low LPR (2:1 by weight, ~120:1 molar ratio) and it is possible that this crowded BAM causes the high activity observed, but may also limit the total substrate folding. Proteoliposomes were therefore created using 1/10 and 1/100 dilutions of BAM in detergent, creating liposomes with 20:1 and 200:1 LPR by weight. Reconstitution appeared successful. However, particularly for the 1/100 dilution of BAM, the protein concentration could not be accurately measured. For this sample therefore total concentration is assumed at 0.07 μM, based on consistent reconstitution of BAM at ~7μM in non-diluted samples. The first assay (Figure 3-22a) compares normal proteoliposomes (made at 2:1 LPR by weight) at final BAM concentrations standard (0.25 μM), ½ (0.125 μM), and ¼

115

(0.0625 μM) with those made with 1/10 (y) and 1/100 (z) less BAM in the proteoliposomes. The legend therefore refers to the final concentration of BAM in that sample, relative to the standard of 0.25 μM with x, y, or z denoting the original LPR. Unsurprisingly, considering previous results, less BAM causes lower activity, and there does not appear to be a compensating effect by higher LPR (y and z).

Experiments were also carried out with a lower concentration of OmpT to more accurately measure activity at low concentrations of BAM (Figure 3-22b). A 1/10 BAM proteoliposome preparation produces very low activity (Figure 3-22a orange line). This becomes easier to compare if the concentration of OmpT is also reduced (Figure 3-22b). In addition, in this experiment, the same concentration of BAM was compared across different LPRs. This allows us to see, for example, that at the same concentration of BAM (0.005 µM, '1/50 BAM') and liposomes made with a 2:1 (x,green) or 200:1(z,pink) LPR, the lower LPR results in a more active system. The same trend is seen for BAM at 0.05 µM ('1/5 BAM') between proteoliposomes made with 2:1 LPR (x,sky blue) or 20:1 LPR (y,purple). Therefore, having more lipid around the BAM likely decreases, rather than increases apparent BAM activity for the same concentration of enzyme and OmpT substrate.
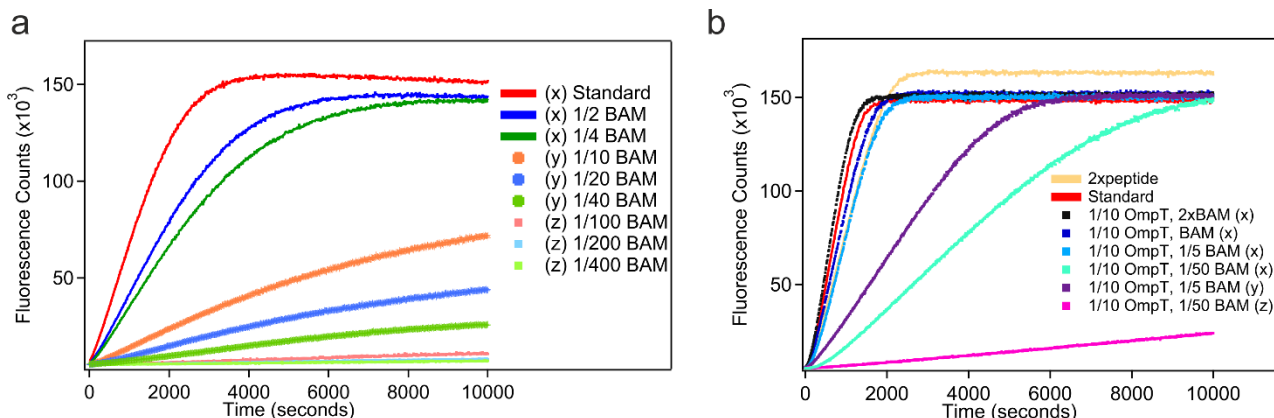
Figure 3-22: Effect of LPR, BAM and OmpT concentration on the OmpT activity assay. The standard conditions, depicted as a red line in both cases utilises 0.25 μM BAM proteoliposomes, 5 μM OmpT, 35 μM SurA, 1 mM peptide, 0.8 M urea in 50 mM glycine-NaOH pH 9.5. In this figure (x) denotes proteoliposomes generated with the original 2:1 LPR, whereas (y) denotes a proteoliposomes with a 20:1 LPR and (z) a 200:1 LPR. Therefore for panel (a), the last three traces, with (z) utilise the proteoliposomes containing 1/100 original concentration of BAM, creating 1/100 (~0.0025 μM final BAM), 1/200 (~0.00125 μM final BAM), and 1/400 (~0.000625 μM final BAM). In panel (b) the format is the same, comparing dilutions across proteoliposomes with different LPRs. The majority of assays for this experiment, were carried out with 1/10 OmpT (0.5 μM) retaining other conditions (35 μM SurA, 1 mM peptide, 0.8 M urea in 50 mM glycine-NaOH pH 9.5) as standard. Each experiment was carried out twice, for which one replicate is shown.

The results of altering BAM concentration and LPR are increasingly interesting when one considers the model of BamA oligomerisation[211,212]. This has been a pervasive hypothesis since original identification of the BamA protein[211], but is strongly supported by studies demonstrating OMPs to co-localise[216,283]. These studies demonstrate that copies of BAM cluster to function. This would suggest that BAM proteoliposomes generated with a lower LPR would exhibit greater activity, as the copies of the BAM complex would be more clustered than for the same concentration of BAM proteoliposomes created with a high proportion of lipid. This is in fact exactly what is observed, with the lower LPR leading to increased activity in BAM folding OmpT, lending support from this experiment to oligomerisation and BAM islands.

A final aspect of the OmpT assay which was of interest and a control for observed activity, was whether isolated BamA is capable of catalysing the folding of OmpT into liposomes formed of *E.coli* polar lipid extract. It has been shown previously that BamA can be assembled by BAM lipoproteins and this is more efficient than it can be assembled by itself[272]. However, BAM lipoproteins are not capable of

117

catalysing OmpA assembly[272]. In order to examine this, proteoliposomes of *E.coli* polar lipid extract were generated containing folded BamA (Methods, Section 2.10.2). The reconstitution and correct folding was verified (Figure 3-23a) and these were then tested in the OmpT assay and compared against proteoliposomes containing the BAM complex. Proteoliposomes containing BamA were tested both at the same lipid (1) or protein (2) concentration used for the BAM complex proteoliposomes (Figure 3-23, see Methods 2.10.2 for details). The results show, remarkably, that BamA cannot fold OmpT under the conditions employed, whilst BAM is a highly efficient catalyst.
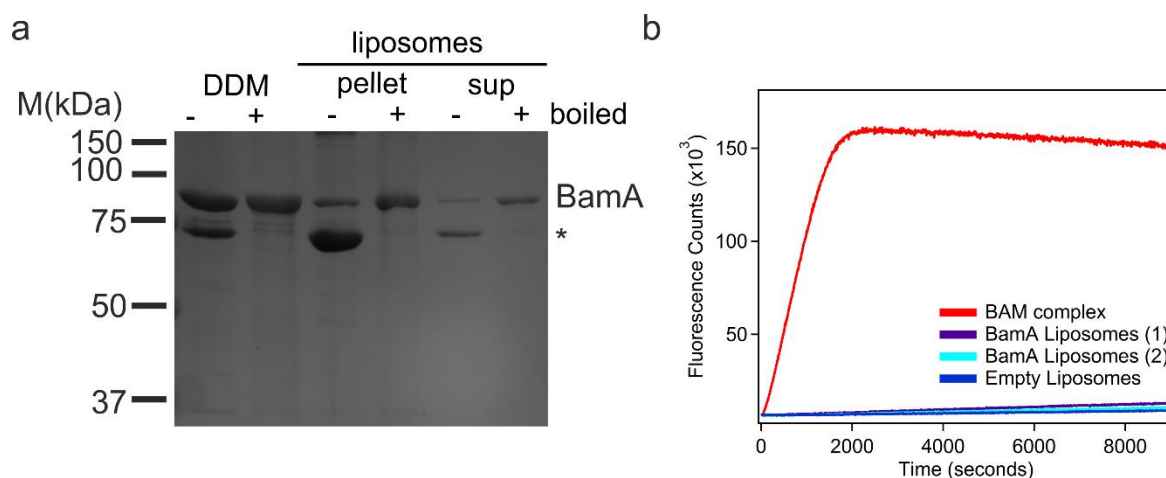
Figure 3-23: BamA in liposomes formed from *E.coli* polar lipids does not assist OmpT folding. (a) Semi-native PAGE with low SDS concentration (0.1 % (*w/v*)) to demonstrate bandshift of folded BamA. BamA was prefolded in TBS+0.05% (*w/v*) DDM and 3 M urea, to mimic the protocol to produce BAM-containing proteoliposomes, before following the proteoliposomes dialysis procedure. BamA has clearly associated with the liposomes (present in pellet) and is mostly folded. A * denotes folded BamA, which is unfolded when boiled (+). (b) An OmpT activity assay was carried out with BAM complex and BamA proteoliposomes. The conditions used for BAM are 0.25 μM BAM proteoliposomes, 5 μM OmpT, 35 μM SurA, 1 mM peptide, 0.8 M urea in 50 mM glycine-NaOH pH 9.5. For BamA, proteoliposomes were created at the same weight LPR as BAM complex proteoliposomes, resulting in a different BamA: lipid molar ratio. The BamA proteoliposomes were either diluted for the same assumed concentration of lipid (1) as in the BAM proteoliposomes and a concentration of ~0.6 μM, or diluted to equivalent concentration of BamA protein (2), ~0.25 μM.

3.5.3 Assessing inhibitors in the OmpT assay

The results presented above show that OmpT can be folded only when catalysed by BAM and delivered by the chaperone SurA (Figure 3-18). The assay was optimized for assessing how alterations to the BAM complex impact its catalytic ability, discussed in Chapter 5 (Section 5.5). However, an important application of the OmpT assay developed here is in screening potential inhibitors of OMP folding or BAM activity. Three different potential inhibitors have been of interest based on the literature, and were tested in this assay, the results of which are summarised below.

The first two "inhibitors" (BamD and 'Peptide2') are based on the same concept and research. It is known that BamA and BamD are the only essential components of the BAM complex[21,25,187,188]. The "β- signal" hypothesised to be present in OMPs and vital for substrate assembly was originally proposed to first bind BamD by *in silico* experiments demonstrating the ability to dock the peptide in the BamD TPR scaffold[195]. The proposed signal, containing a conserved Glycine residue and patterns of hydrophobic residues (i.e. GxxΦxΦ, where Φ denotes hydrophobic)[174] is found in the β14 strand of BamA[175]. Mutagenesis experiments have shown this signal to be both necessary and sufficient for binding of substrate BamA to BamD[175]. Furthermore, a 15 amino-acid stretch (NIRMSAGIALQWMSP, henceforth denoted as Peptide 2) containing the recognition signal is able to inhibit the folding of BamA by BAM, is toxic *in vivo* and may act as a general inhibitor of OMP assembly[175]. This peptide was therefore purchased and its effect on OmpT folding assayed. The effects of the peptide had not been characterised in *in vitro* activity assays such as ours. Additionally, this and other research suggested that BamD binds OMPs prior to their assembly in the membrane[175,220]. Therefore, the addition of soluble BamD to a folding reaction would be anticipated to slow OMP folding by sequestering substrate. Due to low solubility of purified BamD, these assays were carried out at reduced OmpT concentration. However no effect of BamD was seen at a 25- or 40- fold molar excess over OmpT (Figure 3-24a).

In the majority of the inhibition assays the component was tested both by pre-incubation in the OmpT-SurA subreaction or the BAM proteoliposome-peptide subreaction. It is indicated for each sample in which subreaction (BAM/OmpT+) preincubation occurred. The β-signal mimic, Peptide 2, was anticipated to be

119

recognised by the BAM complex and thus may compete and slow folding of OmpT. It was thus anticipated that a specific effect would be seen for the peptide when pre-incubated with BAM proteoliposomes. However, any effect in this case was indistinguishable from the effect of the DMSO control (Figure 3-24b). The peptide only demonstrated an effect when pre-incubated with OmpT in low SurA conditions (Figure 3-24b, light blue&green). Due to the effect only in low SurA conditions, the peptide is possibly causing aggregation of OmpT, rather than acting as a specific inhibitor.
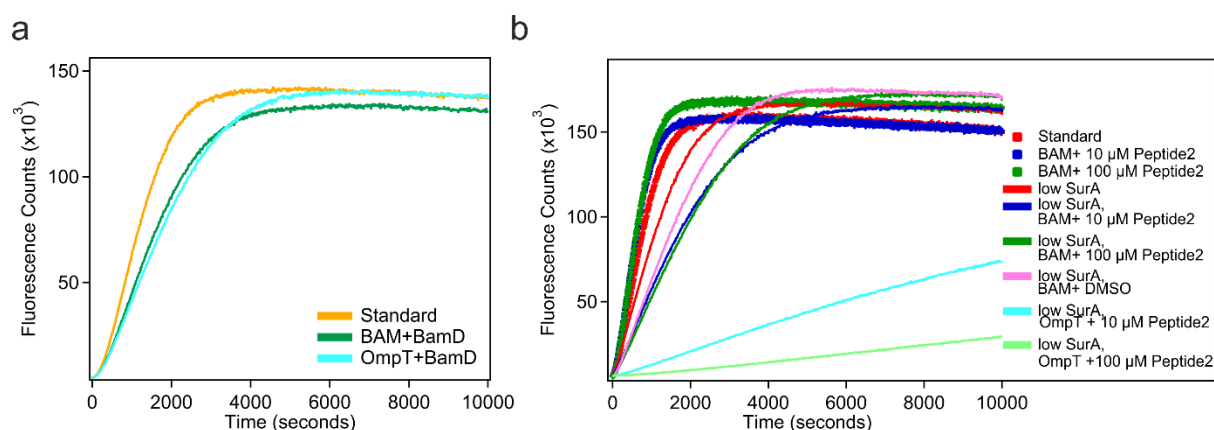
Figure 3-24: Inhibition of OmpT folding by BAM by a) BamD and b) 15aa "Peptide2". (a) Standard conditions, shown in orange utilise 0.25 μM BAM proteoliposomes, 0.5 μM OmpT, 35 μM SurA, 1 mM fluoropeptide, 0.8 M urea in 50 mM glycine-NaOH pH 9.5. BamD in pre-incubation with BAM (green line) is at 20 μM final concentration and with OmpT (cyan) is at 12.5 μM. (b) Standard conditions, denoted by a red line, contain 0.25 μM BAM proteoliposomes, 5 μM OmpT, 35 μM SurA, 1 mM fluoropeptide, 0.8 M urea in 50 mM glycine-NaOH pH 9.5. Peptide 2 is made up in DMSO in 10x stocks, therefore an equal volume DMSO control is included. Conditions are as standard for thicker lines, but were also carried out with low SurA (10 μM final concentration), denoted by thinner lines. Each experiment was carried out twice for which one representative example is shown.

The final inhibitor tested was a macrocyclic peptide (Figure 3-25). This peptide, JB-95, was of interest following research demonstrating it to possess antimicrobial activity, to increase OM permeability, and to downregulate expression of several OMPs[47]. An interesting possibility therefore was that this peptide affects BAM. A macrocylic peptide, L27-11 which was shown to be active against LptD in *Pseudomonas aeruginosa*[314] was used as a control.
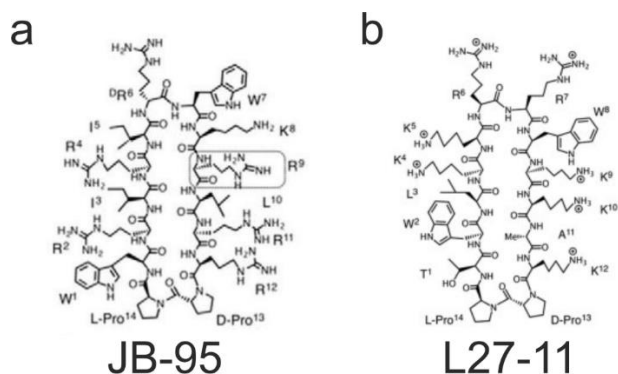
Figure 3-25: Structures of Macrocyclic peptides. a)JB-95, image from Urfer *et al.*, 2016[47]. b) L27-11, image from Schmidt *et al.*, 2013[315].

While the macrocyclic peptide does apparently show a titratable effect of inhibition, with 25 μM of peptide ablating any observed folding, the reoccurring trend is that the control peptide (L27-11) demonstrates the same effects (Figure 3-26). In addition to assaying these peptides by pre-incubation in BAM or OmpT subreactions (Figure 3-26a), they were also tested on OmpT prefolded in DUPC LUVs (Figure 3-26b), see Methods 2.12.3 for details. In the cases of OmpT prefolded in DUPC LUVs, inhibition by the peptides is less (Figure 3-26b, thin lines, pink to blue/green) than with OmpT folding in BAM (thick lines, brown to blue/green). However, the control peptide L27-11 demonstrates the same inhibition (Figure 3-24 thick blue/green). Therefore we cannot conclude JB-95 to be a specific inhibitor from this assay.

121
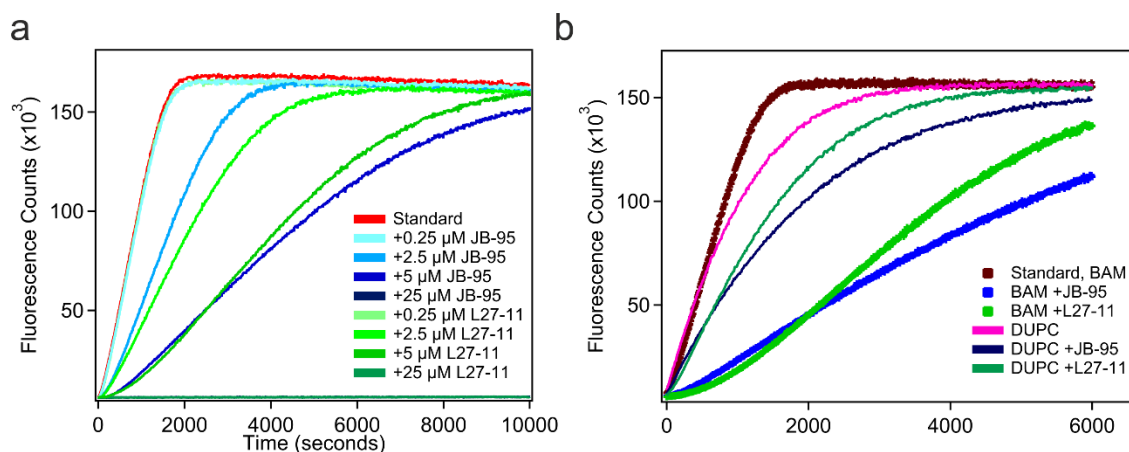
Figure 3-26: Inhibition of OmpT folding with macrocylic peptides. a) Macrocyclic peptides JB-95 and L27-11 are dissolved in glycine buffer and pre-incubated with BAM before commencing the assay. Each reaction contains 0.25 μM BAM proteoliposomes, 5 μM OmpT, 35 μM SurA, 1 mM fluoropeptide, 0.8 M urea in 50 mM glycine-NaOH pH 9.5, with the described final concentrations of peptide. (b) Macrocyclic peptides were tested both with OmpT folded by BAM, by pre-incubation of peptide with the BAM subreaction, and OmpT in DUPC. OmpT DUPC samples were prefolded in DUPC overnight at 25 ⁰C and then mixed in plate with LPS, fluoropeptide and inhibitor. For ease of folding in DUPC, and for consistency OmpT concentration is 0.8 μM throughout and where SurA is used this is 5.6 μM, to be at the normal 7x excess, all other BAM-assay concentrations are as standard (0.25 μM BAM proteoliposomes, 1 mM fluoropeptide, 0.8 M urea in 50 mM glycine-NaOH pH 9.5). Peptides are used at 5 μM final concentration. DUPC samples contain 0.24 M urea, 1mg/ml LPS and 2.56 mM DUPC (molar LPR 3200:1). The experiments were carried out three times, for which one representative example is shown.

There were confounding effects in this case as it was later noticed that the peptide of interest possesses sequential charged residues (Figure 3-25), which are the recognition site for cleavage by OmpT[268,275]. Therefore it may compete with fluoropeptide as a cleavage substrate, and slow apparent fluorescence by this means, rather than inhibition. It was attempted to untangle the effects of the macrocyclic peptides on BAM and OmpT utilising OmpT prefolded in DUPC LUVs as opposed to folded by BAM proteoliposomes. It would be expected in this case that if the peptide is specific against BAM, inhibition would not occur, but competition with the fluoropeptide would still be observed. As noted, the magnitude of inhibition by the peptides is less for OmpT prefolded in DUPC LUVs (Figure 3-26, thin lines) than folded by BAM proteoliposomes, therefore perhaps the competition effect is minimal. However, both JB-95 and the control peptide L27-11 consistently demonstrate the same effect. It is unlikely that specific BAM inhibition is being observed in this case. Furthermore, the peptides in question were designed resembling cationic antimicrobial peptides (CAMPs)[316], and are

122

therefore short, possessing positively charged residues. These consequently resemble the sequences of cell-penetrating peptides (CPP)[317]. CPPs can be synthetic or natural, but are characterised by their ability to cross the membrane with minimal toxic effect[317]. One of the best examples of CPPs is the Tat peptide of Human Immunodeficiency Virus (HIV)[318]. One mechanism by which CPPs are proposed to enter cells is membrane disruption. Therefore it is likely that the peptide inhibitors in question play a non-specific role in membrane disruption, which would be obscuring any specific effect in inhibition of BAM. While the peptide L27-11 has been specifically characterised as functioning against the OM protein LptD[319], in the context of these assays, critical controls on the function of each peptide on empty liposomes would be necessary before assessing inhibitory effects towards BAM function.

3.5.4 The effect of different chaperones of BAM-mediated OmpT folding

The OmpT enzymatic assay also provides an effective and rapid way to determine the effects of many different players in the OMP folding system. In addition to probing the effects of substrate, BAM and inhibitors, it is also possible to examine the role of SurA in delivering OMPs to the BAM complex. This work was performed in conjunction with Julia Humes (University of Leeds), who was examining the role of the different domains of SurA on OMP folding and delivery to BAM.

SurA is a conserved periplasmic chaperone, vital to the assembly of OMPs. SurA possesses four domains: two parvulin-like peptide prolyl isomerase domains (P1 and P2) and N- and C-terminal domains[166]. The removal of one or both PPIase domains does not damage OM integrity or lead to an increase in the σ^E stress response or reduction of membrane integrity[171,172]. However, the PPIase domains have been suggested to regulate the chaperone activity of the vital N-Ct domains of the chaperone[172]. It was of interest to test how the different domains of SurA may contribute to, or regulate, SurA chaperone ability. Variants were constructed that lacked either the P2 domain (ΔP2) or both PPIase 1 and 2 domains, fusing the N- and C-terminal domains together (N-Ct), see Methods 2.3.3. Various assays were then carried out to determine the ability of these different variants to bind OMPs, prevent aggregation and deliver to BAM (Humes&Schiffrin, *in*

preparation). The SurA variants were additionally compared with other *E.coli* chaperones (Skp, Spy and SecB).

The OmpT assay was then used to determine the effectiveness of the SurA variants and other chaperones to fold and deliver OmpT to BAM. This exploits the finding described above, that in the absence of SurA there is no fluorescence increase (Figure 3-18). Aggregation data from light-scattering has shown that OmpT is aggregation prone (Humes&Schiffrin, *in preparation*), and requires a 100-fold excess of SurA to prevent aggregation when incubated in glycine buffer containing 0.24 M NaCl. In the no Nacl conditions used in the OmpT activity assay, OmpT aggregation is greatly decreased. However, it is likely that in the absence of any SurA, some OmpT will aggregate and not be delivered to BAM. The aggregation data has shown that neither SurA variant was able to prevent the aggregation of OmpT as effectively as WT(Humes&Schiffrin, *in preparation*).

The OmpT activity assay reports the ability of SurA to chaperone OmpT and deliver the OMP to the BAM complex for folding. The OmpT activity assay data (Figure 3-27) clearly demonstrate that while the ΔP2 variant was able to aid OmpT folding nearly to the level of wild-type SurA, all other chaperones functioned at a considerably lower level. The N-Ct SurA variant demonstrates worse folding of OmpT than wild-type or ΔP2 SurA. Additionally, other *E.coli* chaperones were tested. SurA and Skp are periplasmic chaperones of OMPs, while Spy is periplasmic and known to bind soluble proteins, and SecB interacts with OMPs in the cytoplasm, therefore it would be anticipated that they would have different OMP-chaperoning abilities. SecB is apparently unable to deliver substrate, with nearly no fluorescence increase seen (Figure 3-27) whilst the periplasmic chaperones (Skp and Spy) demonstrate some ability to chaperone for OmpT folding, less than that of wild-type SurA. As the different chaperones demonstrate different behaviour not adequately reflected in the t_{50} values, the initial rate of the folding assays were also quantified and compared (Figure 3-27c). This more accurately reflects the ability of SurA variants and Skp to partially aid folding in the OmpT assay, while SecB and Spy cannot. The results present an interesting contrast with aggregation data, in which other chaperones, particularly Skp, may function nearly to WT levels. These chaperones, however are not able to perform SurA's specific role of delivery to BAM in the membrane.

124
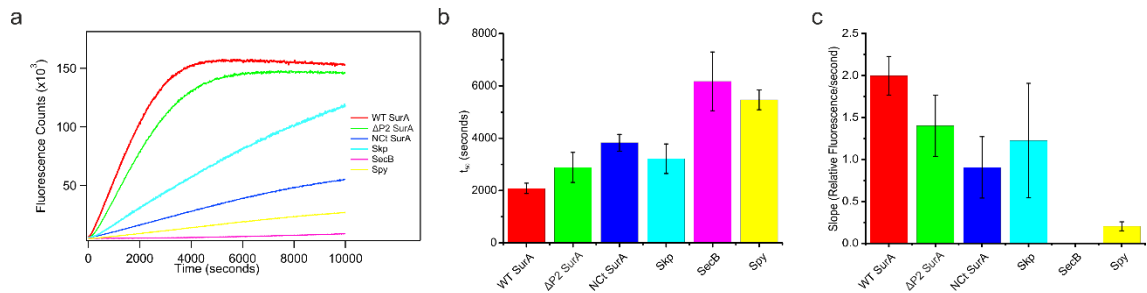
Figure 3-27: SurA variants and other chaperones assist in OmpT assay but not to wild-type levels. (a) Example OmpT assay comparing different chaperones in the same conditions. The setup in these experiments was 0.25 µM BAM, 5 µM OmpT, 35 µM chaperone, 1mM fluorogenic peptide, 0.8 M urea in 50 mM glycine-NaOH pH 9.5 b) t_{50} with average and SEM across a minimum of 3 repeats, with the exception of Spy, which is 2. c) Initial rate, calculated as slope for normalised fluorescence increase over initial 500 seconds. Shown is the average and SEM across a minimum of 3 repeats, with the exception of Spy, which is 2. SecB shows a negligible negative rate due to a considerable lag-time.

Based on these results it appeared likely that other chaperones and SurA variants were functioning, simply not as effectively as wild-type SurA. This was additionally tested with a reduced chaperone and OMP concentration relative to BAM (2 µM OmpT, 20 µM chaperone, 0.25 µM BAM) and the same trend was observed across the chaperones. Additionally, whether the SurA variants could function as effectively as wild-type SurA if used at an increased chaperone: OMP ratio was explored. Particularly for the chaperone N-Ct, which is considerably smaller than WT SurA, it may simply not have sufficient surface area to bind substrate OMPs when used at an equivalent concentration. The typical concentrations in the OmpT assay are 35 µM SurA, with 5 µM OmpT. The setup of this assay already involves a seven-fold excess of chaperone over substrate. This was now tested for N-Ct at 2- and 4- fold greater chaperone:substrate ratio (effective ratio 14- and 28- fold excess) and with wild-type SurA at a 4-fold greater concentration for comparison. The comparison of t_{50} values for repeated assays across the conditions (Figure 3-28) demonstrates that increasing the amount of SurA does not alter folding t_{50}. Assays containing N-Ct SurA consistently demonstrate a higher t_{50}, indicating slower folding, than those with wild-type SurA. In this assay, the ability of wild-type SurA to chaperone OmpT cannot be matched even by a vast excess of N-Ct SurA. In conclusion, data from the OmpT assay has contributed to understanding the roles of SurA domains. This

additionally shows that OMP delivery, performed by SurA in the OmpT assay may differ from its role preventing aggregation.
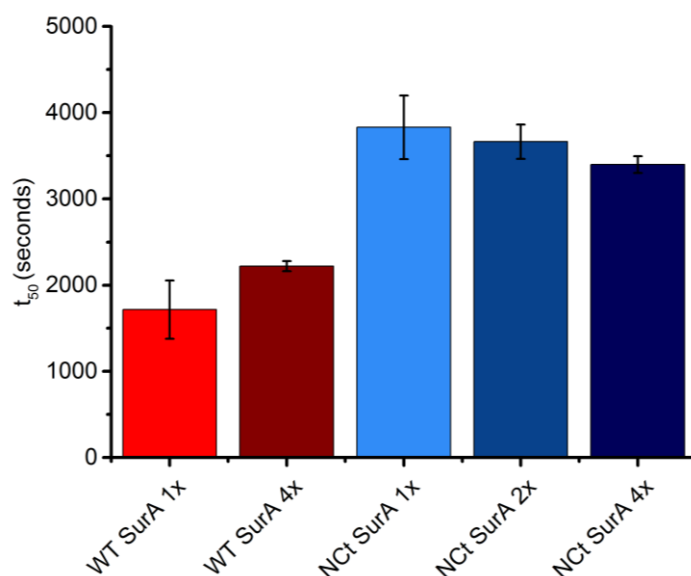
Figure 3-28: Comparison of t_{50} for WT and N-Ct SurA at increased SurA:OMP ratios. The average and SEM is shown across a minimum of three repeats. The standard in this case (1x) was 35 μM SurA, with 5 μM OmpT, 0.25 μM BAM, 1 mM peptide, 0.8 M urea in 50 mM glycine-NaOH pH 9.5. All other conditions were kept constant and only the concentration of chaperone altered, see Methods, Section 2.12.3 for details. Both wild-type SurA results are significantly different from all N-Ct sample results, but within wild-type and N-Ct subsets differences are not significant. Two sample t-tests were used to assess significance, with a p-value of <0.05 considered significant.

3.6 Membrane mimetics

In any discussion of membrane proteins one cannot ignore the effect of the membrane on protein function. The examples discussed in this thesis primarily involve proteoliposomes: either synthetic lipid 100 nm LUVs, or proteoliposomes of *E.coli* polar lipid extract, created by dialysis or dilution and structural studies in detergent. It was therefore also of interest to study the BAM complex utilising other membrane mimetics.

Protein-supported nanodiscs involve the reconstitution of a membrane protein into phospholipids encircled by a helical protein[320]. In this case, the membrane protein of interest is solubilized in detergent and mixed with phospholipids and the "membrane scaffolding protein" (MSP). The detergent is removed and the phospholipid assembles into a bilayer, around the target protein. Two molecules of MSP wrap around the edges, in a belt-like fashion, with one covering each side of the hydrophobic alkyl chains of the leaflet (Figure 3-29c)[306], a conformation confirmed by magic-angle spinning NMR[321]. Nanodiscs are attractive as the MSP belt maintains stability, and structural and functional studies of the membrane protein may be carried out on the same sample[320]. While there is as yet no crystal structure of membrane proteins in nanodiscs[322], cryo-EM has been used, with the structure of a ryanodine receptor resolved to a 6.1 A resolution[323]. Obtaining a cryo-EM structure of BAM in a nanodisc would be the first insight into the structure of the complex in a lipid, with the added advantage that activity assays can be applied to the same sample.

Preparation of nanodiscs containing the BAM complex resembles preparation of proteoliposomes. It first involves purification of BAM from the membrane using detergent. Although a non-ionic detergent such as DDM is considered 'mild', and less likely to denature or inactivate a protein[324], it is clearly disruptive to the native environment. This is why the use of SMALPs is an attractive new possibility. The SMALP, or styrene-maleic acid (SMA) lipid particle, uses the amphiphathic synthetic copolymer SMA to extract proteins from their native membrane, in a pH-dependent manner (Figure 3-29a&b)[325]. The protein can then be purified by affinity chromatography or size-exclusion chromatography, and remains encapsulated within its native lipid by a belt of the copolymer[326]. This is evidently similar to the use of amphipathic polymers, named amphipols[327], but is now directly able to solubilise the biological membrane[326]. This technique has slowly

127

advanced since its advent in 2009[305], where one of its first demonstrations was with the OMP PagP, and the enzyme was shown to be active. SMALPs have already lent themselves well to structural studies. One crystal structure, of *Haloquadratum walsbyi* bacteriorhodopsin was solved in lipidic cubic phase, reconstituted directly from SMALPS[328]. Cryo-EM has been used to solve the structure in SMALPs of the ABC transporter P-glycoprotein/ABCB1 by single particle cryo-EM[329] and the multidrug efflux pump AcrB has been visualised by negative stain single particle EM[330].

Like nanodiscs, SMALPs make concurrent structural and functional studies of membrane proteins possible, and as yet there are no published examples of BAM reconstitution in SMALPs, therefore this was an exciting and novel project.
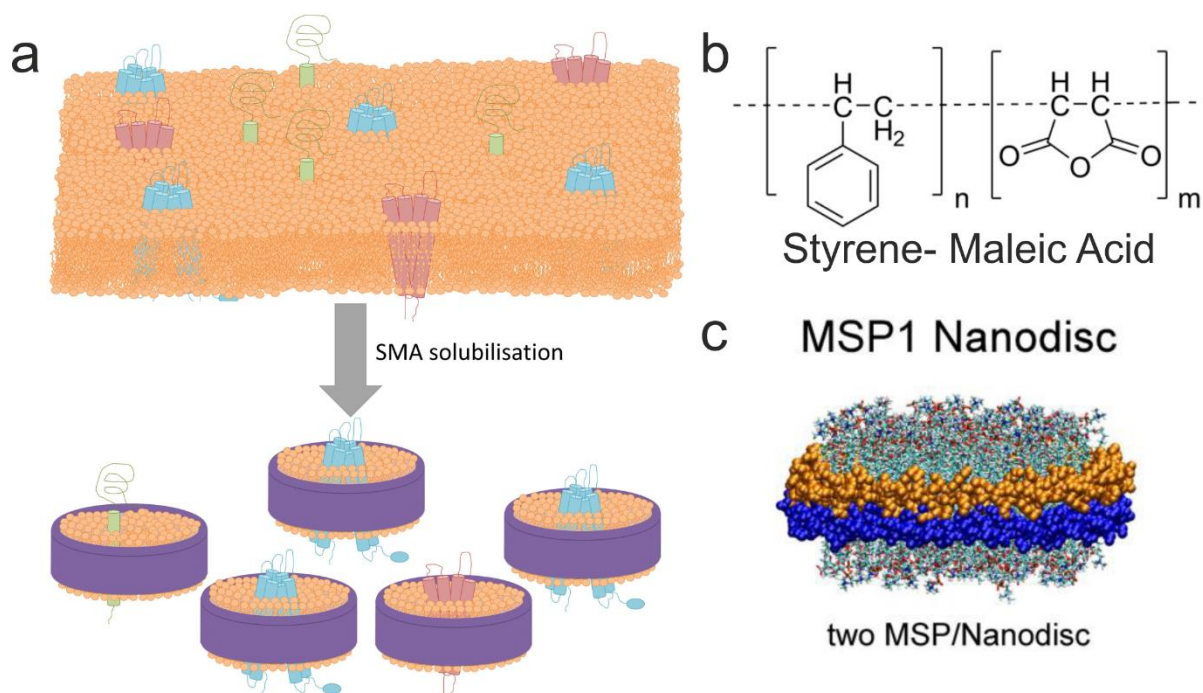
Figure 3-29: SMALP and Nanodisc Reconstitution of Membrane Proteins. a) Schematic of solubilisation of membrane proteins by SMA. Lipids of the membrane are shown in orange, the SMA in purple, with multi-coloured membrane proteins encapsulated. Image adapted from Pollock *et al.*, 2018 [326]. b) Structure of Styrene-Maleic acid. The most commonly used, and that used in this work is 2:1 styrene:maleic acid. c) Composition of MSP1 nanodisc with two membrane-scaffolding proteins (shown in gold and blue) bounding lipids and protein. Image adapted from Bayburt & Sligar 2010[306].

3.6.1 Preparation of BAM in SMALPs

In order to extract BAM with SMALPs, the same initial protocol was followed to grow and express BAM in *E.coli* and extract membranes by ultracentrifugation (Methods, Section 2.3.5). Following the first ultracentrifugation step, membranes were hand homogenised in resuspension buffer (50 mM Tris, 0.5 M NaCl, 1 mM DTT, pH 8). This was then mixed with SMA at 5% (*w/v)* in the same buffer and allowed to resuspend for ~3 hours. The insoluble fraction was pelleted, the supernatant filtered and applied to a HisTrap column. Following overnight binding to HisTrap, the sample was eluted and analysed by SDS-PAGE. The original protocol involved a second purification step by SEC. However, significant amounts of protein were lost in pre- and post-SEC concentrating and on the column, likely due to the low solubility of SMA. This is immediately evident in SDS-PAGE analysis of elution fractions from the nickel affinity and size exclusion chromatography columns (Figure 3-30).
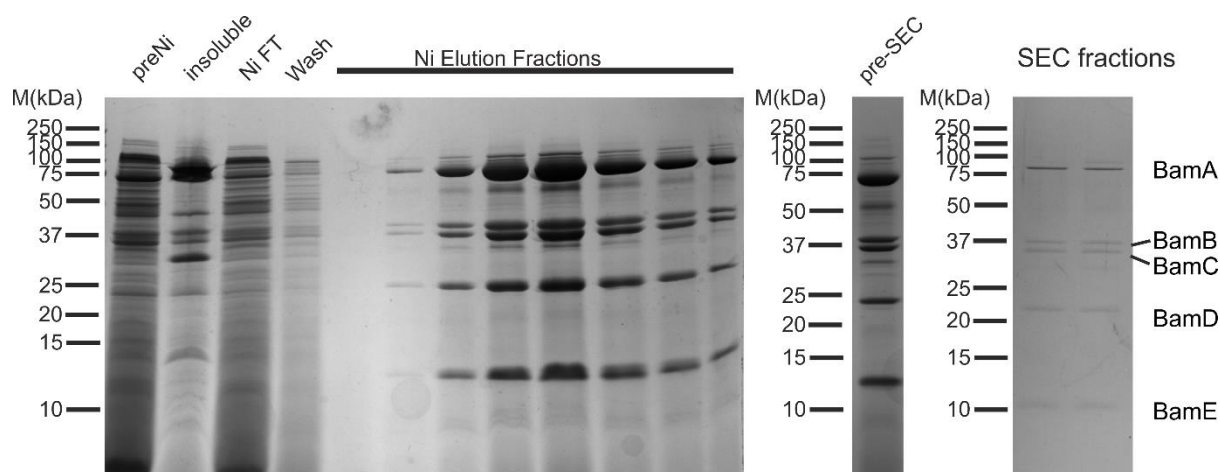
Figure 3-30: Analysis of BAM-SMALPs purification by nickel affinity and SEC by SDS-PAGE. Following solubilisation of BAM membranes with SMA the sample is centrifuged and a scraping of the insoluble pellet resuspended in SDS loading buffer (insoluble). The supernatant is filtered and applied to a 5 mL HisTrap column. Samples are analysed for the pre-Ni solution, flow-through (FT) and Wash (with 10 mM imidazole). Sample is eluted in twenty 1 mL fractions with buffer containing 500 mM imidazole. The elution fractions containing BAM are pooled, concentrated 10-fold (pre-SEC sample shown in 1/10 dilution) and applied in 0.5mL injections to an analytical Superdex S200, whereupon 0.5 mL fractions are collected. No distinct peak was seen in SEC by monitoring of A_{280} and instead fractions were analysed across the typical volume where BAM is anticipated to elute. Shown are samples of the solution pre-SEC and representative fractions across the volume range analysed.

At this point the protocol was repeated using a phosphate-based buffer with glycerol (50 mM phosphate pH 8, 500 mM NaCl, 10 % glycerol) instead of Tris-

129

based throughout, following a published protocol[304], see Methods (2.14) for details. This increased stability of the SMALP samples, but did not increase yield post-SEC. It was noted that following purification by nickel affinity chromatography the sample was reasonably pure; this was improved by carrying out additional washes of the Ni column pre- and post- binding of sample, at increasing low (20-100 mM) imidazole concentrations prior to elution. Following analysis by SDS-PAGE (Figure 3-31) it was concluded that the SEC step was unnecessary in this case, and therefore final yield could be significantly increased.
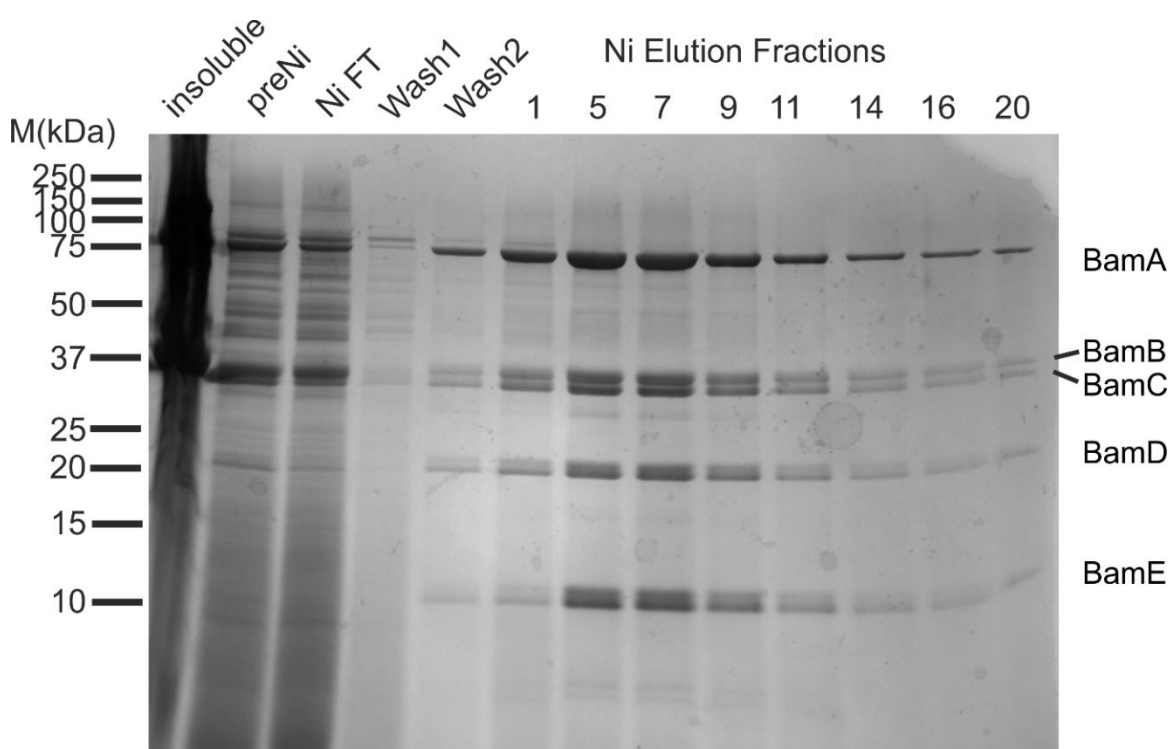
Figure 3-31: Purification of BAM-SMALPs by nickel affinity. As before, samples were taken of the insoluble pellet, solution pre-HisTrap, flow-through and 2 washes. Resuspension of membranes and subsequent steps were carried out with 50 mM phosphate pH 8, 500 mM NaCl, 10 % (*v/v*) glycerol. Wash1 was carried out with buffer containing 20 mM imidazole and wash2 100 mM imidazole. Sample is eluted from the HisTrap in twenty 1 mL fractions with buffer containing 500 mM imidazole. Sample was diluted in non-imidazole buffer prior to concentrating the protein or dialysed following the concentrating step.

BAM protein concentration was measured by the BCA assay (Methods, Section 2.3.9) and SMALPs were used in activity assays or snap-frozen and stored at -80 °C.

3.6.2 Preparation of BAM nanodiscs

Unlike SMALPs which offer an alternative method of extraction from the membrane and conservation of native lipids, nanodiscs were created from membrane scaffold proteins (MSPs) binding around detergent-solubilised pure BAM and *E.coli* polar lipid extract. In this way they more closely resemble proteoliposomes, but are an attractive alternative for structural studies. There is considerable precedent in cryo-EM studies of MSP-nanodiscs[323,331,332]. It would be highly desirable for our work to be able to carry out structural and functional studies of the same sample, for example with disulphide-locked BAM complex variants.

The preparation of MSP-nanodiscs involves the preparation of the BAM complex in DDM as previously described (Methods 2.3.5) and preparation of membrane scaffold proteins. There are a number of different choices of membrane scaffold proteins, however based on the size and literature precedent, we utilized MSP1D1[274]. This protein was kindly expressed and purified by Dr Anton Calabrese (Methods, Section 2.3.8) and utilised in His-tagged or cleaved forms. Simply, creation of nanodiscs involves mixing of BAM, scaffold protein and lipid with multiple washes with Biobeads to remove detergent and promote formation of discs (for details see Methods Section 2.15.2). While SDS-PAGE demonstrated that all original components were present, it was desirable to purify the sample further, and to verify integrity of the disc.

One method to demonstrate formation of the disc is native PAGE[274,333]. If the scaffold protein has bound and encapsulated the BAM complex then the nanodisc should migrate at a molecular weight higher than that of the BAM complex in DDM. Protein in DDM detergent, nanodisc and SMALP were analysed and compared by native PAGE (Methods, Section 2.6.4) (Figure 3-32). Detergent-solubilised BAM consistently migrated as a double band by native PAGE. The reason for this is unclear, as it may denote two conformations of BAM, but has been consistently observed in our studies of the BAM complex. Interestingly, while SMALPS show the same migration pattern, with a double band, nanodiscs migrate as a single, higher molecular weight band. This verifies the formation of the nanodisc, with the presence of the membrane-scaffold proteins. The single band implies that the nanodisc is possibly constraining the movements of BAM to one conformation.

131
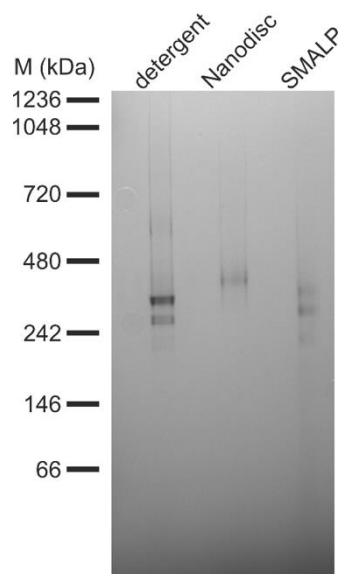
Figure 3-32: Native PAGE of BAM in detergent, nanodiscs and SMALPs.
Blue-Native PAGE was carried out to demonstrate presence of the BAM complex after its reconstitution into different environments. Precast Invitrogen NativePAGE 4-16 % Bis-Tris gels were used according to the manufacturer's instructions. Approximately 10 µg of each sample were loaded, as well as Native Mark Standard (LifeTechnologies). Electrophoresis is carried out at 150 V for 120 minutes at room temperature (see Methods, Section 2.6.4).

One method for analysis and purification of the sample was SEC, in which the sample should elute as a single peak, containing all component proteins. SEC was attempted for multiple preparations of nanodiscs. However, while increasing purity, SEC caused a reduction in yield. Comparison of analysis by SDS-PAGE (Figure 3-33) of the preSEC and SEC fractions clearly shows a significant loss of protein following size-exclusion. The SEC trace, however, shows a single peak, of low absorbance, demonstrating the successful reconstitution of BAM into the nanodiscs.
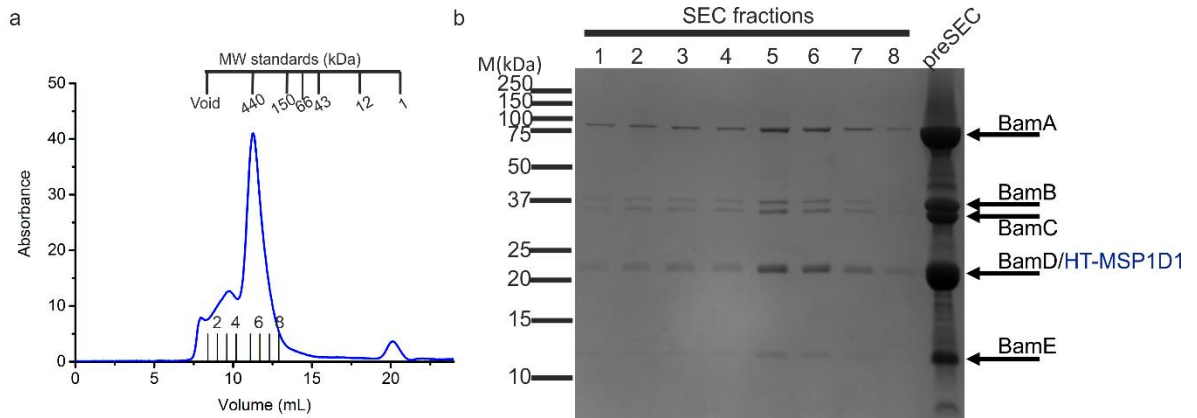
Figure 3-33: Purification of BAM-containing nanodiscs using SEC. Example trace for analysis of BAM nanodiscs on analytical Superdex S200 column. (b) SDS-PAGE analysis for fractions across the size-exclusion peak, indicated with black bars on (a).

SEC and native PAGE provide proof of formation of nanodiscs, and while SEC additionally increases purity, similarly to with SMALPs there was significant loss of yield following SEC. While nanodiscs samples are less likely to be dropping below solubility limits during chromatography, recovery after SEC was low. Additionally, as the starting concentration of BAM in the nanodiscs is low (~6 μM) significant loss of protein renders the desired activity assays impossible. A suitable concentration and volume of protein is required to both accurately assay concentration and carry out activity assays. For these reasons it was decided to increase the scale of the original nanodisc preparation (from 300 μL to 1 mL), while maintaining the original start concentration of 6 μM BAM and carry out nickel affinity purification rather than SEC. In order to carry out nickel affinity purification of BAM-containing nanodiscs it is necessary to use MSP1D1 with the His-tag cleaved. The nickel beads bind the His-tag on BamE and unbound MSP1D1 is washed away. Additionally, the sample can be eluted in a smaller volume than start volume, thus increasing the concentration.

Preparation and purification of nanodiscs was also carried out for different BAM complex variants. Shown below is the simultaneous purification carried out for MSP1D1 nanodiscs of wild-type (WT) and lid-lock (LL) variants (Figure 3-34). This demonstrates that while small amounts of protein are lost in every step, the final product is pure and at high concentration (elution sample diluted 1:10, all other samples undiluted). Empty nanodiscs were usually prepared in parallel and used as a control, typically with untagged MSP1D1, as with the BAM nanodiscs.

133

Where necessary, His-tagged MSP1D1 was used for Empty discs and further purification or concentration could be achieved with Nickel affinity chromatography. When not immediately used, samples of nanodiscs were snap-frozen and stored at -80 °C.
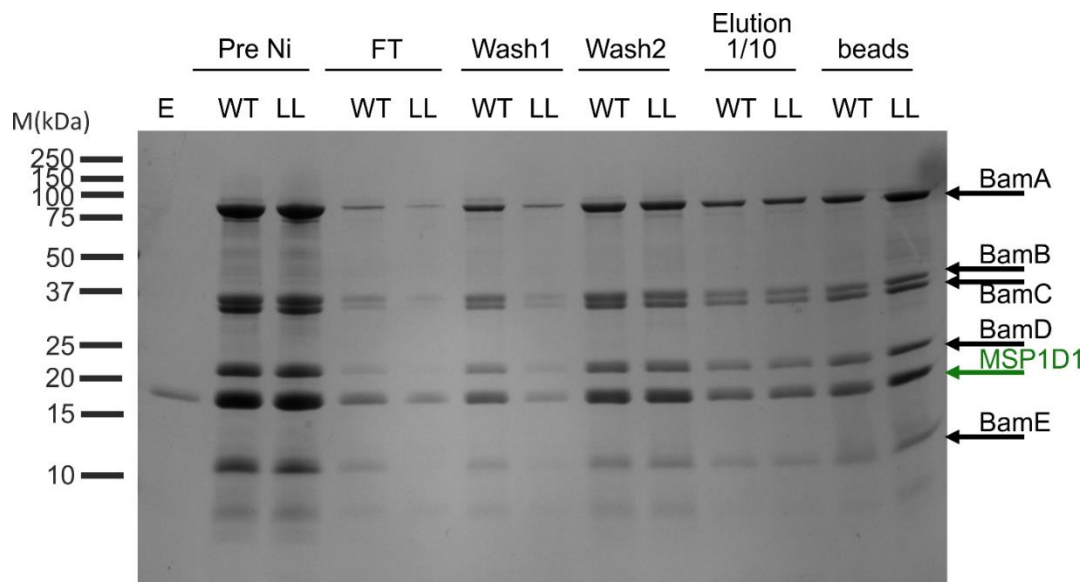
Figure 3-34: Purification of BAM nanodiscs by Ni affinity. The BAM nanodisc preparation in a 1 mL sample (Pre Ni) was applied to 100 µL pre-washed nickel beads. Following 3 hours incubation, the beads were washed twice with buffer containing 50 mM imidazole and sample eluted with buffer containing 500 mM imidazole. A small sample of beads was also boiled in SDS loading buffer demonstrating that some protein was still bound. All nanodiscs contain untagged MSP1D1, E= empty nanodiscs, BAM nanodiscs contain WT = wild-type or LL = lid-lock BAM variants.

3.6.3   Activity of BAM in membrane mimetics

As previously discussed (0), the use of membrane mimetics is attractive as they not only would enable future structural studies such as cryo-EM in the native lipid, but functional studies could be carried out on the same preparation of protein. Following preparation of BAM in MSP1D1 nanodiscs and SMALPs, the OmpT activity assay was carried out. Shown is one representative example of the activity assay for BAM proteoliposomes, nanodiscs and SMALPs and empty proteoliposomes and nanodiscs. The t_{50} of BAM-containing samples was calculated and compared across a minimum of three repeats (Figure 3-35).

It is evident that both BAM nanodiscs and SMALPs appear to show activity in folding OmpT while empty nanodiscs consistently show no activity. This is the first known reconstitution of BAM in SMALPs and only the second time that BAM

complex reconstitution in nanodiscs has been demonstrated and proved to form active complex[274]. This result is significant and interesting, as the activity of BAM in nanodiscs is evidence against models of BAM acting in an oligomeric complex. The nature of the MSP-encapsulated BAM permits no room for multiple copies of the BAM complex. Activity in these nanodiscs means that folding of protein into must occur by one copy of BAM. BAM-containing SMALPs with more native-like lipid, show significant activity in folding OmpT, intermediate between nanodiscs and proteoliposomes, demonstrating once again the importance of the membrane environment.
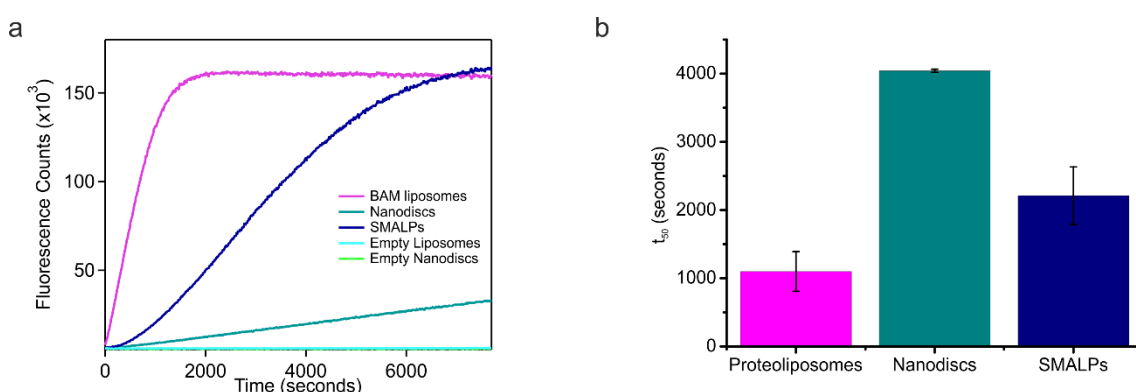
Figure 3-35: BAM-SMALPs and nanodiscs show activity in OmpT assay. (a) An example OmpT assay comparing WT BAM in proteoliposomes, nanodiscs and SMALPs and empty proteoliposomes and nanodiscs. The assay was set up as previously, with 0.25 µM BAM, 5 µM OmpT, 35 µM SurA, 1mM fluorogenic peptide, 0.8 M urea in 50 mM glycine-NaOH pH 9.5. All proteoliposomes, SMALPs and nanodiscs were assayed for accurate BAM concentration prior to use using the Pierce BCA Protein Assay, and diluted to an appropriate concentration. Empty samples were used to an equivalent amount of lipid (proteoliposomes) or concentration of MSP1D1. (b) Average t_{50} with SEM across a minimum of three replicates.

The assay for analysis of tOmpA folding by BAM by SDS-PAGE was optimised around this time (see Chapter 5, Section 5.5) and one experiment was carried out with wild-type BAM nanodiscs. While BAM proteoliposomes show efficient folding of tOmpA in these conditions, with folding nearly complete after one hour, the BAM nanodiscs show no appearance of a tOmpA folded band (Figure 3-36). This is highly surprising when compared to OmpT data that consistently shows activity of BAM in nanodiscs. Further experiments will be needed to understand this difference in activity, for example by tOmpA folding and analysis by SDS-PAGE in parallel with OmpT activity assays.

135
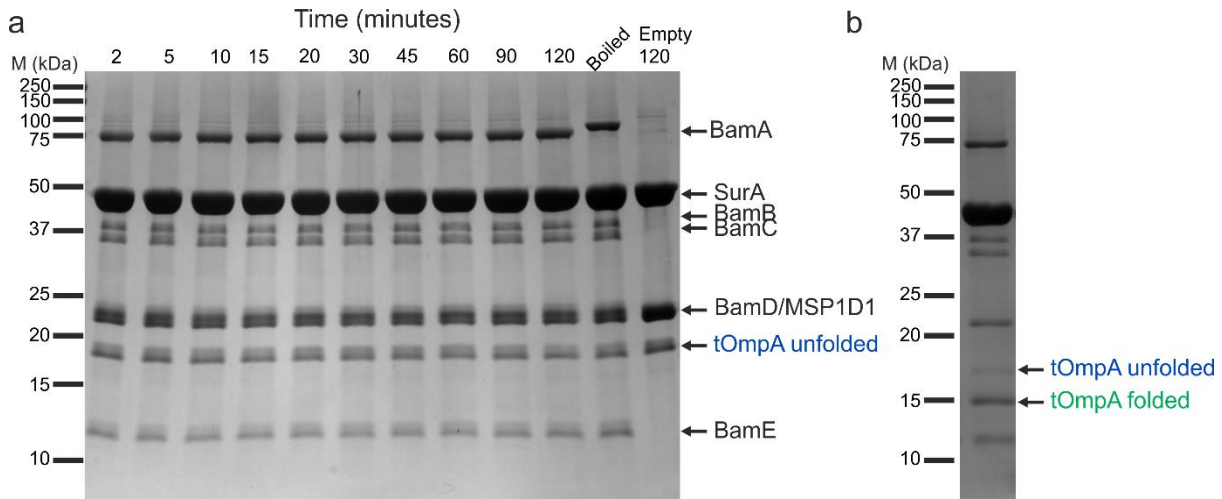
Figure 3-36: tOmpA shows no folding by SDS-PAGE with WT nanodiscs. a) SDS-PAGE analysis of tOmpA folding demonstrates no appearance of the folded band over time. b) Comparison of folding of tOmpA by wild-type BAM in proteoliposomes at 1 hour, which shows near completion of folding. The assay contains 2 µM tOmpA, 10 µM SurA, 1 µM wild-type BAM in nanodiscs, 0.8 M urea in 20 mM Tris-HCl pH 8, 150 mM NaCl. The reaction is maintained at 25 °C, samples are taken at the indicated timepoints and quenched by addition to 6x SDS loading buffer. One sample is boiled for 10 minutes, the rest are electrophoresed without boiling. One control lane contains Empty nanodiscs at equivalent concentrations of MSP1D1, and other conditions identically, for which sample was only taken at the final timepoint of 120 minutes.

3.7 Discussion

The work carried out in this chapter presents structural studies of the BAM complex and sets the scene for further work understanding BAM complex activity. The optimization of protein and proteoliposome preparation and of the OmpT assay permits the investigation into BAM complex catalysis presented in Chapter 5.

The optimization of expression and purification of the BAM complex in DDM micelles as discussed in this chapter permitted its analysis by cryo-EM, carried out by Dr Matthew Iadanza (University of Leeds). This remains the only EM structure of the complex and the structure is the sole representation of the full BamABCDE complex containing BamA in a lateral-open conformation. This refutes the hypothesis that the presence of BamB is linked to the lateral closed state of BamA[32,207-210]. Instead the change in POTRA domain conformation, linked to presence of BamB suggests a mechanism of communication across the complex. Additionally, the detergent micelle, visible in EM but not crystal structures, creates a membrane mimetic and highlights regions of the BAM complex for potential membrane interactions. This is particularly evident in BamD where the location for membrane interaction causes a hinge and conformational change within the protein (Figure 3-11 & Figure 3-12).

This chapter also delves into understanding the assay widely used for BAM complex activity: the OmpT protease assay. BAM within the proteoliposomes generated by the 'dialysis' method developed here is more active, as measured by this assay, than those produced by 'dilution' here or in the literature[159,189,272,274]. Optimisation of the OmpT protocol has produced a robust assay, consistent across proteoliposome batches, with measurable kinetics which can be used to tease out elements of BAM-OMP interaction. Whilst there are aspects which remain puzzling, the assay has proved useful, both in determining the effects of BAM dynamics, as will be discussed in Chapter 5, and in screening inhibitors and examining SurA mutations. The screening of potential inhibitors in two cases (Figure 3-24 BamD and Peptide2) has determined that these inhibitors are not significantly active in this assay, demonstrating little effect when at significant excess over the proposed substrate. In the third case, however (Figure 3-26, JB-95), it is evident that a different assay is required. The macrocyclic peptide JB-95 is of considerable interest as a potential inhibitor of

137

the BAM complex[47], but due to possessing sequential charged residues, cannot be used in an assay containing OmpT. Further work using this peptide is clearly of interest and has been begun, by my colleague Dr Bob Schiffrin, using the tOmpA folding assay discussed in Chapter 5. The results of this assay have demonstrated that both Peptide 2 and JB-95 are effective inhibitors of BAM-assisted tOmpA folding when utilised at 20- and 50- fold excess of BAM, respectively (Dr Bob Schiffrin, personal communication). As BAM concentration in this assay is only 1 µM this still represents inhibition at a low concentration. However, as discussed above, controls are necessary with JB-95 to ensure that the peptide is not functioning as a cell-penetrating peptide and disrupting the membrane in a non-specific manner.

Examination of the SurA variants by substitution in the OmpT assay appears to show that while ΔP2 SurA is capable of fulfilling the function of WT SurA, N-Ct SurA and other chaperones (Figure 3-27) are not. The capability of wild-type SurA is not recovered at lower OmpT concentrations or increased chaperone:OmpT ratio (Figure 3-28). Additionally, while binding with nanomolar Kd was detected for WT SurA to the BAM complex in detergent, no binding could be accurately measured for the mutants, implying a much weaker interaction (Julia Humes, unpublished data).

However, this does not currently agree with data using the SurA variants in the tOmpA folding assay (Humes & Schiffrin, in preparation), which show that the ΔP2 SurA is only partially active compared with WT, and more similar to N-Ct SurA. The results seen for OmpT are therefore unexpected, particularly as OmpT is a slightly larger substrate, and aggregation data suggest that the P2 domain of SurA is required to prevent aggregation of OmpT (Humes&Schiffrin, *in preparation*). This difference requires further study with folding of OmpT or other OMPs by the BAM complex as measured by SDS-PAGE to resolve the substrate specificity of the effects observed.

Finally, two membrane mimetics were used for BAM complex studies: SMALPs and nanodiscs. For both of these purification of the sample was optimised and function of BAM in both environments demonstrated using the OmpT assay. This is the first demonstration that BAM can be purified using SMALPs to create an active complex, and only the second demonstration of reconstitution in nanodiscs[274]. On-going work is now proceeding, using cryo-EM in both of these

138

alternative forms to obtain structural information, and to elucidate how the membrane surrounding BAM may impact its structure.

A wide range of SMA-like polymers, of varying sizes and physical properties are being developed. Some of these, of longer size than the 2:1 styrene:maleic acid SMA used here[325], may be more suitable and facilitate studies with a large complex such as BAM.

The sample of BAM in nanodiscs, identical to that presented here, is currently being analysed by Dr Matt Iadanza by cryo-EM. This initial data is highly interesting, with a bigger variation in BAM structures than noticed in previous detergent datasets. This suggests that the complex is considerably more dynamic in the lipid bilayer present in the nanodisc than in a detergent micelle. This is in contrast to data showing that OmpA is more dynamic in a micelle than lipid bilayer[334], but strongly supported by NMR data showing increased dynamics of OmpX in DMPC-nanodiscs compared to a detergent micelle[335]. This highlights the necessity of structural studies of the BAM complex in more native-like environments.

4 Results Chapter 2: Investigating the lateral gating hypothesis and the role of the β-signal for BamA-assisted OMP folding

4.1 Introduction

The work described in this chapter addresses two aspects of existing models of BAM catalysis: lateral gating and targeting by the β-signal. These concepts are not mutually exclusive and are in fact complementary, although one may be correct without the other. The experiments and hypotheses behind both concepts have been introduced (1.10-4 and 1.11) as well as the alternative models existing in the case of lateral gating (1.10) and are introduced again only briefly here.

4.1.1 Lateral gating in BamA

The lateral opening in the BAM complex is the theory that BamA opens via a separation of the β1 and β16 strands and this is linked to its catalytic mechanism in folding OMPs. There is a long-existing "BamA hybrid barrel" model[212] wherein the opening of the strands allows substrate OMP hairpins to template on and form a new, mixed OMP barrel before the substrate buds off into the membrane (Figure 4-1a). New models integrate aspects of BamA lateral opening while suggesting a hybrid barrel is energetically unfavourable and unlikely[33] and it is possible templating occurs on one strand while the barrel does not close. Irregardless, the lateral opening of BamA has now been accepted to occur. This was originally hypothesised from molecular dynamics simulations, and supported by experiments demonstrating that introduction of cysteines on β1 and β16 to disulphide cross-link BamA in the lateral closed conformation caused synthetic lethality (Figure 4-1b)[199]. Recent structures of the BAM complex[207-210], however, show BamA in both the lateral open and closed conformation, proving that this dynamic change occurs (Figure 4-1c). The observed conformations sampled, and the *in vivo* lethality of disulphide cross-linking, however, do not explain how BamA lateral gating links to functional activity. It was a key aim of this thesis to examine the role of lateral gating, beginning in this chapter with its importance in *in vitro* catalytic activity of isolated BamA. The aim was to utilise the same cysteine pairs demonstrating lethality *in vivo*, introduce these in *in vitro* experiments on BamA-catalysed folding and analyse their potential inhibition of BamA function. The data ultimately obtained, on BamA-assisted folding of tOmpA in DMPC LUVs (Section

4.2.5) is published in Schiffrin *et al.*, 2017, "Effects of Periplasmic Chaperones and Membrane Thickness on BamA-Catalyzed Outer-Membrane Protein Folding", Journal of Molecular Biology, **429**, 3776-3792. For this, I carried out all experiments and data analysis on the BamA variants, and the manuscript was largely written by Dr Bob Schiffrin (University of Leeds) with input from all authors.
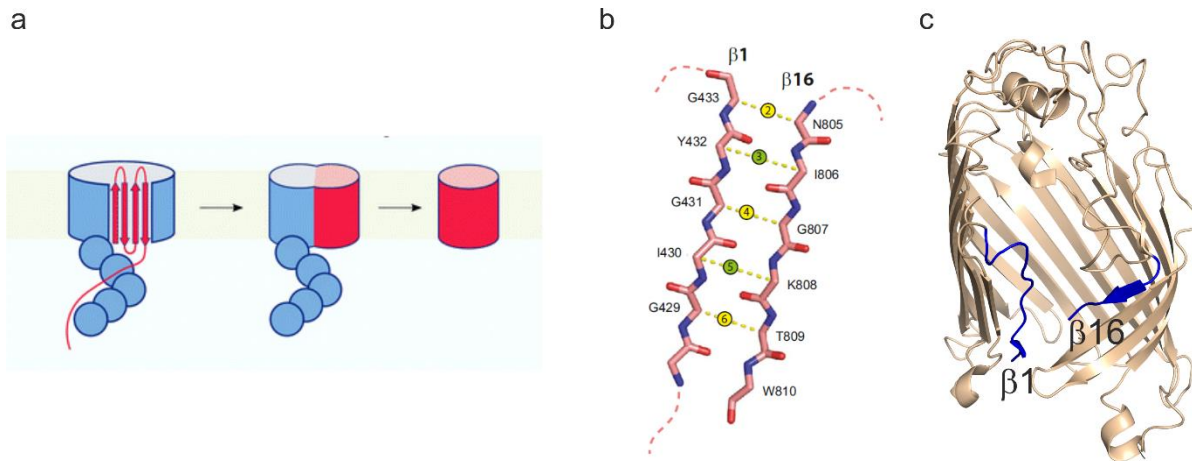
Figure 4-1: Lateral opening of BamA. a) Hypothesised model of BamA hybrid barrel formation and substrate budding with substrate in red and BamA in blue. Adapted from Schiffrin *et al.,* (2017)[33]. b) Cysteine pairs along β1 and β16 which are lethal *in vivo*. Green denotes disulfides which would point into the membrane surrounding BamA, whereas yellow denotes those which would point into the lumen. Figure adapted from Noinaj *et al.*, (2014)[199]. c) BamA barrel (residues 424-806) seen in lateral-open conformation from the EM structure of the complex [5LJ0][210].

4.1.2 The β-signal

The concept of the β-signal is that a 'signal sequence' to direct OMPs to BAM is encoded within the sequence[28,71,211,285]. As previously discussed (Introduction 1.11), this sequence is highly conserved, is characterised by alternating hydrophobic residues, and a vital C-terminal Phe[285]. The sequence is species-specific[211] and mutagenesis, while not necessarily detrimental to folding, usually affects BAM-catalysed folding[71].

Direct studies of the role of the β-signal remain scattered and minimal, with a mixture of *in vivo* and *in vitro* data. We wished to examine the hypothesis of species-specificity at the residue level, and the high conservation of the sequence by analysing OMP folding and its catalysis by BamA and the BAM complex. Two different approaches were taken, firstly for the species specificity and secondly examining a single conserved residue: the highly conserved Gly approximately

six residues from the C-terminus (Figure 4-2). It was hypothesised that both approaches would yield OMPs capable of folding but with altered recognition by BamA, and thus altered BamA- or BAM complex- catalysed folding.

a

OMP	1	2	3	4	5	6	7	8	9	10
BtuB	E	Y	T	L	S	G	S	Y	T	F
FadL	L	F	G	T	N	F	N	Y	A	F
OmpA	M	L	S	L	G	V	S	Y	R	F
OmpC	I	V	A	L	G	L	V	Y	Q	F
OmpF	T	V	A	V	G	I	V	Y	Q	F
OmpLA	G	V	G	V	M	L	N	D	L	F
OmpT	I	T	T	A	G	L	K	Y	T	F
OmpX	T	W	I	A	G	V	G	Y	R	F
PagP	V	Y	F	A	W	M	R	F	Q	F
PhoE	I	V	A	V	G	M	T	Y	Q	F

b

	+9		+7		+5		+3		+1
OmpA	M	L	S	L	G	V	S	Y	R	F
PorA	A	A	S	V	G	L	R	H	K	F

Figure 4-2: OMP β-signal comparisons. (a) The C-terminal 10 amino acids of a selection of OMPs from *E.coli* displays the high level of conservation in the β-signal. There is a pattern of alternating hydrophobic residues, highlighted in blue, a conserved terminal Phe, highlighted in yellow and a mostly conserved Gly, highlighted in green. (b) Comparison of the C-terminal 10 amino acids of *E.coli* OmpA with *N.meningitidis* PorA, numbered by alternate residues from the C-terminus (eg. +1). Residues of tOmpA mutated to those of PorA are highlighted in orange. Other colours are as in (a).

In the first approach, a tOmpA variant was created that incorporated the penultimate three residues of *N.meningitidis* PorA, replacing the corresponding residues in tOmpA (Figure 4-2b). *In vitro* studies measuring channel opening of BamA by OMP sequences had suggested incompatability between β-signal sequences from *Neisseria* and *Escherichia* due to the charged residue found before the C-terminal Phe in *Neisseria* sequences (+2 position)[211]. Later bioinformatics analysis suggested incompatibility was more likely due to the Histidine found at the +3 position in *Neisseria* OMPs. Comparison of frequency plots for *Escherichia* and *Neisseria* C-terminal signal peptides (Figure 4-3) demonstrates that alternating hydrophobic residues and C-terminal Phe are conserved across both genera while the Histidine that is common at the +3 position in *Neisseria* is absent in *Escherichia*[286]. As *Escherichia coli* tOmpA sequence possesses a positively charged +2 residue (Arg) but not the distinctive Histidine (Figure 4-2), this was a good candidate for testing how the substitution may impact recognition by BamA and the BAM complex.

143
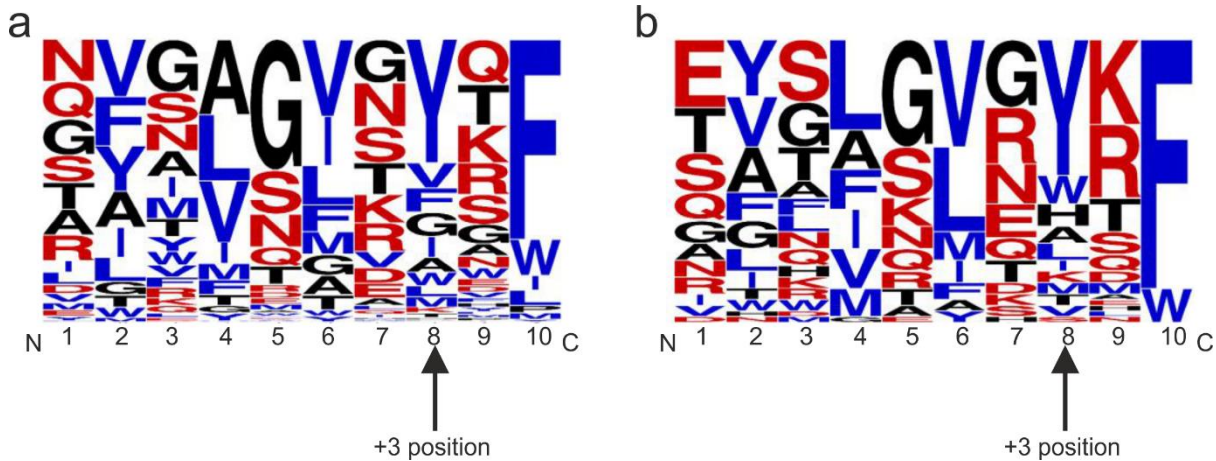
Figure 4-3: Comparison of C-terminal insertion signal for (a)*Escherichia* **and (b)***Neisseria* **strains.** Frequency plots are constructed with C-terminal insertion signal peptides, with 188 unique peptides from 31 *Escherchia* strains and 50 unique peptides of 7 *Neisseria* strains. The +3 position is indicated with an arrow. None of the *Escherichia* C-terminal β-strands in the database used have His at the +3 position, whereas it is found in up to 57% of the peptides derived from β-Proteobacteria. Figure adapted from Paramasivam *et al.*, (2012)[286].

The structure of tOmpA with the residues of interest to be mutated is shown (Figure 4-4).
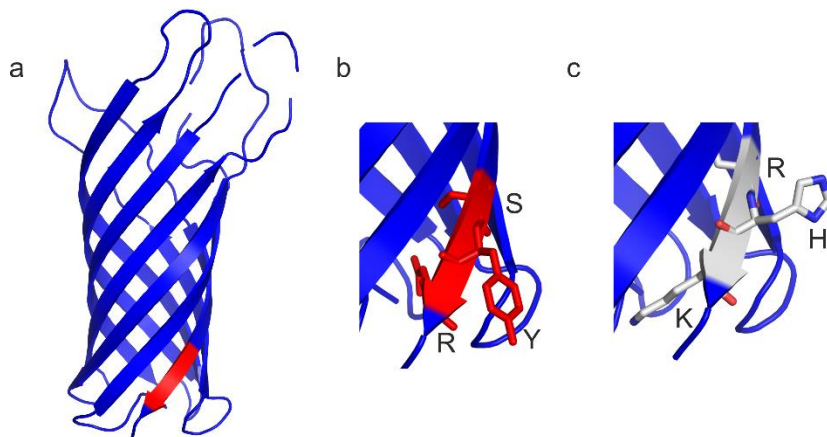
Figure 4-4: Structure of tOmpA highlighting mutagenesis. tOmpA [1BXW][153] is shown with residues SYR 168-170 highlighted in red b) Zoom centred on residues SYR 168-170 with a stick representation. c) Same region as (b) displaying mutagenesis of residues: S168R, Y169H, R170K. Images were created in Pymol.

The second aspect of investigating the role of the β-signal in BAM-catalysed OMP folding examines the highly conserved Gly approximately six residues from the C-terminus. This Gly is conserved across a variety of OMPs within *E.coli* (Figure 4-2) and across all families of Proteobacteria (Figure 4-5)[286].

144
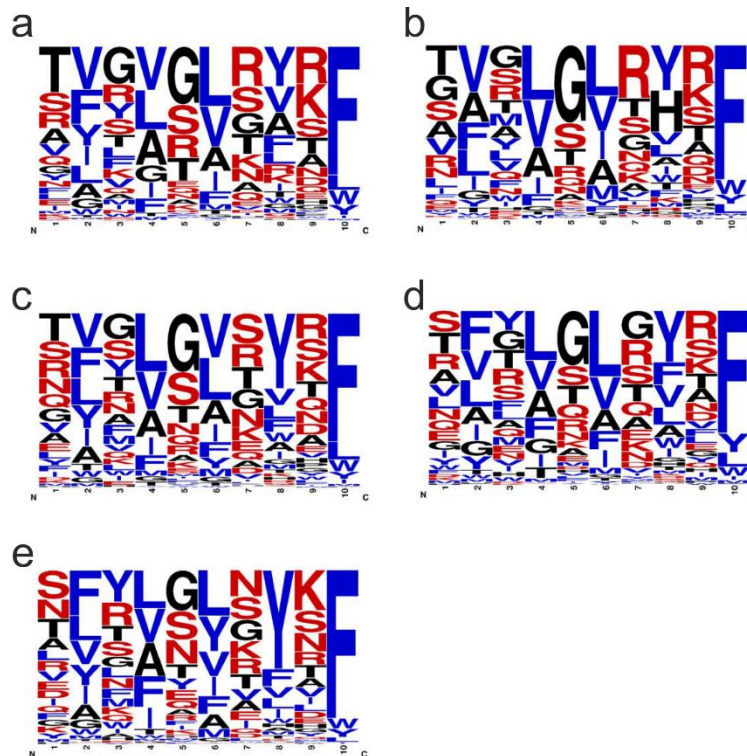
Figure 4-5: Frequency plot of C-terminal β-strands from Proteobacteria. Figure from Paramasivam *et al.*[286], demonstrates the frequency of the conserved Gly across Proteobacteria OMPs. Plots show (a) α-Proteobacteria (b) β-Proteobacteria (c) γ-Proteobacteria (d) δ-Proteobacteria (e) ε–Proteobacteria. For the +6 position, glycine is the amino acid most likely to occur, across all Proteobacteria. This residue conservation is only found for the +6 Gly and the terminal Phe residues.

These studies initially utilised OmpT, with the intention of examining the effect of mutating the conserved Gly measuring catalysis of folding with the full BAM complex using the OmpT assay (Chapter 3, Section 3.5). Initially a mutant of OmpT, Gly306Pro, was designed, purified and characterised, and subsequently a further OmpT variant was made, with the conserved Gly mutated to Ala (G306A). Finally, to investigate the effect of substitution of the equivalent Gly in another OMP, tOmpA-G166A was generated and analysed. The structures of the proteins, position of the mutations, and structural change is shown in Figure 4-6.
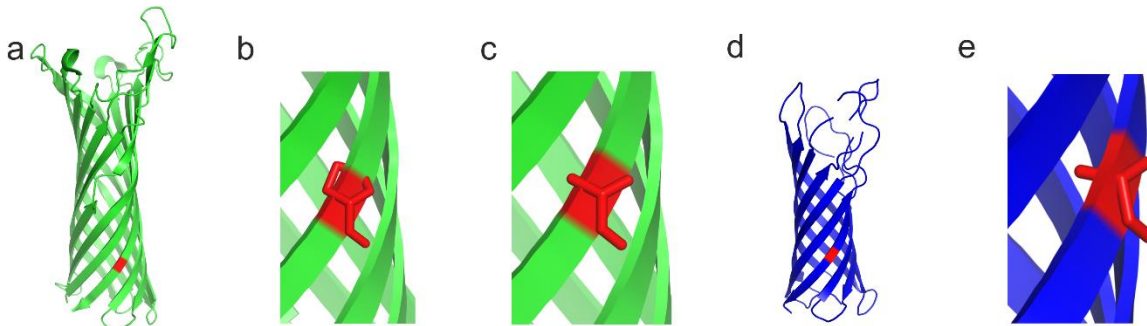
Figure 4-6 Structural models of β-signal mutants a) OmpT [1I78][336] with G306 highlighted in red. (b) Zoom centred on OmpT-G306 with a stick representation in red displaying predicted conformation of the mutant b) G306P and c) G306A. d) Transmembrane domain of OmpA (tOmpA) [1BXW][153] with G166 highlighted in red e) Zoom centred on tOmpA-G166, with a stick representation displaying mutagenesis of G166A.

As previously discussed, little work has been performed previously on unravelling the role of the OMP β-signal in folding and insertion by detailed *in vitro* studies. In particular, studies are lacking examining how variation in the β-signal affects recognition by BAM. The aim of this work, therefore, was to investigate how BamA-mediated catalysis of folding is impacted by changes to the β-signal. This was performed measuring BamA- and the BAM complex-catalysed folding *in vitro.* Additionally how the folding of one mutant, tOmpA-RHK is catalysed by the BamA[430/808] X-link variant was also examined.

4.2 Lateral gating in BamA

The importance of lateral gating in BamA function has been supported by *in vivo* data showing that double cysteine mutants purported to close the BamA gate are lethal to *E.coli*[199]. These variants however, have not previously been examined *in vitro*. To address this question, the same mutagenesis approach as that used for the *in vivo* studies was employed. Firstly, a Cys-free BamA mutant (C690S/C700S) was created and then new double cysteine pairs to disulphide lock the BamA lateral gate were introduced. Although site-directed mutagenesis to create four of the disulphide pairs reported in the literature was initially attempted (G429C/T809C, I430C/K808C, G431C/G807C and G433C/N805C) (Figure 4-1)[199], the I430C/K808C and G431C/G807C pairs were the first to be cloned successfully. These BamA mutants were created using Q5 site-directed mutagenesis (primers and protocol are detailed in Methods 2.1.5 and 2.2.3 respectively). Consequently, these double cysteine pairs, the Cys-free pseudo wild-type, and wild-type BamA were those expressed and characterised as described in the sections below.

4.2.1 Expression and purification of BamA and its variants

Following successful generation of the mutants of BamA by site-directed mutagenesis, the variant proteins were expressed and purified as described in Methods Section 2.3.1. Briefly, each protein was expressed in *E.coli* BL21 (DE3) and purified by inclusion body isolation followed by size exclusion chromatography under denaturing conditions (see Methods Section 2.3.1 for details). The elution profile obtained by SEC for each BamA variant is shown in Figure 4-7. The protein composition of the elution peak was visualised by electrophoresis on SDS-PAGE (Figure 4-7), from which a clear band for BamA was observed. Fractions were then selected to be pooled and concentrated (see Section 2.1 for details). BamA wild-type (wt), Cys-free (C690S/C700S), BamA[430/808] (C690S/C700S/I430C/K808C) and BamA[431/807](C690S/C700S/ G431C/G807C) were thus all successfully produced, with yields of 141, 109, 159 and 130 mg pure protein/ L culture respectively.
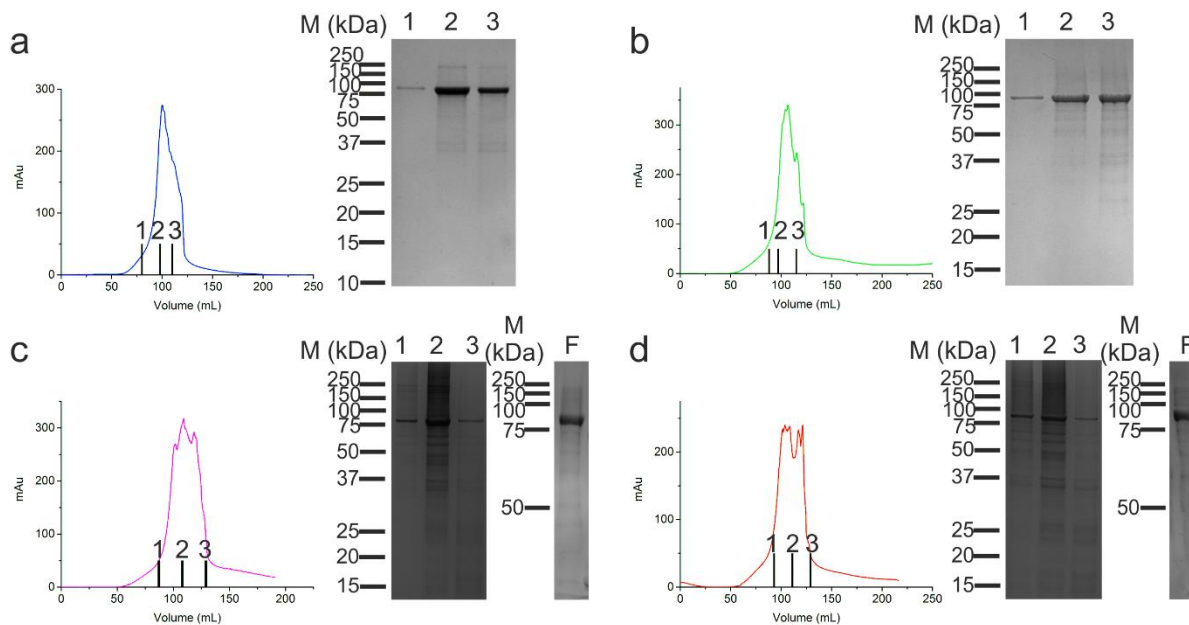
Figure 4-7: Purification of BamA. Shown is an example SEC trace of purification of BamA and fractions analysed by SDS-PAGE for a) wt; b) Cys-free ; c) BamA[430/808] ; d) BamA[431/807]. SEC was carried out using a Sephacryl-S200 column with 25 mM Tris, 6M GuHCl pH 8 (see Methods 2.3.1 for details). Three fractions are shown by SDS-PAGE across the peak of protein elution, indicated on the elution trace with black bars. BamA has a molecular mass of 88 kDa and can be seen compared to the protein marker to the left of each gel image. Protein is shown buffer-exchanged from 25 mM Tris, 6M GuHCl pH 8 to 8 M urea, 50 mM glycine-NaOH pH 9.5 for a) and b), but not c) and d) thus the apparent smearing of protein bands. For c) and d) as elution fractions are not clear, a final (F) sample, of pooled, purified fractions is shown, demonstrating these proteins to be pure.

4.2.2 Characterisation of BamA variants

The need to assess BamA variants includes their characterisation *in vitro* followed by an assessment of their catalytic capabilities on OMP folding. While initial experiments showed that the disulphide variants are expressed in cells[199] an assessment of their ability to be reconstituted into liposomes *in vitro* had not been carried out.

This chapter focuses principally on folding assays in synthetic Large Unilamellar Vesicles (LUVs), and using BamA catalytic activity to unravel these intricacies. As discussed (Introduction Section 1.8), while the native lipid head groups in the outer membrane impose a kinetic barrier on OMP folding, this is relieved by BamA[71]. In studies of membrane protein folding, lipids with phosphatidylcholine head groups have been widely employed[71,72] as these support fast folding. To allow reliable and measurable kinetics using tryptophan fluorescence

emission[163,250,337]; initial experiments in this chapter used 100 nm LUVs created from the 11-carbon chain diundecanoyl-*sn*-glycero-3-phosphatidylcholine (DUPC). For these lipid preparations, protein folding was carried out at 25 °C in 50 mM glycine-NaOH, pH 9.5 (see Methods Sections 2.7 and 2.8 for details).

4.2.2.1 Band-shift assays in DUPC liposomes

BamA protein variants were folded into 100 nm DUPC liposomes and folding was verified by means of a band shift assay (Figure 4-8) using semi-native (cold) SDS-PAGE in low (0.1 % (*w/v*)) SDS (Methods Section 2.6.2). This permits separation of bands of folded and unfolded BamA[307]. This heat modifiability is a common property of OMPs[72,307] and can be used to monitor the progress and yield of OMP folding and insertion into lipid bilayers[71,72,79,159,189]. Samples are boiled (+) to cause unfolding, while those remaining unboiled (-), and thus folded, migrate faster in semi-native SDS-PAGE. For BamA it is necessary to use semi-native conditions and low SDS to maintain the stability of the BamA barrel, whereas for other OMP substrates, the same heat modifiability folding band-shift can be seen without the need for low temperatures and concentrations of SDS (Methods Section 2.6.2).

The band-shift assay (Figure 4-8) demonstrated that all of the BamA variants created fold successfully into the DUPC liposomes. Analysis of the bandshift by densitometry indicated that although not matching the wild-type folding yield of 90%, high (~70%) folding efficiency is seen for all BamA variants. A discrepancy is seen in this experiment between anticipated and observed concentrations of BamA variants due to mis-measurement of the stock concentration, this was corrected in later experiments using BamA variants.

149
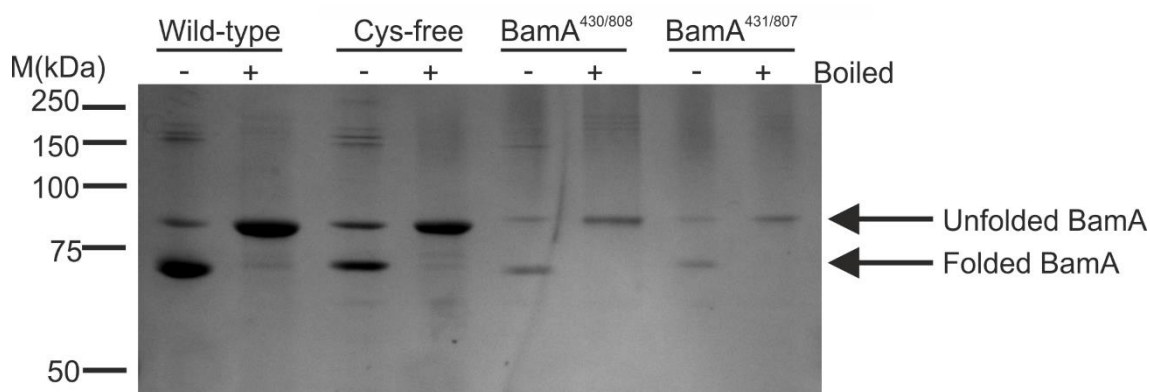
Figure 4-8: Bandshift analysis of all BamA variants using semi-native SDS PAGE. BamA variants of wild-type, Cys-free, BamA[430/808] and BamA[431/807] proteins folded into DUPC liposomes, with no boiling (-) or unfolded after boiling (+). Samples contained 0.8 µM BamA, 1.28 mM DUPC (molar LPR 1600:1), and 0.24 M urea in 50 mM glycine buffer, pH 9.5 and were folded at 25 °C for 2 hours prior to analysis by electrophoresis.

4.2.2.2 Fluorescence Emission Spectroscopy

To demonstrate successful folding of wild-type BamA and the variants created, fluorescence emission spectroscopy was next carried out for all BamA variants, folded into DUPC liposomes or unfolded in 8 M urea (see Methods Section 2.6.1). Due to the nature of the intrinsic tryptophan fluorescence[250], a different emission spectrum will be observed for folded versus unfolded protein. For BamA, folded proteins show a blue shift in Trp fluorescence, with wavelength of maximum fluorescence intensity (λ_{max}) occurring at a shorter wavelength, and with a higher fluorescence intensity relative to the unfolded state[250]. This was observed for wild-type BamA and all of the purified variants (Figure 4-9) and also by comparison of calculated λ_{max} (Table 4-1). The results provide a clear indication that all variants of BamA are folded, and display the same characteristic tryptophan fluorescence emission spectra noted for BamA wild-type in folded and unfolded forms. This is further evidence that the BamA variants are folding correctly and act similarly to wild-type, although perhaps show lower folding efficiency than the wild-type protein.
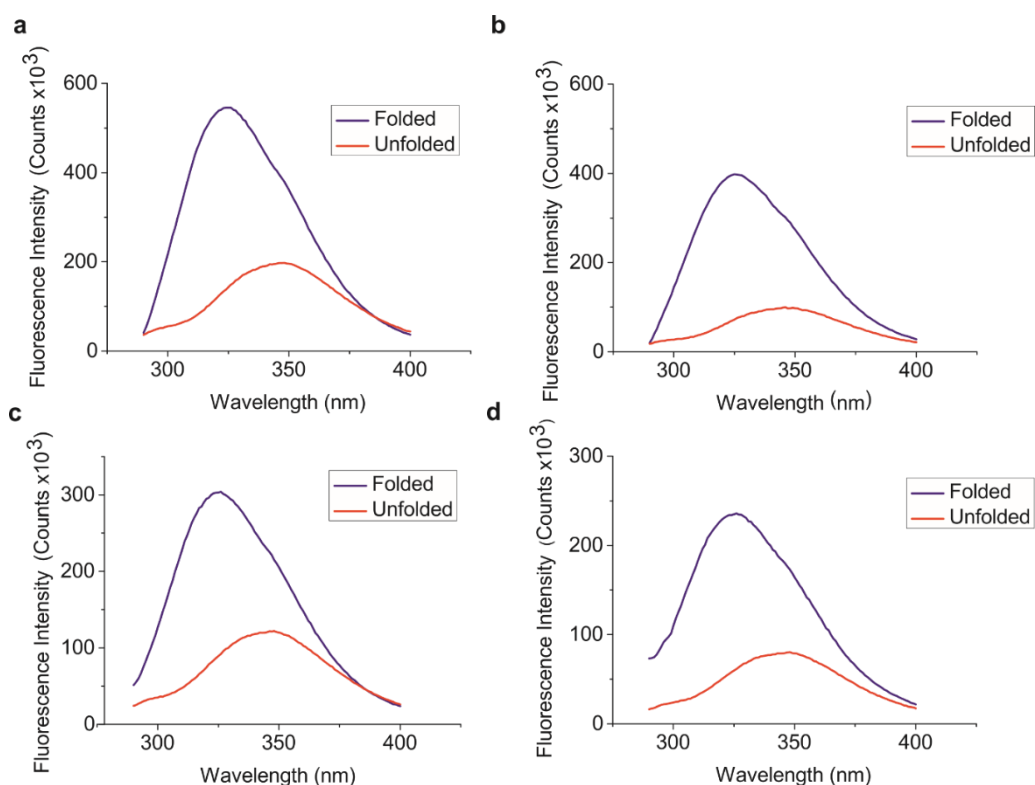
Figure 4-9: Fluorescence emission spectra for folded and unfolded samples of all BamA variants. a) Wild-type BamA; b) Cys-free BamA; c) BamA[430/808]; d) BamA[431/807]. Samples contained 0.8 μM BamA, 1.28 mM DUPC, and 0.24 M urea in 50 mM glycine buffer, pH 9.5 for folded samples, or 0.8 μM BamA in 8 M urea for unfolded samples. Samples were folded by incubation with LUVs at 25 °C for two hours prior to measurement. Each spectrum was recorded from 280 nm to 400 nm in 1 nm increments, using an excitation wavelength of 280 nm. An appropriate "blank" sample was subtracted from measurements, to remove light scattering by liposomes from the final spectra observed (see Methods Section 2.8.1 for details).

	λ_{max} (nm)			
	Wild-Type	**Cys-free**	**BamA[430/808]**	**BamA[431/807]**
Folded	325	325	326	326
Unfolded	348	346	348	348

Table 4-1: Comparison of λ_{max} values for BamA wild-type, Cys-free (C690S/C700S), and BamA[430/808] and BamA[431/807]. The wavelength at which the fluorescence spectrum is at its maximum is shown, and is consistent across variants, and a clear difference is seen between unfolded and folded samples for all BamA proteins.

151

4.2.2.3 Circular Dichroism (CD) spectroscopy of BamA and variants

Circular dichroism was also utilised to determine whether the BamA variants adopt the expected β-barrel architecture when folded into different environments, and also to enable a comparison between the extent of folding of all the BamA variants. Folding of each of the BamA variants into DUPC liposomes (Figure 4-10a) resulted in far UV CD spectra typical of a β-sheet protein, with a negative maximum at ~220 nm. This confirms that all proteins are capable of folding in this lipid type. In addition, all variants gave rise to CD spectra that differ substantially from the spectra of their unfolded states obtained in 8 M urea (Figure 4-10b).
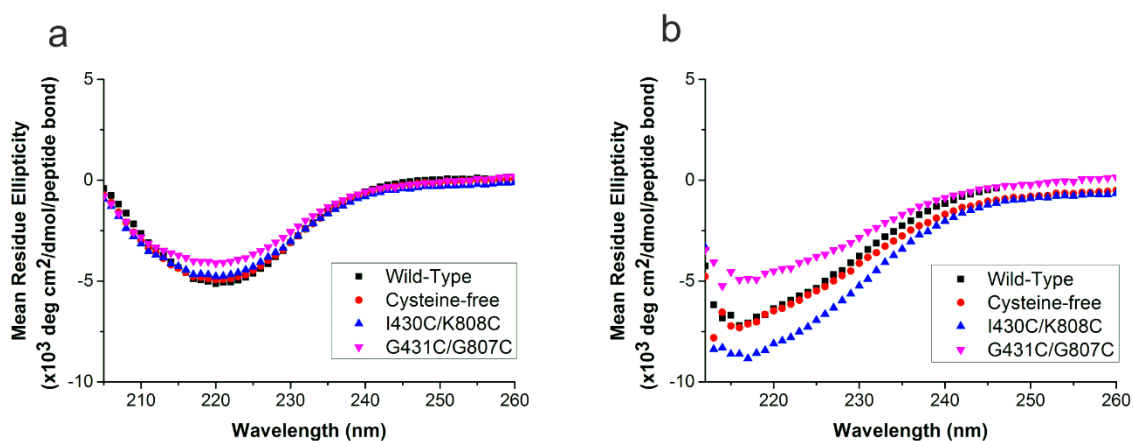
Figure 4-10: Comparison of far UV CD spectra of BamA wild-type and variants in a) DUPC LUVs and b) unfolded in 8 M urea. a) All BamA protein variants folded in DUPC liposomes contained 0.8 µM BamA, 1.28 mM DUPC LUVs, and 0.24 M urea in 50 mM glycine buffer, pH 9.5. All folded samples were incubated at 25 °C for two hours prior to measurement. b) Unfolded BamA protein variants (0.8 µM BamA) in 8 M urea 50 mM glycine buffer, pH 9.5. An appropriate blank was subtracted for each sample. The Mean Residue Ellipticity (for derivation see Methods Section 2.8.2) is plotted against wavelength.

4.2.3 Kinetics of BamA-assisted OMP folding

BamA is of interest as this β-barrel protein, even when isolated from the BAM complex, is capable of accelerating the folding of substrate OMPs into synthetic liposomes[71,271]. This effect is specific to BamA as prefolded OmpA in the LUVs does not exert the same catalytic effect[241]. This was hypothesised to be a useful means to assess the importance of BamA lateral gating *in vitro* as BamA variants with the β-barrel disulphide locked may provide little or no assistance to substrate OMP folding if gating is vital for function. Consequently, experimental conditions were set up in which the acceleration of OMP folding by BamA can be reliably measured utilising the natural tryptophan fluorescence of OMPs. The truncated β-barrel of the small outer membrane protein OmpA (tOmpA, residues 1-171) was used as a substrate in these experiments. This was chosen because it is known that tOmpA will fold spontaneously into liposomes formed from the synthetic lipids DUPC, DUPC:DDPE, or later DMPC used here, on a measurable timescale and gives rise to a large change in fluorescence intensity[288].

As discussed above, initially DUPC LUVs were the synthetic liposomes of choice for observing the catalytic activity of BamA disulphide lock variants on tOmpA folding. This is because the liposomes formed and BamA-assisted folding into the liposomes had been well-characterised hitherto[71,72,241,271]. The experiments yield folding transients that can be fit to exponential functions, with reliable folding rate constants. In addition, folding occurs in presence or absence of BamA at measurable timescales and at room temperature (25 °C), which is not close to the sub-zero phase transition temperature for DUPC. The first kinetic experiments performed here focused on validating the experimental set-up by comparison to previous findings, and were used to establish that consistent data are obtained across varying liposome batches. In all experiments folding of tOmpA was monitored following the rapid dilution of denatured tOmpA (in 8 M urea, 50 mM glycine-NaOH pH 9.5) into 100 nm LUVs in 50 mM glycine-NaOH pH 9.5 containing BamA (in the presence or absence of Skp as required) at predetermined concentrations. For all kinetic experiments, the traces were fitted globally to a single- or double- exponential function, as appropriate (Methods Section 2.9), and rate constants k_1 and k_2 are reported. Skp and tOmpA proteins were kindly provided by Bob Schiffrin (University of Leeds) and were purified as previously described[288] (see Methods 2.3.1 and 2.3.3).

153

Firstly the folding of tOmpA in DUPC liposomes upon dilution 200-fold from 8 M urea was measured (Figure 4-11a). The results show that tOmpA folds with an observed rate constant of $21.8 \pm 0.2 \times 10^{-3}$ s^{-1}. BamA-assisted folding of tOmpA in DUPC is exceptionally fast in these conditions, complete within ~200 seconds[241]. This fast kinetic rate means any experimental errors in sample handling would cause a significant portion of the first kinetic phase to be missed, and small differences between BamA-accelerated sample folding would be nearly impossible to determine. The addition of chaperone, Skp was used to slow folding in order that small differences may be observed. The "holdase" activity of the chaperone Skp is known to prevent the folding of tOmpA, resulting in no fluorescence change in the absence of BamA[163,271](Figure 4-11b). The presence of BamA, prefolded into liposomes allows the release of tOmpA from Skp, permitting folding[271]. In addition, this experimental setup permits examination of the potential importance of BamA lateral gating not only in catalysing OMP assembly, but also in the handover from chaperones.

Upon pre-incubation of tOmpA with a 2-fold molar excess of Skp trimer without BamA, no fluorescence increase and thus no folding is observed (Figure 4-11b). This indicates that in the absence of BamA, Skp functions as a "holdase" sequestering the substrate tOmpA, consistent with previous results[163,271].
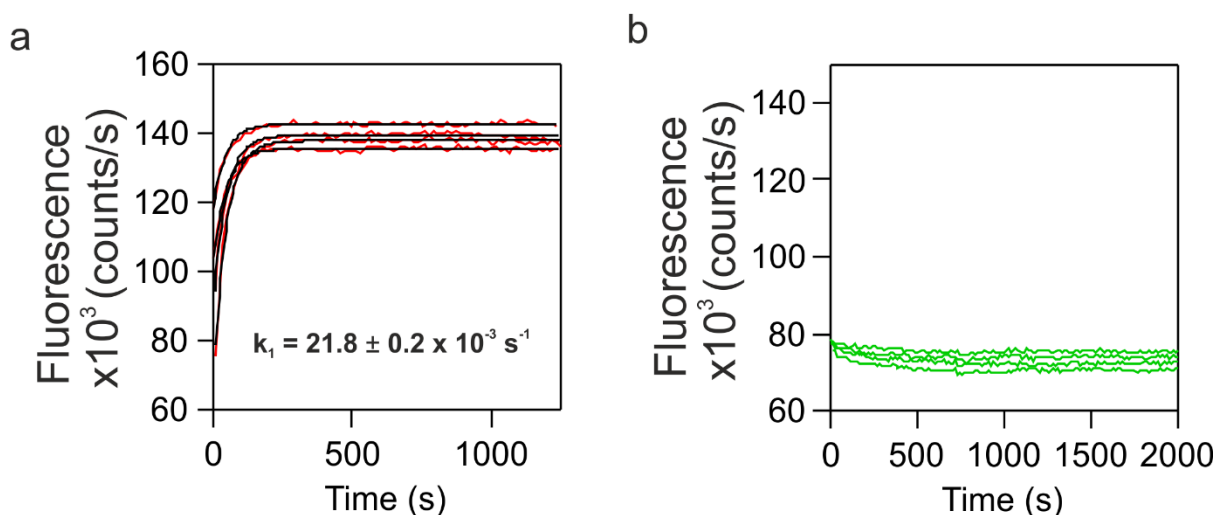
Figure 4-11: Kinetic traces for tOmpA folding into DUPC liposomes in the (a) absence or (b) presence of two-fold molar excess of Skp trimers monitored by intrinsic tryptophan fluorescence. Black lines in (a) represent the fits of the data to a single exponential function. Four replicate samples of each assay are shown. Samples contained 0.4 µM tOmpA, 1.28 mM DUPC LUVs, 0.8 µM Skp trimer for (b) and 0.24 M urea in 50 mM glycine buffer, pH 9.5 and were measured at 25 °C.

Having validated the set-up and use of DUPC liposomes for folding of tOmpA the next step was to examine the catalytic effect of BamA and the effect of barrel cross-linking on tOmpA folding by prefolding wild-type BamA or BamA[430/808] into DUPC liposomes. It was hypothesised that the BamA double cysteine variant would form an intramolecular disulphide cross-link, preventing lateral gating[199]. If lateral gating was a prerequisite of its function, cross-linking the lateral gate would be expected to diminish the ability of BamA to facilitate tOmpA folding. To be sure of determining the effect in a barrel-locked state, measurements were also made with the addition of oxidizing agents (1 mM diamide or 100 µM $CuSO_4$).

The folding of tOmpA from Skp into DUPC liposomes containing prefolded wild-type BamA (Figure 4-12a), at a rate constant of $7.4 \pm 0.1 \times 10^{-4}$ s^{-1} , is consistent with the rate constant of 1×10^{-3} s^{-1}, determined previously following repeated experiments[241]. However, the folding of tOmpA with prefolded BamA[430/808] (Figure 4-12b), which was anticipated to be slower than with wild-type BamA, yielded a rate constant of $24.7 \pm 0.5 \times 10^{-4}$ s^{-1} and is therefore more than 3-fold faster than wild-type BamA. Furthermore, the addition of oxidizing agents (Figure 4-12c & d), anticipated to slow the observed rate constant still further, caused high variability between kinetic transients, with the same or higher observed rate constants in the presence of diamide or $CuSO_4$ respectively.
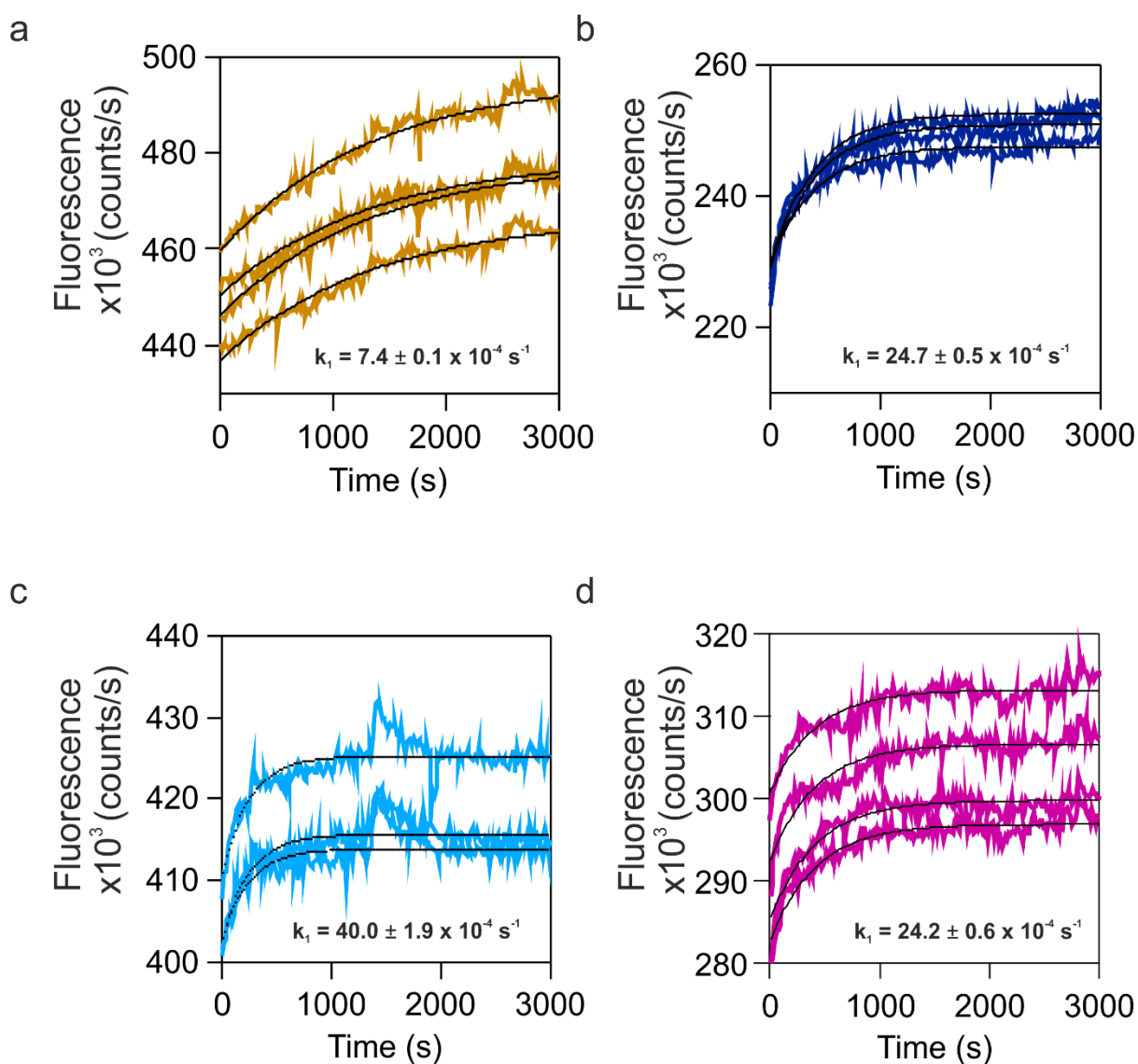
Figure 4-12: Folding of tOmpA into DUPC liposomes with BamA and Skp.
Four replicate traces are shown for folding of tOmpA into liposomes containing prefolded a) wild-type BamA; b) BamA[430/808]; c) BamA[430/808] + 100 µM CuSO$_4$; and d) BamA[430/808] + 1 mM diamide. Black lines represent the fits of the data to a single exponential function. Three or four replicate samples of each measurement are shown. Samples contained 0.4 µM tOmpA, 0.8 µM BamA, 0.8 µM Skp trimer, 1.28 mM DUPC LUVs, and 0.24 M urea in 50 mM glycine buffer, pH 9.5 and were measured at 25 °C.

The results obtained with prefolded BamA in DUPC liposomes were highly variable, with inconsistent effects on the addition of different oxidizing agents. In addition, the data appeared noisy (Figure 4-12) rendering interpretation of the results difficult. This appears partly attributable to the fast rate of folding, as slight inconsistencies in sample preparation, or dead time in beginning the experiment could lead to high variability in the observed rate constants of folding between experiments containing BamA variants. For these reasons it was decided to

repeat these experiments utilising lipids shown previously to result in a slower rate of tOmpA folding[71]. In addition, the slower intrinsic rate of folding of OMPs into longer chain, or more complex lipids would be expected to lead to a greater catalytic effect of BamA[71,72].

4.2.4   Kinetics of BamA assisted OMP folding in DUPC: DDPE

It was decided next to use more native-like lipids and emulate the method of Gessman *et al*[71] whereby phosphatidylethanolamine lipids (*di*C$_{10:0}$PE DDPE) are doped in DUPC to create a DUPC:DDPE lipid bilayer. 100 nm LUVs created from DUPC:DDPE (80:20 molar ratio) were thus used to investigate the efficiency of BamA-assisted folding of tOmpA. DUPC is commonly used for OMP folding studies into liposomes, as it has been shown previously that OMPs fold efficiently into phosphatidylcholine LUVs with short (12 or less carbon) chain length[71,72]. Increasing the proportion of lipid with 'native' headgroups, such as phosphatidylethanolamine or phosphatidylglycerol slows the rate of OMP folding into liposomes, and more effectively mimics the lipid that may be present in the cell and increases the effect of pre-folded BamA[71].

Studies demonstrate that even a molar percentage of 20% DDPE in DPPC LUVs will slow the folding of all OMPs measured (tOmpA, OmpA, OmpX and OmpLA) compared to DPPC alone[71]. Prefolded BamA is capable of relieving the kinetic effect of the native lipid headgroups, accelerating folding to near that found in DPPC-alone LUVs[71]. Incorporation of DDPE creating DUPC:DDPE liposomes thus allows for more effective study of BamA-aided folding, as the addition of BamA may have a more substantial effect on substrate folding rates in lipid bilayers that do not support rapid, spontaneous OMP folding and insertion.

Based on this rationale, a mixed liposome of DUPC:DDPE (80:20 molar ratio), similar to those used by Gessman et al 2014[71] (see Methods Section 2.7) was used to characterize BamA-assisted OMP folding. As OMPs fold less efficiently into this lipid mixture it is not necessary to use Skp as a holdase to determine whether BamA has an effect on the observed rate of folding. This simplifies the experiment as the chaperone handover to BamA is no longer a contributing factor to observed folding rate.

157

Firstly, a band shift assay (Figure 4-13) was carried out to determine whether effective folding occurs for all BamA variants in LUVs of this lipid composition. The band shift assay demonstrated that all of the BamA variants studied here are capable of folding into 100 nm DUPC:DDPE LUVs. Samples which are "folded" show an unfolded band of relatively higher intensity than observed previously (Figure 4-13), indicating that BamA folds with lower efficiency in this lipid type, as anticipated[71]. Nonetheless, the amount of folded BamA was sufficient to measure the effect of BamA on OMP folding into these liposomes.
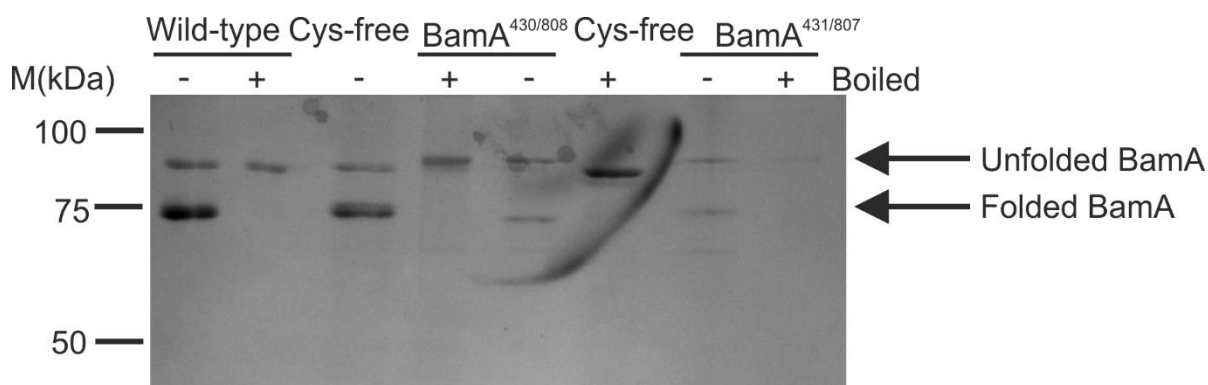
Figure 4-13: Band shift assay in DUPC:DDPE liposomes for all BamA variants. Wild-type, Cysteine-free and two double cysteine mutants in DUPC:DDPE LUVs. Samples contained 0.8 µM BamA, 1.28 mM DUPC or DUPC/DDPE LUVs, and 0.24 M urea in 50 mM glycine buffer, pH 9.5 and were folded at 25 °C for 2 hours prior to analysis by electrophoresis. Samples are with (+) or without (-) 30 minutes boiling at 100 °C demonstrating heat modifiability of BamA with altered electrophoretic mobility in the folded sample.

The results showed, as expected, that tOmpA folds spontaneously and efficiently into DUPC:DDPE lipids alone (Figure 4-14). The kinetics fit to a double exponential function, with rate constants ($k_1 = 16.2 \pm 0.7 \times 10^{-4}$ s^{-1} and $k_2 = 2.1 \pm 0.2 \times 10^{-4}$ s^{-1}), significantly slower than that obtained ($k_1 = 21.6 \pm 0.2 \times 10^{-3}$ s^{-1}) for tOmpA alone in DUPC liposomes (Figure 4-11a). This slow spontaneous rate of folding shows that DUPC:DDPE liposomes are a good choice to investigate BamA-assisted folding of this protein. The fit to single- or double- exponential is poor, suggestive of a complex folding or insertion mechanism that was not investigated further here. Therefore, the t_{50} or half-time to maximum fluorescence, for each of the four transients was calculated by fitting a horizontal line to the end of the data, see Methods 2.9 for details. The average t_{50} calculated for tOmpA into these LUVs is 403.7 ± 18.8 s.
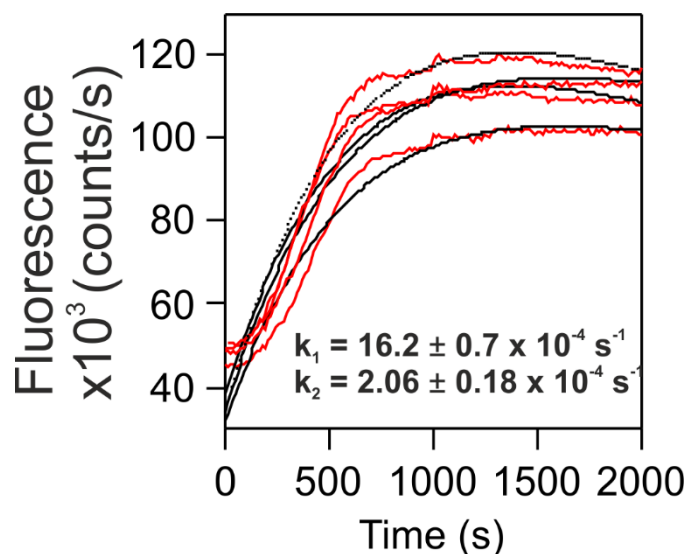
Figure 4-14: Kinetic traces for tOmpA folding in DUPC:DDPE liposomes monitored by intrinsic tryptophan fluorescence. Grey broken lines represent the attempted fits of the data to a double exponential function. This shows that the data does not fit a double exponential due to due to the lag time observed, but yielded smaller residuals than fit to the single-exponential. Four replicate samples are shown. Samples contained 0.4 μM tOmpA, 1.28 mM DUPC:DDPE LUVs, and 0.24 M urea in 50 mM glycine buffer, pH 9.5 and were measured at 25 °C.

The presence of prefolded wild-type BamA in DUPC:DDPE LUVs leads to an increase in the observed rate constant of tOmpA folding (Figure 4-15) with rate constants $k_1 = 8.9 \pm 0.9 \times 10^{-3}$ s^{-1} and $k_2 = 0.2 \pm 0.2 \times 10^{-3}$ s^{-1}. In these experiments the data fit well to a double exponential, and the folding times are in accordance with those noted in the literature for similar liposomes, monitored by gel assays[72]. For comparison with observed rates of tOmpA folding without BamA the t_{50} of each transient was also calculated. The average is 86.2 ± 14.1 s. This provides a second measure of the catalytic effect provided by BamA. However, for the majority of traces in DUPC:DDPE the final fluorescence is not flat, therefore an accurate t_{50} cannot be obtained.

159
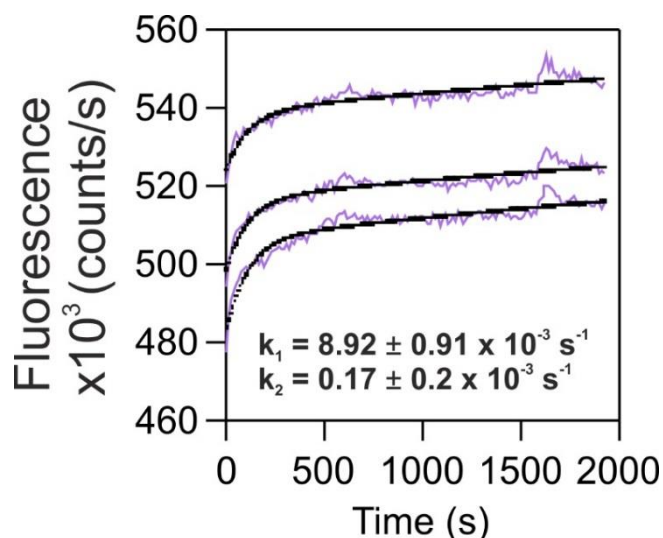
Figure 4-15: Kinetic traces for tOmpA folding in DUPC:DDPE LUVs containing prefolded BamA. Purple indicates each replicate, which were fit globally to a double exponential (indicated by black lines). For details see Methods Section 2.9. BamA was prefolded in 100 nm LUVs at a concentration of 0.8 µM by incubation at 25 °C for two hours prior to measurement. Samples contained 0.4 µM tOmpA, 0.8 µM BamA, 1.28 mM DUPC:DDPE(80:20 molar ratio), and 0.24 M urea in 50 mM glycine buffer, pH 9.5 at 25 °C.

The experiment was repeated with BamA[430/808] and BamA[431/807] (Figure 4-16). Initially both double cysteine variants of BamA appeared capable of accelerating tOmpA folding, as the rate constants of folding are many-fold higher than for tOmpA in isolation. However, variability is observed between the lateral-lock BamA variants, with fit to a single-exponential function optimal for folding transients with prefolded BamA[431/807] but not for the kinetics containing prefolded BamA[430/808].

160
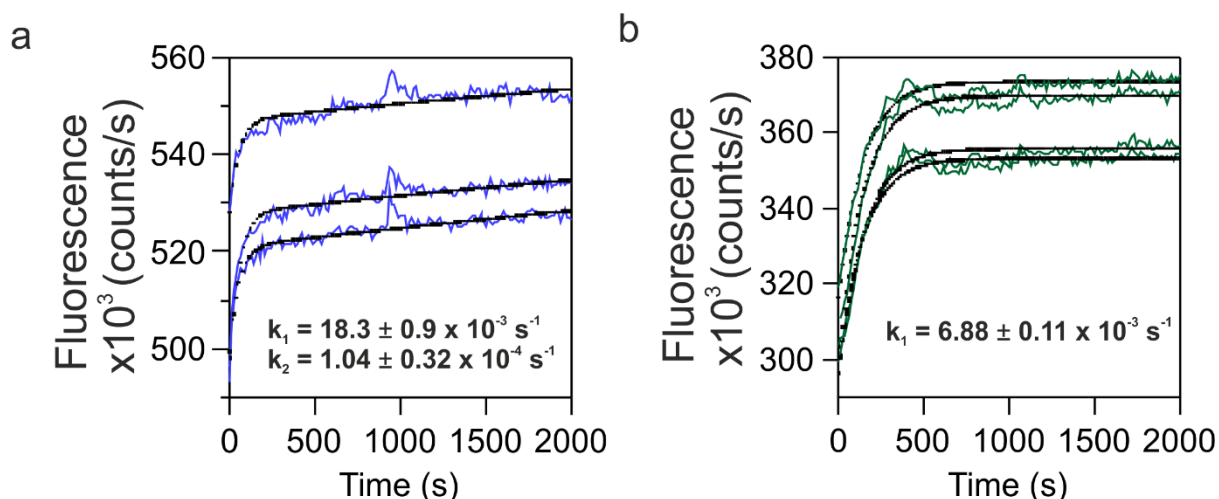
Figure 4-16: Kinetic traces for tOmpA folding in DUPC:DDPE LUVs containing prefolded (a) BamA[430/808] or (b) BamA[431/807] fit to double, or single exponential functions, respectively. Experiments were carried out with final concentrations 0.4 µM tOmpA, 0.8 µM BamA, 1.28 mM DUPC:DDPE (80:20 molar ratio) LUVs, and 0.24 M urea in 50 mM glycine buffer, pH 9.5.

Despite the differences in fit to exponential function, the results from comparison of Figure 4-14 and Figure 4-16 demonstrate that both double-cysteine BamA variants accelerate tOmpA folding. However, folding of tOmpA with prefolded BamA[431/807] fits to a single exponential, unlike the double-exponential seen with wild-type BamA and therefore these cannot be easily compared, although it appears the k_1 extracted is lower for BamA[431/807] than wild-type. Kinetic transients with prefolded BamA[430/808] fit well to a double-exponential and therefore can be compared to wild-type. In this case the first rate constant (k_1) extracted is higher ($18.3 \pm 0.9 \times 10^{-3}$ s^{-1}) than for that of wild-type ($8.92 \pm 0.9 \times 10^{-3}$ s^{-1}). This is evidently the opposite effect than that anticipated.

Folding of tOmpA with prefolded BamA[430/808] was also tested in the presence of reducing and oxidizing agents to influence the extent of cross-linking, however both appeared to decrease the observed rate. The inconsistencies observed in the data and difficulty in quantification led us to move away from DUPC:DDPE LUVS. The majority of kinetic traces do not demonstrate flat final fitting of fluorescence values, precluding extraction of a t_{50}, while the mixture of single- and double- exponential fitting to kinetic transients renders comparison across all conditions impossible. In addition, the kinetic trace for folding of tOmpA in the absence of BamA (Figure 4-14) demonstrates a sigmoidal-like curve, clearly

different from that in the presence of BamA(Figure 4-15). This implies a more complex mechanism of folding than was addressed here.

4.2.5 Kinetics of BamA assisted tOmpA folding in DMPC liposomes

As previously mentioned, in addition to complex effects of polar head group on the rate of OMP folding, the longer the fatty acid chain length, the slower the substrate OMP will fold[71]. It has now been demonstrated in LUVs with phosphatidylcholine head groups that increasing the lipid chain length by single carbons incrementally (from 12 carbon DLPC to 14 carbon DMPC), thus incrementally increasing bilayer thickness[269] will substantially increase the fold rate enhancement provided by BamA[241]. The 14-carbon chain 1,2-dimyristoyl-sn-glycero-3-phosphatidylcholine (DMPC) lipids generated liposomes in which BamA increases the folding rate of tOmpA by 12-fold[241]. It was anticipated that as substrate OMP folding rates were lower[72], but the catalytic effect of BamA in assisting folding was greater[241] any effects of inhibiting BamA lateral gating by disulphide bond formation may be more clearly seen in this lipid type.

For tOmpA folding into DMPC lipids, only BamA[430/808] was taken forward as a cross-link example, henceforth referred to as BamA X-link, as this variant generated the most reproducible folding transients. Experiments were initially attempted with DTT and $CuSO_4$ as reducing and oxidizing agents, respectively. However, the addition of DTT to prefolded X-link BamA resulted in an unexpected fluorescence decrease upon folding (Figure 4-17b), and therefore the alternative reducing agent TCEP was used (Figure 4-20). In addition, as the phase transition temperature of DMPC is 24 °C[279], close to the previous experimental temperature of 25 °C, unlike for previous lipid types used, both BamA pre-folding and measured tOmpA folding were carried out at 30°C to ensure that the lipid remained in liquid phase rather than gel phase. Furthermore, folding of BamA into DMPC liposomes was carried out overnight to increase folding yield prior to the addition of the OMP substrate.

162
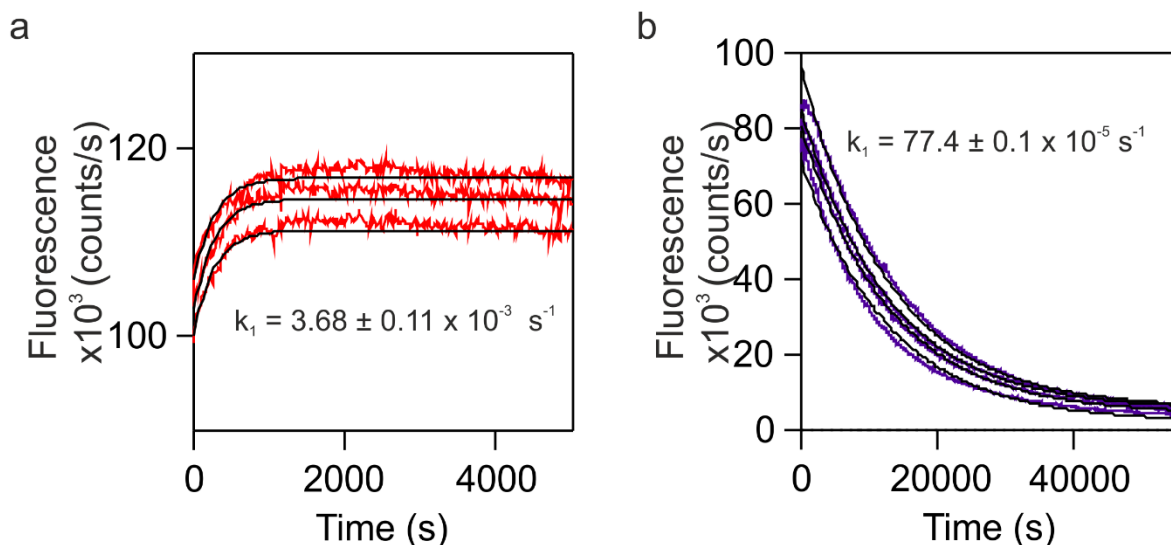
Figure 4-17: Kinetic traces for tOmpA folding in DMPC liposomes containing prefolded BamA X-link with a) TCEP and b) DTT. Experiments were performed as previously described with final concentrations of 0.4 µM tOmpA, 0.8 µM BamA, 1.28 mM DMPC LUVs, and 0.24 M urea in 50 mM glycine buffer, pH 9.5, with 10 mM TCEP or 25 mM DTT where applicable. BamA was first allowed to fold in the liposomes, here by incubation overnight at 30 °C. Reducing agents were then added to the folded sample, mixed thoroughly and the reaction started on the addition of tOmpA diluted 200-fold from 8 M urea. Each replicate trace is indicated in (a) red or (b) purple, with the global fit to a single exponential indicated by black lines.

It was first verified that wild-type, cysteine-free and X-link BamA variants are all able to fold into DMPC liposomes. It was anticipated that folding yield would be greatly reduced in these longer chain lipid LUVs[72] but it was verified that folding yield between BamA variants was approximately equal (Figure 4-18). Bandshift assays were carried out as previously detailed (see Methods Section 2.6.2 for details), with three repeats in different liposome batches and the folding yield quantified by densitometry analysis (Table 4-2).
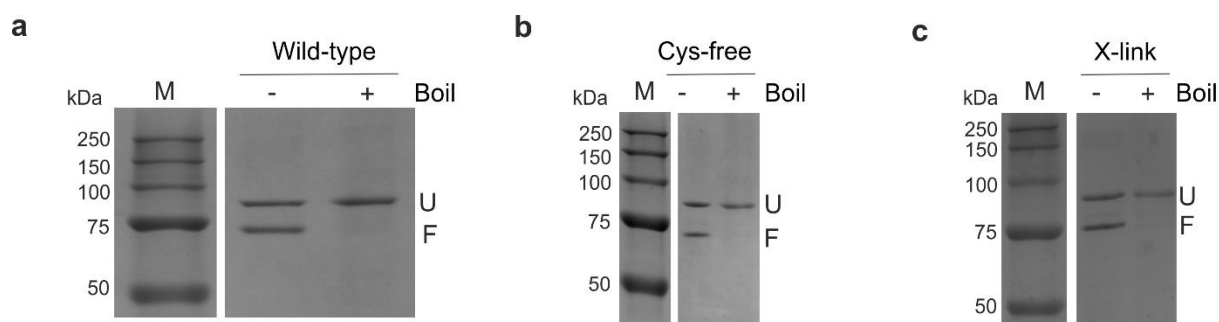
Figure 4-18: Bandshift of BamA variants in DMPC liposomes. Samples contained 0.8 µM BamA, 1.28 mM DMPC LUVs, and 0.24 M urea in 50 mM glycine buffer, pH 9.5 and were folded at 30 °C overnight prior to analysis by semi-native SDS-PAGE. Samples are shown with (+) and without (-) boiling prior to analysis. U denotes unfolded, and F folded bands of BamA variants.

BamA construct	BamA folding yield (%)
Wild-type	51.7 ± 1.7
Cys-free	55.9 ± 17.4
X-link	51.4 ± 11.9

Table 4-2: Folding yield of BamA variants and wild-type BamA in DMPC liposomes, observed by bandshift assay, quantified by densitometry. Three repeats in different liposome batches were independently analysed by semi-native SDS-PAGE. The data shown are mean ± standard deviation.

For each liposome preparation, the folding of tOmpA in the absence of BamA was first measured as a control (Figure 4-19). The data do not fit well to a single exponential function, but demonstrate that the folding rate constant ($k_1 = 39.9 \pm 0.2 \times 10^{-6}$ s^{-1}) is slower than that observed in previous lipid types used.
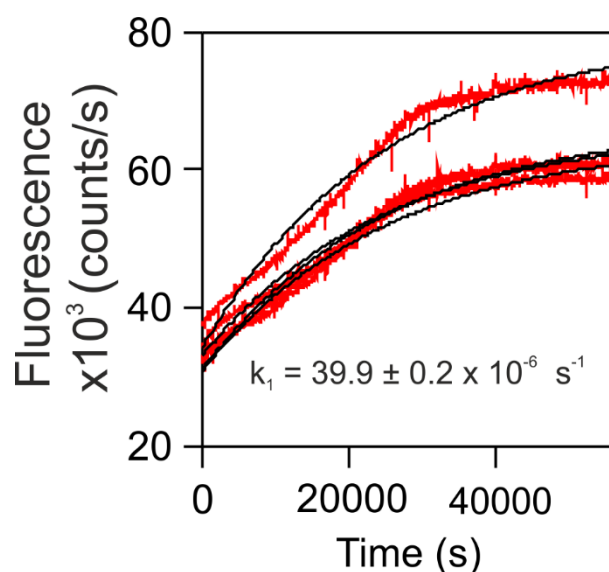
Figure 4-19: Kinetic traces for tOmpA folding in the absence of BamA in DMPC liposomes. Black lines represent the fits of the data to a single exponential function. Four replicate samples are shown. Samples contained 0.4 µM tOmpA, 1.28 mM DMPC LUVs, and 0.24 M urea in 50 mM glycine buffer, pH 9.5 and were measured at 30 °C.

BamA-catalysis of tOmpA folding in DMPC liposomes was then assessed. Following overnight folding of BamA into the LUVs, a 10x stock of TCEP (reducing), $CuSO_4$ (oxidizing) or buffer, 50mM glycine-NaOH pH 9.5 was added to the sample and incubated for a minimum of 30 minutes at 30°C before addition of tOmpA. A set of four transients was obtained (Figure 4-20), and each experiment was repeated a minimum of 3 times, with separate liposome batches.
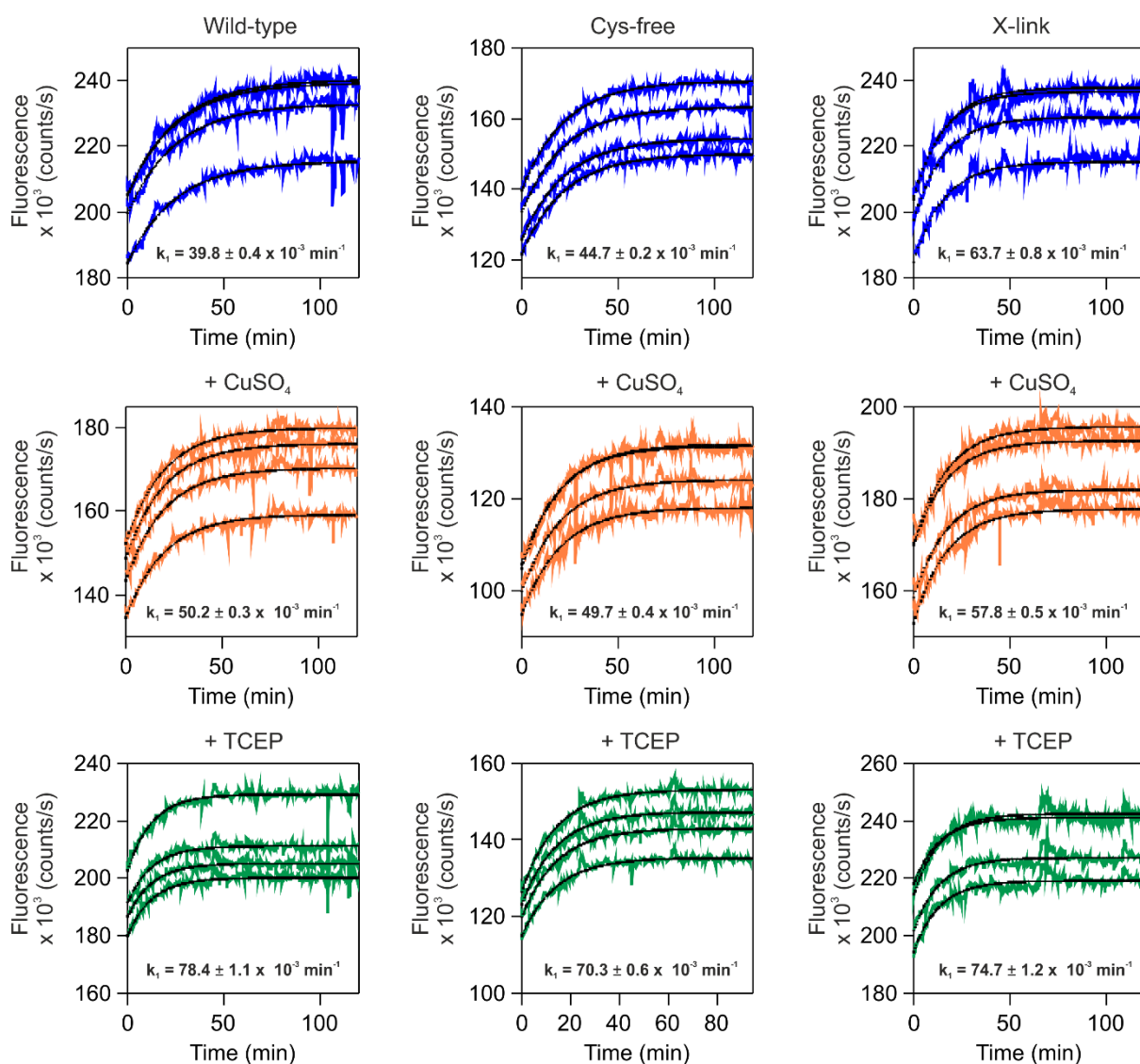
Figure 4-20: Example folding transients for BamA-catalysed folding of tOmpA, with wild-type, Cys-free and X-link BamA with addition of buffer, CuSO₄ or TCEP. Four replicate samples of each assay are shown. Samples contained 0.4 μM tOmpA, 0.8 μM BamA, 1.28 mM DMPC LUVs, and 0.24 M urea in 50 mM glycine buffer, pH 9.5 and were measured at 30 °C. Experiments were performed with the addition of buffer (blue), 1 mM CuSO₄ (orange) or 25 mM TCEP (green).

A first order rate equation was globally fit to each set of four transients and the rate constant k_1 reported for each example. However, due to the notable lag phase present in DMPC folding reactions in the absence of BamA (see Figure 4-19), the t_{50} value, or time taken to reach 50% of the total fluorescence change on folding was used to compare the tOmpA folding rates (Table 4-3, Figure 4-21b).

166

Folding condition	t_{50} (minutes)		
	+buffer	+CuSO$_4$	+TCEP
-BamA	276 ± 6	-	-
+WT BamA	22.3 ± 1.5	15.7 ± 1.1	7.9 ± 0.7
+BamA (Cys-free)	18.8 ± 0.6	18.6 ± 2.0	12.4 ± 1.0
+BamA (X-link mutant)	17.3 ± 1.7	16.8 ± 1.3	8.55 ± 0.45

Table 4-3: Average t_{50} values for tOmpA folding in each condition. t_{50} values were extracted to analyse the folding rate. Each transient was independently analysed with a horizontal line fit to the final section of data. Three repeats of each experiment (12 transients in total) were used to calculate the average t_{50} for each condition and standard error of the mean.

From comparison of the t_{50} values, one can observe that although the addition of TCEP lowers the t_{50} ~2-3 fold in the case of all BamA variants (Table 4-3) the general trend is near identical (Figure 4-21b). The difference between wild-type, Cys-free and X-link BamA catalysis of tOmpA folding in the same conditions is negligible. Overlay of a normalised transient for all conditions of Cys-free and X-link BamA-catalysed folding (Figure 4-21a) shows that these rates are near identical. In addition, visual comparison of t_{50} values (Figure 4-21b) demonstrates the significant catalytic effect on tOmpA folding provided by all BamA variants and the substantial increase in rate relative to absence of BamA and the insignificant differences between variants and conditions. This considerable catalytic effect, with ~12-fold rate enhancement is specific to BamA, as prefolding of OmpA has been shown to have no catalytic effect on tOmpA folding[241].
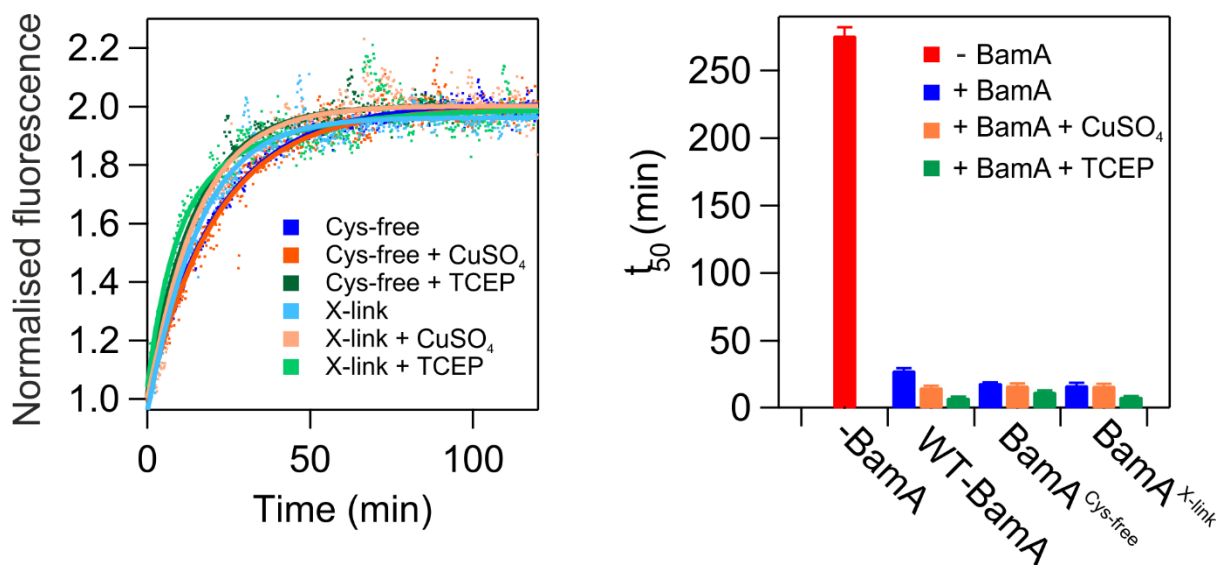
Figure 4-21: Comparison of BamA-catalysed folding of tOmpA. a) Overlay of single normalised transients comparing BamA-catalysis of tOmpA folding by Cys-free mutant and X-link mutant in all conditions. b) Comparison of t_{50}, as a measure of folding rate for tOmpA folding alone, or with prefolded wild-type, Cys-free, or X-link BamA in all reduced and oxidized conditions. Three repeats of each experiment (12 transients in total) were used to calculate the average t_{50} for each condition with error bars showing standard error of the mean.

It has previously been noted that removal of the two natural cysteines of BamA has little effect on function, as measured *in vitro* or *in vivo*[199,210,231] and this variant therefore forms an excellent pseudo wild-type control. Due to the proposed role of lateral gating it had been anticipated that the catalytic effect of the X-link variant would be different to that of the wild-type or Cys-free. However, as overlay of the normalised transients (Figure 4-21a) renders apparent, the X-link variant also has the same catalytic activity as the Cys-free BamA. The lack of significant difference between BamA X-link catalytic activity in reduced or oxidized conditions demonstrates that the lateral opening of BamA is not critical in this case.

4.2.6 Redox gels for BamA X-link mutant

As a final control for this section of the work, conditions were optimised to enable the reduced and oxidized states of BamA to be resolved by SDS-PAGE. The process for this is detailed for the BAM complex, in Section 5.6. Results were optimised with 5% Tris-glycine gels (Methods Section 2.6.3) (Figure 4-24). Two examples are shown, firstly with cysteine-free and X-link variants folded in DUPC (Figure 4-22) and in DMPC (Figure 4-23).
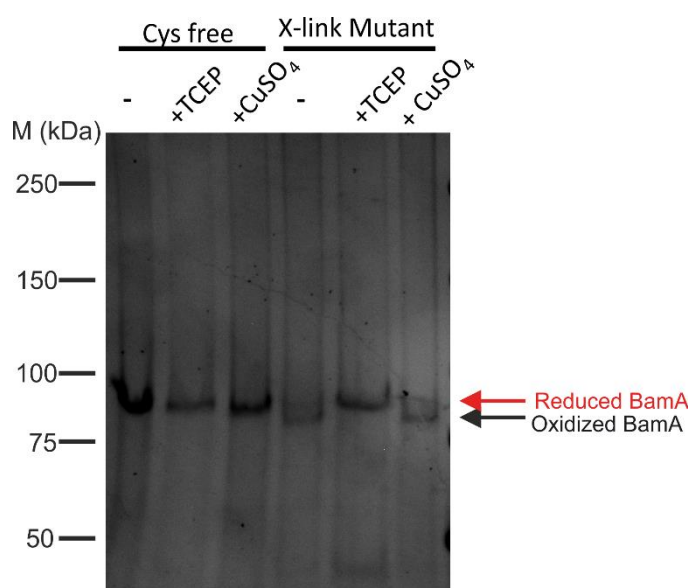
Figure 4-22: Non-reducing SDS-PAGE of BamA Cys-free and X-link mutant.
BamA protein samples folded into DUPC liposomes at 2µM, were incubated for 30 minutes with TCEP or CuSO$_4$ at final concentrations 25 mM or 1 mM, respectively. Samples were mixed with 6x loading buffer, containing 0.6 % (*w/v*) SDS in the absence of DTT and loaded on the 5% acrylamide, Tris-Glycine gel, see Methods Section 2.6.3.

In both examples the X-link variant in both buffer and in the presence of oxidizing agent (CuSO$_4$/diamide) shows a double band. This clearly resolves to a single band upon treatment with reducing agent (DTT/TCEP). This demonstrates that BamA is in a partially oxidized state that can be reduced, but not oxidized to completion. Wild-type or Cys-free BamA remains as a single band in all redox conditions, with migration approximately equivalent to that of reduced lateral-lock variant.

169
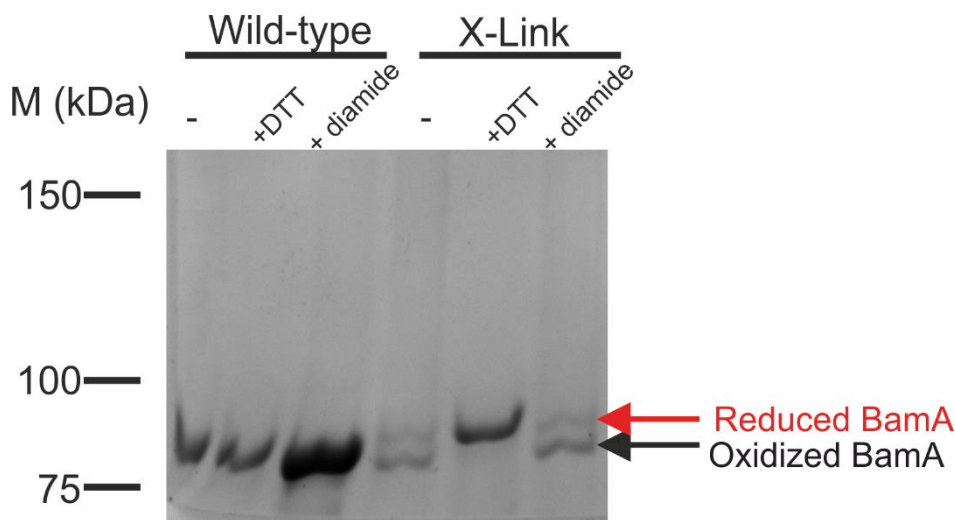
Figure 4-23: Non-reducing SDS-PAGE of BamA Wild-type and X-link variant.
BamA protein samples folded into DMPC liposomes at 2µM, were incubated for 1hour with DTT or diamide at final concentrations 25mM or 100 µM, respectively. Samples were mixed with 6x loading buffer, containing 0.6 % (*w/v*) SDS and boiled for 30 minutes before being loaded on the 5% acrylamide, Tris-Glycine gel, see Methods Section 2.6.3.

The extent of oxidation for BamA in DMPC was determined by densitometry. This revealed the fraction of total protein sample oxidized for X-link protein as 60% in buffer, and 65% with the addition of diamide.

4.2.7 BamA Lateral Gating Conclusions

This section begins examination of the role of BamA lateral gating in its *in vitro* catalysis of OMP folding. Following initial studies in DUPC and DUPC:DDPE LUVs, assays of BamA-assisted folding of tOmpA in DMPC are carried out for most reproducible results. Non-reducing SDS-PAGE was used to show that greater than ~60% of the BamA X-link protein will be in the oxidized form in the conditions used for tOmpA folding assays. The results demonstrate that the X-link BamA variant is able to catalyse tOmpA folding, and this occurs to the same extent as with wild-type BamA (Figure 4-21). It therefore appears that at least for the BamA-catalysed folding of tOmpA in synthetic DMPC liposomes, the opening of the BamA lateral gate is not essential for its function. This supports alternative hypotheses over lateral gating, particularly that of membrane destabilization[71,212,279]. It appears highly likely, with this data in mind, that the presence of any BamA variant in the bilayer of these synthetic LUVs is sufficient to aid the folding of the substrate tOmpA, likely by inducing local membrane

170

disorder. As previously noted, controls, carried out by Dr Bob Schiffrin concurrently, have proved that this effect is specific to BamA: prefolding OmpA into LUVs before addition of tOmpA had no catalytic effect on tOmpA folding[241].

4.3 β-signal: tOmpA-RHK

The tOmpA-RHK protein variant discussed previously (4.1.2, Figure 4-4) was designed for studies on the role of the β-signal in BAM-mediated OMP folding and was previously cloned, expressed and purified by Dr. Bob Schiffrin (University of Leeds) according to the method used for wild-type tOmpA (see Methods 2.3.1). Aliquots of the protein in 6M GuHCl 25 mM Tris pH 8 had been snap-frozen and stored at -80 °C and were thawed and buffer exchanged into the correct urea buffer immediately prior to use.

Initial experiments examined the intrinsic folding rate and recognition of the β-signal variant by BamA using fluorescence kinetic studies. These were performed by analysing tOmpA folding alone and BamA-assisted folding of tOmpA wild-type and RHK variants in 12 carbon chain 1,2-dilauroyl-sn-glycero-3-phosphatidylcholine (DLPC) and 14 carbon chain 1,2-dimyristoyl-sn-glycero-3-phosphatidylcholine (DMPC) LUVs. As previously discussed, while synthetic liposomes are not a native-like system, DMPC liposomes provide the lipid bilayer thickness (~23 Å)[269] most likely to mimic the *E.coli* outer membrane[270]. In addition, with increasing lipid length the fold rate enhancement provided by BamA increases incrementally[241]. Carrying out experiments in DMPC LUVs therefore allows us to better observe small differences in BamA catalysed rates of OMP folding while utilising two different lipid types enables a better understanding of how tOmpA-RHK folding depends on lipid type. This variant has not previously been characterised and therefore this work is seminal in understanding its folding capabilities. In addition to wild-type BamA, the BamA X-link variant (430/808) was also used to better understand how the models of lateral locking and β-signal targeting may complement one another.

Kinetic folding experiments were carried out as described previously, for wild-type tOmpA(4.2.5). Folding of tOmpA was monitored upon rapid dilution 200-fold from 8 M urea in the presence or absence of prefolded wild-type or X-link BamA in LUVs formed from DLPC (prepared and used at 25 °C) and DMPC (at 30 °C).

171

Example folding kinetic traces are shown for all conditions in DLPC (Figure 4-24) and DMPC (Figure 4-25) liposomes. For all kinetic experiments, the traces were fitted globally to a single exponential function (Methods Section 2.9), and the rate constant k_1 is reported.
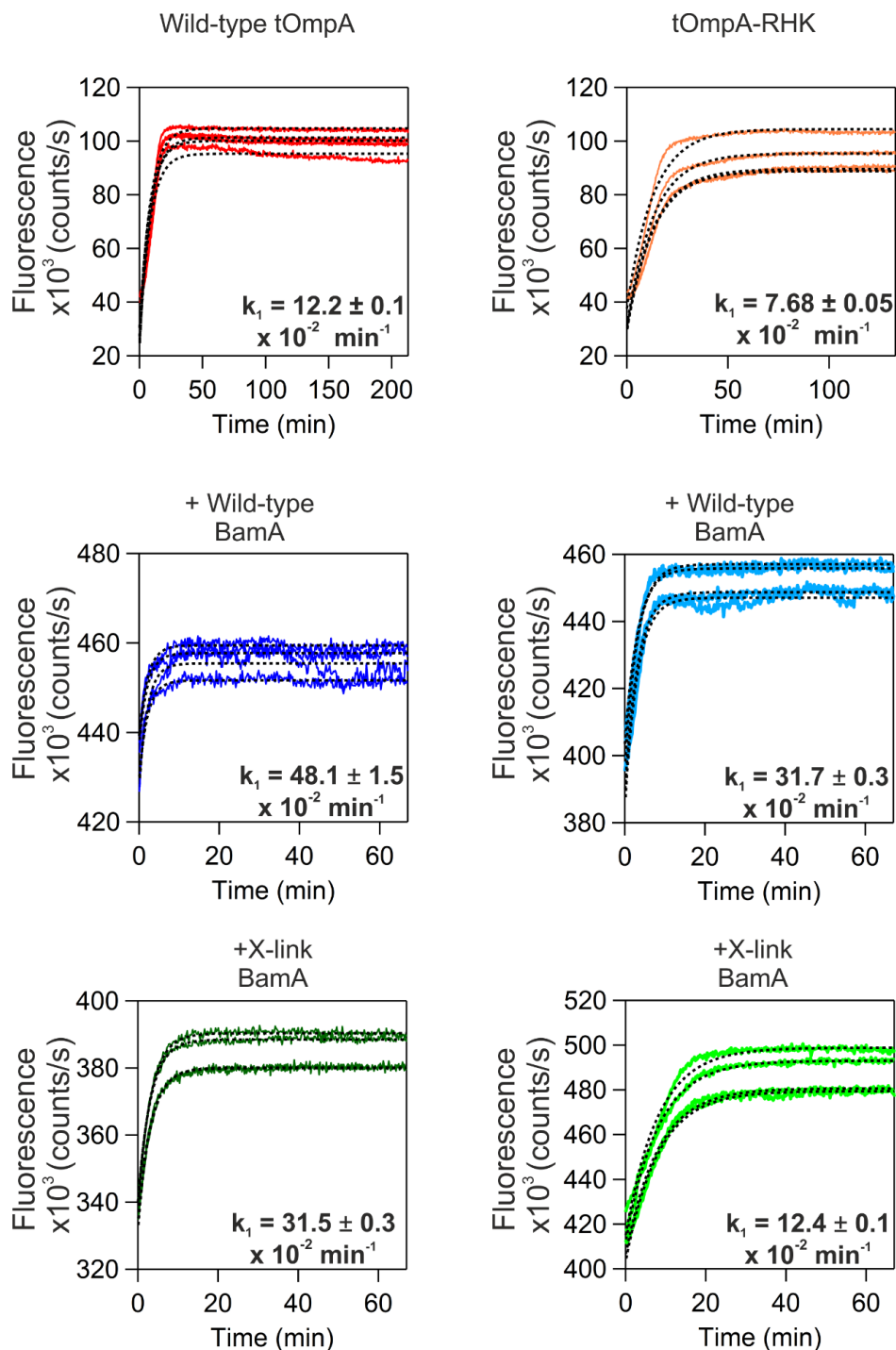
Figure 4-24 Example folding kinetic transients for wild-type or RHK tOmpA in DLPC liposomes with no BamA, wild-type BamA or X-link BamA. Four replicate samples of each assay are shown. Samples contained 0.4 µM tOmpA, 0.8 µM BamA where applicable, 1.28 mM DLPC LUVs, and 0.24 M urea in 50 mM glycine buffer, pH 9.5 and were measured at 25 °C. Transients are globally fit to a single exponential, fits are indicated in dashed black lines.
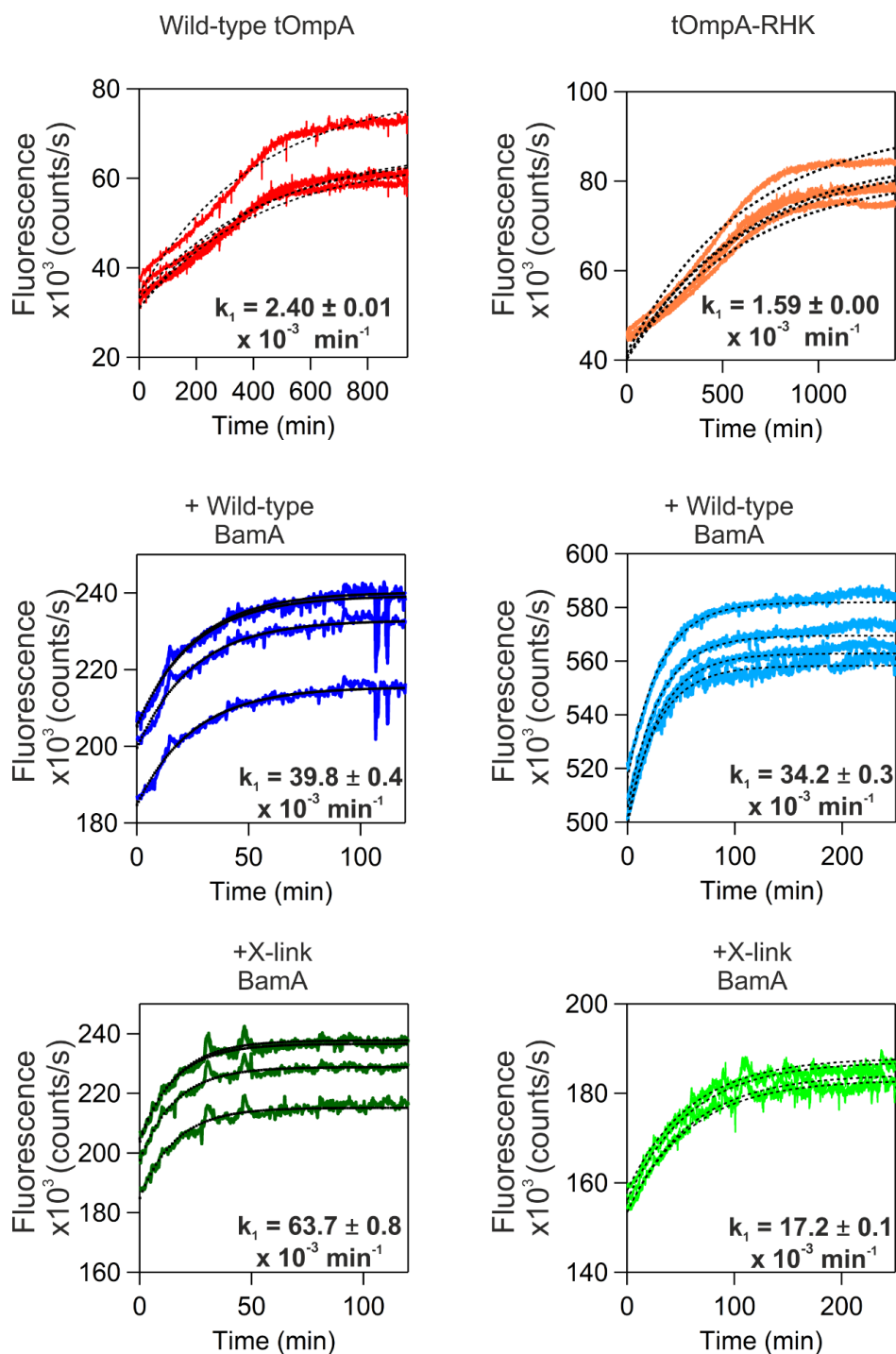
Figure 4-25 Example folding kinetic transients for wild-type or RHK tOmpA in DMPC liposomes with no BamA, wild-type BamA or X-link BamA. Four replicate samples of each assay are shown. Samples contained 0.4 µM tOmpA, 0.8 µM BamA where applicable, 1.28 mM DMPC LUVs, and 0.24 M urea in 50 mM glycine buffer, pH 9.5 and were measured at 30 °C. Transients are globally fit to a single exponential, fits are indicated in dashed black lines.

As previously, traces are quantified and compared by extraction of the t_{50} (see Methods 2.9 for details). Comparison of the folding traces immediately demonstrates the altered folding of the tOmpA-RHK variant, which folds ~2-fold slower than wild-type tOmpA in both lipid types. In addition, a significant rate enhancement provided by prefolded wild-type BamA or X-link BamA is observed in both cases (Figure 4-26).
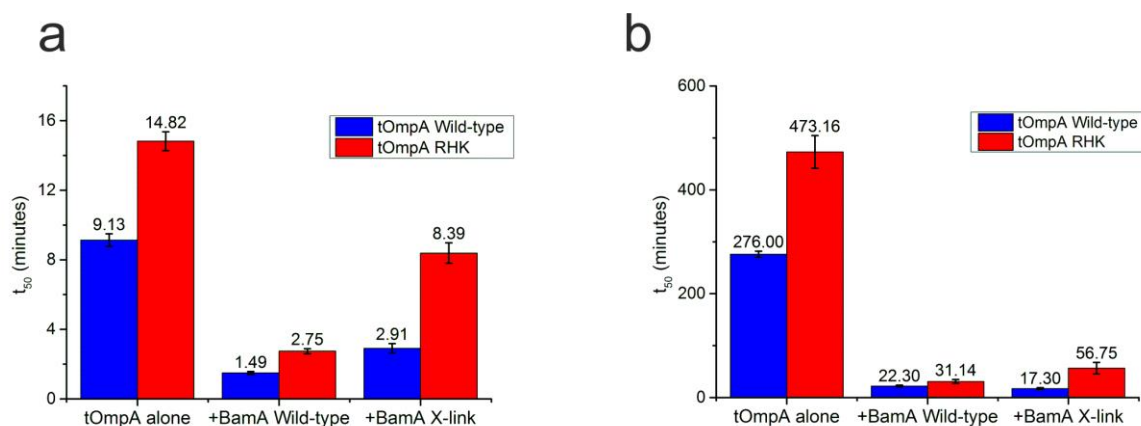
Figure 4-26: Comparison of t_{50}s for folding kinetics in a) DLPC and b) DMPC for tOmpA wild-type (blue) and tOmpA-RHK (red). The t_{50} is the time taken to reach the fluorescence halfway between the minimum and a horizontal line fitted to the final 10% of data. A minimum of three replicates with 4 transients each, each with an independently calculated t_{50} were used. Shown is the average, and error bars indicate SEM.

The tOmpA-RHK variant (red) folds more slowly than wild-type tOmpA (blue) in all conditions (Figure 4-26). Comparison of fold change in t_{50} of wild-type tOmpA over tOmpA-RHK highlights the key differences (Figure 4-27). Firstly, while tOmpARHK folds ~1.6x slower than wild-type (in both lipid types) approximately the same fold difference is observed for the two proteins when folding is accelerated by wild-type BamA (Figure 4-27). Therefore wild-type BamA is exerting a catalytic effect on both tOmpA variants, but maintaining the fold difference between them. In considering the X-link BamA variant, however, the story changes. The fold difference between tOmpA-RHK and wild-type catalysed by X-link BamA is nearly twice that previously observed (~3x), in both DLPC and DMPC lipids. This indicates that X-link BamA is less effective at catalysing the folding of tOmpA-RHK than of wild-type tOmpA, in both lipid types. Thus, while the BamA X-link variant is capable of catalysing wild-type tOmpA folding, the
174

combination of the X-link BamA barrel and a mutated substrate β-signal sequence reduces the catalytic effect of BamA on tOmpA folding. This suggests a correlation between lateral gate opening of BamA and β-signal recognition, where both are required for maximum enhancement of substrate folding rate *in vitro*.
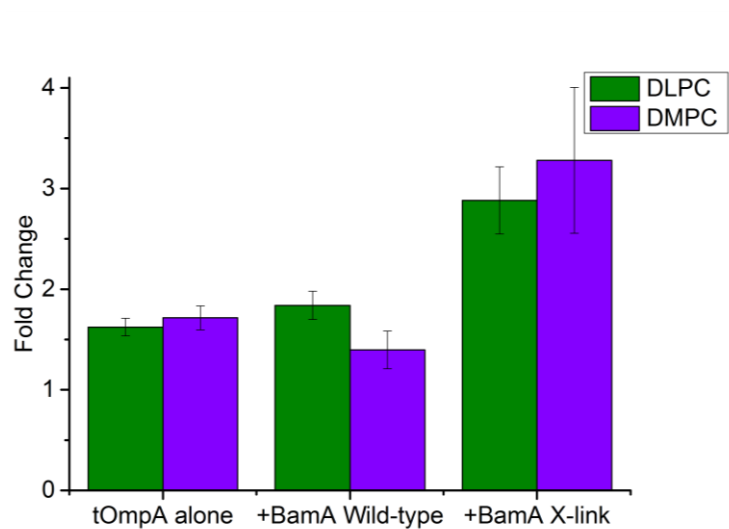
Figure 4-27: Fold change in t_{50} values between tOmpA wild-type and RHK in all conditions and two lipid types. The t_{50} for tOmpA-RHK is slower (larger) than wild-type in all cases. Therefore the fold change is calculated by t_{50}(tOmpARHK)/t_{50}(tOmpAwt) for all conditions. Error bars show propagated SEM (for details see Methods 2.9).

4.4 β-signal: Gly variants

The second approach to studying the roles of the β-signal in BamA-catalysed folding involved mutagenesis of the conserved Gly, firstly to Pro using OmpT as substrate and subsequently to Ala in OmpT and tOmpA. Q5 site-directed mutagenesis was carried out for all variants (primers and protocol are detailed in Methods Table 2-5 and Section 2.2.3).

Following successful generation of the variants OmpT-G306P, OmpT-G306A and tOmpA-G166A by site-directed mutagenesis, the proteins were expressed and purified as described in Methods Section 2.3.1. Briefly, each protein was expressed in *E.coli* BL21 (DE3) and purified by inclusion body isolation followed by size exclusion chromatography under denaturing conditions (see Methods Section 2.3.1 for details). The elution profile obtained by SEC and protein composition of the elution peak as analysed by electrophoresis on SDS-PAGE is shown (Figure 4-28). Fractions were then selected to be pooled and concentrated (see Section 2.3.1 for details).
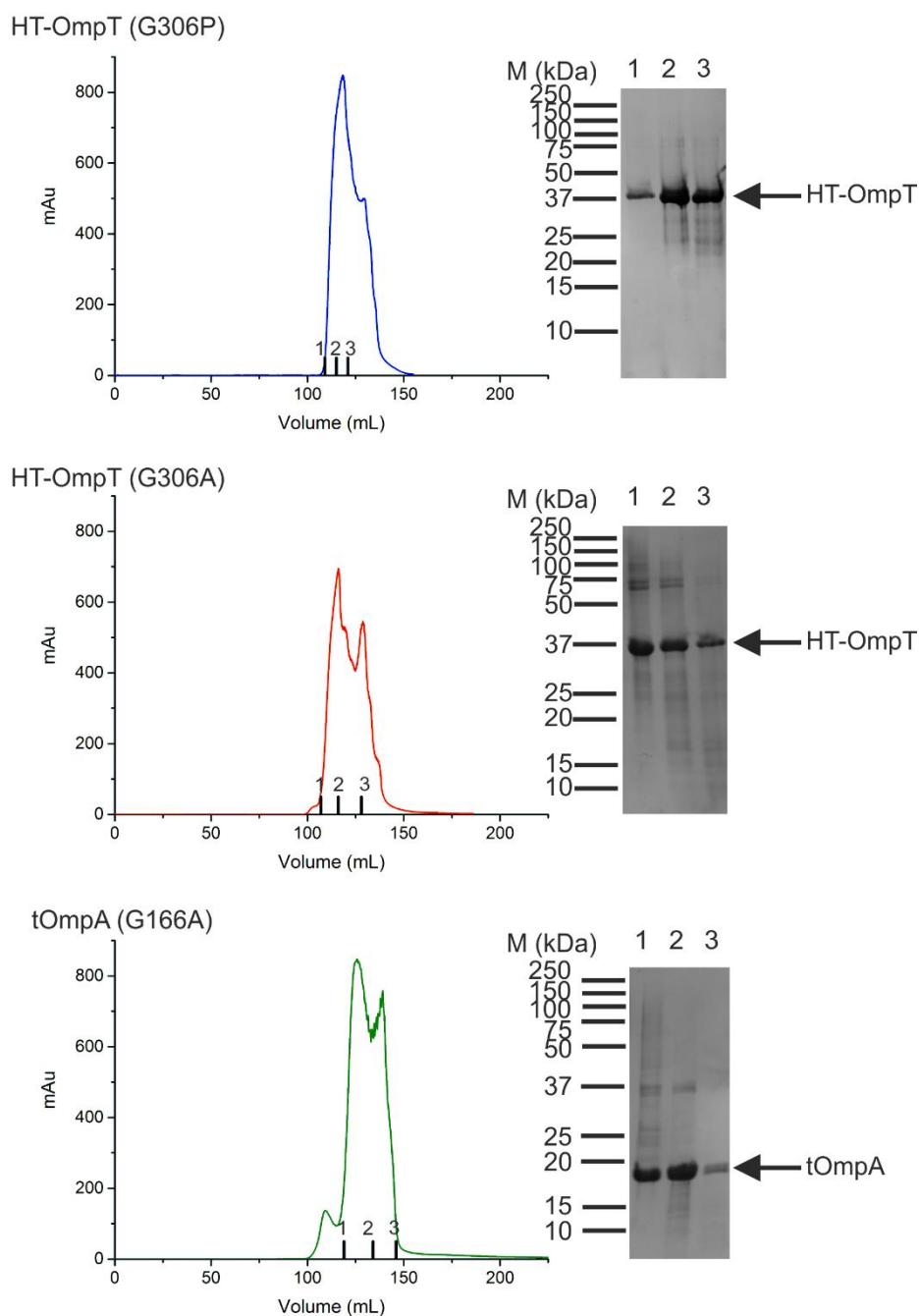
Figure 4-28: Purification of β-signal mutants. Shown is an example SEC trace of purification of each protein and fractions analysed by SDS-PAGE for HT-OmpT-G306P, HT- OmpT-G306A, tOmpA-G166A. SEC was carried out using a Sup75 column with 25 mM Tris, 6M GuHCl pH 8 (see Methods 2.3.1 for details). Three fractions are shown by SDS-PAGE across the peak of protein elution, indicated on the elution trace with black bars. Proteins have a molecular mass of 35 kDa (HT-OmpT -G306A & -G306P) and 18 kDa (tOmpA) and are shown compared to a protein marker to the left of each gel image. Protein is shown buffer-exchanged from 25 mM Tris, 6M GuHCl pH 8 to 8 M urea, 50 mM glycine-NaOH pH 9.5 for b) and c) but not a) thus the apparent band smearing.

4.4.1 Characterisation of β-signal variants

As these were novel protein variants, a full characterisation of the folding of these proteins in synthetic liposomes was carried out. Folding in DUPC liposomes was examined by a number of techniques, firstly heat modifiability. As previously mentioned, this allows us to distinguish between folded and unfolded populations of OMPs due to their SDS-resistant properties when folded and left unboiled[248,307]. Unlike with BamA, however, most OMP barrels are sufficiently heat and SDS-resistant once folded that experiments can be carried out at room temperature and with typical Tris-Tricine SDS-PAGE (Methods, Section 2.6). OmpT-G306P was the first variant created, and the first to be tested. It was immediately apparent that the folding of this protein differed substantially from wild-type as this variant displayed no folding in the initial electrophoresis experiment (Figure 4-29).
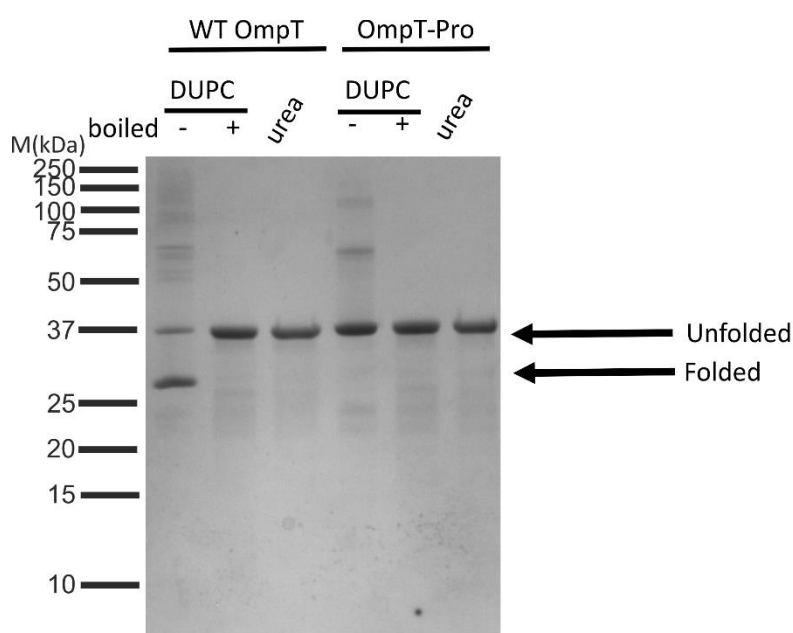
Figure 4-29: Folding of OmpT wild-type and G306P variant in DUPC liposomes analysed by SDS-PAGE. Samples contained 5 µM protein either with 4 mM (800:1 molar LPR) DUPC LUVs, 2 M urea in 50 mM glycine-NaOH pH 9.5 (DUPC samples) or kept unfolded at 5 µM in 8 M urea, 50 mM glycine-NaOH pH 9.5 (urea samples). Folding was carried out for 3 hours at 25 ⁰C prior to electrophoresis. A sample of folded protein is boiled (+) for 30 minutes prior to electrophoresis. HT-OmpT is 35 kDa and when unfolded migrates close to its calculated molecular mass, while folded HT-OmpT migrates at ~29 kDa[268].

It is possible that this lack of folding was due to limited folding time (3 hours in the initial experiment), the protein concentration, or the lipid-protein ratio (LPR)

178

used. It was subsequently verified that the OmpT-G306P variant did not show SDS-resistant folding properties by bandshift with longer folding times (3-16 hours) in a wide range of protein concentrations (0.4 – 5 μM) and LPR conditions(800-3200 :1 molar LPR) (Figure 4-30).
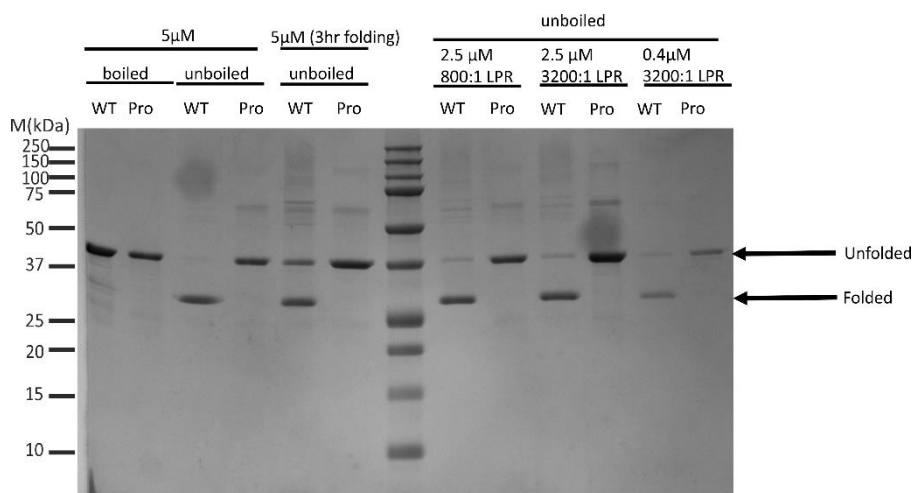
Figure 4-30: Folding of OmpT wild-type (WT) and G306P (Pro) variant in DUPC liposomes by SDS-PAGE. From the left: samples contained 5 μM protein with 4 mM (800:1 LPR) DUPC LUVs, 2 M urea in 50 mM glycine-NaOH pH 9.5; other concentrations and LPRs are as indicated, all with 2 M urea and in 50 mM glycine-NaOH pH 9.5. All folding was carried out overnight at 25 °C unless indicated otherwise.

As all electrophoresis experiments for this protein utilised standard SDS-PAGE, and the OmpT-G306P variant appears sensitive to SDS the experiments were repeated utilising semi-native SDS-PAGE as used for bandshift assays of BamA (see Methods Section 2.6.2) (Figure 4-31). These gels contain no SDS in the gel and only 0.1% (*w/v*) SDS in the loading buffer, which is added to the samples immediately prior to gel loading. In addition, the gels are run at 4°C and low (10-20) mA to avoid any heat-denaturation of sample. These experiments conclusively demonstrate the OmpTG306P variant is not able to adopt an SDS-resistant folding conformation under any of the conditions explored, by contrast with the wild-type protein.
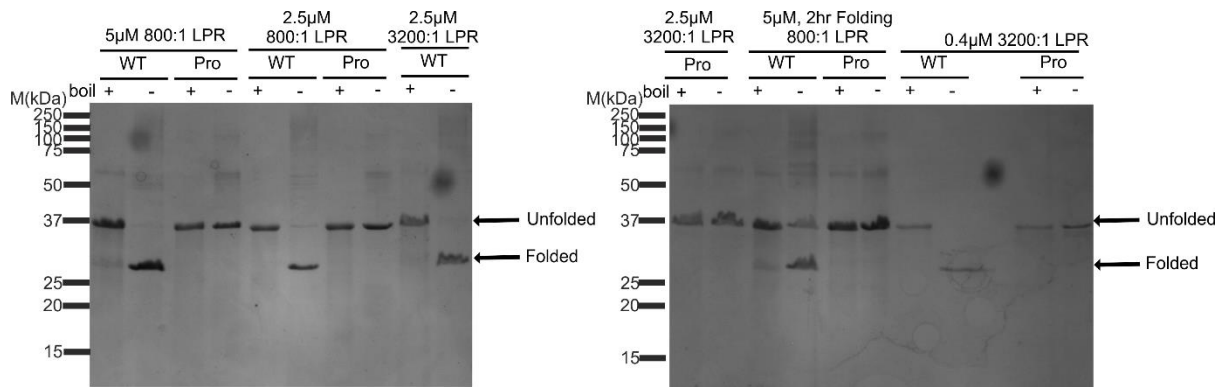
Figure 4-31: Folding of HT-OmpT wild-type (WT) and OmpT-G306P (Pro) variant in DUPC liposomes by semi-native SDS-PAGE Samples contained the indicated protein concentration and LPR with 2 M urea in 50 mM glycine-NaOH pH 9.5. All folding was carried out overnight at 25 °C unless otherwise indicated. Samples were mixed with low-SDS loading buffer without boiling (-) or prior to 30 minutes boiling (+).

Bandshift electrophoresis experiments were next attempted with all β-signal variants including the tOmpA-RHK variant for comparison (Figure 4-32). As it was known that folding may be kinetically slower or occur with lower yield than for the wild-type proteins all experiments were carried out with proteins folded in DUPC liposomes overnight at 25 °C. In these conditions wild-type tOmpA folding goes to completion. Complete (~100%) folding was observed for all tOmpA variants, however while wild-type OmpT folds nearly to completion (~74%), no folding is observed for OmpT- G306P or -G306A variants.
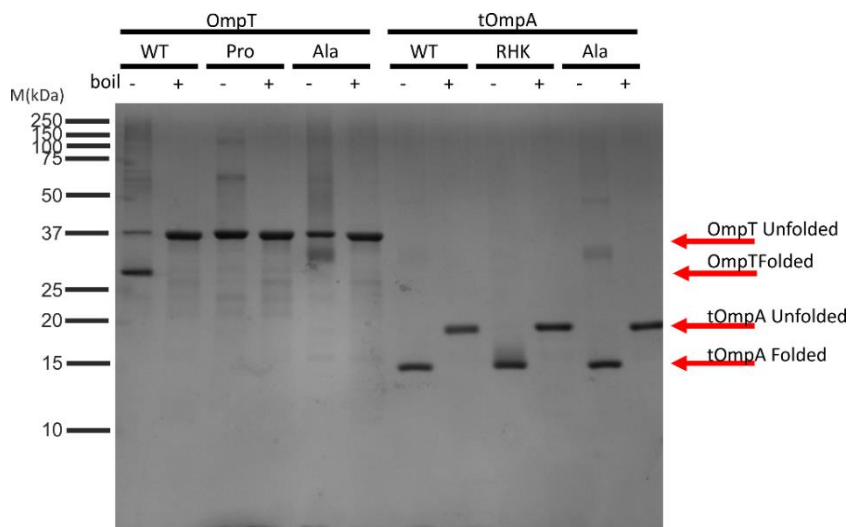
Figure 4-32: Folding of all OmpT and tOmpA mutants in DUPC analysed by SDS PAGE. Samples contained 5 μM protein with 4 mM (800:1 LPR) DUPC LUVs, 2 M urea in 50 mM Glycine-NaOH pH 9.5 Folding was carried out overnight at 25 °C prior to electrophoresis. Samples were mixed with low-SDS loading buffer without boiling (-) or after 30 minutes boiling (+).

180

Further characterisation of the proteins was next carried out in DUPC LUVs using fluorescence emission spectra (Figure 4-33). As with BamA discussed previously (4.2.2.2), folded OMPs display a blue shift, with wavelength of maximum fluorescence intensity (λmax) occurring at a shorter wavelength, and with a higher fluorescence intensity relative to the unfolded state. This is observed for all variants analysed here for both proteins. The results for OmpT can be misleading, as OmpT has been shown previously to display a folded fluorescence emission spectrum when collapsed in buffer[163], due to folding of the extracellular β-strands. However, it should be noted that the spectra of the variants still do not differ significantly from those of wild-type protein.
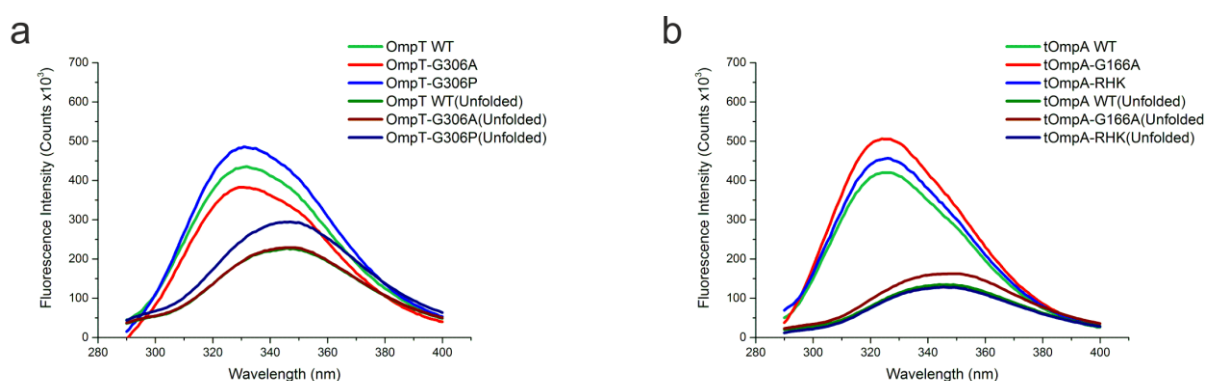
Figure 4-33: Fluorescence emission spectra for a) OmpT and b) tOmpA protein variants. Shown are spectra of variants both folded in DUPC LUVs and unfolded in 8 M urea. Protein was folded in DUPC LUVs at 0.4 µM OmpT/tOmpA, 1.28 mM DUPC LUVs (3200 LPR), and 2 M urea in 50 mM glycine buffer, pH 9.5. All folded samples were incubated at 25 °C overnight prior to measurement. Unfolded protein variants contain 0.4 µM OmpT/tOmpA in 8 M urea 50 mM glycine buffer, pH 9.5. Each spectrum was recorded from 280 nm to 400 nm in 1 nm increments, using an excitation wavelength of 280 nm. An appropriate "blank" sample was subtracted from measurements, to remove light scattering by liposomes from the final spectra observed (see Methods Section 2.8.1 for details).

4.4.2 Analysis of Gly variants using Far UV CD

Far UV CD was also utilised to determine whether the variants adopt the expected β-barrel architecture. Folding of each of the OmpT/tOmpA variants into DUPC liposomes resulted in far UV CD spectra typical of a β-sheet protein (

181

Figure 4-34) with a negative maximum at 220 nm, confirming that all proteins are capable of forming β-sheet structure in this lipid. In addition, all variants gave rise to far UV CD spectra that differ substantially from the spectra of their unfolded states obtained in 8 M urea.
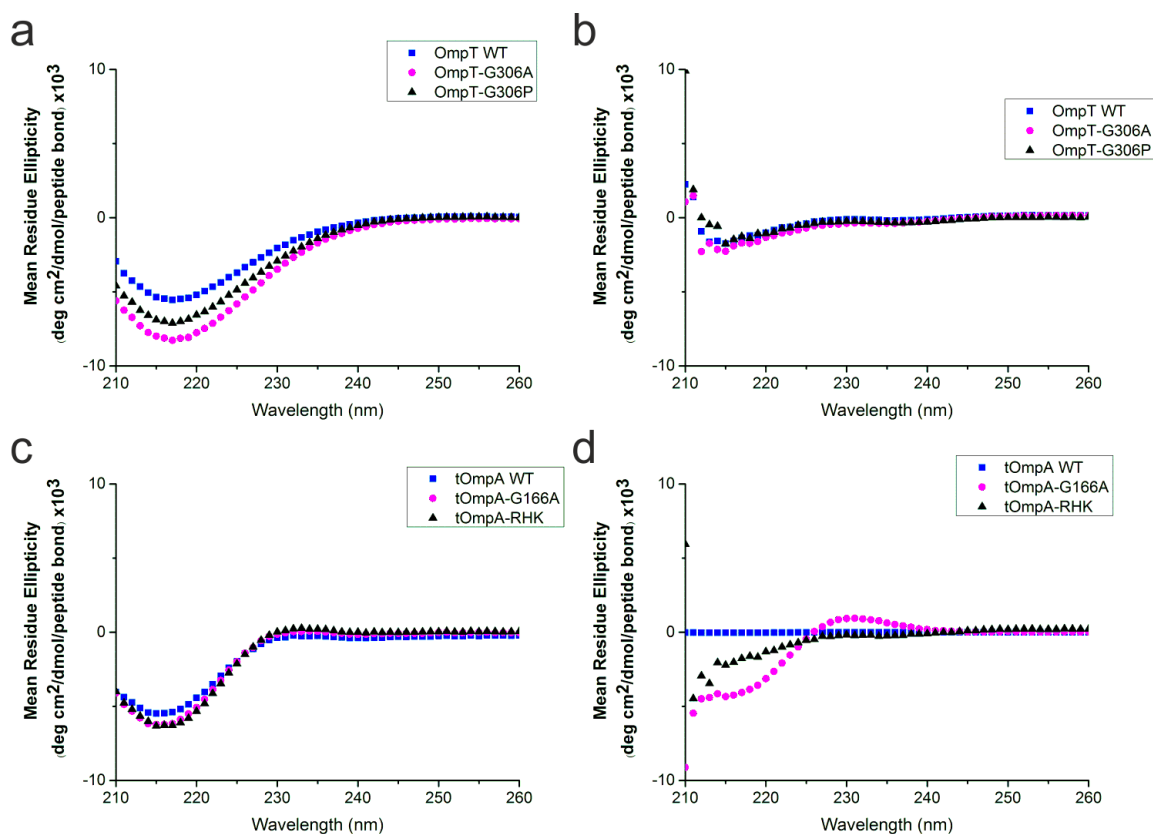
Figure 4-34: Comparison of CD spectra for OmpT (a & b) and tOmpA (c & d) variants in folded (a & c) and unfolded (b & d) forms. Protein was folded in DUPC LUVs at 5 μM OmpT/tOmpA, 4 mM DUPC LUVs (800:1 molar LPR), and 2 M urea in 50 mM glycine buffer, pH 9.5. All folded samples were incubated at 25 °C overnight prior to measurement. Unfolded protein variants are 5 μM OmpT/tOmpA in 8 M urea 50 mM glycine buffer, pH 9.5. An appropriate blank was subtracted for each sample. The Mean Residue Ellipticity (MRE) is plotted against wavelength, for how MRE is derived see Methods Section 2.8.2.

As the OmpT variants were demonstrating β-sheet structure but no SDS resistance in any condition, CD spectra over a temperature ramp from 20 – 90 ºC were also obtained to determine the variants' relative stability (Figure 4-35). Even at the highest temperature of 90 °C all proteins show unperturbed β-sheet

structure. The results obtained here indicate that the OmpT Gly variants fold to a stable β-barrel structure, that surprisingly is not SDS-resistant.
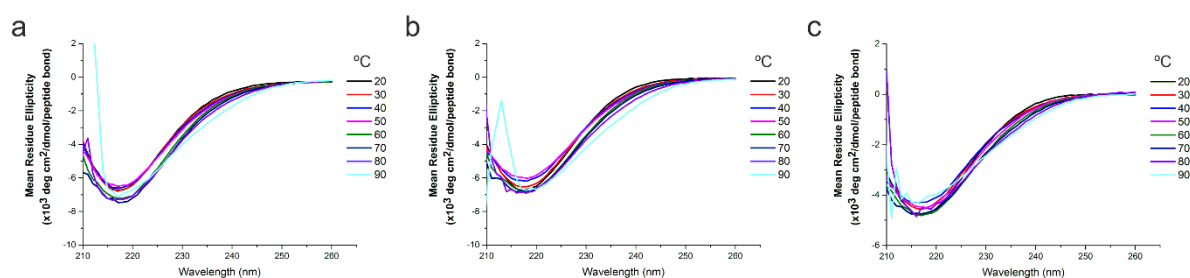
Figure 4-35: Temperature Ramp of OmpT (a) wild-type (b) G306A (c) G306P. The protein was folded in DUPC LUVs at 5 μM OmpT, 4 mM DUPC LUVs (800:1 molar LPR), and 2 M urea in 50 mM glycine buffer, pH 9.5. All folded samples were incubated at 25 °C overnight prior to measurement. An appropriate blank was subtracted for each sample. The spectra was measured from 20- 90 ºC with a 1 ºC step and 120 seconds settling time for each reading. The spectra are depicted for every ten degrees for simplicity.

4.4.3 BAM-mediated folding of the β-signal Gly variants

As previously discussed, the original experimental directive behind the mutagenesis was to understand the relevance of the β-signal to OMP folding by BAM. This had partially been begun by analysing catalysis of tOmpA-RHK folding by BamA (Figure 4-24-Figure 4-27), and the aim moving to OmpT was to utilise the OmpT assay and thus the BAM complex. It had been assumed that single point mutations would not be highly detrimental to the OMP's intrinsic folding ability, but may inhibit its' ability to be catalysed by BAM. It is immediately apparent with the OmpT Gly variants that this is not the case, and the single amino acid mutation significantly impairs the protein's ability to adopt a stable SDS-resistant structure, however we proceeded to determine how interaction with BAM is affected by substitution of the conserved Gly in the β –signal.

Fortunately, for OmpT, folding can be measured by the catalytic activity of native OmpT to cleave a fluorogenic peptide substrate[189,268]. This indirect assay is complex as it reports on whether the OmpT variants are capable of folding, if these structures are active and how they might interact with BAM. Samples were set up as described previously (3.5.1 and Methods 2.12) to examine OmpT folding as catalysed by BAM. In parallel the catalysis of OmpT and its variants

prefolded in DUPC LUVs, at the same concentration and LPR as the fluorescence and CD experiments (molar LPR 800:1). The results are surprising, with OmpT activity resulting in all cases, but with very different rates (Figure 4-36).

Due to the setup of the reaction, the DUPC and +BAM samples cannot be fairly compared. Not only is there a slight concentration difference of OmpT between them, but DUPC samples involve prefolded OmpT, whereas in +BAM samples the OmpT is being folded simultaneously to the peptide cleavage that is monitored. However this makes the magnitude of the catalytic effect of BAM upon the folding of OmpT even more apparent. The +BAM rates for wild-type OmpT and OmpT-G306A are considerably faster than those same proteins folded in DUPC (Figure 4-36) despite none of the OmpT being folded in its functional form at the start of the reaction.
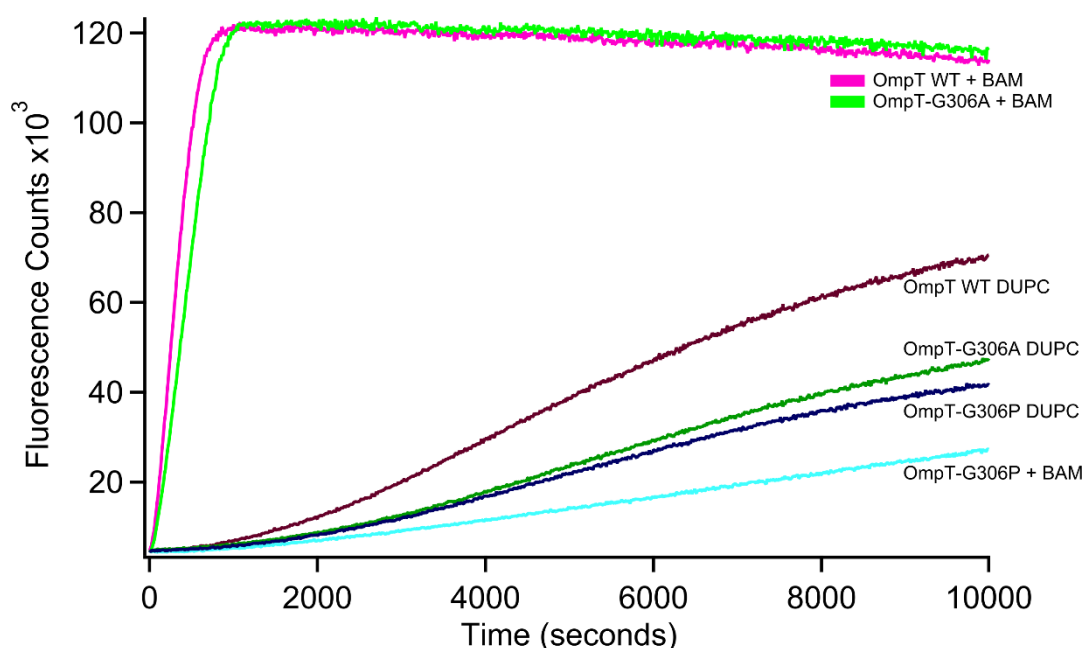
Figure 4-36: OmpT protease assay for OmpT wild-type and variants folded in DUPC or BAM complex proteoliposomes. The OmpT assay was carried out as previously described for +BAM samples. These contained 5 µM OmpT, 35 µM SurA, 1mM fluorogenic peptide, 0.4 M urea, 0.25 µM BAM, *E.coli* polar lipid proteoliposomes, 50mM glycine-NaOH pH 9.5. DUPC samples used OmpT variants prefolded into DUPC (overnight, 25 °C) at 5 µM protein, 4 mM DUPC. This subreaction was then mixed with LPS and fluoropeptide in the assay plate, with final concentrations 4 µM OmpT, 1 mM fluoropeptide, 1mg/ml LPS, 1.8 M urea, 50 mM Glycine-NaOH pH 9.5. The reaction was monitored using a Clariostar immediately after mixing of subreactions.

184

Many traces do not reach completion over the time-course measured, therefore an accurate t_{50} cannot be extracted in these cases. Thus while only qualitative comparison of the rates of folding can be drawn, the results show that wild-type and OmpT-G306A in the presence of BAM show near indistinguishable and rapid reaction rates. This implies efficient folding by BAM, and full protease activity as expected for the wild-type OmpT sample. Interestingly, however, the OmpT-G306P under the same conditions displays a significantly slower trace. This has several possible conclusions: that the OmpT-G306P variant has lower protease activity than the other variants, that catalysis by BAM is slower or to a lower yield.

The presence of any activity in the OmpT variant samples, the high activity seen for OmpT-G306A in the presence of BAM, but particularly the activity observed for OmpT-DUPC samples is surprising as from the SDS-PAGE analysis of the same samples (prior to addition of LPS and fluoropeptide) no folded band is observed for OmpT-G306P or OmpT-G306A (Figure 4-32). The protease activity only occurs when OmpT is correctly folded, confirming that variants are folded both in synthetic DUPC LUVs and in liposomes created from *E.coli* polar lipid extract, but do not adopt an SDS-resistant structure in DUPC.

In addition to the OmpT assay, a second assay for determining BAM folding of OMPs utilising SDS-PAGE was developed (see Methods 2.13 and Chapter 5, Section 5.7). This relies on the heat modifiability property of OMPs and the ability to distinguish folded and unfolded populations of protein by SDS-PAGE. It can therefore be applied to a wide range of SDS-resistant OMP sequences. This assay can be used with the full BAM complex in the presence of the chaperone, SurA, and is ideal for monitoring the folding of tOmpA as both the folded and unfolded bands can be clearly seen (Figure 4-38), but less so for OmpT where the unfolded protein band overlaps with the BamB and C subunits on SDS-PAGE. This assay was predominantly used to monitor BAM-mediated folding of tOmpA. The setup of the assay will be discussed further (Section 5.7) however controls demonstrate that only very low folding of tOmpA occurs in empty proteoliposomes lacking the BAM complex, even after significant incubation time (Figure 5-12).

As previously stated, the setup is better suited for tOmpA as the unfolded and folded protein populations can be easily distinguished. In addition to allowing us to better observe folding, this enables us to show that no protein is lost or in an "elusive state" [230] as near constant protein intensity is observed by summing the intensity of folded and unfolded populations. The experiment was carried out with comparison of all β-signal mutants, in OmpT and tOmpA (Figure 4-37). Folding with BAM proteoliposomes was carried out with time-points taken after 1 and 3 hours.

One can observe that wild-type tOmpA is nearly completely folded following 1 hour, and 100% after 3 hours, while the tOmpA-G166A(Ala) variant retains a small population in the unfolded state after 3 hours (Figure 4-37). The tOmpA-RHK mutant is considerably slower still, with less than 50% of protein obtaining the folded state after 3 hours. All are better, however, than any OmpT variants, including wild-type which appear to demonstrate very low folding yield.
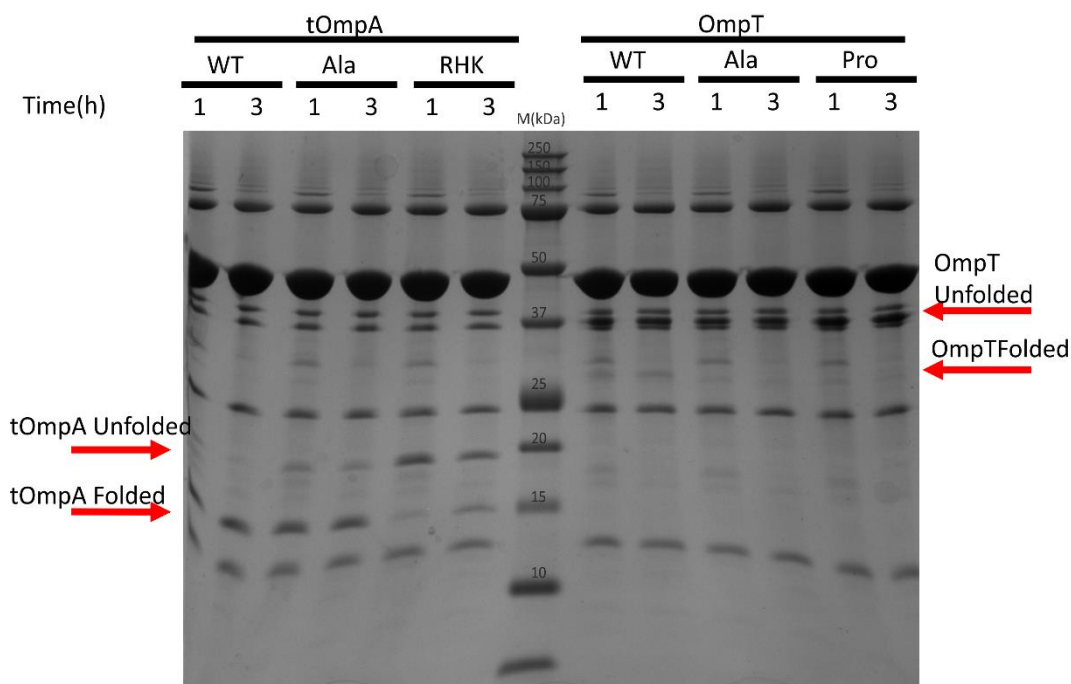
Figure 4-37: SDS-PAGE demonstrating folding of tOmpA/OmpT β-signal variants in BAM proteoliposomes. Samples contain 2µM tOmpA/OmpT, 10µM SurA, 1µM BAM, *E.coli* polar lipid proteoliposomes, TBS pH8. Folding is carried out at 25 ⁰C with time-points taken after 1 or 3 hours, and mixed 1:4 with 6x SDS loading buffer prior to electrophoresis. No samples are boiled to retain the correct folded and unfolded populations.

The assay can be used to measure multiple time-points over the course of the folding reaction, analyse fraction folded/total and obtain a kinetic readout of folding time. The time-course has been optimised for folding of wild-type tOmpA in BAM *E.coli* polar lipid proteoliposomes, as will be discussed in Chapter 5, and involves ten time-points from 2- 120 minutes. This enables us to obtain a reasonable kinetic trace to which a first order exponential can then be fit.

One preliminary experiment was carried out to compare the two tOmpA variants to wild-type using this assay. For all three tOmpA variants in this particular assay the SDS-PAGE showed extra protein bands, not typically seen. Thus, although results were fully analysed, these may not be accurate. A representative gel, of wild-type tOmpA folding in this experiment is shown (Figure 4-38).
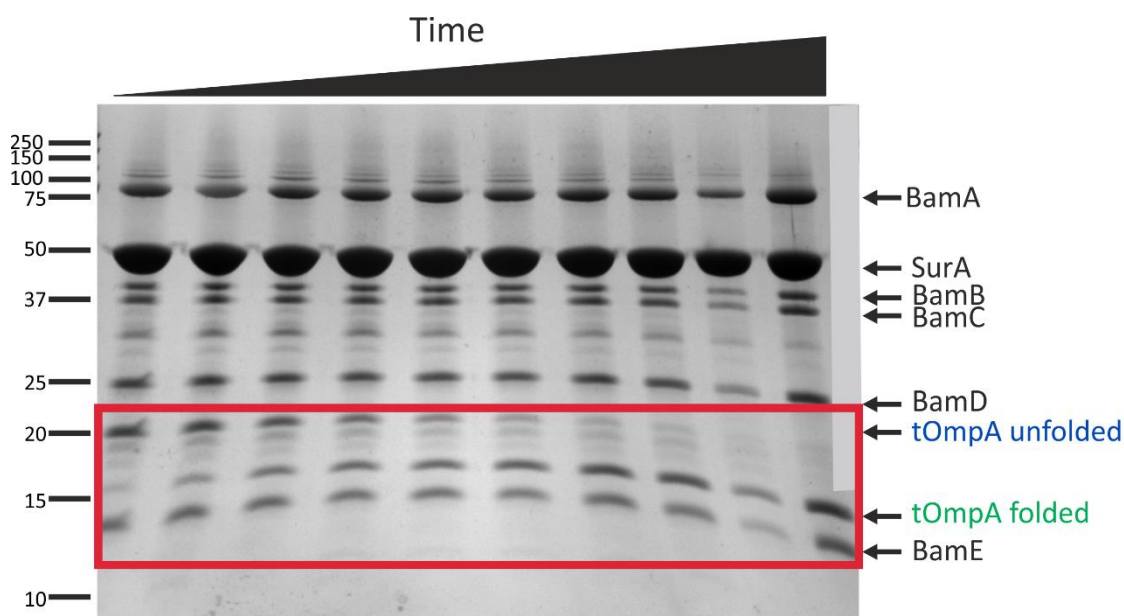
Figure 4-38: Analysis of folding of wild-type tOmpA by BAM proteoliposomes by SDS-PAGE. Samples contain 2µM tOmpA, 10µM SurA, 1µM BAM, *E.coli* polar lipid proteoliposomes, TBS pH8. Folding is carried out at 25 °C with time-points taken at 2, 5, 10, 15, 20, 30, 45, 60, 90 and 120 minutes, and mixed 1:4 with 6x SDS loading buffer prior to electrophoresis. No samples are boiled to retain the correct folded and unfolded populations.

Identical experiments were carried out in parallel for tOmpA-G166A and tOmpA-RHK variants. The results were analysed by gel densitometry, folding yield calculated, plotted and fitted to a single exponential (see Methods Section 2.13). The folding of each variant is shown (Figure 4-39a) and rate constant k_1 for folding transients are compared (Figure 4-39b). Comparison of rate constants can clearly be seen to be problematic, as from the graph both tOmpA wild-type and tOmpA-

G166A variants start with near-identical initial traces but the tOmpA-G166A variant does not reach the same folding yield. Consequently the rate constant appears higher for this variant, and this does not accurately reflect the lower folding achieved. In addition the tOmpA-RHK variant clearly does not fit to a single exponential. The fraction folded at 1 hour is therefore also tabulated, as this time-point provides a good comparison between the folding of different tOmpA variants.

a

b

tOmpA variant	Rate constant	Fraction folded 1 hour (%)
tOmpA WT	1.03 ± 0.06 $\times 10^{-3}$ s^{-1}	94%
tOmpA-G166A	1.78 ± 0.16 $\times 10^{-3}$ s^{-1}	63%
tOmpA-RHK	No fit	11%
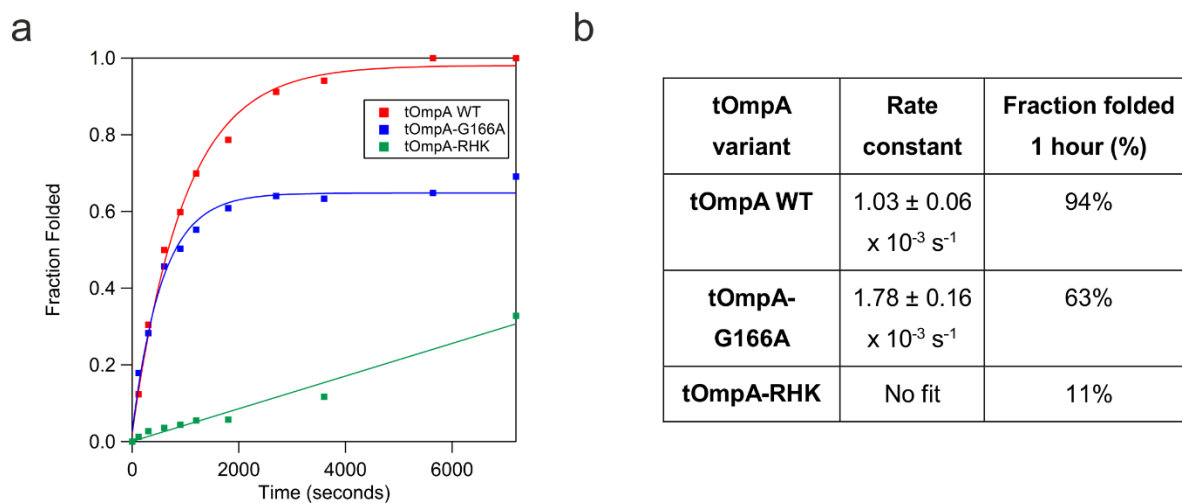
Figure 4-39: Kinetic plot of folding of tOmpA variants (a) and table of analysis (b). Fraction folded at each time-point is plotted and a single exponential fit using the Igor Graphing programme (a). The subsequent rate constant of the fit and the fraction folded at 1 hour time-point are shown (b).

4.5 Discussion

This chapter discusses progress towards investigating the role of lateral gating in BamA-mediated OMP folding and insertion, and the role of the OMP β-signal in BAM-mediated folding. The lateral-gating aspect of the project began with the hypothesis from *in vivo* work, that disulphide-locking BamA in its lateral closed conformation will negatively impact its catalytic ability[199]. Utilising the same cross-link mutant pairs shown to be lethal *in vivo*[199] two X-link mutant proteins (I430C/K808C and G431C/G807C) were expressed, purified and characterised, in addition to the Cys-free BamA variant. The proteins were shown to be folded using synthetic Large Unilamellar Vesicles (LUVs), and cold SDS bandshift. CD spectroscopy and tryptophan fluorescence were employed to demonstrate that these BamA variants have no substantial differences to wild-type in folding capability *in vitro*. Next, the activity of BamA variants in catalysing substrate folding was determined utilising tryptophan fluorescence emission spectroscopy. Systematically moving from LUVs composed of the 11-carbon lipid DUPC, to those containing a proportion of native-like phosphatidylethanolamine (DUPC:DDPE 80:20 molar ratio), to the 14-carbon chain phosphatidylcholine DMPC the ability of BamA variants to catalyse folding relative to wild-type was examined.

The OMP substrate used in these experiments was the β-barrel (residues 1-171) of the 8-stranded β-barrel OmpA (tOmpA). While able to fold in each lipid type used, a significant folding rate enhancement was observed in the presence of BamA, which increases with increasing acyl chain length[241]. It was observed that all BamA variants, including X-link variants were able to accelerate folding in every lipid type used (Figure 4-12, Figure 4-16, Figure 4-20). As any difference in BamA variant catalytic rate enhancement would be small, and therefore best observed in longer chain lipids where folding is slow [72,241] this body of work was concluded by thorough studies of BamA-assisted folding in DMPC lipids.

Experiments were conducted in the 14-carbon chain LUVs as previously, and it was observed that wild-type, Cys-free and X-link BamA variants were all able to accelerate tOmpA folding to the same extent (Figure 4-21). In addition, studies were carried out in the presence of reducing agent (TCEP) and oxidizing agent (CuSO$_4$) with no significant effect on folding rate. The BamA X-link variant was demonstrated to be in a mostly oxidized state, which could be reduced by TCEP

189

as visualized by non-reducing SDS-PAGE (Figure 4-24). Therefore it was concluded that the X-link BamA variant, regardless of oxidation state, was capable of accelerating substrate OMP folding. The data demonstrate that at least for BamA-assisted folding of tOmpA in synthetic LUVs, the lateral gating of the BamA β-barrel is not required.

While this project has been in progress this work has been validated by the findings of another research group, who utilised the BamA-assisted folding of substrate OmpX into DDPC:DDPE (80:20 molar ratio) LUVs[231]. The work utilised three sets of disulphide pairs (Figure 4-40b), located along the β1 : β16 seam, with one pair (G431C/G807C) identical to that used in this chapter. The BamA-assisted folding of OmpX, as measured by heat-modifiability, was first shown for the Cys-free variant of BamA (C690S/C700S) (Figure 4-40a). It was next shown that all disulphide-pair variants, in both reduced and oxidized form, are equally capable of accelerating OmpX folding. Thus, they reach the same conclusion as found here, that regardless of oxidation state, barrel-locked BamA is capable of accelerating substrate folding [231] at least into LUVs *in vitro*.
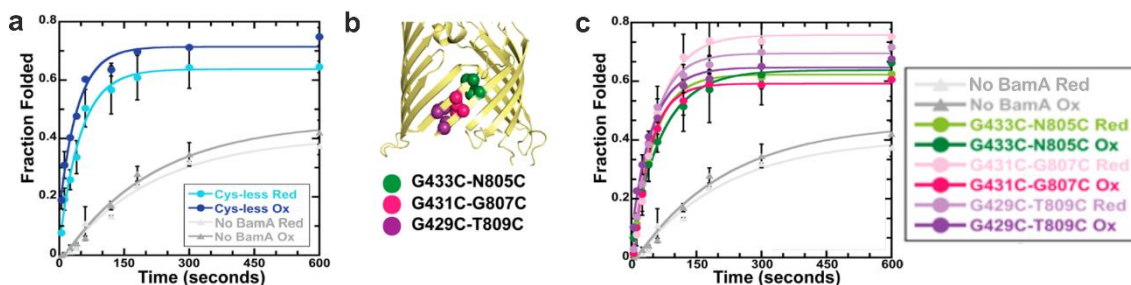
Figure 4-40: Barrel locked BamA assists folding of OmpX[231]. a) Fraction OmpX folded, as measured by heat modifiability, with no BamA (grey lines) and in the presence of Cys-free BamA in reducing (Red) and oxidizing (Ox) conditions b) Representation of the location of disulphide pairs on the BamA β1 and β16 strand seam c) Folding of OmpX in the presence of BamA double-cysteine mutants in reducing (Red) and oxidizing (Ox) conditions. Figure adapted from Doerner *et al.,* 2017 [231].

The second section of work in this chapter focussed on the β-signal and its importance for folding catalysed by BamA or the BAM complex. Systematic folding studies were carried out comparing wild-type tOmpA and tOmpA-RHK in which three residues on the terminal strand are mutated to more closely resemble that of neisserial OMPs. These studies, in DLPC and DMPC LUVs demonstrated that while tOmpA-RHK shows slower intrinsic folding rates than wild-type, the rate

of folding is equally accelerated by wild-type BamA, but not by BamA X-link (Figure 4-26; Figure 4-27). These novel findings are interesting on three counts. Firstly, like the neisserial signal (RHK), the tOmpA residues replaced (SYR) possess a positively charged residue in the +2 position (R170) (Figure 4-2). Contrary to a previous hypothesis that the charged residue may cause incompatibility between *E.coli* and *Neisseria* β-signals[211] it is likely that the distinctive Histidine, found only in neisserial OMPs is responsible for any altered folding[286]. Secondly, while tOmpA-RHK folds more slowly than tOmpA wild-type, the fold-change between them (~1.6x) remains the same in wild-type BamA-catalysed folding (Figure 4-26, Figure 4-27). This implies that while BamA is not able to compensate for the slower folding of tOmpA-RHK, the catalytic rate enhancement is equal. Lastly, it is interesting that the X-link variant does not equally accelerate wild-type and RHK tOmpA folding. The X-link BamA variant shows the same catalytic activity as wild-type BamA when folding wild-type tOmpA in DMPC (Figure 4-21), supporting the hypothesis that BamA acts as a membrane disruptase, rather than a specific recognition partner in this setup. However, the differential activity of X-link BamA with respect to tOmpA-RHK implies that while X-link BamA is a sufficient catalyst in the case of wild-type tOmpA, acting perhaps as a membrane disruptase, it is insufficient for the impaired tOmpA-RHK. This suggests that for BamA-mediated folding of tOmpA in the absence of an appropriate β-signal, such as in the tOmpA-RHK variant, perhaps BamA catalysis must play a more active role. An increased importance for BamA dynamics in this case would explain the slower folding of tOmpA-RHK by X-link BamA compared to wild-type BamA. Further experiments remain to be done to unravel these interconnected models of Bam-assisted substrate folding. Current results cannot support or refute the hypothesis of species-specificity as in these conditions BamA appears to show no specific recognition of substrate, acting primarily as a membrane disruptase. Perhaps by further study using the BAM complex, where substrate folding is more specifically catalysed, one can more thoroughly probe recognition by *E.coli* BamA of a hybrid tOmpA substrate.

Other experiments on the OMP β-signal involved mutation of the conserved Gly in the β-signal of OmpT and tOmpA. These results were surprising, as in OmpT the effects were drastic. These experiments demonstrated that the mutation of glycine 166 to alanine in tOmpA (G166A) resulted in a protein largely

191

indistinguishable from wild-type, with similar folding in DUPC liposomes as characterised by bandshift, fluorescence emission spectra and CD. From preliminary experiments, however, the tOmpA-G166A variant demonstrated impaired folding by the BAM complex (Figure 4-38, Figure 4-39). In addition to confirming this slower rate, other studies remain to be done with this variant. Firstly, it would be informative to examine tOmpA-G166A folding in DMPC liposomes and determine, as with tOmpA-RHK, whether slower folding was seen, and how this was accelerated by both wild-type and X-link BamA. Secondly, a more thorough study would involve sequential mutations along the β-signal. This would help deconstruct the role of the β-signal in intrinsic and BamA-catalysed folding.

In OmpT, the results of mutating the conserved Gly were striking. While folding of the two variants (OmpT-G306A and OmpT-G306P) into DUPC LUVs is comparable to wild-type OmpT as assessed by fluorescence emission spectra and far UV CD (Figure 4-33, Figure 4-34), SDS-resistant band shift of OmpT variants was not observed in any folding conditions for DUPC LUVs (Figure 4-32). BAM complex catalysed folding demonstrates a small amount of folding of both variants by SDS PAGE (Figure 4-37) and activity of the OmpT-G306A variant in the protease assay resembles that of wild-type (Figure 4-36). It had been anticipated that mutation of this highly conserved Gly may impact recognition by BamA, but the drastic change, particularly in the inability to form an SDS-resistant folded structure in DUPC, is unprecedented. It appears, from this limited study, that it is OmpT-specific and even the mild mutagenesis of Gly306Ala significantly impacts the folding landscape. As discussed, this Gly is conserved across Proteobacteria. It is the amino acid occurring with the highest frequency in that position, for all studied β-signals, across all classes of Proteobacteria (Figure 4-5)[286].

There is one precedent in OMP literature of studies of this Gly residue. In studies of the folding of BamA, mutation of the conserved Gly (G771A), on the strand 14 β-signal did not impact ability to bind BamD (in a prerequisite to folding) but caused no folding detectable by SDS-PAGE[175]. This was attributed in that case to Gly being integral to the structure, in a manner unique to BamA due to internal stabilizing interactions[175]. While not evident in the structure of OmpT: the inability of OmpT-G306A and OmpT-G306P to form SDS-resistant structures suggests

the conserved Gly likely plays an important structural role. However, as these variants form β-sheet structure, as analysed by far UV CD and fluorescence emission spectra, they are perhaps trapped in a folding intermediate while the conserved Glycine is crucial to formation of the final folded barrel. Further studies on this would again preferably include alanine scanning of the entire terminal strand of OmpT, a more thorough investigation into the altered folding and SDS-resistance properties and on how the variants are catalysed by BAM.

Altogether the results presented in this chapter shed light on the hypotheses of lateral gating and OMP β-signal but demonstrate that while BamA-assisted substrate folding can elucidate a great deal on the interactions between protein, lipid and substrate these may not represent the same interactions seen *in vivo.* For BamA lateral gating for example, while the X-link examined is lethal *in vivo* and impairs activity in the BAM complex, it shows no alteration to catalysis of wild-type tOmpA folding in DMPC. In the following chapter, studies will move away from isolated BamA to examining the effect of lateral gating and other aspects of BamA dynamics on BAM complex activity *in vitro* utilising two complementary activity assays.

5 Results Chapter 3: Dynamics of the BAM complex

5.1 Introduction

As previously discussed, a key aim throughout the project was to determine the extent to which the lateral opening of BamA and the dynamics of its β-barrel are essential for its catalytic function. Having shown that lateral opening was not necessary for BamA catalysis of tOmpA folding into DMPC liposomes (4.2.5), it was desirable to move to the full complex and more native-like lipids. Following successful purification of the wild-type BAM complex (3.2.1), this could now be undertaken. Despite the demonstration that cysteine cross-links constraining the BamA barrel lateral gate or lid are lethal *in vivo*[199], their effect on BAM activity has never been examined *in vitro*. Here I use two assays and two substrates to begin to unravel this fundamental question.

In order to examine the role of BamA dynamics, a series of variants were created (Figure 5-1). Initially, the same Lateral-lock variant used in BamA alone (I430C/K808C) and the cysteine-free control were generated and studied in the context of the full BAM complex. It was also desirable to study a different aspect of the dynamics of BamA: the mobile loop 6 thought to be important for capping the BamA pore. Loop 6, at the top of the BamA barrel, is highly conserved, is thought to be important for the folding of BamA and of substrate proteins[338,339] and has been detected in differing conformations[277]. Most significantly, however, this long extracellular loop closes BamA on the extracellular side[11] and a cysteine pair that would disulphide-lock the loop to the top of strand 1, over the pore (E435C/S665C) has also been shown to be lethal *in vivo*[199]. This same "Lid-lock" variant was therefore created for these studies. Subsequently, it was of interest to further constrain the dynamics of BamA and mutations were made to engineer the Lateral-lock (I430C/K808C) and Lid-lock (E435C/S665C) cysteine pairs into the same protein. This was named "Double-lock". A final Lateral-lock variant was also added ('Lateral-lock2': G433C/N805C). This was attempted as an alternative to Lateral-lock1 as in the case of Lateral-lock2 the disulphide formed would theoretically be in the lumen of the BamA barrel, unlike in Lateral-lock1 where it may point into the membrane surrounding BamA[199](Figure 5-1a,b). This, as with all the other disulphide pairs, had been shown to be lethal *in vivo*[199] and the Double-lock was therefore the only entirely novel variant.

194
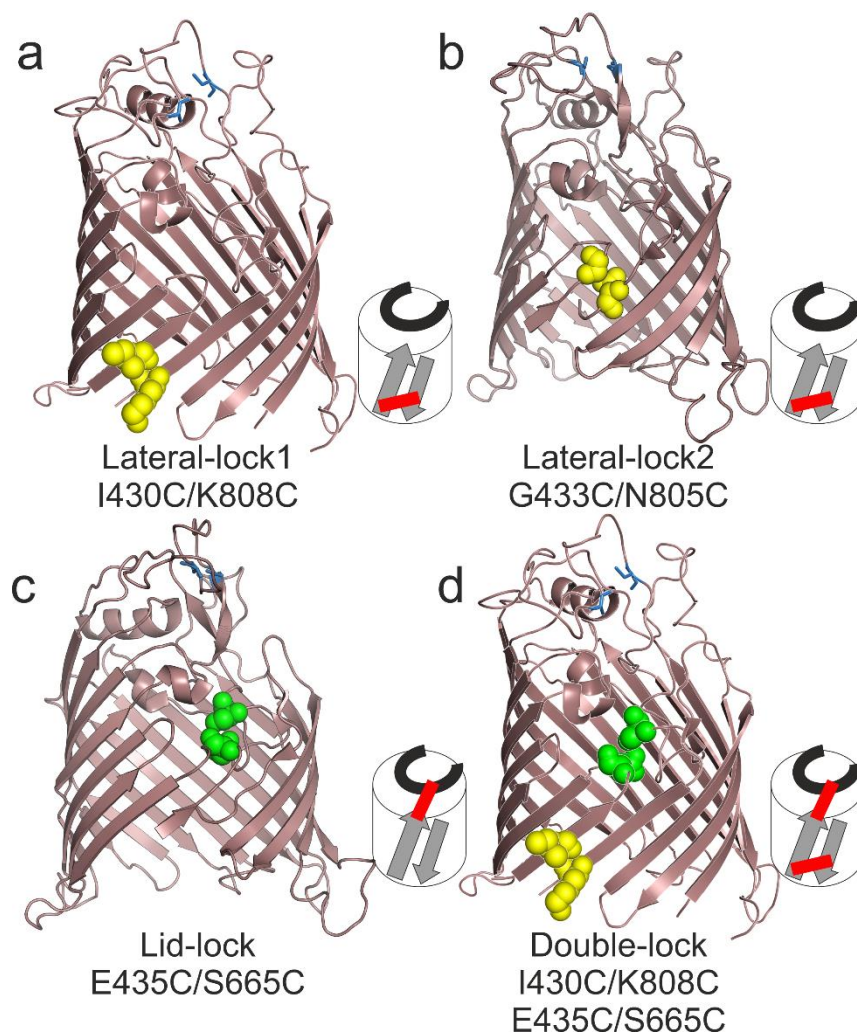
Figure 5-1: Depiction of four disulphide-lock variants in BamA. Positions of all the disulphide-lock pair variants created on the BamA barrel, together with a schematic for each. The two wild-type cysteines mutated to serine are indicated in blue sticks (C690/C700). Lateral-lock mutations are indicated by yellow spheres. Cross-linking across the proposed exit pore of the BamA barrel creates the Lid-lock variant (c), with mutated residues indicated in green. The Double-lock variant (d) is created by the double-cysteine pairs of both Lateral-lock1 and Lid-lock. Images are created in Pymol with structure 4N75[340] used for (a) and (d) and 5AYW[209] for (b) and (c).

5.2 Purification of BAM complex variants

BAM complex variants were created using the wild-type pTrc99a BAM complex plasmid with site-directed mutagenesis to remove the two wild-type cysteines of BamA (C690S/C700S) and sequential mutagenesis to introduce each new cysteine. Details of the primers used and properties of proteins created can be found in Methods (Table 2-1 and Table 2-3). The optimized protocol for BAM

195

preparation using the detergent DDM was then applied to preparation of all the protein variants (Figure 5-2). A good yield and pure complex was obtained for all variants; the nomenclature given to each protein and yield following successful purification in DDM is given below (Table 5-1).
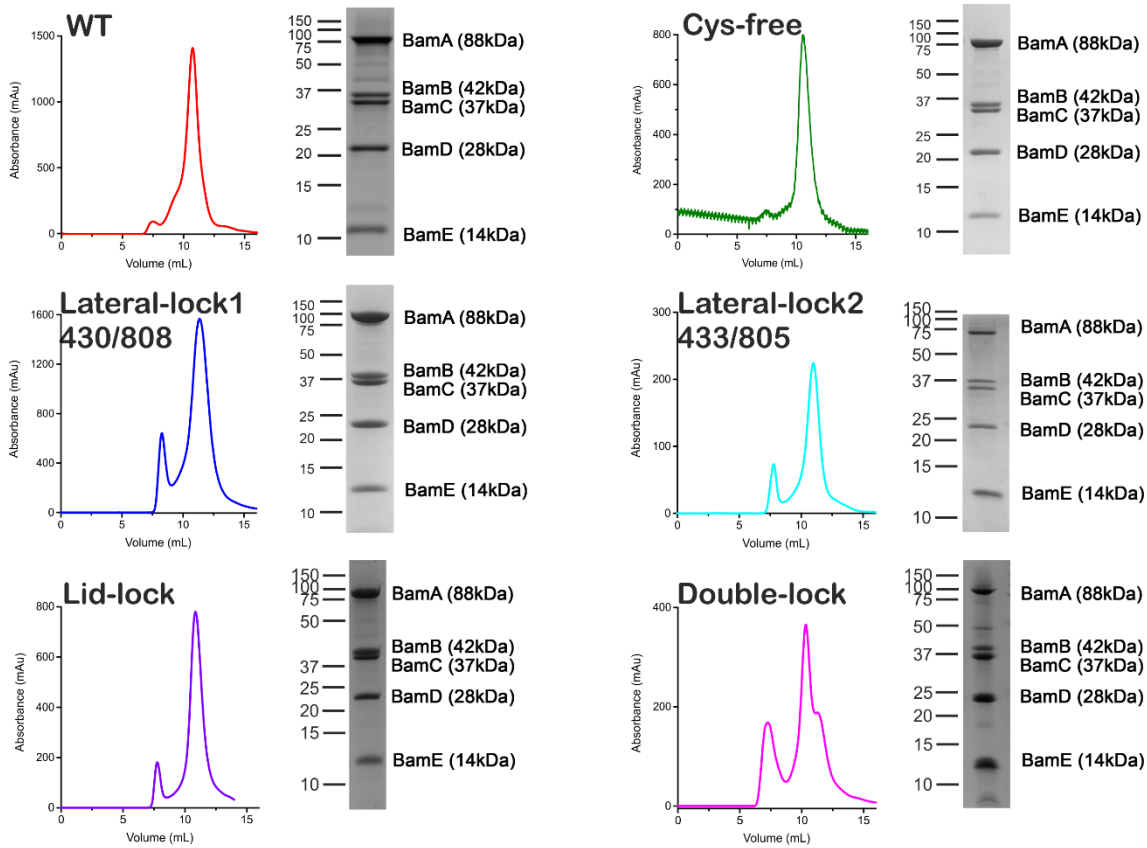
Figure 5-2: Size-exclusion chromatography and SDS-PAGE for purification of all BAM complex variants. Shown is an example trace for elution from Superdex S200, 10/300 GL column for each variant and SDS-PAGE analysis of a central fraction of the principal peak. SEC was performed with TBS containing 0.05 % *(w/v)* DDM.

Name	Position and identity of substitutions	Yield (mg/L grow)
Wild-type	-	2.1*
Cys-free	C690S/C700S	1.9
Lateral-lock1	C690S/C700S/**I430C/K808C**	1.8*
Lateral-lock2	C690S/C700S/**G433C/N805C**	1.8
Lid-lock	C690S/C700S/**E435C/S665C**	1.9
Double mutant	C690S/C700S/**I430C/E435C/S665C/K808C**	1.4

Table 5-1: Nomenclature, mutagenesis and final yield of BAM complex proteins. The yield is calculated as total pure protein per litre of bacterial culture. An asterisk (*) denotes proteins for which preparation was carried out more than once, and the average yield is given. The mutagenesis to introduce disulphide pairs is indicated in bold.

5.3 Reconstitution of BAM variants

Following optimisation of the protocols for the purification of the wild-type BAM complex (3.2.1) and for reconstitution in proteoliposomes (3.4), the other BAM complex variants were reconstituted using the same method. Following each round of 7-day dialysis, SDS-PAGE was carried out for each BAM variant to verify successful reconstitution and presence of all five proteins (BamABCDE). Additionally a Pierce BCA assay was carried out to determine an accurate concentration of the BAM complex in each proteoliposome batch. Shown is one example of reconstitution in proteoliposomes for each variant (Figure 5-3). The pelleted proteoliposomes display a clear bandshift of BamA upon boiling, utilising the heat modifiability property of OMPs to demonstrate that BamA is correctly folded.
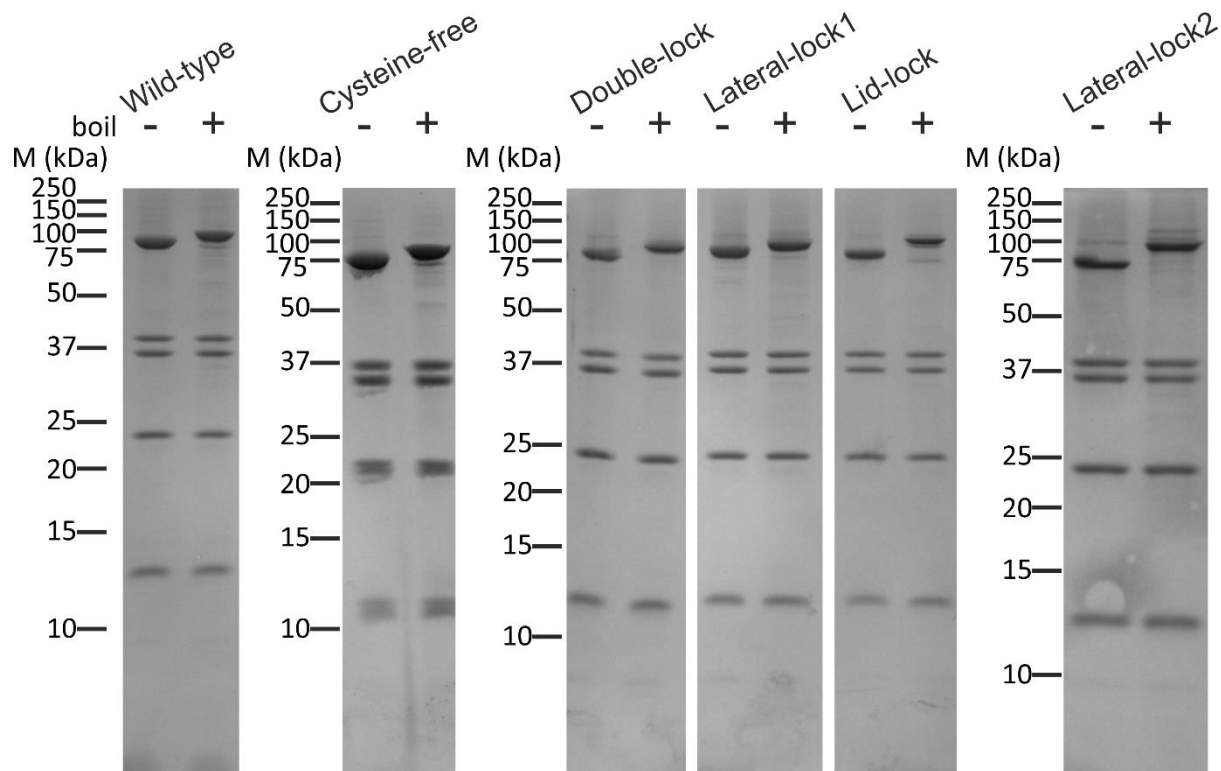
Figure 5-3: BAM variants are intact and fully reconstituted in *E.coli* polar lipid proteoliposomes as verified by SDS PAGE. Proteins in TBS +0.05% (*w/v*) DDM (at 50-70µM) were reconstituted in proteoliposomes (to ~7 µM) by extensive dialysis. Following this, the samples were centrifuged, the pellet resuspended and analysed by electrophoresis with (+) or without (-) boiling. In addition to verifying the presence of the full complex, at 1:1:1:1:1 stoichiometry, this shows the bandshift of BamA upon boiling, demonstrating successful folding into liposomes.

5.4 *In vivo* lethality of disulphide-lock variants

It was *in vivo* assays that initially suggested the importance of the dynamics of BamA, demonstrating lethality when disulphide-lock variants were substituted for wild-type[199]. It was decided to repeat this *in vivo* work to ensure we could reproduce this seminal data and to test the effect of other novel mutations. This utilises JCM166 cells and a pZS21 plasmid, both kind gifts from Professor Tom Silhavy, Princeton University. The pZS21 plasmid has a kanamycin resistance gene and contains HT-BamA under control of an arabinose-inducible pBAD promoter. The JCM166 cells are carbenicillin resistant, and will naturally express wild-type BamA but this is suppressed in the presence of glucose. Growth on

glucose-containing medium is only possible if the BamA on the pZS21 plasmid is functional[25,199]. Plasmids used are summarised in Methods Table 2-1.

Mutagenesis for each disulphide pair had to be done in the pZS21 plasmid by Q5 site-directed mutagenesis; primers used are detailed in Methods Table 2-4. Plasmids were transformed into JCM166 cells, with a pRSFDuet-1 plasmid used as an empty vector control. Outgrowth of cells was carried out in arabinose-containing medium and the transformation mixture was streaked on an arabinose/kanamycin/carbenicillin plate. All transformants are anticipated to grow in these conditions, supplemented by arabinose, and this was the case (Figure 5-4). Colonies were subsequently picked, grown further in LB+arabinose, then pelleted, washed and resuspended to equivalent OD_{600} (see Methods, Section 2.16 for details). Cells of different BamA transformants could then be streaked on an LB agar plate containing glucose and incubated at 37 °C overnight (Figure 5-5).
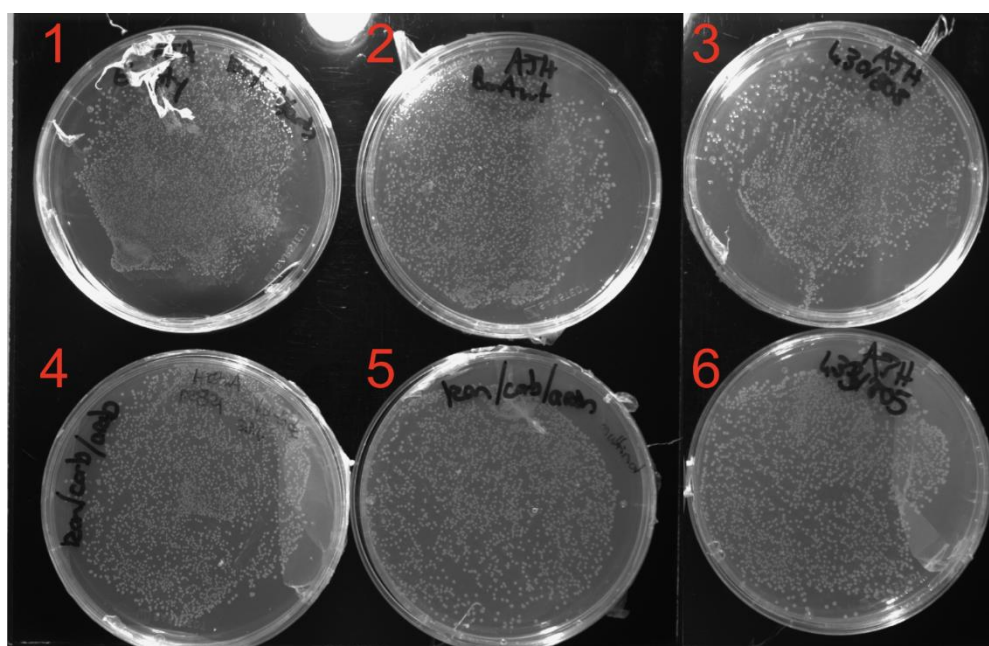
Figure 5-4: All BAM complex variants in JCM166 cells are able to grow when supplemented by arabinose. The plates show clear growth on LB agar + 100 µg/ml carbenicillin + 50 µg/ml kanamycin + 0.2% (*w/v*) arabinose for all conditions. The plates are: 1) Empty pRSF-Duet1 vector, 2-6 pZS21 plasmid with the noted BamA: 2) Wild-type BamA; 3) Lateral-lock1 (430C/808C), 4) Lid-lock (435C/665C), 5) Double-lock, 6) Lateral-lock2 (433C/805C). Note, all disulphide pairs were introduced into a cysteine-free (C690S/C700S) pseudo wild-type. Plasmid containing the cysteine-free is not shown and was grown on arabinose subsequently.

All plasmids, including empty vector, demonstrate good growth in the presence of arabinose (Figure 5-4), while the disulphide-lock variants are not capable of growth in the presence of glucose (Figure 5-5). Four of the lateral-lock cysteine pairs used in the literature were validated here, although only two, Lateral-lock1 (430C/808C) and Lateral-lock2 (433C/805C), were used in these studies. Our findings were consistent with the literature[199], with growth observed for cells transformed with plasmids containing wild-type or cysteine-free BamA and with none of the disulphide-lock pairs or empty vector (Figure 5-5). Literature studies had shown that this effect was specific to formation of the disulphides: single cysteine mutations were non-lethal and the viability of cysteine pair mutants was rescued by the presence of TCEP[199]. These controls were not repeated in this study. As anticipated, the double-lock variant was shown to be lethal; this had not been previously studied.
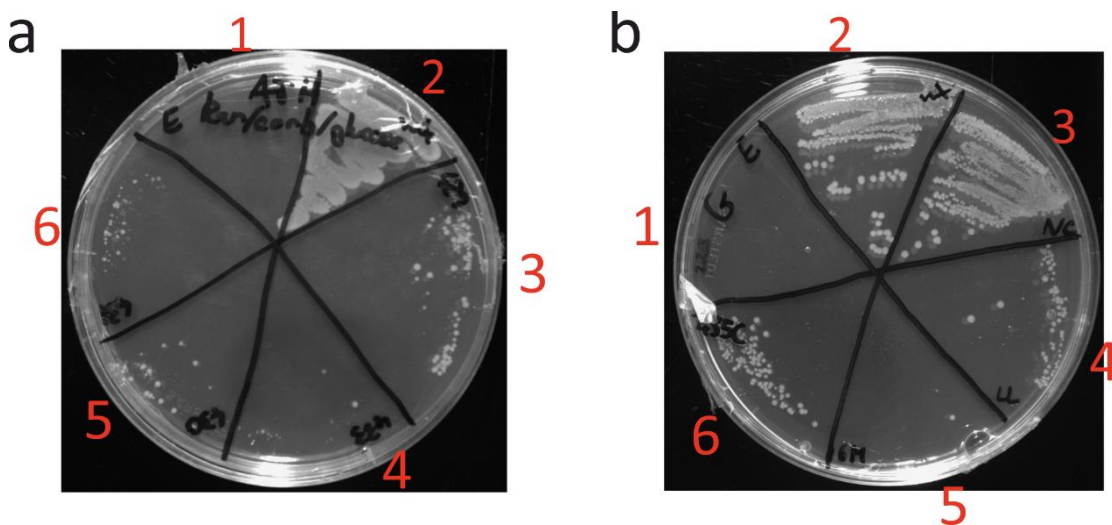
Figure 5-5: Disulphide-lock variants in JCM166 cells are not able to grow in glucose conditions. The plates show growth on LB agar + 100 µg/ml carbenicillin + 50 µg/ml kanamycin + 0.2% (*w/v*) glucose. In both (a) and (b) condition 1 is empty vector, the rest contain BamA on pZS21 as follows: a) 2) Wild-type 3) 429C/809C 4) Lateral-lock2: 433C/805C 5) Lateral-lock1: 430C/808C 6) 431C/807C. b) 2) Wild-type 3) Cysteine-free 4) Lid-lock 5) Double-lock 6) 435C. All cysteine mutations are carried out in the cysteine-free (C690S/C700S) background.

5.5 Assessing activity of BAM complex variants with the OmpT assay

Having purified and reconstituted the BAM complex variants it was possible to assess their activity in OMP folding. This was initially carried out using the OmpT activity assay by comparing wild-type and cysteine-free to Lateral-lock1 and subsequently the Lid-lock variant. The other two protein variants were not generated until later in the project and subsequently not tested in this assay. As previously discussed (Chapter 3, 3.5) the OmpT assay is indirect, but provides a robust and reproducible means to observe BAM complex activity in folding this substrate.

Testing activity was the crux of the creation of the BAM variants. These disulphide-lock variants are all lethal *in vivo*[199] (Figure 5-5). While the lateral-lock mutations in the context of BamA-alone catalysis had no effect on tOmpA folding (Chapter 4, Figure 4-21), the effect in the BAM complex was anticipated to be different. It was unknown whether the disulphide-lock variants would demonstrate any activity at all, or perhaps only slightly altered activity compared to wild-type BAM complex. This was the purpose behind the optimisation of the OmpT assay, as discussed in Chapter 3. It was necessary to find conditions in which changes in BAM activity could be easily observed, while minor alterations in proteoliposomes or technical handling would not hinder the ability to draw conclusions. The conditions optimised in Chapter 3 could now be applied to assaying differences between the BAM complex variants.

It was first demonstrated that wild-type and cysteine-free BAM complex proteoliposomes show nearly identical, fast folding activity in all redox conditions (Figure 5-6a). The Lateral-lock1 variant, however, demonstrated decreased activity relative to cysteine-free and wild-type but this was partially rescued on addition of reducing agent (DTT) to break the disulphide bond (Figure 5-6b). Example traces are shown, and these data were quantified by the t_{50}, for which the average of four replicates is shown (Figure 5-7b). This demonstrates the significant difference between wild-type and Lateral-lock1 catalysis of OmpT folding.
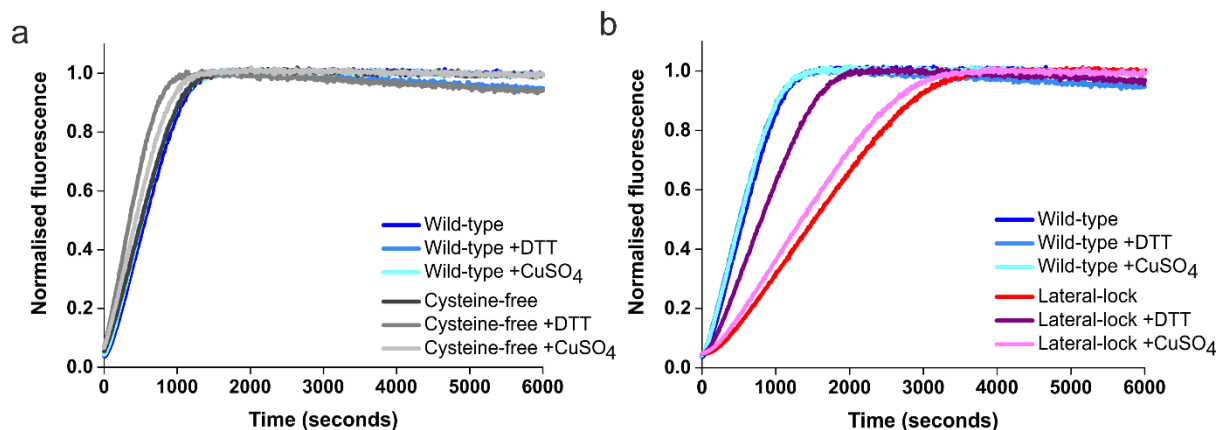
Figure 5-6: OmpT assay shows decreased activity of the Lateral-lock variant. Example kinetic traces of OmpT folding by BAM proteoliposomes comparing: a) wild-type versus cysteine-free, where all traces overlay and b) wild-type and Lateral-lock1 variant in all conditions. All experiments were performed with final concentrations of 0.25 µM BAM proteoliposomes, 5 µM OmpT, 1 mM fluorogenic peptide, 35 µM SurA, with the addition of DTT (50 mM) or $CuSO_4$ (1mM). All experiments were performed in 50 mM glycine-NaOH pH 9.5, 25 °C.

Following this, the activity of the Lid-lock BAM complex variant was assayed. The result was even more striking, with activity more significantly decreased (Figure 5-7a). Reduction of the Lid-lock disulphide bond by DTT also caused an apparent rescue, such that OmpT activity generated is even slightly faster than by wild-type folding. The dramatically slower folding in buffer and oxidizing conditions was consistently observed, and is clearly not only significantly slower than wild-type and cysteine-free BAM protein, but also slower than the Lateral-lock1 variant activity (Figure 5-7b). Altering concentrations of reducing and oxidizing agents were tested but did not show significant difference to the trends observed.
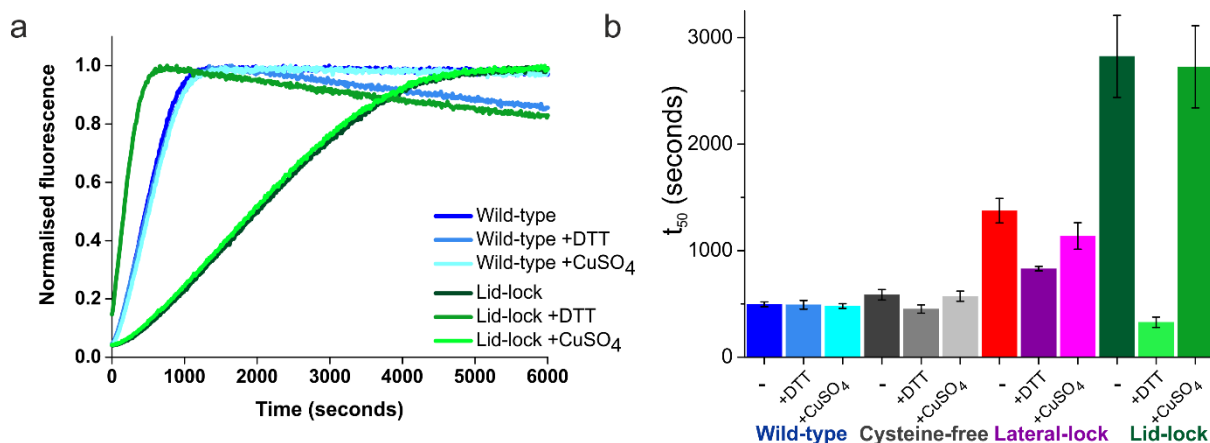
Figure 5-7: Lid-lock variant shows lower activity by the OmpT assay. a) Example kinetic traces of OmpT folding by BAM proteoliposomes, comparing wild-type and Lid-lock variant in all conditions. All experiments were performed with final concentrations of 0.25 µM BAM proteoliposomes, 5 µM OmpT, 1 mM fluorogenic peptide, 35 µM SurA, with the addition of DTT (50 mM) or $CuSO_4$ (1mM). All experiments were performed in 50 mM glycine-NaOH pH 9.5, 25 °C. b) Bar chart for the average half-time of folding reactions with error bars showing standard error of the mean across a minimum of four repeats.

5.6 Investigating the redox status of disulphide cross-links

In order to interpret these results it is necessary to ascertain the redox states of the proteins. As all the cross-linked variants displayed some activity, as opposed to no activity anticipated from their lethality (Figure 5-5)[199] it is unclear whether this is due to partial disulphide formation or a partial decrease in activity upon full cross-link formation. To answer this question it was intended to resolve and view the oxidized and reduced populations of protein by SDS-PAGE. This would also allow quantification of the extent of oxidation. This, however, was not straightforward.

Optimization of the method was carried out on Lateral-lock1, initially using DTT and $CuSO_4$ as used in the OmpT activity assays. BioRad 4-20% acrylamide (*w/v*) gradient gels, as had been used in publications showing the redox state of BamA in DMPC[231] were first used. In addition, another larger gradient gel (4-20% (*w/v*) Novex gel) was also tested. Neither demonstrated noticeably different migration of BamA in reduced or oxidized conditions (Appendix1, Figure A1-1-2). The next gel type assayed was a homemade Tris-Glycine 5% (*w/v*) acrylamide gel, previously used to show the formation of the same disulphides studied here in the *in vivo* experiments[199] (see Methods 2.6.3 for details). Separation of reduced

and oxidized forms of BamA was possible, revealing that Lateral-lock1 BAM appeared incapable of complete oxidation (Figure 5-8).
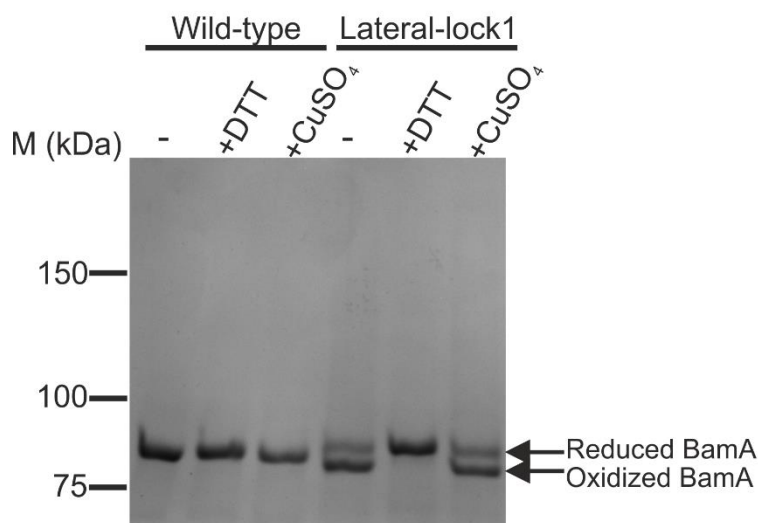
Figure 5-8: SDS-PAGE for redox state of wild-type and Lateral-lock1 BAM complex. Proteoliposomes at 2 µM in TBS pH 8 were incubated with TBS (-), DTT (25 mM) or $CuSO_4$ (1 mM) for 1 hour at room temperature. Samples were mixed with 6x SDS loading buffer and boiled for 30 minutes. The samples were run on a 5% (*w/v*) acrylamide Tris-Glycine gel with MOPS buffer at 30 mA, 180 minutes, 4ºC.

In an attempt to drive oxidation to completion multiple different oxidizing agents were tested, at varying concentrations, in both protein solution (in TBS+ 0.05% (*w/v*) DDM) and reconstituted proteoliposomes, for longer incubations and at higher temperatures (Appendix 1, Figure A1-3-Figure A1-4). None of these alterations appeared to impact the relative populations of reduced and oxidized Lateral-lock1 BamA observed. The oxidizing agent was switched from $CuSO_4$ to diamide at this point, as this is commonly used in experiments requiring cell membrane permeation[341,342]. It appeared that a lower concentration was showing the same oxidative potential. It was also easily soluble in the TBS pH 8 buffer used and did not significantly alter pH. It was noted that the Lid-lock variant showed a fully oxidized population in the presence of oxidizing agent (Appendix1, Figure A1-3). It was hypothesised that full oxidation could not be achieved for Lateral-Lock1 due to the position of the disulphide bond, facing into the membrane surrounding the barrel (Figure 5-1)[199]. Previous *in vivo* work demonstrated a greater extent of oxidation for all disulphides than seen here, and notably marginally higher for those directed towards the lumen of BamA relative to those facing the membrane[199]. Consequently a Lateral-lock2 variant (433/805)

204

was generated, where the disulphide would point into the lumen of the barrel and perhaps be easier to oxidize. The Lid-lock variant is clearly capable of full reduction and oxidation, migrating as a single band reproducibly, with distinct mobility under oxidizing and reducing conditions (Figure 5-9). However Lateral-lock2 was not capable of full oxidation (Figure 5-9). The Double-lock variant shows a more confusing pattern. While capable of full reduction, to a single band, the buffer and +diamide conditions appear to display a mixed population, but with consistent smearing between the bands (Figure 5-9). This suggests formation of one or both of the potential disulphides.
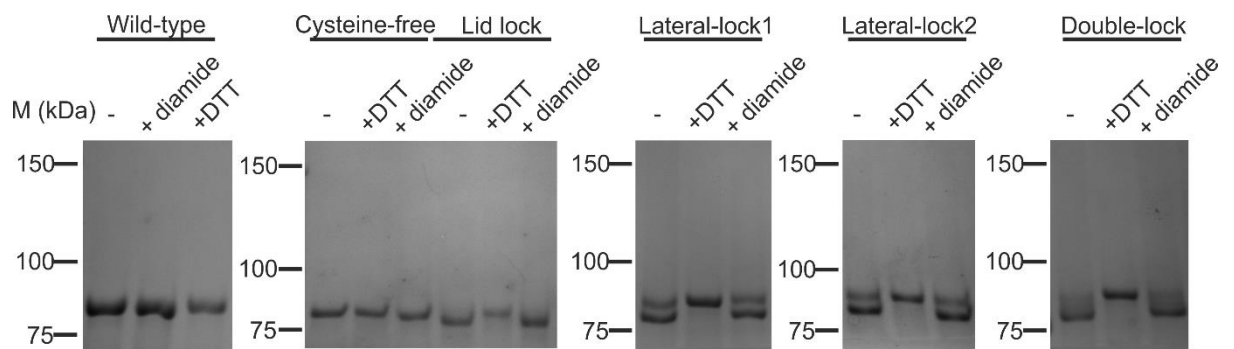
Figure 5-9: Redox SDS-PAGE for all BAM complex variants. BAM proteoliposomes in TBS pH 8 were diluted to 2 µM with the addition of buffer (-), 25 mM DTT or 100 µM diamide. 5% (*w/v*) acrylamide Tris-Glycine gels were used, run with MOPS buffer at 4°C, 3 hours, 30 mA per gel and stained with Instant Blue.

These results inform our understanding of the OmpT assay results. While the activity of the Lateral-lock1 variant may be due to the population of protein that is not fully oxidized, this cannot be true for the Lid-lock BAM variant which is completely oxidized. Additionally, in both cases, reduction with DTT resolves protein to a single, reduced BamA band (Figure 5-9). However in the OmpT assay, the Lid-lock BAM proteoliposomes in reducing conditions demonstrate better than wild-type activity, while the Lateral-lock activity does not appear to fully recover (Figure 5-7b). One potential explanation is that the mutations introduced in the Lid-lock variant intrinsically improve activity while those of the Lateral-lock variant decrease it.

One further assay was carried out to determine whether the protein was recalcitrant to oxidation and to obviate the possibility that one or both of the

sulfhydryls were already oxidized (by forming a disulphide bond with a small molecule for example). Firstly, as it is evident that both lateral-lock variants can be fully reduced (by the appearance of a single higher MW band) it appeared that perhaps by first reducing, then re-oxidizing the protein, it might be possible to reach full oxidation of the protein.

This was attempted using the protein in detergent, fully reducing it and then binding to nickel beads and washing to remove reducing agent, then incubating with oxidizing agent (see Methods 2.6.3.1 for details). Samples pre-experiment (P), following DTT treatment (Reduced:R) and final (F) were mixed with SDS loading buffer and analysed by gel electrophoresis (Figure 5-10). The experiment demonstrates that while the proteins are fully reduced, with a single higher apparent molecular weight band for R sample in all variants, the final sample is once again a mixed population. This is particularly evident for Lateral-lock2, for which all samples: Pre (P), reduced (R), wash (W) and final (F) are shown (Figure 5-10).
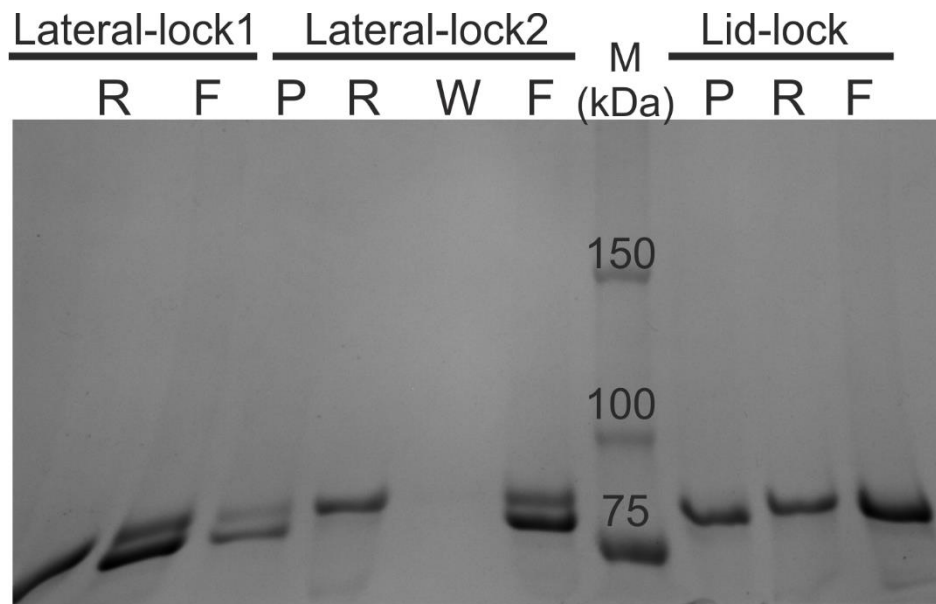
Figure 5-10: SDS-PAGE analysis of "Reduce then Oxidize" for disulphide variants. Protein in TBS+DDM diluted to 4 µM was treated with DTT, incubated with nickel beads and washed and then treated with diamide. Samples are shown for Pre DTT **(P)**, Reduced **(R)**, first Wash **(W)**, and Final **(F)**. Samples were mixed with 6x loading buffer, boiled for 15 minutes and analysed on a 5% (*w/v*) acrylamide Tris-Glycine gel with MOPS buffer at 40 mA, 180 minutes, 4ºC.

206

The samples were also submitted for mass spectrometry analysis. It was hypothesised that a modification on the free cysteine that would impede formation of a disulphide, would be detectable as a secondary population by mass spectrometry. On the contrary, deconvolution of the mass spectrometry of both Lateral-lock proteins in detergent (where a mixed population is observed by gel) showed a single peak for the membrane protein region. It was determined that both lateral-lock BAM complex variants could not be fully oxidized and would remain in a mixed population. The extent of oxidation was consistent across proteoliposome preparations, and could be quantified (Figure 5-11). Analysis of the average fraction oxidized determines that this does not differ greatly between the two lateral-lock variants, or with the addition of (oxidizing agent) diamide.
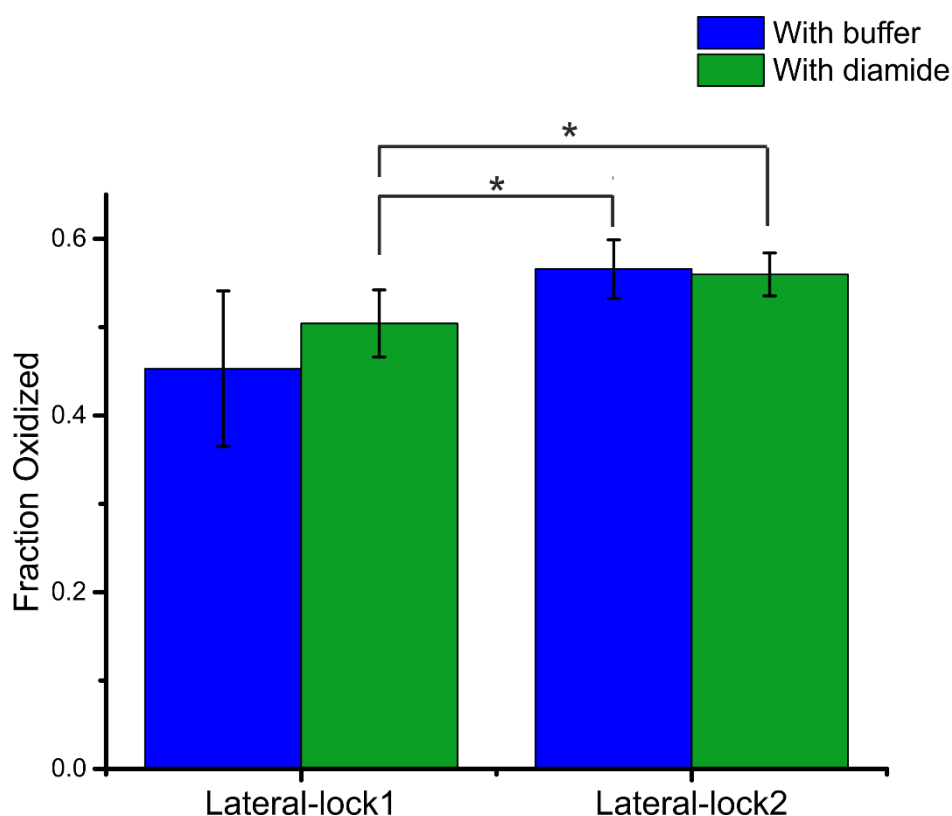
Figure 5-11: Fraction Oxidized for BAM proteoliposomes containing Lateral-lock1 and Lateral-lock2 variants. Analysis is carried out by densitometry using ImageJ. Fraction oxidized is calculated as the ratio between intensity of the oxidized band and the sum of the oxidized and reduced band intensities. Analysis was carried out across 5% (*w/v*) acrylamide redox gels (minimum 3 for every condition) with average and standard deviation shown. The significance of variation between conditions was assessed with two-sample t-tests. * indicates a significant difference with a p-value of <0.05. All other differences are non-significant.

5.7 Assessing activity of BAM complex variants with a novel tOmpA assay

The OmpT enzymatic assay is the most widely used method to assess BAM complex activity *in vitro*[159,189,272,274]. Yet this is an indirect assay, is not without considerable limitations, some of which are discussed (Section 3.5). Orthogonal assays used in the literature include assessing substrate protein folding by SDS-PAGE followed by autoradiography[159,189] or western blot[272,274]. These both exploit the heat modifiability property of OMPs that they will separate according to their folded and unfolded populations on SDS-PAGE. These assays are both indirect, assuming that folded and unfolded populations will be detected equally. While a fair assumption for autoradiography, this is not always the case for western blot, as has been shown for OmpG which exhibits lower detection of the folded form[273]. Detection by an antibody will depend on the peptides to which the antibody has been raised. Controls are necessary to ensure that the region of protein is equally exposed in both folded and unfolded protein conformations, that these migrate into the blotting membrane equally and are detected proportionately by antibody.

Observing the folding of proteins directly by SDS-PAGE, while widely-used for monitoring spontaneous or BamA-assisted OMP folding in liposomes[71,72,241] has not been performed for BAM-assisted OMP folding, likely due to the large number of proteins on the resulting gel and the low concentrations of OMP substrate typically used. Many substrate proteins are unsuitable for such an analysis, overlapping with one or other of the BAM subunits (unfolded OmpT 35 kDa with BamC 37 kDa; OmpA 37 kDa, between BamB 42 kDa and BamC 37 kDa). However, a deletion variant of the widely used substrate protein OmpA that is comprised of just the transmembrane domain (tOmpA) is 18 kDa, folds identically to full-length OmpA[273] and migrates between BamD and BamE in both folded (~15 kDa) and unfolded (~18 kDa) forms. In order to be easily detectable and quantifiable by SDS-PAGE, the concentration of substrate OMP had to be suitably high. After some optimization, Dr Bob Schiffrin (University of Leeds) found that a 2 µM concentration of tOmpA and a 1 µM concentration of BAM provided conditions in which all proteins could be visualized by SDS-PAGE and the relative abundance of tOmpA folded and unfolded populations could be easily

quantified. The concentration of SurA, used to maintain high solubility of tOmpA, was less important, but was maintained at 10 µM, providing a 5-fold excess over substrate. Under these conditions the folding of tOmpA by the BAM complex could be reliably, consistently and quickly monitored. Folding of tOmpA by wild-type BAM complex was complete after ~1 hour, enabling a time course of folding to be constructed by a discontinuous assay. Folding was initiated by mixing the protein components with proteoliposomes and then quenched after each timepoint by addition to SDS loading buffer (see Methods, Section 2.13).

Analysis over longer folding times show that while folding by wild-type or cysteine-free BAM proteoliposomes is complete after ~2 hours, little folding (0-2%) of tOmpA occurs in an equal volume of empty liposomes, in the absence of the BAM complex (Figure 5-12). Additionally, removal of SurA diminishes folding (Figure 5-12).
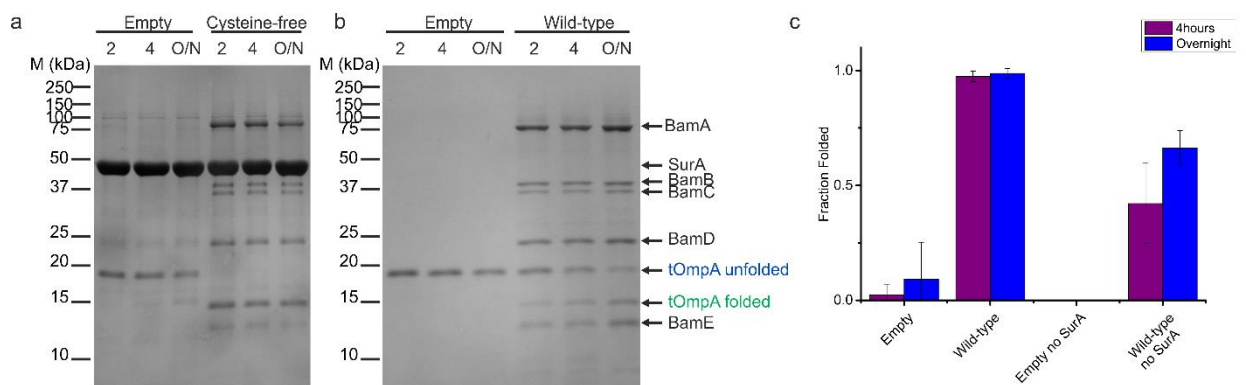
Figure 5-12: Minimal folding is observed in empty liposomes and in the absence of SurA. The assay involves 1 µM BAM proteoliposomes, 2 µM tOmpA, 10 µM SurA, 0.8 M urea, TBS pH 8, 25°C. Experiments were carried out at 25°C and, at the indicated time point, an aliquot of 15 µL was quenched by addition to 5 µL of 6x SDS loading buffer. Controls involved incubation for 2 and 4 hours and overnight (O/N) ~20 hours. Example control SDS-polyacrylamide gels are shown with (a) and without (b) SurA. In (c) average and standard deviation of at least two replicates is shown. No folded tOmpA band is seen for empty liposomes in the absence of SurA.

This assay therefore is robust and was next used to determine changes in catalytic activity for variants of the BAM complex. Two sub-reactions were set up: BAM proteoliposomes were diluted to 4 µM (2x final concentration) in TBS pH 8 containing redox agents where necessary (also at 2x final concentration). The second subreaction comprised of SurA and tOmpA at 2x final concentration. The folding reaction was initiated by addition of equal volume of the SurA-tOmpA mix

to the BAM proteoliposomes (see Methods Section 2.13 for details). Following initiation of the folding reaction, the sample was maintained at 25 °C and folding of the samples was quenched at the appropriate time-points by addition of 15 µL sample to 5 µL 6x SDS-loading buffer. Samples were maintained at 25 ºC until all time-points had been taken and were immediately loaded on 15% (*w/v*) acrylamide Tris-Tricine buffered SDS-PAGE at room temperature, without boiling. An example SDS-PAGE of the folding reaction is shown (Figure 5-13). Ten time points were taken, between 2 minutes and 2 hours.
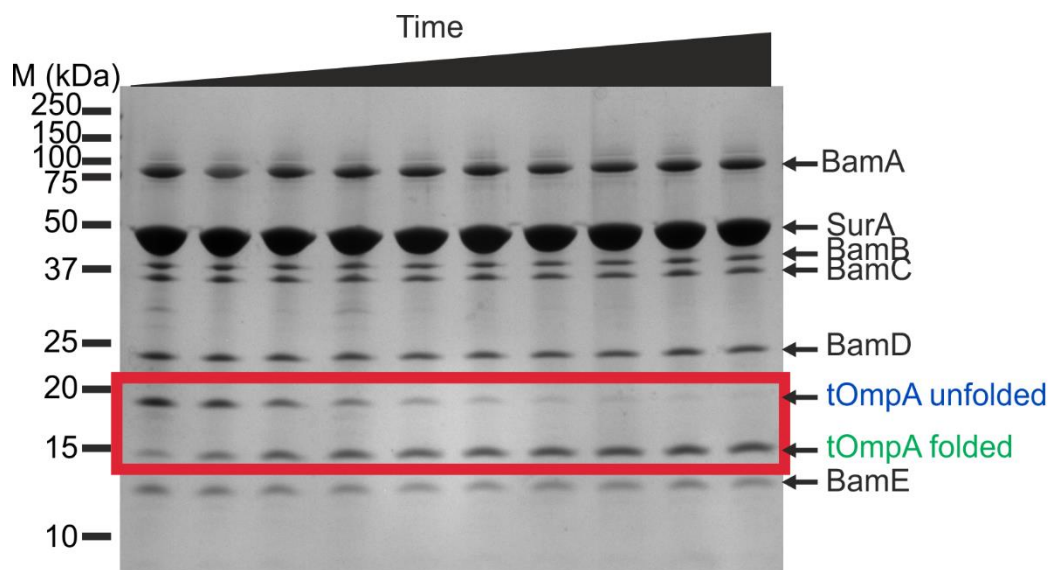
Figure 5-13: BAM-catalysed folding of substrate can be measured by SDS-PAGE. Example SDS-polyacrylamide gel demonstrating the analysis of the folding of OMP substrate tOmpA by BAM proteoliposomes in the presence of SurA. The assay involves 1 µM BAM proteoliposomes, 2 µM tOmpA, 10 µM SurA, 0.8 M urea, 20 mM Tris pH 8 150 mM NaCl, 25°C. Experiments were carried out at 25°C and at the indicated time point an aliquot of 15 µL was quenched by addition to 5 µL of 6x SDS loading buffer.

The assay was carried out for wild-type, cysteine-free and all four disulphide-lock BAM complex variants in buffer, oxidizing and reduced conditions, see Appendix 2 for an example gel in each condition. Folding was quantified by densitometry using ImageJ, of every lane within a gel using:

Equation 5-1: $Fraction\ folded = \frac{folded\ band\ intensity}{(folded+unfolded)band\ intensities}$.

It has been observed previously that tOmpA populates intermediate 'elusive' states during folding[230]. By contrast, we observed that the total band intensity (folded +unfolded) remained relatively constant across the folding time course

210

ruling out population of such species under the conditions employed here. Increase in folded band intensity was observed with a corresponding decrease in unfolded band intensity. This justifies quantitation of fraction folded using Equation 5-1.

The result of the experiment comparing buffer conditions for the proteoliposome variants is immediately striking. While wild-type and cysteine-free BAM complex show relatively fast and similar folding rates of tOmpA, all four disulphide-lock variants show similar inhibited activity (Figure 5-14).
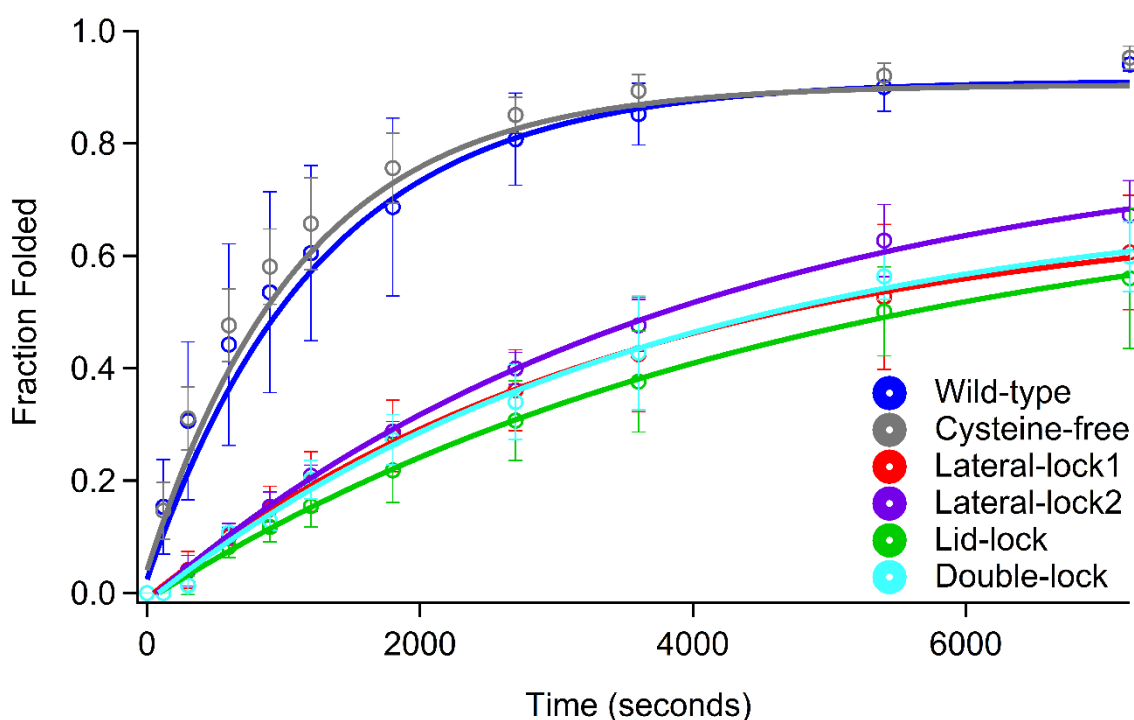
Figure 5-14: All disulphide-locked BAM variants show similarly impaired activity. Average kinetic traces for all BAM variants folding tOmpA with fraction folded over time. Fraction folded for tOmpA is quantified by densitometry using ImageJ, of every lane within a gel using Equation 5-1. SDS-PAGE experiments were repeated a minimum of three times with the average and standard deviation shown and fit to a single exponential function.

It is striking that the variants are able to catalyse folding tOmpA where *in vivo* lethality might predict an absence of activity. It is also notable that all variants show near identical traces in buffer conditions, indicating a consistent residual level of folding in the presence of the BAM complex. Comparison of the rates of BAM-catalysed tOmpA folding in buffer, reduced and oxidised conditions for each variant (Figure 5-15), demonstrates that in all disulphide-lock variants with the

211

exception of Lateral-lock1, folding is rescued to equal or greater than wild-type levels on addition of DTT. Shown are the average traces for folding by each variant, with wild-type shown in each for consistency and clarity (Figure 5-15).
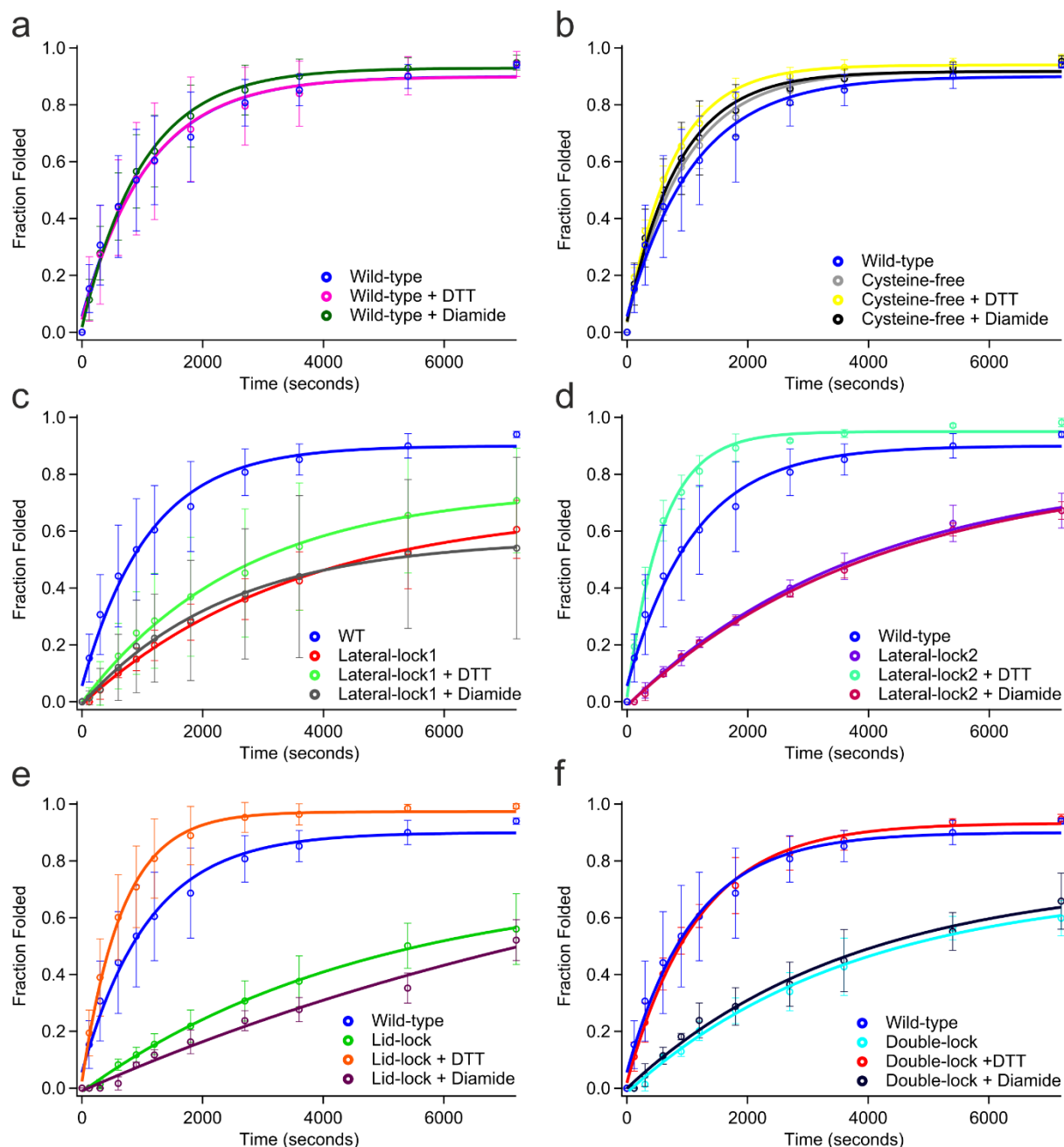
Figure 5-15: Average tOmpA folding by each BAM complex proteoliposomes in all redox conditions. Averaged kinetic traces for the folding of tOmpA catalysed by each BAM variant in buffer, reduced and oxidized conditions. SDS-PAGE experiments were repeated a minimum of three times, and quantified by Equation 5-1 with the average and standard deviation shown. Lid-lock+Diamide is only 2 repeats. Experiments were performed with the addition of 25 mM DTT or 100 µM diamide where indicated. All other conditions were identical to those in Figure 5-14.

In every case the average trace is fit to a single exponential from which a rate constant may be extracted. It is possible to compare across the wide range of variants and conditions by comparison of the exponential rate constants, extent of folding at a single time-point (eg. 1 hour) or t_{50}. The 1 hour time-point is used as at this point wild-type and cysteine-free BAM complex variants show nearly complete (>84%) folding of substrate, whereas all disulphide-lock variants show ~50% folding in buffer conditions. The comparison shows that in wild-type and cysteine-free BAM proteoliposomes the addition of redox agents does not alter activity. In all disulphide-lock variants the addition of reducing agent increases the extent of folding observed (Figure 5-16). This indicates a strong trend for rescue of the variants upon reducing agent breaking the disulphide bond. In the case of Lateral-lock2, Lid-lock and Double-lock the variants are fully active, to greater than wild-type levels, when reduced (Figure 5-16). This is not the case for Lateral-lock1, which shows only partial increase in activity. This is unexpected considering the more significant rescue of this variant seen in OmpT folding assays (Figure 5-6b & Figure 5-7b), but also surprising as the Double-lock variant, which shows full rescue, contains the cysteine pair of Lateral-lock1. The evident difference between Lateral-lock1 and Lateral-lock2 may also be affected by the positions of the cysteines, which in Lateral-lock1, pointing into the membrane (Figure 5-1a) may diminish activity. It is significant, however, that for Lateral-lock2, Lid-lock and Double-lock variants the reduced form is fully active.

213
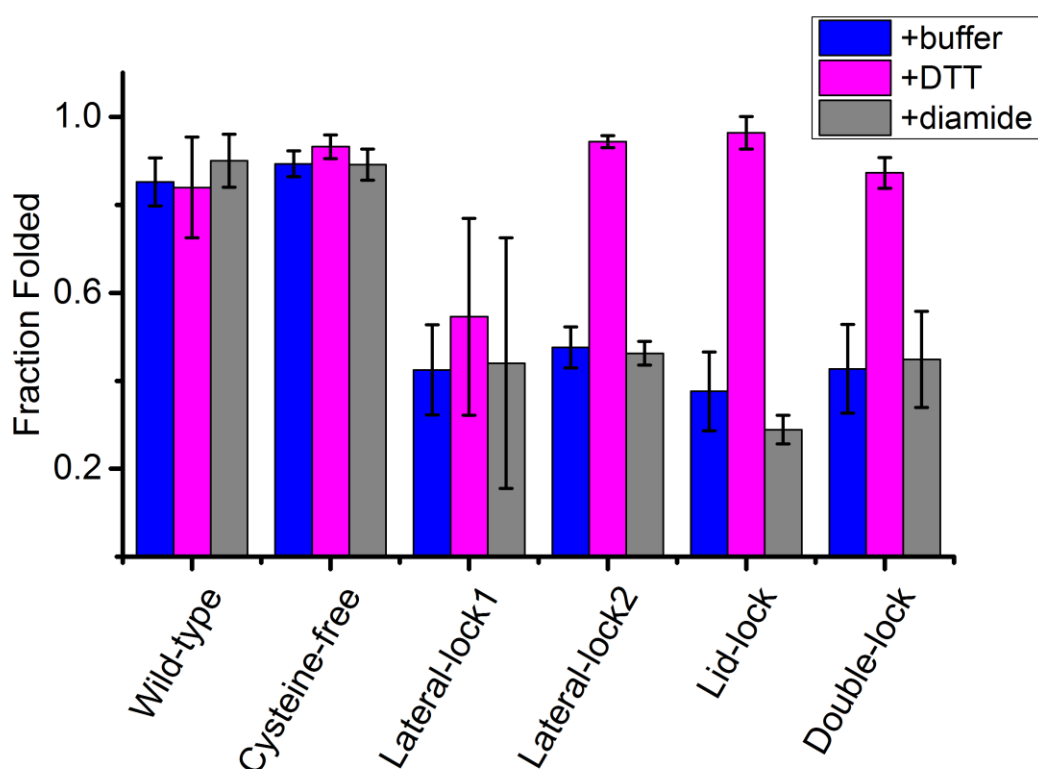
Figure 5-16: All disulphide-lock variants show impaired activity, rescued in the majority of cases by addition of DTT. Comparison of all conditions using the average fraction folded at 1 hour time-point. Shown are the averages and standard deviation of three replicates, with the exception of Lid-lock+diamide which is only 2 repeats.

It was also of interest to quantify folding over longer timescales to determine whether the disulphide-lock variants were capable of folding tOmpA to completion. Folding assays were therefore performed as described previously. The reactions were set to fold, but time-points were taken at 2 and 4 hours and overnight (~20 hours) and analysed on SDS-PAGE with comparison to other variants at long time-points. Example SDS-PAGE are shown in Figure 5-17 and Figure 5-18. This demonstrated that given sufficient time, the variants are able to fold tOmpA to completion (Figure 5-19). This is in contrast to the controls previously shown (Figure 5-12) demonstrating that in empty proteoliposomes only minimal folding was observed overnight.
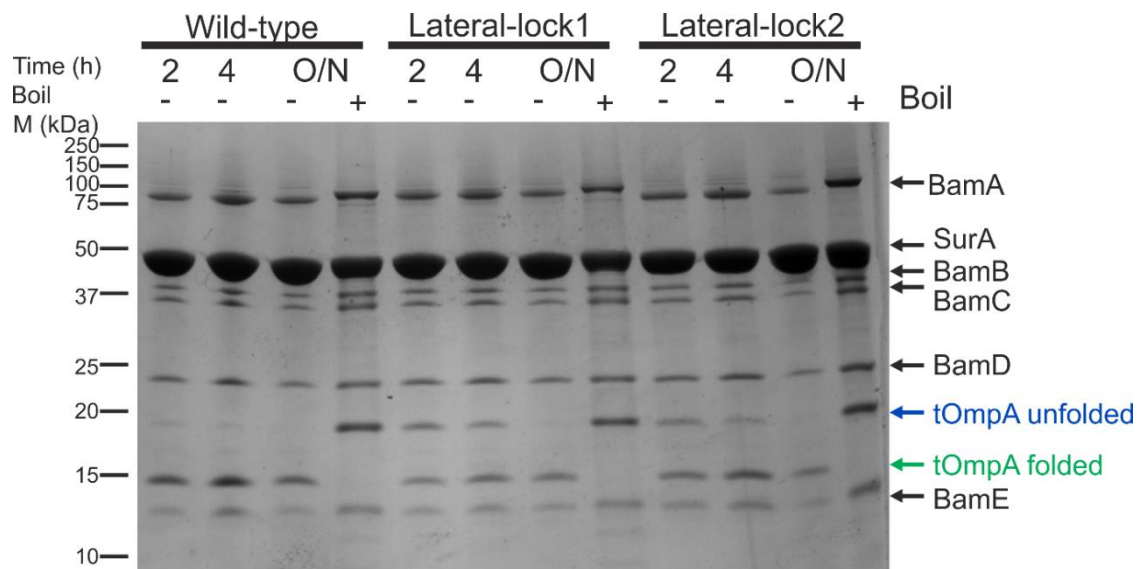
Figure 5-17: Example of SDS-PAGE for longer time-points of folding by wild-type, Lateral-lock1 and Lateral-lock2 BAM proteoliposomes. The same experiment was carried out as previously with time-points taken after 2 and 4 hours and overnight (O/N, ~20 hours). Most samples are shown without boiling (-), but overnight samples are also shown boiled (+) where BamA and tOmpA migrate according to their expected molecular weight.
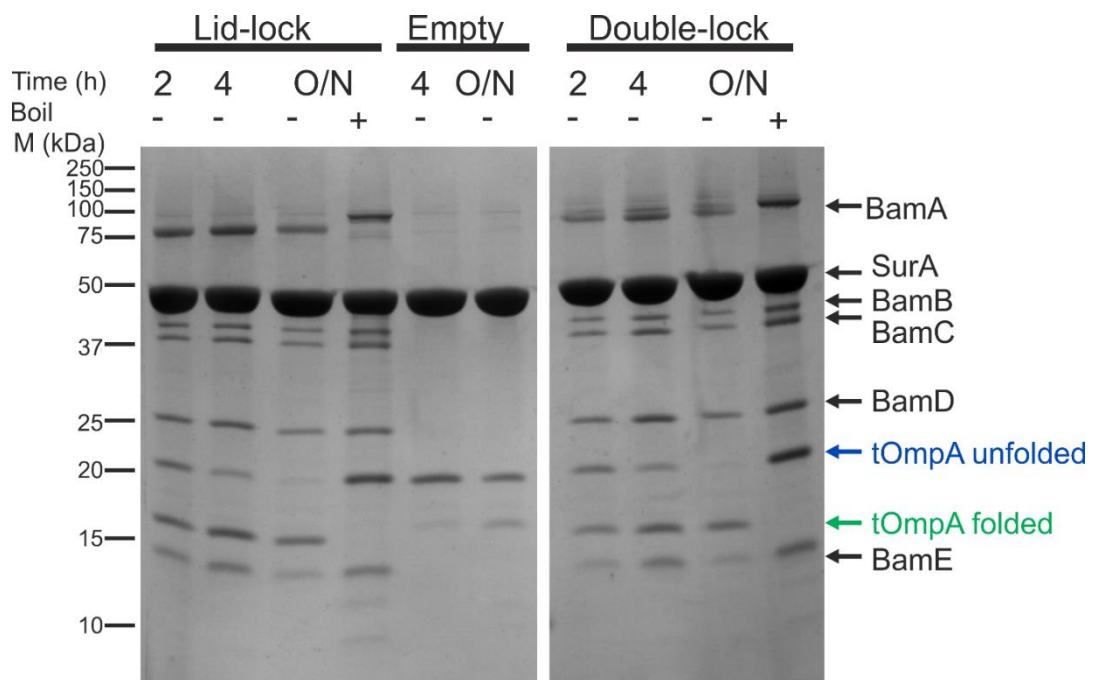
Figure 5-18: Example of SDS-PAGE for longer time-points of folding by Lid-lock and Double-lock BAM proteoliposomes and empty liposomes. The same experiment was carried out as previously with time-points taken after 2 and 4 hours and overnight (O/N, ~20 hours). Most samples are shown without boiling (-), but overnight BAM-folded samples are also shown boiled (+) where BamA and tOmpA migrate according to their expected molecular weight.

215
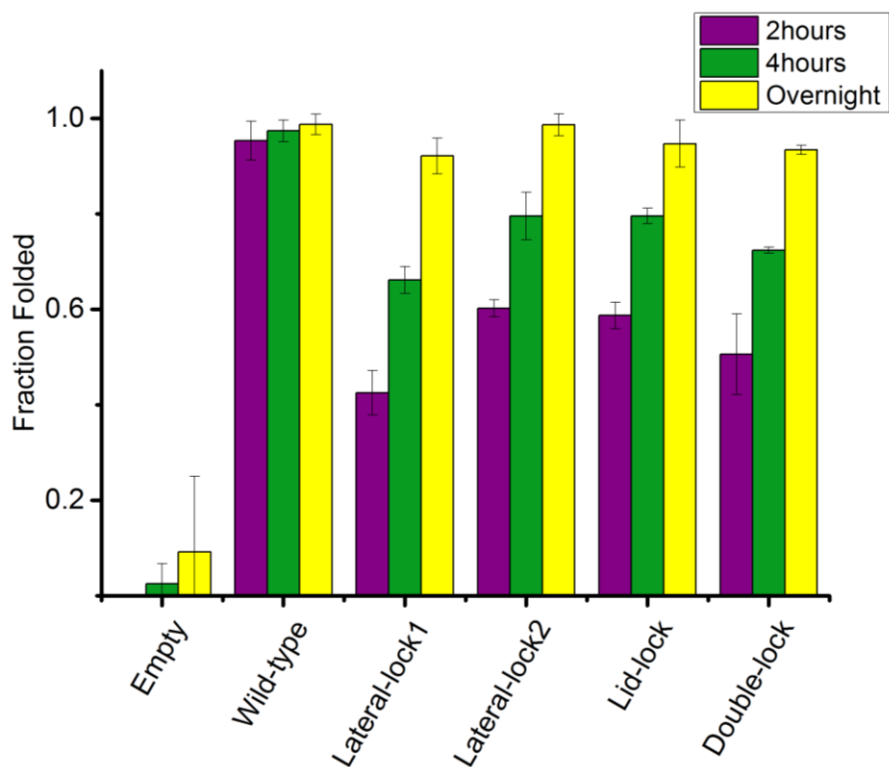
Figure 5-19: Folding with all BAM complex variants eventually reaches completion. The same experiment was carried out as previously with time-points taken after 2, 4 or ~16 hours and quantified according to Equation 5-1. Shown are the averages and standard deviation of a minimum of two repeats.

5.8 Concentration titration of BAM proteoliposomes

In both lateral-lock samples the oxidized population in proteoliposomes is, on average ~50% of the protein sample (Figure 5-11). In addition, both variants show approximately 50% of the activity of wild-type BAM proteoliposomes for folding tOmpA in the same conditions (Figure 5-16). One might therefore deduce that the reduced fraction of the sample (~50%) is contributing to this observed activity (~50%) while the oxidized portion is non-functional.

It was decided to test this hypothesis by carrying out the tOmpA folding assay with a titration of Lateral-lock2 at decreasing concentrations in the presence of DTT. The tOmpA folding reaction was therefore initiated with different concentrations of BAM and the fraction tOmpA folded at the 1 hour time-point was compared. Controls included Lateral-lock2 in the absence of DTT and titration of the concentration of wild-type BAM.

Should the oxidized protein be inactive, then the activity of the 100% concentration of Lateral-lock2 without DTT (Figure 5-20, green bar) would be approximately matched by the 50% concentration of Lateral-lock2+DTT. This folding yield is indicated in Figure 5-20 with a dotted line. Instead, the 50% concentration of Lateral-lock2+ DTT (0.5 µM, indicated with an asterisk) demonstrated a higher fraction folded of tOmpA. Low concentrations of Lateral-lock2 +DTT exhibit greater activity than the Lateral-lock2 without DTT (Figure 5-20, green bar, dotted line). This indicates that the reduced portion of Lateral-lock2 protein is in fact more active and the oxidized form is somehow diminishing that activity.
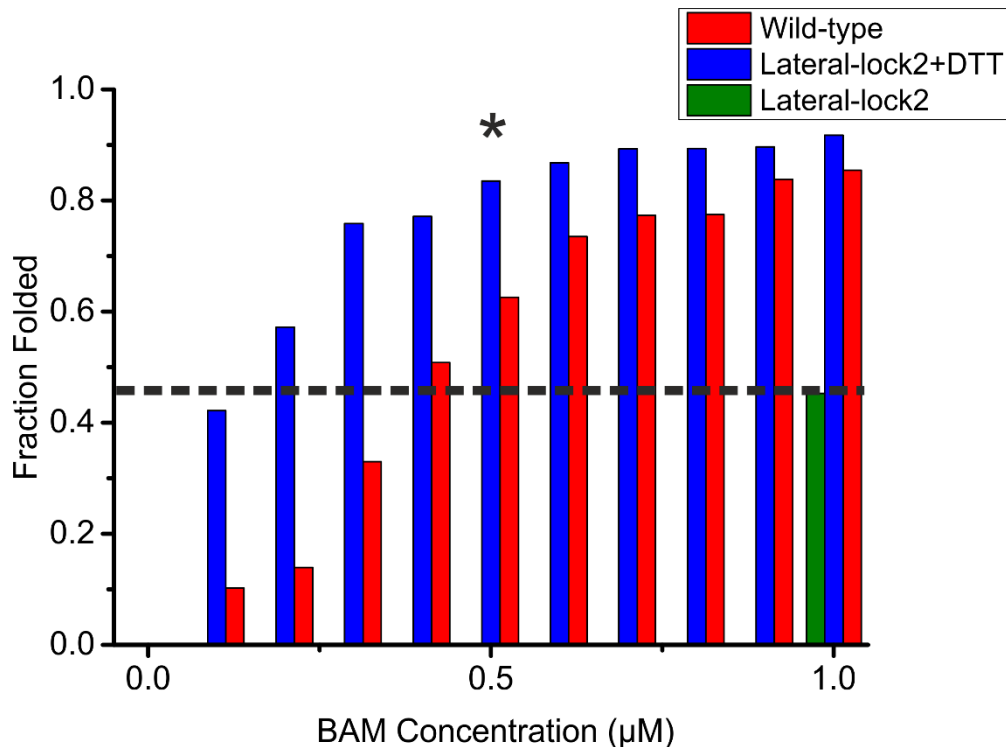
Figure 5-20: Decreased concentration of Lateral-lock2 BAM proteoliposomes in the presence of DTT demonstrates higher than anticipated activity. The assay typically involves 1 µM BAM proteoliposomes, 2 µM tOmpA, 10 µM SurA, 0.8 M urea, TBS pH 8, 25°C. BAM proteoliposomes were diluted in TBS pH 8 to final experimental concentrations of 0.1- 1.0 µM and pre-incubated with DTT (to final concentration 25 mM) where appropriate. Experiments were carried out at 25 °C. Folding was quenched after one hour by addition to 6x SDS loading buffer. Samples were analysed by SDS-PAGE with all samples from one variant on the same gel.

The data appear to suggest that the oxidized form of Lateral-lock2 diminishes the otherwise high activity of the reduced form in folding tOmpA. One potential explanation is that the oxidized form creates a non-productive interaction: able to recognise and bind tOmpA but unable to catalyse folding. This would create a tOmpA "sink" such that the tOmpA folding yield of Lateral-lock2 (without DTT) would be lower than that seen for folding by a 50% concentration of reduced Lateral-lock2 alone, where the non-productive interaction does not occur. This explanation fits, however it is difficult to presently draw conclusions as at the concentrations and time-points measured here, folding of substrate is nearly complete in the majority of samples. The relationship between fraction folded and BAM concentration is clearly not linear for wild-type or Lateral-lock2+DTT in the conditions used. One cannot be certain of the effect of the Lateral-lock2 oxidized populations, as it is evident that halving the concentration of BAM (eg.

218

comparison of 1 µM and 0.5 µM) is not halving the subsequent tOmpA folding yield for either wild-type or Lateral-lock2. Rather than an endpoint assay, as in these data, to examine BAM as an enzyme I wish to extract initial rates of substrate folding, which should increase linearly with respect to BAM concentration. In order to do this in the future, the substrate concentration will be decreased, such that enzyme (BAM) excess can be assumed. Initial rates will be measured by increasing the number of early time-points measured in the folding of tOmpA. The behaviour of BAM as an enzyme will be verified by demonstrating that an increasing concentration of wild-type BAM yields a corresponding increase in initial rate. Finally, the initial rate of oxidized and reduced Lateral-lock2 proteoliposomes will be determined. For Lateral-lock2 BAM without reducing agent, containing a mixed population, three clear outcomes are possible, with different explanations. If the oxidized population is inactive, then initial rate of Lateral-lock2 would be at 50% that of Lateral-lock2+DTT. If the oxidized population is detrimental to overall activity, the resulting initial rate would be lower than fully reduced protein and if the oxidized population is contributing to activity then initial rate would be higher. Theoretically these comparisons will allow us to determine the extent to which BAM, locked across the β-barrel can contribute to catalytic activity. These simple experiments should help to determine the nature of the lateral-lock in the BAM complex in addition to examining the enzymatic properties of BAM complex catalysis.

5.9 Discussion

This chapter applies the optimisation of purification and reconstitution of the BAM complex described in Chapter 3 to studies of the importance of BamA dynamics. I generated four BAM complex variants with cysteine pairs to produce disulphide cross-links, and also a cysteine-free pseudo wild-type control. These complexes were purified (Figure 5-2) and reconstituted in proteoliposomes (Figure 5-3). I demonstrated that all of the disulphide-locking variants are lethal *in vivo* (Figure 5-5), replicating literature findings[199] with a novel finding in the case of the Double-lock variant. Utilising the OmpT activity assay in the conditions optimised previously (Section 3.5.1) I assessed the catalytic activity of lethal disulphide cross-linking of the BAM complex for the first time.

It is now widely understood that BamA visits both lateral-open and –closed conformations by structural studies showing the BAM complex in both states[207-210]. While it is known that disulphide lateral-locking or Lid-locking of BamA is lethal to cells[199], presumably as it is detrimental to BamA function, studies by myself, and another group[231] have demonstrated that this effect does not translate to the catalytic activity of BamA in LUVs. In these BamA is equally functional in its lateral locked form. The effect of these disulphide locks, constraining BamA dynamics, on the catalytic activity of the full BAM complex have never previously been studied *in vitro*.

I have demonstrated that both the Lid-lock and the Lateral-lock1 variants have diminished activity as assessed by the OmpT assay, which is rescued by the addition of reducing agent (Figure 5-7). All of the BAM complex disulphide variants display near identical decreased activity in the folding of tOmpA which is rescuable in the cases of Lateral-lock1, Lid-lock and Double-lock by addition of reducing agent (Figure 5-16). The consistent diminished activity appears to imply a base level of folding on constraining the dynamics of the BAM complex. This level of folding is not seen in empty proteoliposomes (Figure 5-12), and with sufficient time all BAM variants are capable of folding substrate to completion (Figure 5-19). This suggests that the presence of the BAM complex, even constrained, catalyses folding. This may support a mixed model of BAM complex function: both by lateral opening dynamics, and by membrane destabilization.

This chapter discusses a novel assay quantifying the folding of substrate by BAM complex proteoliposomes directly using SDS-PAGE. In contrast to previous reports of a tOmpA 'elusive state' in folding[230], with an apparent disappearance of protein intensity, the sum of folded and unfolded band intensities remains relatively constant. The assay is robust, reliable and consistent, with reproducible kinetics of tOmpA folding by wild-type BAM proteoliposomes across different preparations of BAM and SurA and carried out by multiple members of the lab. In addition the assay has proved sensitive to alterations in the BAM complex and to altered concentrations of BAM. This assay is now being used further to examine the folding of other substrates by the BAM complex (eg. OmpX), to look at the role of SurA (as mentioned in Chapter 3, 0) and will be used to characterise the tOmpA variants previously mentioned (Sections 4.3 and 4.4).

The concentration titration carried out (Figure 5-20) is fascinating on two counts. Not only does it contradict the assumption that the oxidized population of the Lateral-lock protein is inactive and instead suggests it is detrimental to BAM catalytic activity, but a titration of the BAM complex such as this has not been carried out in studies of substrate folding. Previous studies have postulated a catalytic mechanism for BamA function by experiments on titration of substrate, demonstrating BamA can fold substrate to a higher concentration than the concentration of folded BamA. These studies on BamA[245] and the BAM complex[159] both suggest a catalytic turnover of ~1.6 OMPs per BAM. The sigmoidal curve seen for titration of wild-type BAM complex (Figure 5-20) demonstrates sensitivity in this assay to low concentrations of BAM complex, but also demonstrates better than anticipated activity of the complex at these concentrations.

The yield of tOmpA folding in this assay appears to exceed expected turnover, with BAM complex at 1 µM readily capable of folding 2 µM tOmpA quickly. The high fraction of tOmpA folded by low concentrations of wild-type and better still by Lateral-lock2 BAM within an hour (Figure 5-20) suggest that catalytic turnover is accelerated in the conditions used in this assay. For example, 0.4 µM Lateral-lock2 +DTT folds nearly 80% of 2 µM tOmpA, suggesting a folding yield of 1.6 µM, which is approximately four times the concentration of BAM complex. The basal rate of folding, in the presence of SurA would need to be more accurately measured to quantify the extent to which this is due to BAM. Once again, further studies will be required to untangle this catalytic rate, but this supports previous findings that BamA works by a catalytic mechanism[159,245] and suggests that the catalytic turnover has been underestimated.

In addition, experiments here demonstrate that disulphide variants, when reduced, may be more active than wild-type BAM, particularly in the cases of Lateral-lock2 and Lid-lock variants. This suggests that mutagenesis introducing cysteines to constrain the BamA barrel, creates a more active BAM complex. For the Lid-lock variant, this is dramatically seen in the OmpT assay (Figure 5-7). For Lateral-lock2 the titration data demonstrates consistently higher catalysis relative to wild-type BAM (Figure 5-20). In studying constraints of the BAM complex we have developed an enzyme that is in fact more active. Further work is needed to understand why this is the case.

221

Conclusions can most easily be drawn from the Lid-lock variant which exhibits disulphides in a fully oxidised state in the presence of buffer and diamide, but is fully reduced in the presence of DTT (Figure 5-9). This is in contrast with the other disulphide variants in which a totally oxidized population can never be obtained (Figure 5-9). The Lid-lock variant is lethal *in vivo*, in our assays (Figure 5-5) and in the literature[199,208]. Yet the Lid-lock variant clearly demonstrates that BAM retains activity, even with a fully oxidized cysteine cross-link (Figure 5-15e) and this is restored to wild-type levels of activity on reduction of the disulphide. Furthermore, folding of tOmpA by the Lid-lock variant in the absence of DTT (where the disulphide is fully oxidized), will eventually reach completion (Figure 5-19). This demonstrates that the cross-link imposes a purely kinetic constraint on Lid-lock catalysis of substrate folding, which translates to lethality *in vivo*. Some explanation may be posited utilising the recent demonstration that the accumulation of unfolded OMPs in the periplasm is lethal to cells[343]. These recent studies, on an inhibitor of the chaperone RseP, demonstrate that reduction in cell viability due to this inhibitor can be overcome by overexpression of DegP, to remove levels of unfolded OMPs[343]. Similarly, deletion of the genes for abundant OMPs OmpA and OmpC confers resistance to the inhibitor, whereas cells possessing a defective BAM complex display increased sensitivity[343]. In the case of the BAM Lid-lock variant therefore, the slower activity of folding observed *in vitro* may be sufficient to cause a toxic level of unfolded OMPs. Therefore we begin to piece together a model where constraining the dynamics of the BamA β-barrel slows the catalytic activity of BAM, likely causing accumulation of unfolded OMPs and toxicity to the cell.

6 Discussion

6.1 Overall Conclusion of Results

This thesis has endeavoured to investigate BAM-assisted OMP folding, particularly the role of BamA dynamics, with a plethora of biochemical and biophysical techniques. From an initial launching point of examining *in vitro* how BamA lateral gating may influence BamA catalytic activity, the project has expanded to examine the BAM complex, membrane mimetics and the β-signal hypothesis.

The data presented in Chapter 3 summarise the optimisation of the BAM complex preparation and the standard assay for its activity, the OmpT protease assay. The optimised purification protocol led to the sole published cryo-EM structure of the complex, which displayed BamA in a lateral-open structure in the presence of the full complex, and remains the only structure of the intact complex in this conformation[207-209].

Two approaches were taken to unpick the mechanism of BAM-assisted OMP folding and the role of BamA dynamics in OMP dynamics. Firstly, the work in Chapter 4 described the catalytic activity of isolated BamA in DMPC lipids in folding the substrate tOmpA. This system has been well characterised[163,241,288] and could easily be applied to investigating the effects of different variants of BamA. The results demonstrated no difference in BamA catalytic activity between the wild-type and lateral-lock forms of BamA. This implies that in DMPC LUVs, for folding of tOmpA, the lateral opening of BamA is not essential.

The second approach investigating the role of BamA dynamics utilised the intact BAM complex, following its successful purification and reconstitution discussed in Chapter 3. A wider range of BamA variants were tested in the BAM complex: two examples of cysteine pairs across the lateral gate, a variant to lock the substrate exit pore ('Lid-lock') and a Double-lock variant. Two assays were employed, the OmpT enzymatic assay on Lateral-lock1 and Lid-lock variants, and tOmpA folding by SDS-PAGE using all BAM variants.

The results demonstrated that cysteine pairs to lock the conformation of the BamA barrel only impair, but do not abolish BAM-catalysed OMP folding, of OmpT and tOmpA in *E.coli* polar lipid proteoliposomes. I further demonstrated

that folding of tOmpA by any of the BAM complex variants in proteoliposomes will eventually reach completion (Figure 5-19). Interestingly, all of the cysteine pairs are lethal *in vivo*[199]. The diminished folding kinetics of the variants render them inadequate in the context of the cell. Perhaps this is due simply to the fast turnover necessary in the cell, with both nascent protein production and minimisation of potential toxic intermediates, or perhaps the BamA cysteine-lock variants are incapable of folding larger substrates.

One must consider the possibility that if the formation of the disulphide in the BAM variants does not reach completion, it is in fact the non-oxidized population of the protein that is providing all activity. In the case of BAM complex variants, activity is partially diminished and rescued on addition of reducing agent, therefore alterations in redox state have a clear effect. However, for BamA catalysis in DMPC no changes in activity are observed with addition of reducing or oxidizing agent (Figure 4-21). Non-reducing PAGE confirmed that the majority of the protein is in the oxidized state in buffer and under oxidizing conditions, but is entirely reduced in the presence of reducing agent. The lack of change in observed BamA activity with changes in redox state leads us to conclude that the lateral lock (and therefore the redox state of it) makes no difference to the ability of BamA to catalyse tOmpA folding *in vitro.*

For the lateral-lock and Double-lock variants of the BAM complex, BamA remains in a mixed population, therefore it has not yet been ascertained what proportion of the activity can be ascribed to the reduced or oxidized populations. A titration experiment was carried out to determine the compensating effect of the mixed population: at what fraction of Lateral-lock2 BAM in reduced state is the resultant activity equal to the partially oxidized population. However the results demonstrate that activity in the reduced state is likely worsened by the presence of protein in the oxidized state (Figure 5-20) and further experiments on the kinetics of each BAM variant are necessary to unpick these data. The finding that folding of tOmpA by the BAM complex variants will reach completion, and differences are primarily kinetic, is particularly insightful for the Lid-lock variant, in which BamA is fully oxidized, as confirmed by non-reducing PAGE. The results conclusively demonstrate that the fully oxidized, and therefore constrained Lid-lock BAM shows partial function in catalysing tOmpA folding.

Additionally, I have used a cumulative perspective of the assays discussed in this thesis to examine two aspects of the OMP β-signal hypotheses. I have examined firstly the hypothesis of species-specificity: that *E.coli* BamA will not recognise signal sequences from a different organism[211] using a hybrid tOmpA mutant containing residues from the signal sequence of *N.meningitidis* PorA with otherwise *E.coli* tOmpA sequence. The results provide further evidence that BamA in DMPC liposomes acts primarily according to the membrane disruptase model of function (Introduction 1.10). Folding of tOmpA-RHK is catalysed by wild-type BamA with the same fold change as for wild-type tOmpA, implying no impaired recognition of the protein. Conversely, however, folding of tOmpA-RHK catalysed by Lateral-lock1 BamA is considerably slower. This suggests that impairing the dynamics of the BamA barrel diminishes its catalytic effect of folding an unfamiliar substrate. It remains possible that other components of the BAM complex increase the specificity of substrate recognition, therefore continuation of this project would focus on BAM-catalysed folding. This work has also included investigation into the conserved Gly of the β-signal which appears to exhibit a structural role in OmpT but not in tOmpA. In OmpT, mutation of Gly306, even to Ala, produces a protein incapable of spontaneous folding to an SDS-resistant structure. Mutation of the conserved Gly both in OmpT (G306A and G306P) and tOmpA (G166A) slows BAM-catalysed folding in *E.coli* liposomes (Figure 4-36 - Figure 4-39). This implies that little variation on this highly conserved residue can be tolerated.

6.2 Evidence towards the models of BAM function

The outer membrane proteins (OMPs) of Gram-negative bacteria must be transported to, and assemble in, the OM in an environment devoid of chemical energy, and far from their site of synthesis. The final step in this pathway is folding, catalysed by the BAM complex. Despite being essential[21], conserved[21,24,57] and with available structural models[207-209] the mechanism of function of the BAM complex is not yet clear. There are several proposed models, summarised as threading, oligomerisation, membrane destabilisation and lateral opening, addressed in detail in Introduction, Section 1.10. The work in this thesis was driven particularly towards understanding the model of BamA lateral opening

and the extent to which this is important in BamA-catalysed OMP folding. The results have provided evidence relevant to several of the models: not only lateral opening, but membrane destabilisation and oligomerisation.

The absence of a role for lateral opening in the case of BamA-catalysed tOmpA folding in DMPC LUVs lends support to the hypothesis that BamA destabilises membranes. In accord with this idea, parallel work by Dr Bob Schiffrin (University of Leeds) demonstrated the increased catalytic effect of BamA in longer chain lipid bilayers[241], evidencing its role in reducing the energetic penalty of folding into these bilayers.

In the context of the BAM complex, however, the results presented in Chapter 5 demonstrate that any constraint on the dynamics of the BamA barrel does indeed reduce, but does not abolish, its ability to catalyse OMP folding. The clear role for lateral opening in the scenario of BAM-catalysed folding into *E.coli* lipid bilayers implies a strong lipid dependence for this mechanism. In addition, the mechanism may be substrate-dependent with an increased importance for lateral opening in larger or multimeric OMPs that may be more difficult to fold spontaneously.

In contrast to the BamA-budding model originally proposed for the role of lateral opening, where the substrate interacts with both β1 and β16 in a lateral open BamA, results now favour a barrel elongation model (Figure 6-1)[33]. This suggests β-strand augmentation occurs on β1, but formation of a hybrid barrel and the repeated associated making and breaking of H-bonds does not occur. This model allows for the role of lateral gating, and accommodates previous observations suggesting that OMPs fold by sequential insertion of β-hairpins into the membrane[237,238,257]. In addition, the proposed interaction between BAM and substrate protein would then predominantly occur in the periplasm, with the periplasmic domains of BamA or the lipoproteins, such as BamD. This is consistent with the essential nature of BamD[25,187], cross-linking of an LptDE complex to BamA and BamD in a stalled intermediate interaction[220], and proposed recognition of substrate β-signal by BamD[175,195,218].
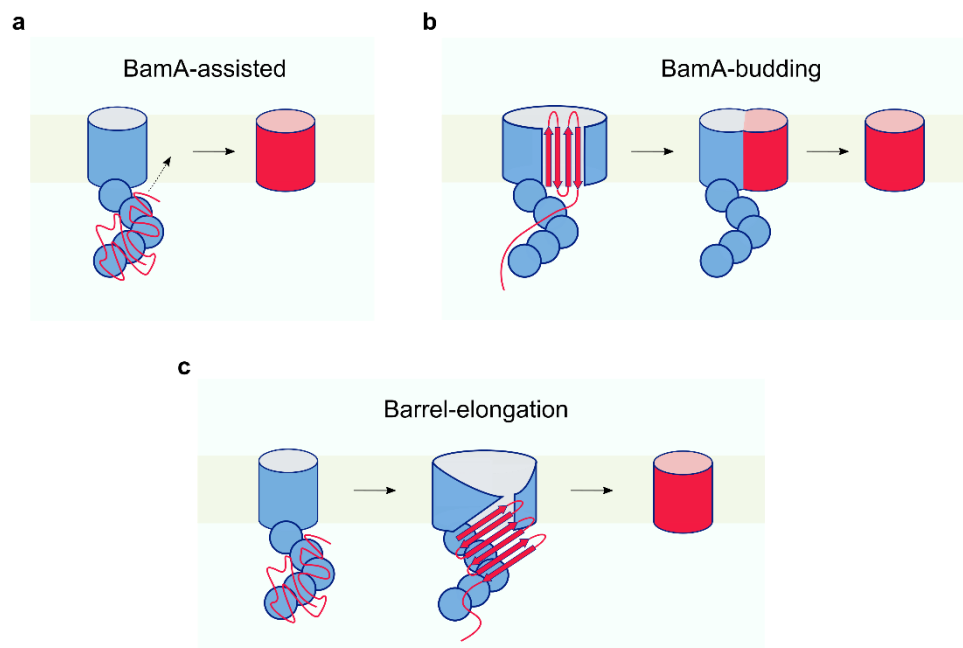
Figure 6-1: Models for OMP assembly by the BAM complex. In all models BamA is depicted in blue and the substrate protein in red. The lipoproteins BamB-E and the chaperone SurA are omitted for clarity. a) BamA-assisted: BamA acts as a "membrane disruptase" to catalyse folding. b) BamA-budding: BamA opens by a separation of β1 and β16, the substrate β-strands sequentially insert and interact before budding off into the membrane. c) Barrel-elongation: similar to the previous model BamA opens via the lateral gate, but the substrate OMP interacts only with β1 of BamA and periplasmic components of the complex. Formation of the barrel and insertion into the membrane completes folding. Figure reproduced from Schiffrin *et al.,*(2017)[33].

While the barrel elongation model leaves an unpaired β16 at the C-terminus of BamA with unsatisfied H-bond interactions, it may also explain the short length of β16 and propensity to form an inward kink (Figure 6-2a)[11,209]. Recent experiments on BamA folded in LDAO have demonstrated the ability of the β1 strand to form H-bonds in addition to those with β16, and shown that this may increase the stability of the complex[254]. These experiments utilised extension of the β16 of BamA with 9 residues from the C-terminus of OmpX to extend the connection between β1 and β16 (Figure 6-2c). This provides strong evidence in support of the barrel elongation model as it proposes β1 as the site for OMP interaction and demonstrates the stability of interaction with a longer β-strand. These studies have also demonstrated the unusual dynamics of the BamA structure that samples register sliding of the β1 and β16. Studies were carried out for BamA in LDAO[254] and had previously been shown in DDPC:DDPE LUVs[231]. In both cases it has been shown that disulphides may form across the lateral

gate, not only in the anticipated pairing, but to residues out of register: up to two higher or lower on the opposite β strand (Figure 6-2b).
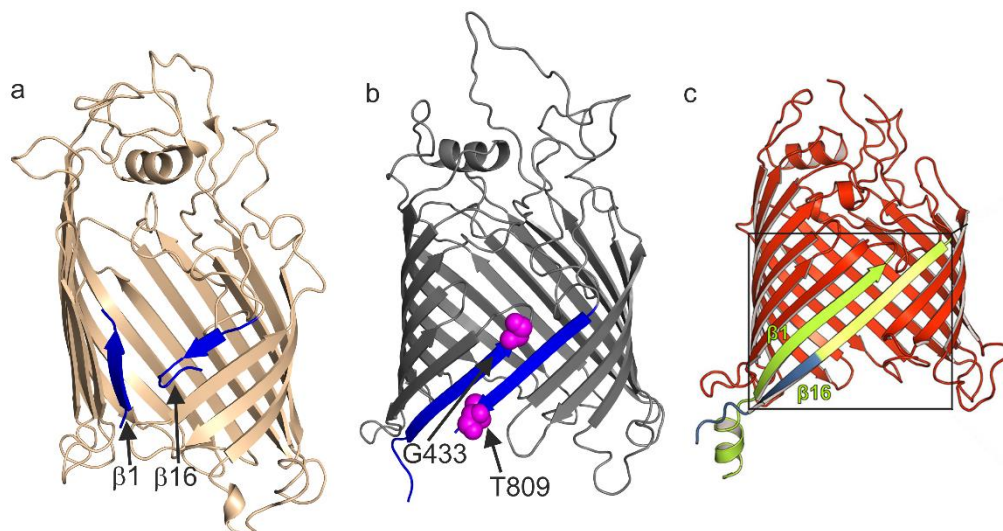
Figure 6-2: *E.coli* BamA transmembrane domain showing (a) inward kink of β16. (b) non-register cross-linking of β1 and β16. (c) Extension of β16 creates a stable structure. (a) BamA from BAM complex structure [5EKQ][207] with β1 and β16 highlighted in blue. The lateral open structure shows the latter β-strands tilted inwards to the barrel. (b) Cysteine residues engineered on G433 and T809 (magenta spheres) are able to form a disulfide despite being two steps out of register. This particular pair was shown for BamA both folded in LDAO[254] and DDPC:DDPE LUVs[231]. β1 and β16 are highlighted in blue. Image created from BAM *E.coli* model[227]. (c) Extension of β16 with 9 residues of OmpX (blue) stabilizes the structure. Image adapted from Hartmann *et al.*, (2018)[254].

A further proposed model of BAM function includes oligomerisation. As originally proposed, the model involves OMP threading through the pore at the centre of a BAM tetramer[211,212]. The structures of the BAM complex demonstrate this to be unlikely due to the anticipated steric clash between components of the complex[207-210]. However, there is increasing evidence that copies of the BAM complex interact, with theories that productive BAM complexes are tightly clustered together in "OMP islands" or "precincts"[216,283]. Activity of the BAM complex in protein-supported nanodiscs[274] (Figure 3-35) was taken as evidence against an oligomerisation model, or suggestive that this is not the obligate form for functional BAM, as an isolated copy of the complex is active. However, reconsideration of the data permits alternative hypotheses. BAM in nanodiscs exhibits lower activity in the OmpT assay than proteoliposomes at the same concentration of BAM (Figure 3-35). One hypothesis as to why this may occur is
228

that the encapsulation of individual copies of the BAM complex in nanodiscs abolishes the productive interactions of copies of the BAM complex. BAM in proteoliposomes, demonstrating a higher level of activity, may be located close together or oligomerise, permitting the optimal functional form. However, no oligomers of BAM were observed in these studies by native PAGE of the complex in detergent, SMALPs or proteoliposomes. In addition, while this was not examined in depth, experiments with altered LPR demonstrated that greater LPR decreased activity for the same concentration of BAM (Figure 3-22). Increased LPR would likely reduce the number of BAM clusters or their size. While these experiments are difficult to control, due to the necessity of making liposomes of different LPRs, and uncertainty about how exactly the BAM complex is clustering, this is further evidence supporting clustering of the BAM complex as increasing its activity.

Furthermore, the results of the dilution series of BAM Lateral-lock2 are intriguing when considered in the context of OMP islands. In this work, the BAM complexes are principally considered separate, disparate enzymatic units. Approximately 50% of the population of BAM complex Lateral-lock2 protein is in the oxidized conformation and 50% in the reduced conformation. However, the results demonstrate that an equal concentration of the reduced protein (50% of typical total concentration) exhibits greater activity than the mixed population. While these results may suggest that the oxidized population has a direct negative effect on the overall activity, by creating a non-productive interaction, it is also possible that the oxidized BAM impacts the activity of the reduced BAM units. This makes sense only in consideration of OMP islands where the proteins are tightly packed together. An oxidized BAM may clearly impact the dynamics and thus activity of its neighbouring BAM. Further studies remain to be done to comprehend how the clustering of BAM may impact activity and whether one copy in the cluster can affect its neighbours.

6.3 The next studies to be done

A great deal of work remains to be done to fully unravel the mechanism of BAM-assisted OMP folding, of which a few experiments present themselves as obvious following the results of this thesis. One of the principal questions persists of whether BAM would function differently for OMPs of varying size. The examples discussed throughout this thesis have focussed predominantly on smaller OMPs, those of 8-10 β-strand size, as these are the more tractable: easier for protein expression, folding in different lipids and monitoring protein folding. The field now requires a thorough investigation into BAM-assisted folding of the larger OMPs. This has been partially begun with studies on 12-stranded autotransporter EspP[273,274,344], 26-stranded LptD[220] and BamA itself[272].

However, the library of unstudied OMPs remains large, and particularly the folding of multimeric OMPs is unexplored. Furthermore, the application of the BAM complex variants generated in this thesis to the folding of larger OMPs remains of interest. The roles of lateral opening, and BamA dynamics in general may be highly substrate-specific, with an increased importance in larger OMPs. This would partially explain the *in vivo* lethality of disulphide variants, which only cause a partial reduction in *in vitro* catalysis of folding.

Secondly, it has only been briefly addressed how the role of the lipid is integral in BAM-assisted OMP folding. We are able to observe this clearly in BamA assisted folding of tOmpA, with LUVs formed of longer chain PC lipids causing retarded folding but a greater catalytic effect of BamA-assisted folding[241]. Preliminary results have been generated in this thesis examining the effect of different lipids (Figure 4-27), LPR (Figure 3-22) and membrane mimetics (Section 3.6). However, not only do all these aspects require further attention, but the questions of membrane curvature, vesicle size (in use of LUVs) and asymmetry to resemble the native bilayer, have of necessity been ignored.

In unilamellar vesicles generated of synthetic phospholipids in the absence of BAM it has been demonstrated that vesicle size and membrane curvature impacts the intrinsic folding rate of OMPs. Smaller and thinner vesicles in this case accelerate folding[72]. However, studies remain to be done on how this alters when BamA or the BAM complex is present in the lipid of interest. Is the purported

230

role of BamA in membrane destabilisation equal to that of generating a vesicle with increased curvature?

Secondly studies on the lipid:protein ratio (LPR) are of key interest in *in vitro* experiments. Not only could studies on LPR shed light on the theories of OMP islands or precincts, with increasing LPR reducing the propensity of such features in proteoliposomes, but they may elucidate the role of BAM oligomerisation in accelerating OMP assembly. A combination of detailed folding assays *in vitro* with studies on OMP localisation *in vivo* would allow us to unravel how the BAM "precincts" may contribute to its function.

The data presented in this thesis raises many more questions in the field of BAM-assisted OMP folding and presented here are simply some of the most evident questions to be examined moving forward.

6.4 Towards a new antibacterial

A key driver to a great deal of the research on Gram-negative bacteria, particularly on essential, conserved systems such as BAM[21,24,81], is the pressing human need for ways to target and eradicate pathogenic Gram-negative bacteria. Gram-negative bacteria include widespread human pathogens, and with limited development of antibacterials and increasing antibiotic resistance the threat they pose can only grow[7]. The work in our laboratory takes one of many approaches towards advancing this field, by increasing our fundamental understanding of Gram-negative bacteria and how they function. BamA is vital in Gram-negative bacteria and therefore represents an obvious target for antimicrobials, rendered more attractive as its membrane location would potentially render cell penetration unnecessary. Despite understanding of the critical nature of BamA for decades[21], and studies in its mutagenesis demonstrating that inhibiting the complex is lethal[21,24,187,199,201] the understanding of BAM mechanism remains poor. Due in part to its intractability as a membrane protein complex, the structure of the complex has not been solved until recently[207-210], and many of the details of its mechanism remain unclear. How can it be that a complex that is so fundamental, so omnipresent, can be so little understood?

The field advances apace with injection of recombinant BamA providing a potential vaccination against *Acinetobacter baumannii* tested in a mouse model[345]. Meanwhile studies by the pharmaceutical company Genentech have developed antibodies that bind to and inhibit BamA in *E.coli*[49,346]. While the antibodies originally published are not useful clinically as binding requires truncated LPS[49], this fuels further study in this area. It has been discussed briefly in this thesis how inhibitors assumed to work against BAM[47,175] show minimal function, or differential function according to substrate in *in vitro* assays. Whilst *in vitro* assays can be useful in screening inhibitors and determining mode of action, an improved panel of *in vitro* and *in vivo* assays are necessary to investigate potential inhibitors of BAM. The macrocyclic peptides, discussed in the context of the potential inhibitor JB-95, are designed as synthetic peptidomimetic antibiotics[47,314], taking inspiration from cationic antimicrobial peptides found as part of the innate immune system[316]. The peptide used as a control in experiments in this thesis, L27-11, was demonstrated to be specifically inhibiting LptD in *Pseudomonas aeruginosa*[314,319]. This led to the development of the closely related peptide Murepavadin, currently in phase III trials as an antibiotic towards *Pseudomonas aeruginosa*[316,347], proving the exceptional potential of this research.

The lateral opening of BamA was proved to be vital in *E.coli* by disulphide-locking of the BamA β-barrel causing lethality in bacteria[199]. Evidently one cannot introduce a lock into BamA opening in live bacteria, however, if one can understand the details of the mechanism perhaps it is possible to design inhibitors. This has been a key real-world goal to studies throughout my thesis. In examination of BamA and the BAM complex, however, caution must be exercised regarding the potential of inhibitory peptides or chemicals, as these may affect not only the mutualistic bacteria of the human intestinal microbiome, but also the Omp85 proteins of mitochondria and chloroplasts[22,26]. These proteins are highly similar, with recent studies on mitochondrial Sam50 proving the mechanism hypothesised for the lateral opening and β-signal recognition in BamA[287]. While substrate proteins do not necessarily show sequence similarity, β-barrel bacterial proteins are efficiently folded in the mitochondrial outer membrane dependent on the C-terminal β-signal[28].

While these caveats remain, and there is still much to do to understand BAM mechanism of action, the examples discussed here show the progress and potential of new inhibitors towards BamA. BamA is essential in Gram-negative bacteria and our advancement of fundamental understanding of its mechanism of function may advance development of novel inhibitors and antibacterials.

References

1. Zgurskaya, H.I., Lopez, C.A. & Gnanakaran, S. Permeability Barrier of Gram-Negative Cell Envelopes and Approaches To Bypass It. *ACS Infect Dis* **1**, 512-522 (2015).

2. Exner, M. et al. Antibiotic resistance: What is so special about multidrug-resistant Gram-negative bacteria? *GMS Hyg Infect Control* **12**(2017).

3. Ghai, I. & Ghai, S. Understanding antibiotic resistance via outer membrane permeability. *Infect Drug Resist* **11**, 523-530 (2018).

4. Shaikh, S., Fatima, J., Shakil, S., Rizvi, S.M. & Kamal, M.A. Antibiotic resistance and extended spectrum beta-lactamases: Types, epidemiology and treatment. *Saudi J Biol Sci* **22**, 90-101 (2015).

5. Blair, J.M., Webber, M.A., Baylay, A.J., Ogbolu, D.O. & Piddock, L.J. Molecular mechanisms of antibiotic resistance. *Nat Rev Microbiol* **13**, 42-51 (2015).

6. Silver, L.L. Challenges of antibacterial discovery. *Clin Microbiol Rev* **24**, 71-109 (2011).

7. May, K.L. & Grabowicz, M. The bacterial outer membrane is an evolving antibiotic barrier. *Proc Natl Acad Sci U S A* **115**, 8852-8854 (2018).

8. Ghai, I. & Ghai, S. Exploring bacterial outer membrane barrier to combat bad bugs. *Infect Drug Resist* **10**, 261-273 (2017).

9. Nikaido, H. Molecular basis of bacterial outer membrane permeability revisited. *Microbiol Mol Biol Rev* **67**, 593-656 (2003).

10. Ieva, R. Interfering with outer membrane biogenesis to fight Gram-negative bacterial pathogens. *Virulence* **8**, 1049-1052 (2017).

11. Albrecht, R. et al. Structure of BamA, an essential factor in outer membrane protein biogenesis. *Acta Crystallogr D Biol Crystallogr* **70**, 1779-89 (2014).

12. Otzen, D.E. & Andersen, K.K. Folding of outer membrane proteins. *Arch Biochem Biophys* **531**, 34-43 (2013).

13. Silhavy, T.J., Kahne, D. & Walker, S. The bacterial cell envelope. *Cold Spring Harb Perspect Biol* **2**, a000414 (2010).

14. Rollauer, S.E., Sooreshjani, M.A., Noinaj, N. & Buchanan, S.K. Outer membrane protein biogenesis in Gram-negative bacteria. *Philos Trans R Soc Lond B Biol Sci* **370**(2015).

15. Pugsley, A.P. The complete general secretory pathway in gram-negative bacteria. *Microbiol Rev* **57**, 50-108 (1993).

16. Macnab, R.M. The bacterial flagellum: reversible rotary propellor and type III export apparatus. *J Bacteriol* **181**, 7149-53 (1999).

17. Soto, G.E. & Hultgren, S.J. Bacterial adhesins: common themes and variations in architecture and assembly. *J Bacteriol* **181**, 1059-71 (1999).

18. Koebnik, R., Locher, K.P. & Van Gelder, P. Structure and function of bacterial outer membrane proteins: barrels in a nutshell. *Mol Microbiol* **37**, 239-53 (2000).

19. Bos, M.P., Robert, V. & Tommassen, J. Biogenesis of the gram-negative bacterial outer membrane. *Annu Rev Microbiol* **61**, 191-214 (2007).

20. Beveridge, T.J. Structures of gram-negative cell walls and their derived membrane vesicles. *J Bacteriol* **181**, 4725-4733 (1999).

21. Voulhoux, R., Bos, M.P., Geurtsen, J., Mols, M. & Tommassen, J. Role of a highly conserved bacterial protein in outer membrane protein assembly. *Science* **299**, 262-5 (2003).

22. Reumann, S., Davila-Aponte, J. & Keegstra, K. The evolutionary origin of the protein-translocating channel of chloroplastic envelope membranes: identification of a cyanobacterial homolog. *Proc Natl Acad Sci U S A* **96**, 784-9 (1999).

23. Webb, C.T., Heinz, E. & Lithgow, T. Evolution of the beta-barrel assembly machinery. *Trends Microbiol* **20**, 612-20 (2012).

24. Voulhoux, R. & Tommassen, J. Omp85, an evolutionarily conserved bacterial protein involved in outer-membrane-protein assembly. *Res Microbiol* **155**, 129-35 (2004).

25. Wu, T. et al. Identification of a multicomponent complex required for outer membrane biogenesis in Escherichia coli. *Cell* **121**, 235-45 (2005).

26. Gentle, I., Gabriel, K., Beech, P., Waller, R. & Lithgow, T. The Omp85 family of proteins is essential for outer membrane biogenesis in mitochondria and bacteria. *J Cell Biol* **164**, 19-24 (2004).

27. Gentle, I.E., Burri, L. & Lithgow, T. Molecular architecture and function of the Omp85 family of proteins. *Mol Microbiol* **58**, 1216-25 (2005).

28. Walther, D.M., Papic, D., Bos, M.P., Tommassen, J. & Rapaport, D. Signals in bacterial beta-barrel proteins are functional in eukaryotic cells for targeting to and assembly in mitochondria. *Proc Natl Acad Sci U S A* **106**, 2531-6 (2009).

29. Walther, D.M., Rapaport, D. & Tommassen, J. Biogenesis of beta-barrel membrane proteins in bacteria and eukaryotes: evolutionary conservation and divergence. *Cell Mol Life Sci* **66**, 2789-804 (2009).

30. Albenne, C. & Ieva, R. Job contenders: roles of the beta-barrel assembly machinery and the translocation and assembly module in autotransporter secretion. *Mol Microbiol* **106**, 505-517 (2017).

31. Bakelar, J., Buchanan, S.K. & Noinaj, N. Structural snapshots of the beta-barrel assembly machinery. *FEBS J* **284**, 1778-1786 (2017).

32. Noinaj, N., Gumbart, J.C. & Buchanan, S.K. The beta-barrel assembly machinery in motion. *Nat Rev Microbiol* **15**, 197-204 (2017).

33. Schiffrin, B., Brockwell, D.J. & Radford, S.E. Outer membrane protein folding from an energy landscape perspective. *BMC Biol* **15**, 123 (2017).

34. Hagan, C.L., Silhavy, T.J. & Kahne, D. Beta-Barrel membrane protein assembly by the Bam complex. *Annu Rev Biochem* **80**, 189-210 (2011).

35. Ranava, D., Caumont-Sarcos, A., Albenne, C. & Ieva, R. Bacterial machineries for the assembly of membrane-embedded beta-barrel proteins. *FEMS Microbiol Lett* **365** (2018).

36. Salton, M.R. The relationship between the nature of the cell wall and the Gram stain. *J Gen Microbiol* **30**, 223-35 (1963).

37. Beveridge, T.J. & Graham, L.L. Surface layers of bacteria. *Microbiol Rev* **55**, 684-705 (1991).

38. Goodsell, D.S. Inside a living cell. *Trends Biochem Sci* **16**, 203-6 (1991).

39. Glauert, A.M. & Thornley, M.J. The topography of the bacterial cell wall. *Annu Rev Microbiol* **23**, 159-98 (1969).

40. Braun, V. Covalent lipoprotein from the outer membrane of Escherichia coli. *Biochim Biophys Acta* **415**, 335-77 (1975).

235

41. Cohen, E.J., Ferreira, J.L., Ladinsky, M.S., Beeby, M. & Hughes, K.T. Nanoscale-length control of the flagellar driveshaft requires hitting the tethered outer membrane. *Science* **356**, 197-200 (2017).

42. Vollmer, W., Blanot, D. & de Pedro, M.A. Peptidoglycan structure and architecture. *FEMS Microbiol Rev* **32**, 149-67 (2008).

43. Neuhaus, F.C. & Baddiley, J. A continuum of anionic charge: structures and functions of D-alanyl-teichoic acids in gram-positive bacteria. *Microbiol Mol Biol Rev* **67**, 686-723 (2003).

44. Pitout, J.D. & Laupland, K.B. Extended-spectrum beta-lactamase-producing Enterobacteriaceae: an emerging public-health concern. *Lancet Infect Dis* **8**, 159-66 (2008).

45. (WHO), W.H.O. Global Priority List of Antibiotic-Resistant bacteria to guide research, discovery, and development of new antibiotics. (2017).

46. Weirich, J. et al. Identifying components required for OMP biogenesis as novel targets for antiinfective drugs. *Virulence* **8**, 1170-1188 (2017).

47. Urfer, M. et al. A Peptidomimetic Antibiotic Targets Outer Membrane Proteins and Disrupts Selectively the Outer Membrane in Escherichia coli. *J Biol Chem* **291**, 1921-32 (2016).

48. Henderson, J.C. et al. The Power of Asymmetry: Architecture and Assembly of the Gram-Negative Outer Membrane Lipid Bilayer. *Annu Rev Microbiol* **70**, 255-78 (2016).

49. Storek, K.M. et al. Monoclonal antibody targeting the beta-barrel assembly machine of Escherichia coli is bactericidal. *Proc Natl Acad Sci U S A* **115**, 3692-3697 (2018).

50. Tripathi, P. et al. Towards a nanoscale view of lactic acid bacteria. *Micron* **43**, 1323-30 (2012).

51. Sperandeo, P., Martorana, A.M. & Polissi, A. The lipopolysaccharide transport (Lpt) machinery: A nonconventional transporter for lipopolysaccharide assembly at the outer membrane of Gram-negative bacteria. *J Biol Chem* **292**, 17981-17990 (2017).

52. Okuda, S., Sherman, D.J., Silhavy, T.J., Ruiz, N. & Kahne, D. Lipopolysaccharide transport and assembly at the outer membrane: the PEZ model. *Nat Rev Microbiol* **14**, 337-45 (2016).

53. Malinverni, J.C. & Silhavy, T.J. An ABC transport system that maintains lipid asymmetry in the gram-negative outer membrane. *Proc Natl Acad Sci U S A* **106**, 8009-14 (2009).

54. Lugtenberg, E.J. & Peters, R. Distribution of lipids in cytoplasmic and outer membranes of Escherichia coli K12. *Biochim Biophys Acta* **441**, 38-47 (1976).

55. Braun, M. & Silhavy, T.J. Imp/OstA is required for cell envelope biogenesis in Escherichia coli. *Mol Microbiol* **45**, 1289-302 (2002).

56. Furse, S. & Scott, D.J. Three-Dimensional Distribution of Phospholipids in Gram Negative Bacteria. *Biochemistry* **55**, 4742-7 (2016).

57. Tommassen, J. Assembly of outer-membrane proteins in bacteria and mitochondria. *Microbiology* **156**, 2587-96 (2010).

58. Bayer, M.E. Areas of adhesion between wall and membrane of Escherichia coli. *J Gen Microbiol* **53**, 395-404 (1968).

59. Vacca, I. Bacterial physiology: Shuttling lipids across bacterial membranes. *Nat Rev Microbiol* **15**, 319 (2017).

60. Freinkman, E., Okuda, S., Ruiz, N. & Kahne, D. Regulated assembly of the transenvelope protein complex required for lipopolysaccharide export. *Biochemistry* **51**, 4800-6 (2012).

61. Ekiert, D.C. et al. Architectures of Lipid Transport Systems for the Bacterial Outer Membrane. *Cell* **169**, 273-285 (2017).

62. Wu, T. et al. Identification of a protein complex that assembles lipopolysaccharide in the outer membrane of Escherichia coli. *Proc Natl Acad Sci U S A* **103**, 11754-9 (2006).

63. Okuda, S. & Tokuda, H. Model of mouth-to-mouth transfer of bacterial lipoproteins through inner membrane LolC, periplasmic LolA, and outer membrane LolB. *Proc Natl Acad Sci U S A* **106**, 5877-82 (2009).

64. Muller, M., Koch, H.G., Beck, K. & Schafer, U. Protein traffic in bacteria: multiple routes from the ribosome to and across the membrane. *Prog Nucleic Acid Res Mol Biol* **66**, 107-57 (2001).

65. Wulfing, C. & Pluckthun, A. Protein folding in the periplasm of Escherichia coli. *Mol Microbiol* **12**, 685-92 (1994).

66. Cronan, J.E. Bacterial membrane lipids: where do we stand? *Annu Rev Microbiol* **57**, 203-24 (2003).

67. Ishinaga, M., Kanamoto, R. & Kito, M. Distribution of phospholipid molecular species in outer and cytoplasmic membrane of Escherichia coli. *J Biochem* **86**, 161-5 (1979).

68. Shibuya, I., Miyazaki, C. & Ohta, A. Alteration of phospholipid composition by combined defects in phosphatidylserine and cardiolipin synthases and physiological consequences in Escherichia coli. *J Bacteriol* **161**, 1086-92 (1985).

69. Killian, J.A. et al. Effect of divalent cations on lipid organization of cardiolipin isolated from Escherichia coli strain AH930. *Biochim Biophys Acta* **1189**, 225-32 (1994).

70. DeChavigny, A., Heacock, P.N. & Dowhan, W. Sequence and inactivation of the pss gene of Escherichia coli. Phosphatidylethanolamine may not be essential for cell viability. *J Biol Chem* **266**, 5323-5332 (1991).

71. Gessmann, D. et al. Outer membrane beta-barrel protein folding is physically controlled by periplasmic lipid head groups and BamA. *Proc Natl Acad Sci U S A* **111**, 5878-83 (2014).

72. Burgess, N.K., Dao, T.P., Stanley, A.M. & Fleming, K.G. Beta-barrel proteins that reside in the Escherichia coli outer membrane in vivo demonstrate varied folding behavior in vitro. *J Biol Chem* **283**, 26748-58 (2008).

73. Casali, N. & Riley, L.W. A phylogenomic analysis of the Actinomycetales mce operons. *BMC Genomics* **8**, 60 (2007).

74. Chong, Z.S., Woo, W.F. & Chng, S.S. Osmoporin OmpC forms a complex with MlaA to maintain outer membrane lipid asymmetry in Escherichia coli. *Mol Microbiol* **98**, 1133-46 (2015).

75. Chng, S.S. et al. Disulfide rearrangement triggered by translocon assembly controls lipopolysaccharide export. *Science* **337**, 1665-8 (2012).

76. Thong, S. et al. Defining key roles for auxiliary proteins in an ABC transporter that maintains bacterial outer membrane lipid asymmetry. *Elife* **5**(2016).

77. Nikaido, H. Restoring permeability barrier function to outer membrane. *Chem Biol* **12**, 507-9 (2005).

237

78. Ruiz, N., Wu, T., Kahne, D. & Silhavy, T.J. Probing the barrier function of the outer membrane with chemical conditionality. *ACS Chem Biol* **1**, 385-95 (2006).

79. Kleinschmidt, J.H. & Tamm, L.K. Secondary and Tertiary Structure Formation of the β-Barrel Membrane Protein OmpA is Synchronized and Depends on Membrane Thickness. *J Mol Biol* **324**, 319-330 (2002).

80. Sampson, B.A., Misra, R. & Benson, S.A. Identification and characterization of a new gene of Escherichia coli K-12 involved in outer membrane permeability. *Genetics* **122**, 491-501 (1989).

81. Genevrois, S., Steeghs, L., Roholl, P., Letesson, J.J. & van der Ley, P. The Omp85 protein of Neisseria meningitidis is required for lipid export to the outer membrane. *EMBO J* **22**, 1780-9 (2003).

82. Bos, M.P., Tefsen, B., Geurtsen, J. & Tommassen, J. Identification of an outer membrane protein required for the transport of lipopolysaccharide to the bacterial cell surface. *Proc Natl Acad Sci U S A* **101**, 9417-22 (2004).

83. Ruiz, N., Falcone, B., Kahne, D. & Silhavy, T.J. Chemical conditionality: a genetic strategy to probe organelle assembly. *Cell* **121**, 307-17 (2005).

84. Freinkman, E., Chng, S.S. & Kahne, D. The complex that inserts lipopolysaccharide into the bacterial outer membrane forms a two-protein plug-and-barrel. *Proc Natl Acad Sci U S A* **108**, 2486-91 (2011).

85. Botos, I. et al. Structural and Functional Characterization of the LPS Transporter LptDE from Gram-Negative Pathogens. *Structure* **24**, 965-976 (2016).

86. Qiao, S., Luo, Q., Zhao, Y., Zhang, X.C. & Huang, Y. Structural basis for lipopolysaccharide insertion in the bacterial outer membrane. *Nature* **511**, 108-11 (2014).

87. Narita, S.I. & Tokuda, H. Bacterial lipoproteins; biogenesis, sorting and quality control. *Biochim Biophys Acta* **1862**, 1414-1423 (2017).

88. Tokuda, H. & Matsuyama, S. Sorting of lipoproteins to the outer membrane in E. coli. *Biochim Biophys Acta* **1694**, 5-13 (2004).

89. Ruiz, N., Chng, S.S., Hiniker, A., Kahne, D. & Silhavy, T.J. Nonconsecutive disulfide bond formation in an essential integral outer membrane protein. *Proc Natl Acad Sci U S A* **107**, 12245-50 (2010).

90. Gu, Y. et al. Lipopolysaccharide is inserted into the outer membrane through an intramembrane hole, a lumen gate, and the lateral opening of LptD. *Structure* **23**, 496-504 (2015).

91. Li, X., Gu, Y., Dong, H., Wang, W. & Dong, C. Trapped lipopolysaccharide and LptD intermediates reveal lipopolysaccharide translocation steps across the Escherichia coli outer membrane. *Sci Rep* **5**, 11883 (2015).

92. Miyake, K. Innate recognition of lipopolysaccharide by Toll-like receptor 4-MD-2. *Trends Microbiol* **12**, 186-92 (2004).

93. Greenfield, L.K. & Whitfield, C. Synthesis of lipopolysaccharide O-antigens by ABC transporter-dependent pathways. *Carbohydr Res* **356**, 12-24 (2012).

94. Zhou, Z., White, K.A., Polissi, A., Georgopoulos, C. & Raetz, C.R. Function of Escherichia coli MsbA, an essential ABC family transporter, in lipid A and phospholipid biosynthesis. *J Biol Chem* **273**, 12466-75 (1998).

95. Bollati, M. et al. Crystal structure of LptH, the periplasmic component of the lipopolysaccharide transport machinery from Pseudomonas aeruginosa. *FEBS J* **282**, 1980-97 (2015).

96.   Malojcic, G. et al. LptE binds to and alters the physical state of LPS to catalyze its assembly at the cell surface. *Proc Natl Acad Sci U S A* **111**, 9467-72 (2014).

97.   Martorana, A.M. et al. Functional Interaction between the Cytoplasmic ABC Protein LptB and the Inner Membrane LptC Protein, Components of the Lipopolysaccharide Transport Machinery in Escherichia coli. *J Bacteriol* **198**, 2192-203 (2016).

98.   Ruiz, N., Gronenberg, L.S., Kahne, D. & Silhavy, T.J. Identification of two inner-membrane proteins required for the transport of lipopolysaccharide to the outer membrane of Escherichia coli. *Proc Natl Acad Sci U S A* **105**, 5537-42 (2008).

99.   Okuda, S., Freinkman, E. & Kahne, D. Cytoplasmic ATP hydrolysis powers transport of lipopolysaccharide across the periplasm in E. coli. *Science* **338**, 1214-7 (2012).

100.   Suits, M.D., Sperandeo, P., Deho, G., Polissi, A. & Jia, Z. Novel structure of the conserved gram-negative lipopolysaccharide transport protein A and mutagenesis analysis. *J Mol Biol* **380**, 476-88 (2008).

101.   Laguri, C. et al. Interaction of lipopolysaccharides at intermolecular sites of the periplasmic Lpt transport assembly. *Sci Rep* **7**, 9715 (2017).

102.   Huber, D. et al. Use of thioredoxin as a reporter to identify a subset of Escherichia coli signal sequences that promote signal recognition particle-dependent translocation. *J Bacteriol* **187**, 2983-91 (2005).

103.   Driessen, A.J. & Nouwen, N. Protein translocation across the bacterial cytoplasmic membrane. *Annu Rev Biochem* **77**, 643-67 (2008).

104.   Chatzi, K.E. et al. Preprotein mature domains contain translocase targeting signals that are essential for secretion. *J Cell Biol* **216**, 1357-1369 (2017).

105.   Hizlan, D. et al. Structure of the SecY complex unlocked by a preprotein mimic. *Cell Rep* **1**, 21-8 (2012).

106.   Lycklama, A.N.J.A. & Driessen, A.J. The bacterial Sec-translocase: structure and mechanism. *Philos Trans R Soc Lond B Biol Sci* **367**, 1016-28 (2012).

107.   Rapoport, T.A., Li, L. & Park, E. Structural and Mechanistic Insights into Protein Translocation. *Annu Rev Cell Dev Biol* **33**, 369-390 (2017).

108.   Beck, K., Wu, L.F., Brunner, J. & Muller, M. Discrimination between SRP- and SecA/SecB-dependent substrates involves selective recognition of nascent chains by SRP and trigger factor. *EMBO J* **19**, 134-43 (2000).

109.   Randall, L.L. & Hardy, S.J. SecB, one small chaperone in the complex milieu of the cell. *Cell Mol Life Sci* **59**, 1617-23 (2002).

110.   Gouridis, G., Karamanou, S., Gelis, I., Kalodimos, C.G. & Economou, A. Signal peptides are allosteric activators of the protein translocase. *Nature* **462**, 363-7 (2009).

111.   Kumamoto, C.A. & Beckwith, J. Evidence for specificity at an early step in protein export in Escherichia coli. *J Bacteriol* **163**, 267-74 (1985).

112.   Kumamoto, C.A. & Gannon, P.M. Effects of Escherichia coli secB mutations on pre-maltose binding protein conformation and export kinetics. *J Biol Chem* **263**, 11554-8 (1988).

113.   Hartl, F.U., Lecker, S., Schiebel, E., Hendrick, J.P. & Wickner, W. The binding cascade of SecB to SecA to SecY/E mediates preprotein targeting to the E. coli plasma membrane. *Cell* **63**, 269-79 (1990).

239

114. Brundage, L., Hendrick, J.P., Schiebel, E., Driessen, A.J. & Wickner, W. The purified E. coli integral membrane protein SecY/E is sufficient for reconstitution of SecA-dependent precursor protein translocation. *Cell* **62**, 649-57 (1990).

115. Van den Berg, B. et al. X-ray structure of a protein-conducting channel. *Nature* **427**, 36-44 (2004).

116. Cranford-Smith, T. & Huber, D. The way is the goal: how SecA transports proteins across the cytoplasmic membrane in bacteria. *FEMS Microbiol Lett* **365**(2018).

117. Allen, W.J. et al. Two-way communication between SecY and SecA suggests a Brownian ratchet mechanism for protein translocation. *Elife* **5**(2016).

118. van der Wolk, J.P., de Wit, J.G. & Driessen, A.J. The catalytic cycle of the escherichia coli SecA ATPase comprises two distinct preprotein translocation events. *EMBO J* **16**, 7297-304 (1997).

119. Gouridis, G. et al. Quaternary dynamics of the SecA motor drive translocase catalysis. *Mol Cell* **52**, 655-66 (2013).

120. Erlandson, K.J. et al. A role for the two-helix finger of the SecA ATPase in protein translocation. *Nature* **455**, 984-7 (2008).

121. Bauer, B.W., Shemesh, T., Chen, Y. & Rapoport, T.A. A "push and slide" mechanism allows sequence-insensitive translocation of secretory proteins by the SecA ATPase. *Cell* **157**, 1416-29 (2014).

122. Whitehouse, S. et al. Mobility of the SecA 2-helix-finger is not essential for polypeptide translocation via the SecYEG complex. *J Cell Biol* **199**, 919-29 (2012).

123. Fessl, T. et al. Dynamic action of the Sec machinery during initiation, protein translocation and termination. *Elife* **7**(2018).

124. Braun, V. & Wu, H.C. Lipoproteins, structure, function, biosynthesis and model for protein export. in *New Comprehensive Biochemistry*, Vol. 27 (eds. Ghuysen, J.M. & Hakenbeck, R.) 319-341 (Elsevier, 1994).

125. Mao, G. et al. Crystal structure of E. coli lipoprotein diacylglyceryl transferase. *Nat Commun* **7**, 10198 (2016).

126. Vogeley, L. et al. Structural basis of lipoprotein signal peptidase II action and inhibition by the antibiotic globomycin. *Science* **351**, 876-80 (2016).

127. Sankaran, K. & Wu, H.C. Lipid modification of bacterial prolipoprotein. Transfer of diacylglyceryl moiety from phosphatidylglycerol. *J Biol Chem* **269**, 19701-6 (1994).

128. Seydel, A., Gounon, P. & Pugsley, A.P. Testing the '+2 rule' for lipoprotein sorting in the Escherichia coli cell envelope with a new genetic selection. *Mol Microbiol* **34**, 810-21 (1999).

129. Terada, M., Kuroda, T., Matsuyama, S.I. & Tokuda, H. Lipoprotein sorting signals evaluated as the LolA-dependent release of lipoproteins from the cytoplasmic membrane of Escherichia coli. *J Biol Chem* **276**, 47690-4 (2001).

130. Yamaguchi, K., Yu, F. & Inouye, M. A single amino acid determinant of the membrane localization of lipoproteins in E. coli. *Cell* **53**, 423-32 (1988).

131. Yakushi, T., Masuda, K., Narita, S., Matsuyama, S. & Tokuda, H. A new ABC transporter mediating the detachment of lipid-modified proteins from membranes. *Nat Cell Biol* **2**, 212-8 (2000).

132. Narita, S., Kanamaru, K., Matsuyama, S. & Tokuda, H. A mutation in the membrane subunit of an ABC transporter LolCDE complex causing outer

membrane localization of lipoproteins against their inner membrane-specific signals. *Mol Microbiol* **49**, 167-77 (2003).

133. Sakamoto, C., Satou, R., Tokuda, H. & Narita, S. Novel mutations of the LolCDE complex causing outer membrane localization of lipoproteins despite their inner membrane-retention signals. *Biochem Biophys Res Commun* **401**, 586-91 (2010).

134. Hara, T., Matsuyama, S. & Tokuda, H. Mechanism underlying the inner membrane retention of Escherichia coli lipoproteins caused by Lol avoidance signals. *J Biol Chem* **278**, 40408-14 (2003).

135. Ito, Y., Kanamaru, K., Taniguchi, N., Miyamoto, S. & Tokuda, H. A novel ligand bound ABC transporter, LolCDE, provides insights into the molecular mechanisms underlying membrane detachment of bacterial lipoproteins. *Mol Microbiol* **62**, 1064-75 (2006).

136. Matsuyama, S., Tajima, T. & Tokuda, H. A novel periplasmic carrier protein involved in the sorting and transport of Escherichia coli lipoproteins destined for the outer membrane. *EMBO J* **14**, 3365-72 (1995).

137. Matsuyama, S., Yokota, N. & Tokuda, H. A novel outer membrane lipoprotein, LolB (HemM), involved in the LolA (p20)-dependent localization of lipoproteins to the outer membrane of Escherichia coli. *EMBO J* **16**, 6947-55 (1997).

138. Taniguchi, N., Matsuyama, S. & Tokuda, H. Mechanisms underlying energy-independent transfer of lipoproteins from LolA to LolB, which have similar unclosed beta-barrel structures. *J Biol Chem* **280**, 34481-8 (2005).

139. Robinson, L.S., Ashman, E.M., Hultgren, S.J. & Chapman, M.R. Secretion of curli fibre subunits is mediated by the outer membrane-localized CsgG protein. *Mol Microbiol* **59**, 870-81 (2006).

140. Drummelsmith, J. & Whitfield, C. Translocation of group 1 capsular polysaccharide to the surface of Escherichia coli requires a multimeric complex in the outer membrane. *EMBO J* **19**, 57-66 (2000).

141. Cowles, C.E., Li, Y., Semmelhack, M.F., Cristea, I.M. & Silhavy, T.J. The free and bound forms of Lpp occupy distinct subcellular locations in Escherichia coli. *Mol Microbiol* **79**, 1168-81 (2011).

142. Konovalova, A. & Silhavy, T.J. Outer membrane lipoprotein biogenesis: Lol is not the end. *Philos Trans R Soc Lond B Biol Sci* **370**(2015).

143. Webb, C.T. et al. Dynamic association of BAM complex modules includes surface exposure of the lipoprotein BamC. *J Mol Biol* **422**, 545-55 (2012).

144. Michel, L.V. et al. Dual orientation of the outer membrane lipoprotein Pal in Escherichia coli. *Microbiology* **161**, 1251-9 (2015).

145. Arnold, M.F. et al. Enteric YaiW is a surface-exposed outer membrane lipoprotein that affects sensitivity to an antimicrobial peptide. *J Bacteriol* **196**, 436-44 (2014).

146. von Heijne, G. The membrane protein universe: what's out there and why bother? *J Intern Med* **261**, 543-57 (2007).

147. von Heijne, G. Principles of membrane protein assembly and structure. *Prog Biophys Mol Biol* **66**, 113-39 (1996).

148. Dong, C. et al. Wza the translocon for E. coli capsular polysaccharides defines a new class of membrane protein. *Nature* **444**, 226-9 (2006).

149. Schulz, G.E. Beta-Barrel membrane proteins. *Curr Opin Struct Biol* **10**, 443-7 (2000).

241

150. Fairman, J.W., Noinaj, N. & Buchanan, S.K. The structural biology of beta-barrel membrane proteins: a summary of recent reports. *Curr Opin Struct Biol* **21**, 523-31 (2011).

151. Wimley, W.C. The versatile beta-barrel membrane protein. *Curr Opin Struct Biol* **13**, 404-11 (2003).

152. Vogt, J. & Schulz, G.E. The structure of the outer membrane protein OmpX from Escherichia coli reveals possible mechanisms of virulence. *Structure* **7**, 1301-9 (1999).

153. Pautsch, A. & Schulz, G.E. Structure of the outer membrane protein A transmembrane domain. *Nat Struct Biol* **5**, 1013-7 (1998).

154. Efremov, R.G. & Sazanov, L.A. Structure of Escherichia coli OmpF porin from lipidic mesophase. *J Struct Biol* **178**, 311-8 (2012).

155. Locher, K.P. et al. Transmembrane signaling across the ligand-gated FhuA receptor: crystal structures of free and ferrichrome-bound states reveal allosteric changes. *Cell* **95**, 771-8 (1998).

156. van den Berg, B., Black, P.N., Clemons, W.M., Jr. & Rapoport, T.A. Crystal structure of the long-chain fatty acid transporter FadL. *Science* **304**, 1506-9 (2004).

157. Snijder, H.J. et al. Structural evidence for dimerization-regulated activation of an integral membrane phospholipase. *Nature* **401**, 717-21 (1999).

158. Schrodinger, LLC. The PyMOL Molecular Graphics System, Version 1.3r1. (2010).

159. Hagan, C.L. & Kahne, D. The reconstituted Escherichia coli Bam complex catalyzes multiple rounds of beta-barrel assembly. *Biochemistry* **50**, 7444-6 (2011).

160. Goemans, C., Denoncin, K. & Collet, J.F. Folding mechanisms of periplasmic proteins. *Biochim Biophys Acta* **1843**, 1517-28 (2014).

161. Harms, N. et al. The early interaction of the outer membrane protein PhoE with the periplasmic chaperone Skp occurs at the cytoplasmic membrane. *J Biol Chem* **276**, 18804-11 (2001).

162. Sklar, J.G., Wu, T., Kahne, D. & Silhavy, T.J. Defining the roles of the periplasmic chaperones SurA, Skp, and DegP in Escherichia coli. *Genes Dev* **21**, 2473-84 (2007).

163. Schiffrin, B.C., Antonio N.; Devine, Paul W.A.; Harris, Sarah A.; Ashcroft, Alison E.; Brockwell, David J.; Radford, Sheena E. Skp is a multivalent chaperone of outer membrane proteins *Nat Struct Mol Biol* **23**, 786-793 (2016).

164. Rizzitello, A.E., Harper, J.R. & Silhavy, T.J. Genetic evidence for parallel pathways of chaperone activity in the periplasm of Escherichia coli. *J Bacteriol* **183**, 6794-800 (2001).

165. Thoma, J., Burmann, B.M., Hiller, S. & Muller, D.J. Impact of holdase chaperones Skp and SurA on the folding of beta-barrel outer-membrane proteins. *Nat Struct Mol Biol* **22**, 795-802 (2015).

166. Bitto, E. & McKay, D.B. Crystallographic structure of SurA, a molecular chaperone that facilitates folding of outer membrane porins. *Structure* **10**, 1489-98 (2002).

167. Walton, T.A. & Sousa, M.C. Crystal structure of Skp, a prefoldin-like chaperone that protects soluble and membrane proteins from aggregation. *Mol Cell* **15**, 367-74 (2004).

242

168. Krojer, T. et al. Structural basis for the regulated protease and chaperone function of DegP. *Nature* **453**, 885-90 (2008).

169. Lazar, S.W. & Kolter, R. SurA assists the folding of Escherichia coli outer membrane proteins. *J Bacteriol* **178**, 1770-3 (1996).

170. Vertommen, D., Ruiz, N., Leverrier, P., Silhavy, T.J. & Collet, J.F. Characterization of the role of the Escherichia coli periplasmic chaperone SurA using differential proteomics. *Proteomics* **9**, 2432-43 (2009).

171. Behrens, S., Maier, R., de Cock, H., Schmid, F.X. & Gross, C.A. The SurA periplasmic PPIase lacking its parvulin domains functions in vivo and has chaperone activity. *EMBO J* **20**, 285-94 (2001).

172. Soltes, G.R., Schwalm, J., Ricci, D.P. & Silhavy, T.J. The Activity of Escherichia coli Chaperone SurA Is Regulated by Conformational Changes Involving a Parvulin Domain. *J Bacteriol* **198**, 921-9 (2016).

173. Hennecke, G., Nolte, J., Volkmer-Engert, R., Schneider-Mergener, J. & Behrens, S. The periplasmic chaperone SurA exploits two features characteristic of integral outer membrane proteins for selective substrate recognition. *J Biol Chem* **280**, 23540-8 (2005).

174. Kutik, S. et al. Dissecting membrane insertion of mitochondrial beta-barrel proteins. *Cell* **132**, 1011-24 (2008).

175. Hagan, C.L., Wzorek, J.S. & Kahne, D. Inhibition of the beta-barrel assembly machine by a peptide that binds BamD. *Proc Natl Acad Sci U S A* **112**, 2011-2016 (2015).

176. Sklar, J.G. et al. Lipoprotein SmpA is a component of the YaeT complex that assembles outer membrane proteins in Escherichia coli. *Proc Natl Acad Sci U S A* **104**, 6400-5 (2007).

177. Chen, R. & Henning, U. A periplasmic protein (Skp) of Escherichia coli selectively binds a class of outer membrane proteins. *Mol Microbiol* **19**, 1287-94 (1996).

178. Jarchow, S., Luck, C., Gorg, A. & Skerra, A. Identification of potential substrate proteins for the periplasmic Escherichia coli chaperone Skp. *Proteomics* **8**, 4987-94 (2008).

179. Qu, J., Mayer, C., Behrens, S., Holst, O. & Kleinschmidt, J.H. The trimeric periplasmic chaperone Skp of Escherichia coli forms 1:1 complexes with outer membrane proteins via hydrophobic and electrostatic interactions. *J Mol Biol* **374**, 91-105 (2007).

180. Wu, S. et al. Interaction between bacterial outer membrane proteins and periplasmic quality control factors: a kinetic partitioning mechanism. *Biochem J* **438**, 505-11 (2011).

181. Burmann, B.M., Wang, C. & Hiller, S. Conformation and dynamics of the periplasmic membrane-protein-chaperone complexes OmpX-Skp and tOmpA-Skp. *Nat Struct Mol Biol* **20**, 1265-72 (2013).

182. Patel, G.J., Behrens-Kneip, S., Holst, O. & Kleinschmidt, J.H. The periplasmic chaperone Skp facilitates targeting, insertion, and folding of OmpA into lipid membranes with a negative membrane surface potential. *Biochemistry* **48**, 10235-45 (2009).

183. Qu, J., Behrens-Kneip, S., Holst, O. & Kleinschmidt, J.H. Binding regions of outer membrane protein A in complexes with the periplasmic chaperone Skp. A site-directed fluorescence study. *Biochemistry* **48**, 4926-36 (2009).

243

184. Burmann, B.M., Holdbrook, D.A., Callon, M., Bond, P.J. & Hiller, S. Revisiting the interaction between the chaperone Skp and lipopolysaccharide. *Biophys J* **108**, 1516-26 (2015).

185. Spiess, C., Beil, A. & Ehrmann, M. A temperature-dependent switch from chaperone to protease in a widely conserved heat shock protein. *Cell* **97**, 339-47 (1999).

186. Krojer, T., Garrido-Franco, M., Huber, R., Ehrmann, M. & Clausen, T. Crystal structure of DegP (HtrA) reveals a new protease-chaperone machine. *Nature* **416**, 455-9 (2002).

187. Onufryk, C., Crouch, M.L., Fang, F.C. & Gross, C.A. Characterization of six lipoproteins in the sigmaE regulon. *J Bacteriol* **187**, 4552-61 (2005).

188. Malinverni, J.C. et al. YfiO stabilizes the YaeT complex and is essential for outer membrane protein assembly in Escherichia coli. *Mol Microbiol* **61**, 151-64 (2006).

189. Hagan, C.L., Kim, S. & Kahne, D. Reconstitution of outer membrane protein assembly from purified components. *Science* **328**, 890-2 (2010).

190. Vuong, P., Bennion, D., Mantei, J., Frost, D. & Misra, R. Analysis of YfgL and YaeT interactions through bioinformatics, mutagenesis, and biochemistry. *J Bacteriol* **190**, 1507-17 (2008).

191. Thomas, W.R., Callow, M.G., Dilworth, R.J. & Audesho, A.A. Expression in Escherichia coli of a high-molecular-weight protective surface antigen found in nontypeable and type b Haemophilus influenzae. *Infect Immun* **58**, 1909-13 (1990).

192. Thomas, K.L. et al. Cloning, overexpression, purification, and immunobiology of an 85-kilodalton outer membrane protein from Haemophilus ducreyi. *Infect Immun* **69**, 4438-46 (2001).

193. Jansen, C. et al. Biochemical and biophysical characterization of in vitro folded outer membrane porin PorA of Neisseria meningitidis. *Biochim Biophys Acta* **1464**, 284-98 (2000).

194. Noinaj, N. et al. Structural insight into the biogenesis of beta-barrel membrane proteins. *Nature* **501**, 385-90 (2013).

195. Albrecht, R. & Zeth, K. Structural basis of outer membrane protein biogenesis in bacteria. *J Biol Chem* **286**, 27792-803 (2011).

196. Clantin, B. et al. Structure of the membrane protein FhaC: a member of the Omp85-TpsB transporter superfamily. *Science* **317**, 957-61 (2007).

197. Gruss, F. et al. The structural basis of autotransporter translocation by TamA. *Nat Struct Mol Biol* **20**, 1318-20 (2013).

198. van den Berg, B. Lateral gates: beta-barrels get in on the act. *Nat Struct Mol Biol* **20**, 1237-9 (2013).

199. Noinaj, N., Kuszak, A.J., Balusek, C., Gumbart, J.C. & Buchanan, S.K. Lateral opening and exit pore formation are required for BamA function. *Structure* **22**, 1055-62 (2014).

200. Maier, T. et al. Conserved Omp85 lid-lock structure and substrate recognition in FhaC. *Nat Commun* **6**, 7452 (2015).

201. Kim, S. et al. Structure and function of an essential component of the outer membrane protein assembly machine. *Science* **317**, 961-4 (2007).

202. Harrison, S.C. Peptide-surface association: the case of PDZ and PTB domains. *Cell* **86**, 341-3 (1996).

203. Gatzeva-Topalova, P.Z., Walton, T.A. & Sousa, M.C. Crystal structure of YaeT: conformational flexibility and substrate recognition. *Structure* **16**, 1873-81 (2008).

204. Jansen, K.B., Baker, S.L. & Sousa, M.C. Crystal structure of BamB bound to a periplasmic domain fragment of BamA, the central component of the beta-barrel assembly machine. *J Biol Chem* **290**, 2126-36 (2015).

205. Chen, Z. et al. Structural basis for the interaction of BamB with the POTRA3-4 domains of BamA. *Acta Crystallogr D Struct Biol* **72**, 236-44 (2016).

206. Fleming, P.J. et al. BamA POTRA Domain Interacts with a Native Lipid Membrane Surface. *Biophys J* **110**, 2698-2709 (2016).

207. Bakelar, J., Buchanan, S.K. & Noinaj, N. The structure of the beta-barrel assembly machinery complex. *Science* **351**, 180-6 (2016).

208. Gu, Y. et al. Structural basis of outer membrane protein insertion by the BAM complex. *Nature* **531**, 64-9 (2016).

209. Han, L. et al. Structure of the BAM complex and its implications for biogenesis of outer-membrane proteins. *Nat Struct Mol Biol* **23**, 192-6 (2016).

210. Iadanza, M.G. et al. Lateral opening in the intact beta-barrel assembly machinery captured by cryo-EM. *Nat Commun* **7**, 12865 (2016).

211. Robert, V. et al. Assembly factor Omp85 recognizes its outer membrane protein substrates by a species-specific C-terminal motif. *PLoS Biol* **4**, e377 (2006).

212. Kim, K.H., Aulakh, S. & Paetzel, M. The bacterial outer membrane beta-barrel assembly machinery. *Protein Sci* **21**, 751-68 (2012).

213. Palomino, C., Marin, E. & Fernandez, L.A. The fimbrial usher FimD follows the SurA-BamB pathway for its assembly in the outer membrane of Escherichia coli. *J Bacteriol* **193**, 5222-30 (2011).

214. Charlson, E.S., Werner, J.N. & Misra, R. Differential effects of yfgL mutation on Escherichia coli outer membrane proteins and lipopolysaccharide. *J Bacteriol* **188**, 7186-94 (2006).

215. Ureta, A.R., Endres, R.G., Wingreen, N.S. & Silhavy, T.J. Kinetic analysis of the assembly of the outer membrane protein LamB in Escherichia coli mutants each lacking a secretion or targeting factor in a different cellular compartment. *J Bacteriol* **189**, 446-54 (2007).

216. Gunasinghe, S.D. et al. The WD40 Protein BamB Mediates Coupling of BAM Complexes into Assembly Precincts in the Bacterial Outer Membrane. *Cell Rep* **23**, 2782-2794 (2018).

217. Kim, K.H., Aulakh, S. & Paetzel, M. Crystal structure of beta-barrel assembly machinery BamCD protein complex. *J Biol Chem* **286**, 39116-21 (2011).

218. Sandoval, C.M., Baker, S.L., Jansen, K., Metzner, S.I. & Sousa, M.C. Crystal structure of BamD: an essential component of the beta-Barrel assembly machinery of gram-negative bacteria. *J Mol Biol* **409**, 348-57 (2011).

219. Gatsos, X. et al. Protein secretion and outer membrane assembly in Alphaproteobacteria. *FEMS Microbiol Rev* **32**, 995-1009 (2008).

220. Lee, J. et al. Characterization of a stalled complex on the beta-barrel assembly machine. *Proc Natl Acad Sci U S A* **113**, 8717-22 (2016).

221. Dong, C., Hou, H.F., Yang, X., Shen, Y.Q. & Dong, Y.H. Structure of Escherichia coli BamD and its functional implications in outer membrane protein assembly. *Acta Crystallogr D Biol Crystallogr* **68**, 95-101 (2012).

245

222. Lewis, C. et al. Small outer-membrane lipoprotein, SmpA, is regulated by sigmaE and has a role in cell envelope integrity and virulence of Salmonella enterica serovar Typhimurium. *Microbiology* **154**, 979-88 (2008).

223. Knowles, T.J. et al. Structure and function of BamE within the outer membrane and the beta-barrel assembly machine. *EMBO Rep* **12**, 123-8 (2011).

224. Kim, K.H. et al. Structural characterization of Escherichia coli BamE, a lipoprotein component of the beta-barrel assembly machinery complex. *Biochemistry* **50**, 1081-90 (2011).

225. Strynadka, N.C. et al. Structural and kinetic characterization of a beta-lactamase-inhibitor protein. *Nature* **368**, 657-60 (1994).

226. Bergal, H.T., Hopkins, A.H., Metzner, S.I. & Sousa, M.C. The Structure of a BamA-BamD Fusion Illuminates the Architecture of the beta-Barrel Assembly Machine Core. *Structure* **24**, 243-51 (2016).

227. O'Neil, P.K., Rollauer, S.E., Noinaj, N. & Buchanan, S.K. Fitting the Pieces of the beta-Barrel Assembly Machinery Complex. *Biochemistry* **54**, 6303-11 (2015).

228. Dong, C., Yang, X., Hou, H.F., Shen, Y.Q. & Dong, Y.H. Structure of Escherichia coli BamB and its interaction with POTRA domains of BamA. *Acta Crystallogr D Biol Crystallogr* **68**, 1134-9 (2012).

229. Tamm, L.K., Hong, H. & Liang, B. Folding and assembly of beta-barrel membrane proteins. *Biochim Biophys Acta* **1666**, 250-63 (2004).

230. Danoff, E.J. & Fleming, K.G. Novel Kinetic Intermediates Populated along the Folding Pathway of the Transmembrane beta-Barrel OmpA. *Biochemistry* **56**, 47-60 (2017).

231. Doerner, P.A. & Sousa, M.C. Extreme Dynamics in the BamA beta-Barrel Seam. *Biochemistry* **56**, 3142-3149 (2017).

232. Fleming, K.G. A combined kinetic push and thermodynamic pull as driving forces for outer membrane protein sorting and folding in bacteria. *Philos Trans R Soc Lond B Biol Sci* **370**(2015).

233. Kleinschmidt, J.H. Membrane protein folding on the example of outer membrane protein A of Escherichia coli. *Cell Mol Life Sci* **60**, 1547-58 (2003).

234. Kleinschmidt, J.H. Folding kinetics of the outer membrane proteins OmpA and FomA into phospholipid bilayers. *Chem Phys Lipids* **141**, 30-47 (2006).

235. Kleinschmidt, J.H. Folding of beta-barrel membrane proteins in lipid bilayers - Unassisted and assisted folding and insertion. *Biochim Biophys Acta* **1848**, 1927-43 (2015).

236. Kleinschmidt, J.H., Bulieris, P.V., Qu, J., Dogterom, M. & den Blaauwen, T. Association of neighboring beta-strands of outer membrane protein A in lipid bilayers revealed by site-directed fluorescence quenching. *J Mol Biol* **407**, 316-32 (2011).

237. Kleinschmidt, J.H., den Blaauwen, T., Driessen, A.J. & Tamm, L.K. Outer membrane protein A of Escherichia coli inserts and folds into lipid bilayers by a concerted mechanism. *Biochemistry* **38**, 5006-16 (1999).

238. Kleinschmidt, J.H. & Tamm, L.K. Folding intermediates of a beta-barrel membrane protein. Kinetic evidence for a multi-step membrane insertion mechanism. *Biochemistry* **35**, 12993-3000 (1996).

239. McMorran, L.M., Brockwell, D.J. & Radford, S.E. Mechanistic studies of the biogenesis and folding of outer membrane proteins in vitro and in vivo: what have we learned to date? *Arch Biochem Biophys* **564**, 265-80 (2014).

240. Moon, C.P., Kwon, S. & Fleming, K.G. Overcoming hysteresis to attain reversible equilibrium folding for outer membrane phospholipase A in phospholipid bilayers. *J Mol Biol* **413**, 484-94 (2011).

241. Schiffrin, B. et al. Effects of Periplasmic Chaperones and Membrane Thickness on BamA-Catalyzed Outer-Membrane Protein Folding. *J Mol Biol* **429**, 3776-3792 (2017).

242. Surrey, T. & Jahnig, F. Kinetics of folding and membrane insertion of a beta-barrel membrane protein. *J Biol Chem* **270**, 28199-203 (1995).

243. Surrey, T. & Jahnig, F. Refolding and oriented insertion of a membrane protein into a lipid bilayer. *Proc Natl Acad Sci U S A* **89**, 7457-61 (1992).

244. Surrey, T., Schmid, A. & Jahnig, F. Folding and membrane insertion of the trimeric beta-barrel protein OmpF. *Biochemistry* **35**, 2283-8 (1996).

245. Plummer, A.M. & Fleming, K.G. BamA Alone Accelerates Outer Membrane Protein Folding In Vitro through a Catalytic Mechanism. *Biochemistry* **54**, 6009-11 (2015).

246. Horne, J.E. & Radford, S.E. A growing toolbox of techniques for studying beta-barrel outer membrane protein folding and biogenesis. *Biochem Soc Trans* **44**, 802-9 (2016).

247. Dornmair, K., Kiefer, H. & Jahnig, F. Refolding of an integral membrane protein. OmpA of Escherichia coli. *J Biol Chem* **265**, 18907-11 (1990).

248. Nakamura, K. & Mizushima, S. Effects of heating in dodecyl sulfate solution on the conformation and electrophoretic mobility of isolated major outer membrane proteins from Escherichia coli K-12. *J Biochem* **80**, 1411-22 (1976).

249. Inouye, M. & Yee, M.L. Homogeneity of envelope proteins of Escherichia coli separated by gel electrophoresis in sodium dodecyl sulfate. *J Bacteriol* **113**, 304-12 (1973).

250. Moon, C.P. & Fleming, K.G. Using tryptophan fluorescence to measure the stability of membrane proteins folded in liposomes. *Methods Enzymol* **492**, 189-211 (2011).

251. Marcoux, J. et al. Mass spectrometry defines the C-terminal dimerization domain and enables modeling of the structure of full-length OmpA. *Structure* **22**, 781-90 (2014).

252. Zheng, C. et al. Cross-linking measurements of in vivo protein complex topologies. *Mol Cell Proteomics* **10**, M110 006841 (2011).

253. Burmann, B.M. & Hiller, S. Chaperones and chaperone-substrate complexes: Dynamic playgrounds for NMR spectroscopists. *Prog Nucl Magn Reson Spectrosc* **86-87**, 41-64 (2015).

254. Hartmann, J.B., Zahn, M., Matecko Burmann, I., Bibow, S. & Hiller, S. Sequence-specific solution NMR assignments of the beta-barrel insertase BamA to monitor its conformational ensemble at the atomic level. *J Am Chem Soc* **140**, 11252–11260 (2018).

255. Morgado, L., Zeth, K., Burmann, B.M., Maier, T. & Hiller, S. Characterization of the insertase BamA in three different membrane mimetics by solution NMR spectroscopy. *J Biomol NMR* **61**, 333-45 (2015).

256. Damaghi, M., Koster, S., Bippes, C.A., Yildiz, O. & Muller, D.J. One beta hairpin follows the other: exploring refolding pathways and kinetics of the transmembrane beta-barrel protein OmpG. *Angew Chem Int Ed Engl* **50**, 7422-4 (2011).

247

257. Thoma, J., Bosshart, P., Pfreundschuh, M. & Muller, D.J. Out but not in: the large transmembrane beta-barrel protein FhuA unfolds but cannot refold via beta-hairpins. *Structure* **20**, 2185-90 (2012).

258. Krainer, G. et al. Slow Interconversion in a Heterogeneous Unfolded-State Ensemble of Outer-Membrane Phospholipase A. *Biophys J* **113**, 1280-1289 (2017).

259. Kang, G. et al. Forster resonance energy transfer as a probe of membrane protein folding. *Biochim Biophys Acta* **1818**, 154-61 (2012).

260. Ubarretxena-Belandia, I. et al. Outer membrane phospholipase A is dimeric in phospholipid bilayers: a cross-linking and fluorescence resonance energy transfer study. *Biochemistry* **38**, 7398-405 (1999).

261. Rodionova, N.A., Tatulian, S.A., Surrey, T., Jahnig, F. & Tamm, L.K. Characterization of two membrane-bound forms of OmpA. *Biochemistry* **34**, 1921-9 (1995).

262. Raschle, T., Rios Flores, P., Opitz, C., Muller, D.J. & Hiller, S. Monitoring Backbone Hydrogen-Bond Formation in beta-Barrel Membrane Protein Folding. *Angew Chem Int Ed Engl* **55**, 5952-5 (2016).

263. Hong, H., Park, S., Jimenez, R.H., Rinehart, D. & Tamm, L.K. Role of aromatic side chains in the folding and thermodynamic stability of integral membrane proteins. *J Am Chem Soc* **129**, 8320-7 (2007).

264. Andersen, K.K., Wang, H. & Otzen, D.E. A kinetic analysis of the folding and unfolding of OmpA in urea and guanidinium chloride: single and parallel pathways. *Biochemistry* **51**, 8371-83 (2012).

265. Pocanschi, C.L. et al. The major outer membrane protein of Fusobacterium nucleatum (FomA) folds and inserts into lipid bilayers via parallel folding pathways. *J Mol Biol* **355**, 548-61 (2006).

266. Krishna, M.M. & Englander, S.W. A unified mechanism for protein folding: predetermined pathways with optional errors. *Protein Sci* **16**, 449-64 (2007).

267. Koebnik, R. Structural and functional roles of the surface-exposed loops of the beta-barrel membrane protein OmpA from Escherichia coli. *J Bacteriol* **181**, 3688-94 (1999).

268. Kramer, R.A., Zandwijken, D., Egmond, M.R. & Dekker, N. In vitro folding, purification and characterization of Escherichia coli outer membrane protease OmpT. *Eur J Biochem* **267**, 885-93 (2000).

269. Lewis, B.A. & Engelman, D.M. Lipid bilayer thickness varies linearly with acyl chain length in fluid phosphatidylcholine vesicles. *J Mol Biol* **166**, 211-7 (1983).

270. Lomize, A.L., Pogozheva, I.D., Lomize, M.A. & Mosberg, H.I. Positioning of proteins in membranes: a computational approach. *Protein Sci* **15**, 1318-33 (2006).

271. Patel, G.J. & Kleinschmidt, J.H. The lipid bilayer-inserted membrane protein BamA of Escherichia coli facilitates insertion and folding of outer membrane protein A from its complex with Skp. *Biochemistry* **52**, 3974-86 (2013).

272. Hagan, C.L., Westwood, D.B. & Kahne, D. Bam Lipoproteins Assemble BamA in vitro. *Biochemistry* **52**, 6108-13 (2013).

273. Hussain, S. & Bernstein, H.D. The Bam complex catalyzes efficient insertion of bacterial outer membrane proteins into membrane vesicles of variable lipid composition. *J Biol Chem* **293**, 2959-2973 (2018).

248

274. Roman-Hernandez, G., Peterson, J.H. & Bernstein, H.D. Reconstitution of bacterial autotransporter assembly using purified components. *Elife* **3**, e04234 (2014).

275. Sugimura, K. & Nishihara, T. Purification, characterization, and primary structure of Escherichia coli protease VII with specificity for paired basic residues: identity of protease VII and OmpT. *J Bacteriol* **170**, 5625-32 (1988).

276. Ruiz, N., Kahne, D. & Silhavy, T.J. Advances in understanding bacterial outer-membrane biogenesis. *Nat Rev Microbiol* **4**, 57-66 (2006).

277. Rigel, N.W., Ricci, D.P. & Silhavy, T.J. Conformation-specific labeling of BamA and suppressor analysis suggest a cyclic mechanism for beta-barrel assembly in Escherichia coli. *Proc Natl Acad Sci U S A* **110**, 5151-6 (2013).

278. Fan, E., Fiedler, S., Jacob-Dubuisson, F. & Muller, M. Two-partner secretion of gram-negative bacteria: a single beta-barrel protein enables transport across the outer membrane. *J Biol Chem* **287**, 2591-9 (2012).

279. Danoff, E.J. & Fleming, K.G. Membrane defects accelerate outer membrane beta-barrel protein folding. *Biochemistry* **54**, 97-9 (2015).

280. Meng, G., Fronzes, R., Chandran, V., Remaut, H. & Waksman, G. Protein oligomerization in the bacterial outer membrane. *Mol Membr Biol* **26**, 136-45 (2009).

281. Li, H., Grass, S., Wang, T., Liu, T. & St Geme, J.W., 3rd. Structure of the Haemophilus influenzae HMW1B translocator protein: evidence for a twin pore. *J Bacteriol* **189**, 7497-502 (2007).

282. Surana, N.K. et al. Evidence for conservation of architecture and physical properties of Omp85-like proteins throughout evolution. *Proc Natl Acad Sci U S A* **101**, 14497-502 (2004).

283. Rassam, P. et al. Supramolecular assemblies underpin turnover of outer membrane proteins in bacteria. *Nature* **523**, 333-6 (2015).

284. Bosch, D., Scholten, M., Verhagen, C. & Tommassen, J. The role of the carboxy-terminal membrane-spanning fragment in the biogenesis of Escherichia coli K12 outer membrane protein PhoE. *Mol Gen Genet* **216**, 144-8 (1989).

285. Struyve, M., Moons, M. & Tommassen, J. Carboxy-terminal phenylalanine is essential for the correct assembly of a bacterial outer membrane protein. *J Mol Biol* **218**, 141-8 (1991).

286. Paramasivam, N., Habeck, M. & Linke, D. Is the C-terminal insertional signal in Gram-negative bacterial outer membrane proteins species-specific or not? *BMC Genomics* **13**, 510 (2012).

287. Hohr, A.I.C. et al. Membrane protein insertion through a mitochondrial beta-barrel gate. *Science* **359**(2018).

288. McMorran, L.M., Bartlett, A.I., Huysmans, G.H., Radford, S.E. & Brockwell, D.J. Dissecting the effects of periplasmic chaperones on the in vitro folding of the outer membrane protein PagP. *J Mol Biol* **425**, 3178-91 (2013).

289. Wilkins, M.R. et al. Protein identification and analysis tools in the ExPASy server. *Methods Mol Biol* **112**, 531-52 (1999).

290. Marty, M.T. et al. Bayesian deconvolution of mass and ion mobility spectra: from binary interactions to polydisperse ensembles. *Anal Chem* **87**, 4370-6 (2015).

291. Kremer, J.R., Mastronarde, D.N. & McIntosh, J.R. Computer visualization of three-dimensional image data using IMOD. *J Struct Biol* **116**, 71-6 (1996).

292. Li, X. et al. Electron counting and beam-induced motion correction enable near-atomic-resolution single-particle cryo-EM. *Nat Methods* **10**, 584-90 (2013).

293. Tang, G. et al. EMAN2: an extensible image processing suite for electron microscopy. *J Struct Biol* **157**, 38-46 (2007).

294. Scheres, S.H. Semi-automated selection of cryo-EM particles in RELION-1.3. *J Struct Biol* **189**, 114-22 (2015).

295. Scheres, S.H. RELION: implementation of a Bayesian approach to cryo-EM structure determination. *J Struct Biol* **180**, 519-30 (2012).

296. Scheres, S.H. Beam-induced motion correction for sub-megadalton cryo-EM particles. *Elife* **3**, e03665 (2014).

297. Kucukelbir, A., Sigworth, F.J. & Tagare, H.D. Quantifying the local resolution of cryo-EM density maps. *Nat Methods* **11**, 63-5 (2014).

298. Pettersen, E.F. et al. UCSF Chimera--a visualization system for exploratory research and analysis. *J Comput Chem* **25**, 1605-12 (2004).

299. Noinaj, N., Fairman, J.W. & Buchanan, S.K. The crystal structure of BamB suggests interactions with BamA and its role within the BAM complex. *J Mol Biol* **407**, 248-60 (2011).

300. Trabuco, L.G., Villa, E., Mitra, K., Frank, J. & Schulten, K. Flexible fitting of atomic structures into electron microscopy maps using molecular dynamics. *Structure* **16**, 673-83 (2008).

301. DiMaio, F. et al. Atomic-accuracy models from 4.5-A cryo-electron microscopy data with density-guided iterative local refinement. *Nat Methods* **12**, 361-365 (2015).

302. Schneider, C.A., Rasband, W.S. & Eliceiri, K.W. NIH Image to ImageJ: 25 years of image analysis. *Nat Methods* **9**, 671-5 (2012).

303. van der Does, C., de Keyzer, J., van der Laan, M. & Driessen, A.J. Reconstitution of purified bacterial preprotein translocase in liposomes. *Methods Enzymol* **372**, 86-98 (2003).

304. Lee, S.C. et al. A method for detergent-free isolation of membrane proteins in their local lipid environment. *Nat Protoc* **11**, 1149-62 (2016).

305. Knowles, T.J. et al. Membrane proteins solubilized intact in lipid containing nanoparticles bounded by styrene maleic acid copolymer. *J Am Chem Soc* **131**, 7484-5 (2009).

306. Bayburt, T.H. & Sligar, S.G. Membrane protein assembly into Nanodiscs. *FEBS Lett* **584**, 1721-7 (2010).

307. Heller, K.B. Apparent molecular weights of a heat-modifiable protein from the outer membrane of Escherichia coli in gels with different acrylamide concentrations. *J Bacteriol* **134**, 1181-3 (1978).

308. Minton, A.P. Recent applications of light scattering measurement in the biological and biopharmaceutical sciences. *Anal Biochem* **501**, 4-22 (2016).

309. Pocanschi, C.L., Patel, G.J., Marsh, D. & Kleinschmidt, J.H. Curvature elasticity and refolding of OmpA in large unilamellar vesicles. *Biophys J* **91**, L75-7 (2006).

310. Wu, E.L. et al. E. coli outer membrane and interactions with OmpLA. *Biophys J* **106**, 2493-502 (2014).

311. Hong, H. & Tamm, L.K. Elastic coupling of integral membrane protein stability to lipid bilayer forces. *Proc Natl Acad Sci U S A* **101**, 4065-70 (2004).

312. Roger, V., Cottet, H. & Cipelletti, L. A New Robust Estimator of Polydispersity from Dynamic Light Scattering Data. *Anal Chem* **88**, 2630-6 (2016).

313. White, G.F., Racher, K.I., Lipski, A., Hallett, F.R. & Wood, J.M. Physical properties of liposomes and proteoliposomes prepared from Escherichia coli polar lipids. *Biochim Biophys Acta* **1468**, 175-86 (2000).

314. Srinivas, N. et al. Peptidomimetic antibiotics target outer-membrane biogenesis in Pseudomonas aeruginosa. *Science* **327**, 1010-3 (2010).

315. Schmidt, J., Patora-Komisarska, K., Moehle, K., Obrecht, D. & Robinson, J.A. Structural studies of beta-hairpin peptidomimetic antibiotics that target LptD in Pseudomonas sp. *Bioorg Med Chem* **21**, 5806-10 (2013).

316. Zerbe, K., Moehle, K. & Robinson, J.A. Protein Epitope Mimetics: From New Antibiotics to Supramolecular Synthetic Vaccines. *Acc Chem Res* **50**, 1323-1331 (2017).

317. Bechara, C. & Sagan, S. Cell-penetrating peptides: 20 years later, where do we stand? *FEBS Lett* **587**, 1693-702 (2013).

318. Ben-Dov, N. & Korenstein, R. The uptake of HIV Tat peptide proceeds via two pathways which differ from macropinocytosis. *Biochim Biophys Acta* **1848**, 869-77 (2015).

319. Werneburg, M. et al. Inhibition of lipopolysaccharide transport to the outer membrane in Pseudomonas aeruginosa by peptidomimetic antibiotics. *Chembiochem* **13**, 1767-75 (2012).

320. Skrzypek, R., Iqbal, S. & Callaghan, R. Methods of reconstitution to investigate membrane protein function. *Methods* **147**, 126-141 (2018).

321. Li, Y., Kijac, A.Z., Sligar, S.G. & Rienstra, C.M. Structural analysis of nanoscale self-assembled discoidal lipid bilayers by solid-state NMR spectroscopy. *Biophys J* **91**, 3819-28 (2006).

322. Denisov, I.G. & Sligar, S.G. Nanodiscs for structural and functional studies of membrane proteins. *Nat Struct Mol Biol* **23**, 481-6 (2016).

323. Efremov, R.G., Leitner, A., Aebersold, R. & Raunser, S. Architecture and conformational switch mechanism of the ryanodine receptor. *Nature* **517**, 39-43 (2015).

324. Seddon, A.M., Curnow, P. & Booth, P.J. Membrane proteins, lipids and detergents: not just a soap opera. *Biochim Biophys Acta* **1666**, 105-17 (2004).

325. Stroud, Z., Hall, S.C.L. & Dafforn, T.R. Purification of membrane proteins free from conventional detergents: SMA, new polymers, new opportunities and new insights. *Methods* **147**, 106-117 (2018).

326. Pollock, N.L., Lee, S.C., Patel, J.H., Gulamhussein, A.A. & Rothnie, A.J. Structure and function of membrane proteins encapsulated in a polymer-bound lipid bilayer. *Biochim Biophys Acta* **1860**, 809-817 (2018).

327. Tribet, C., Audebert, R. & Popot, J.L. Amphipols: polymers that keep membrane proteins soluble in aqueous solutions. *Proc Natl Acad Sci U S A* **93**, 15047-50 (1996).

328. Broecker, J., Eger, B.T. & Ernst, O.P. Crystallogenesis of Membrane Proteins Mediated by Polymer-Bounded Lipid Nanodiscs. *Structure* **25**, 384-392 (2017).

329. Gulati, S. et al. Detergent-free purification of ABC (ATP-binding-cassette) transporters. *Biochem J* **461**, 269-78 (2014).

330. Postis, V. et al. The use of SMALPs as a novel membrane protein scaffold for structure study by negative stain electron microscopy. *Biochim Biophys Acta* **1848**, 496-501 (2015).

331. Gao, Y., Cao, E., Julius, D. & Cheng, Y. TRPV1 structures in nanodiscs reveal mechanisms of ligand and lipid action. *Nature* **534**, 347-51 (2016).

332. Denisov, I.G. & Sligar, S.G. Nanodiscs in Membrane Biochemistry and Biophysics. *Chem Rev* **117**, 4669-4713 (2017).

333. Alami, M., Dalal, K., Lelj-Garolla, B., Sligar, S.G. & Duong, F. Nanodiscs unravel the interaction between the SecYEG channel and its cytosolic partner SecA. *EMBO J* **26**, 1995-2004 (2007).

334. Bond, P.J. & Sansom, M.S. Membrane protein dynamics versus environment: simulations of OmpA in a micelle and in a bilayer. *J Mol Biol* **329**, 1035-53 (2003).

335. Frey, L., Lakomek, N.A., Riek, R. & Bibow, S. Micelles, Bicelles, and Nanodiscs: Comparing the Impact of Membrane Mimetics on Membrane Protein Backbone Dynamics. *Angew Chem Int Ed Engl* **56**, 380-383 (2017).

336. Vandeputte-Rutten, L. et al. Crystal structure of the outer membrane protease OmpT from Escherichia coli suggests a novel catalytic site. *EMBO J* **20**, 5033-9 (2001).

337. Huysmans, G.H., Baldwin, S.A., Brockwell, D.J. & Radford, S.E. The transition state for folding of an outer membrane protein. *Proc Natl Acad Sci U S A* **107**, 4099-104 (2010).

338. Leonard-Rivera, M. & Misra, R. Conserved residues of the putative L6 loop of Escherichia coli BamA play a critical role in the assembly of beta-barrel outer membrane proteins, including that of BamA itself. *J Bacteriol* **194**, 4662-8 (2012).

339. Wzorek, J.S., Lee, J., Tomasek, D., Hagan, C.L. & Kahne, D.E. Membrane integration of an essential beta-barrel protein prerequires burial of an extracellular loop. *Proc Natl Acad Sci U S A* **114**, 2598-2603 (2017).

340. Ni, D. et al. Structural and functional analysis of the beta-barrel domain of BamA from Escherichia coli. *FASEB J* **28**, 2677-85 (2014).

341. Hochgrafe, F., Mostertz, J., Albrecht, D. & Hecker, M. Fluorescence thiol modification assay: oxidatively modified proteins in Bacillus subtilis. *Mol Microbiol* **58**, 409-25 (2005).

342. Leichert, L.I. & Jakob, U. Protein thiol modifications visualized in vivo. *PLoS Biol* **2**, e333 (2004).

343. Konovalova, A. et al. Inhibitor of intramembrane protease RseP blocks the sigma(E) response causing lethal accumulation of unfolded outer membrane proteins. *Proc Natl Acad Sci U S A* **115**, 6614-6621 (2018).

344. Ieva, R. & Bernstein, H.D. Interaction of an autotransporter passenger domain with BamA during its translocation across the bacterial outer membrane. *Proc Natl Acad Sci U S A* **106**, 19120-5 (2009).

345. Singh, R., Capalash, N. & Sharma, P. Immunoprotective potential of BamA, the outer membrane protein assembly factor, against MDR Acinetobacter baumannii. *Sci Rep* **7**, 12411 (2017).

346. Vij, R. et al. A targeted boost-and-sort immunization strategy using Escherichia coli BamA identifies rare growth inhibitory antibodies. *Sci Rep* **8**, 7136 (2018).

347. Martin-Loeches, I., Dale, G.E. & Torres, A. Murepavadin: a new antibiotic class in the pipeline. *Expert Rev Anti Infect Ther* **16**, 259-268 (2018).

Appendices

Appendix 1: Optimisation of SDS-PAGE conditions for resolution of intramolecular cross-links in the BAM complex

Throughout, unless otherwise indicated, samples are incubated with redox agents for 1 hour at room temperature, following which 5 µL of 6x SDS loading buffer is added to a 15 µL sample. Samples are boiled for 30 minutes unless otherwise indicated and 15 µL of sample is loaded per well. Varying concentrations of oxidizing agents are denoted by the following scale: 1 (4 µM), 2 (10 µM) 3 (40 µM), 4 (100 µM), 5 (1 mM), 6 (10 mM). Two precast gradient gel types were first assessed, before moving to homemade Tris-Glycine gels with low acrylamide concentration.
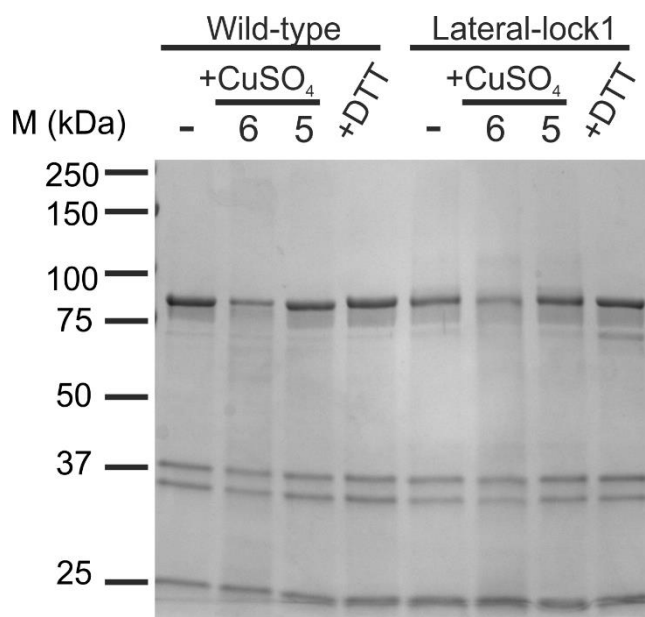
Figure A1-1: Wild-type and Lateral-lock1 proteoliposomes on 4-20% (*w/v*) gradient gel. BAM proteoliposomes at 1 µM in TBS pH 8 were incubated with TBS alone (-), 1 mM (5) or 10 mM (6) CuSO$_4$ or 25 mM DTT. Samples were incubated with redox agents for 1 hour at room temperature, then boiled for 30 minutes with addition of 6x SDS loading buffer. Electrophoresis was carried out on a BioRad 4-20% (*w/v*) gel with cathode buffer at 30 mA, 150 minutes, 4ºC.
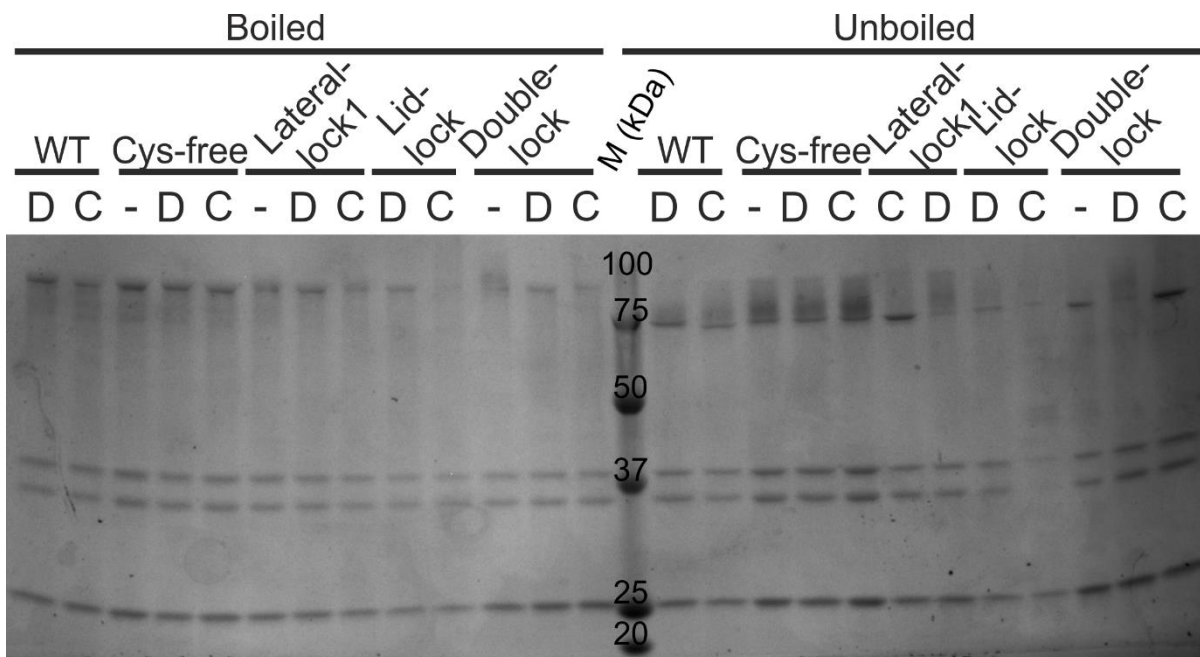
Figure A1-2: Proteoliposomes on 4-20% (*w/v*) polyacrylamide Novex gradient gel. BAM proteoliposomes at 1 µM in TBS pH 8 were incubated with 1 mM CuSO₄ (C), or 10 mM DTT (D), or TBS alone (-). Samples were incubated with redox agents for 2 hours at room temperature, then boiled for 30 minutes where indicated, with addition of 6x SDS loading buffer. The samples were analysed using a Novex 4-20% (*w/v*) polyacrylamide gel with Novex Tris-Glycine buffer at 125V for 4 hours.

In addition to the change to a low acrylamide Tris-Glycine (TGS) gel, several different oxidizing agents were tested (Figure A1-3). 4,4'-dypyridyl-disulphide (4-DPS), iodine and diamide were all hypothesised to be more membrane-permeable than CuSO₄ and it was concluded these might be better oxidizing agents in the case of Lateral-lock1. These were tested at increasing concentrations and in combination (Figure A1-3, 5,5: 1 mM diamide + 1 mM iodine). Intriguingly, iodine at 1 or 10 mM final concentrations (Figure A1-3, iodine 5,6) appeared unable to migrate into the gel. No alterations of oxidizing agent or concentration appeared to affect the proportion of protein in the oxidized state.
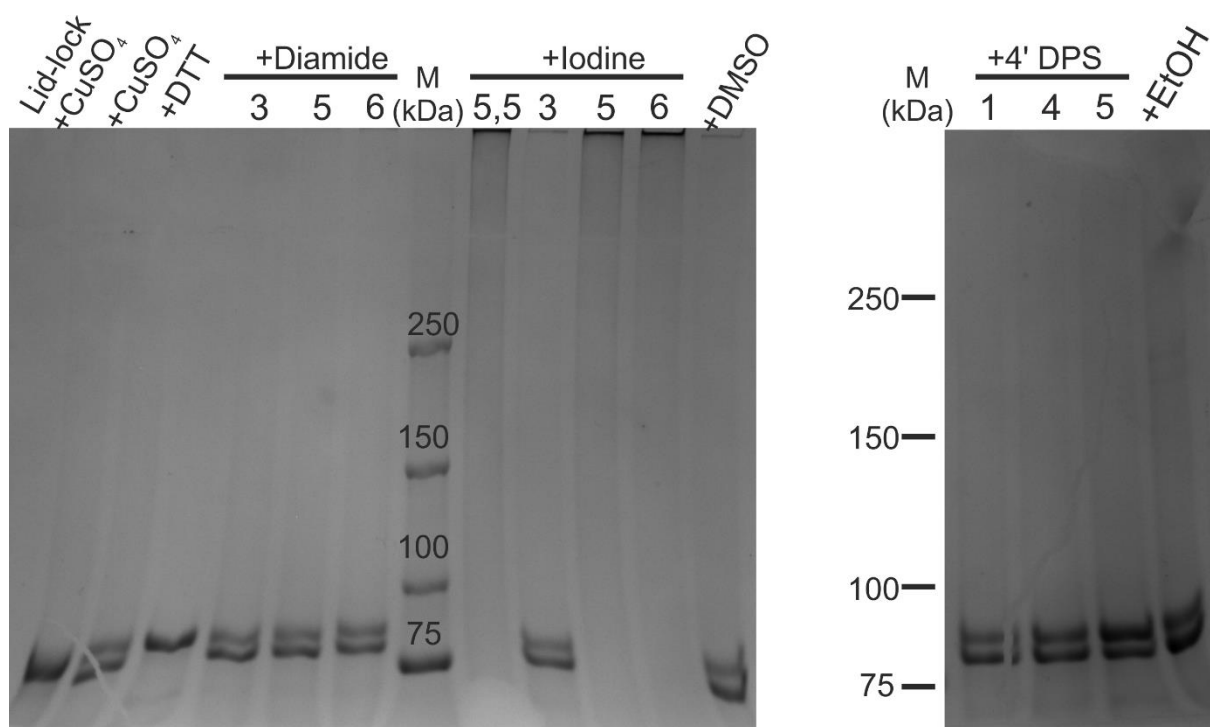
Figure A1-3: Lateral-lock1 proteoliposomes in the presence of oxidizing agents. Oxidation of Lateral-lock1 proteoliposomes was tested with a variety of oxidizing agents. The left-hand lane shows Lid-lock protein (in TBS+DDM) in the presence of 1 mM CuSO$_4$ exhibits a single band. With the exception of the left-most lane, all samples are 2 µM Lateral-lock1 proteoliposomes. Diamide, iodine and 4' DPS were added to final concentrations as indicated by the scale 1 (4 µM), 2 (10 µM) 3 (40 µM), 4 (100 µM), 5 (1 mM), 6 (10 mM). In addition, a final concentration of 1 mM diamide + 1 mM iodine was also tested (indicated as 5,5). Other final concentrations were CuSO$_4$ (1 mM), DTT (25 mM). As iodine is dissolved in DMSO and 4' DPS in EtOH, equivalent volumes of solvent were used as a control. All other agents were made up to 10x stock concentration in TBS pH8. Samples were incubated with redox agents for 1 hour at room temperature, then boiled for 30 minutes with addition of 6x SDS loading buffer. The samples were run on a 5% (*w/v*) acrylamide Tris-Glycine gel with MOPS buffer at 30 mA, 180 minutes, 4ºC.

The Lateral-lock1 proteoliposomes proved impossible to fully oxidize, showing a mixed population with all oxidizing agents, but it was hypothesised perhaps protein (in detergent) would be more amenable or accessible. The study was carried out on protein with varying concentrations of diamide and CuSO$_4$ (Figure A1-4). It was determined that no increased oxidation was seen, but longer incubation and higher temperature were subsequently tested for both protein (P) and proteoliposomes (PL) (Figure A1-5).
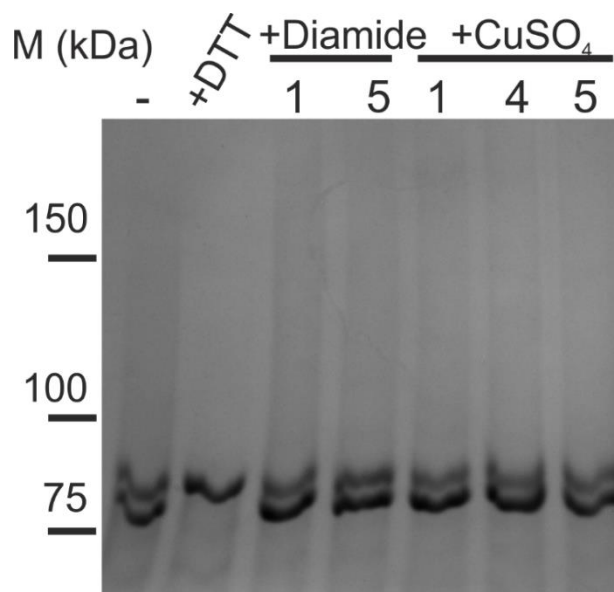
Figure A1-4: Oxidation of Lateral-lock1 protein. The oxidation of Lateral-lock1 protein as opposed to proteoliposomes was tested. Protein was diluted to 2 µM in TBS + 0.05% (*w/v*) DDM. Samples were incubated with redox agents for 1 hour at room temperature, then boiled for 30 minutes with addition of 6x SDS loading buffer. Final concentrations of diamide and $CuSO_4$ were 1 (4 µM), 4 (100 µM) and 5 (1 mM), while the final concentration of DTT was 25 mM. The samples were run on a 5% (*w/v*) acrylamide Tris-Glycine gel with MOPS buffer at 30 mA, 180 minutes, 4ºC.
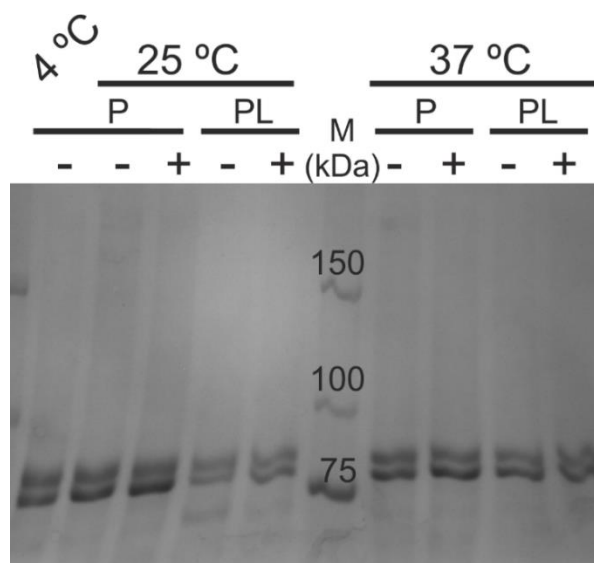

Figure A1-5: Heat and long incubation times do not increase the oxidation of Lateral-lock1 proteoliposomes (PL) or protein (P). The effect of longer incubation and higher temperatures on the reduced:oxidized ratio was tested. Samples of Lateral-lock1 protein (P) in TBS+DDM, and proteoliposomes (PL) in TBS were diluted to 2 µM with (+) or without (-) diamide to a final concentration of 100 µM. Samples were incubated at the indicated temperature for ~ 72 hours. Following this samples were boiled for 30 minutes with addition of 6x SDS loading buffer. The samples were run on a 5% (*w/v*) acrylamide Tris-Glycine gel with MOPS buffer at 30 mA, 180 minutes, 4ºC.

The Lateral-lock2 variant, with sulphydryl groups facing the lumen (Figure 5-1) also showed a mixed population when tested in protein (Figure A1-6), or proteoliposomes (Figure 5-9), with a variety of oxidizing agents.
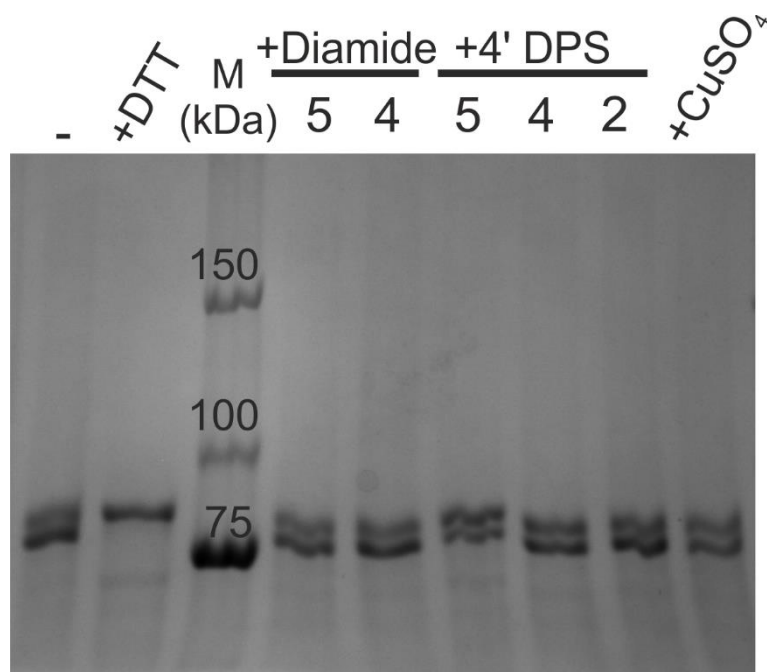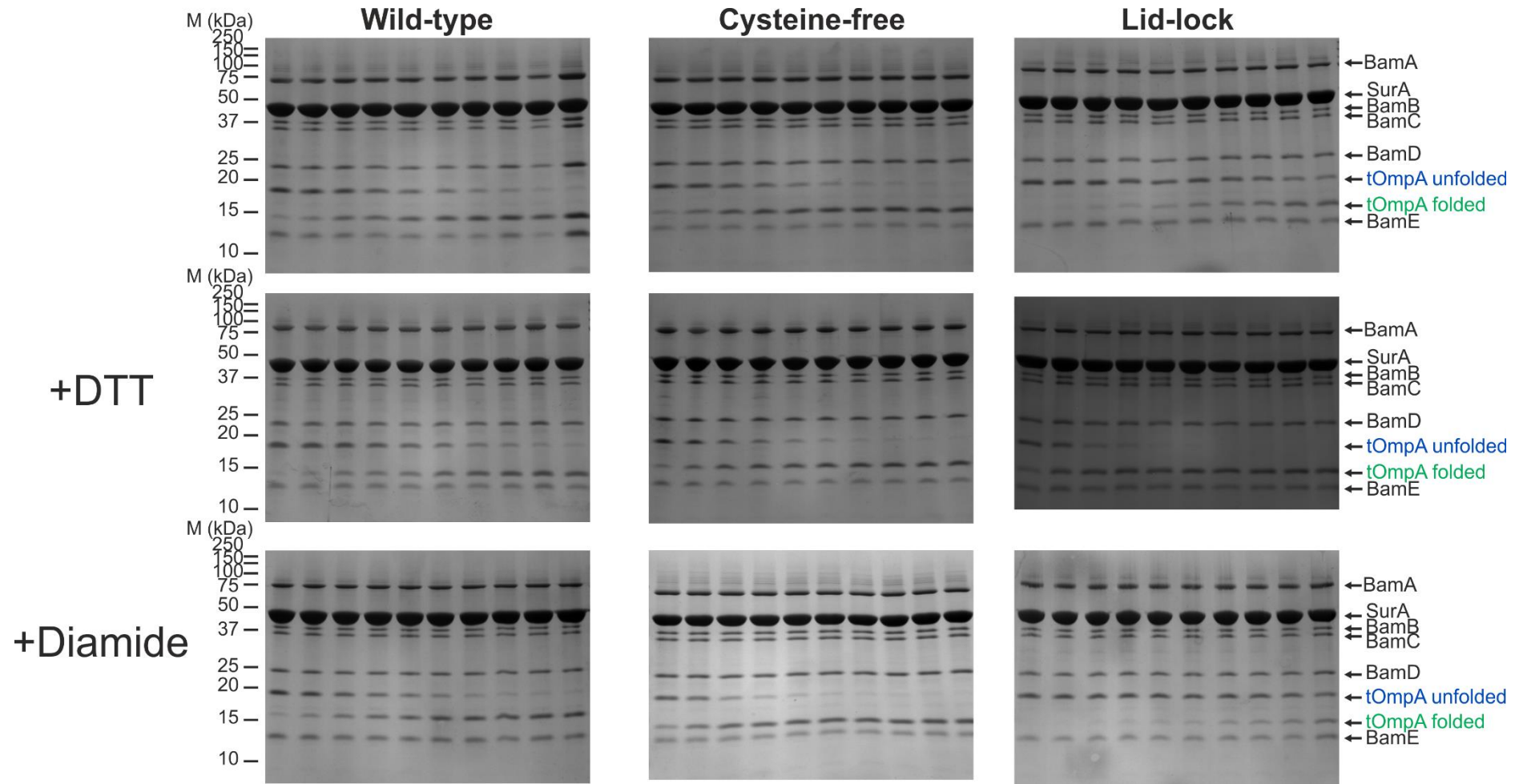
257

Figure A1-6: Lateral-lock2 cannot be fully oxidized. Following generation of the new, Lateral-lock2 (433/805) protein variant, the oxidation state was tested on protein (in TBS + 0.05% (*w/v*) DDM) with a variety of redox agents. Protein at 2 µM is incubated with redox agents overnight (~16 hours) at 25 ºC then boiled for 30 minutes with addition of 6x SDS loading buffer. Final concentrations of diamide and 4'DPS are 2 (10 µM), 4 (100 µM) and 5 (1 mM), while final concentration of DTT is 25 mM and $CuSO_4$ 1 mM. The samples are run on a 5% (*w/v*) acrylamide Tris-Glycine gel with MOPS buffer at 30 mA, 180 minutes, 4ºC.

Appendix2: Examples of the SDS-PAGE tOmpA folding assay for each BAM complex variant in buffer, +DTT and +diamide conditions (Part I)

Examples of the SDS-PAGE tOmpA folding assay for each BAM complex variant in buffer, +DTT and +diamide conditions (Part II)